UNIVERSITY OF CALIFORNIA SAN DIEGO

Secondary Marine Aerosol: A Chemical Link Between Oceans and Clouds

A dissertation submitted in partial satisfaction of the

requirements for the degree Doctor of Philosophy

in

Chemistry

by

Kathryn J. Mayer

Committee in charge:

Professor Kimberly Prather, Chair
Professor Amato Evan
Professor Vicki Grassian
Professor Judy Kim
Professor Haim Weizman

2021

The dissertation of Kathryn J. Mayer is approved,

and it is acceptable in quality and form for publication

on microfilm and electronically.

University of California San Diego

2021

DEDICATION

In memory of my godmother, Dorothy Depgen.

I will always be grateful for your love and support.

TABLE OF CONTENTS

LIST OF ABBREVIATIONS

AF	Activated Fraction
AFM	Atomic Force Microscopy
AMS	Aerosol Mass Spectrometer
APS	Aerodynamic Particle Sizer
ATOFMS	Aerosol Time of Flight Mass Spectrometer
CCN	Cloud Condensation Nuclei
CCNc	Cloud Condensation Nuclei Counter
CN	Condensation Nuclei
CPC	Condensation Particle Counter
Chl-a	Chlorophyll-a
D_a	Aerodynamic Diameter
D_{act}	Activation Diameter
D_d	Dry Diameter
D_m	Mobility Diameter
D_p	Physical Diameter
DMA	Differential Mobility Analyzer
DMS	Dimethyl Sulfide
DMSP	Dimethylsulfoniopropionate
DOC	Dissolved Organic Carbon
DOM	Dissolved Organic Matter
f_{org}	Fraction of Organics
hetSSA	Heterogeneously Aged SSA

ISV	Isolated Sampling Vessel
κ	Hygroscopicity Parameter
κ_{app}	Apparent Hygroscopicity Parameter
LPM	Liters per Minute
MART	Marine Aerosol Reference Tank
MSA	Methanesulfonic Acid
NS-VOC	Non-sulfur VOC
nSSA	Nascent Sea Spray Aerosol
nss-SO_4	Non-sea-salt Sulfate
OAIF	Ocean-Atmosphere Interaction Facility
OFR	Oxidation Flow Reactor
OMF	Organic Mass Fraction
PAM	Potential Aerosol Mass
ppb	Parts-per-billion
ppt	Parts-per-trillion
RH	Relative Humidity
S	Saturation Ratio
S_c	Critical Supersaturation
SS	Supersaturation
SeaSCAPE	Sea Spray Chemistry and Particle Evolution Experiment
SEMS	Scanning Electrical Mobility Spectrometer
SIA	Secondary Inorganic Aerosol
SIO	Scripps Institution of Oceanography

SMA	Secondary Marine Aerosol
SMPS	Scanning Mobility Particle Sizer
SOA	Secondary Organic Aerosol
SOARS	Scripps Ocean Atmosphere Research Simulator
SSA	Sea Spray Aerosol
SSML	Sea Surface Microlayer
VOC	Volatile Organic Compound

LIST OF FIGURES

LIST OF TABLES

ACKNOWLEDGEMENTS

I would like to acknowledge Professor Kim Prather for her support as my advisor and the chair of my committee. This dissertation work would not have been possible without her guidance. Kim never loses sight of the big picture applications of her research. She always challenges her students to push the boundaries of science and make the impossible possible. I would also like to thank Kim for her support of my interest in chemical education. She has encouraged me to pursue opportunities that would further my career goals in teaching and help me develop as an educator. Working with her as a teaching assistant for Atmospheric Chemistry was one of the defining aspects of my graduate school experience. I sincerely thank Prof Prather for all of the guidance and advice she has given me over the past five years.

I would also like to acknowledge my committee members, Professor Vicki Grassian, Professor Judy Kim, Professor Haim Weizman, and Professor Amato Evan for their advice and feedback over the years.

Working with the NSF Center for Aerosol Impacts on Chemistry of the Environment (CAICE) has been an amazing opportunity for collaboration and research. Thank you to all of my CAICE collaborators, especially the SeaSCAPE team. Special thanks to Professor Chris Cappa for his guidance and mentorship. I would also like to acknowledge Liora Mael, Mike Alves, Emily Barnes, Kim Carter, Dan Crocker, Dr. Rich Cochran, Ryan Tumminello, Prof. Dale Stokes (and Odin), Dr. Jeanette McConnell, and Dr. Neal Arakawa.

This dissertation work would not have been possible without the support of the entire Prather Lab. It has been an amazing experience to work with all of you. Thank you to Dr. Jon Sauer, Dr. Chris Lee, Prof. Xiaofei Wang, Dr. Olivia Ryder, Brock Mitts, Dr. Camille Sultana, Dr. Gavin Cornwell, Matt Pendergraft, Mitchell Santander, Alexia Moore, Dr. Louise Kristensen,

Charlotte Dewald (née Beall), Kathryn Moore, Hashim Al-Mashat, Dolan Lucero, Clare Morris, Ke'La Kimble, Lucia Cancelada, Dr. Rebecca Simpson, Dr. Julie Dinasquet, Dr. Daniel Petras, Tyler Price, and Ben Rico. I would also like to acknowledge the undergraduate researchers who worked with me in the lab: Catherine Mullenmeister, Cristina Bahaveolos, Chi-Min Ni, Matt Sprague, Lee Elmont, and Young Jeong. Thank you to Joe Mayer for fabricating whatever was necessary to make our experiments happen. Thank you to Monica Castrejon always going above and beyond.

I would also like to acknowledge the people outside of the lab who supported me throughout graduate school. A million thanks to my boyfriend, Michael Lazear, for putting up with the late nights spent working and for always taking care of me when I was stressed. Thank you to my friends for always brightening my day, especially my climbing partners Felix, Ryan, and Katia, and my adventuring companions, Taylor, Vince, Shawn, Brett, and Maura. Finally, I would like to thank my family for their endless love and support. My parents Lisa and Frank, and my brothers, William and James. I could not have done this without you.

Chapter 2 is, in full, a reprint of material as it appears in *Accounts of Chemical Research.* Reprinted with permission from Mayer, K.J., Sauer, J.S., Dinasquet, J., and Prather, K.A. (2020). CAICE Studies: Insights from a Decade of Ocean–Atmosphere Experiments in the Laboratory, *Acc. Chem. Res.*, 53, 11, 2510-2520. The dissertation author and Dr. Jon Sauer were lead authors of this paper.

Chapter 3 is, in full, a reprint of material as it appears in *ACS Central Science.* Reprinted with permission from Mayer, K.J., Wang, X., Santander, M.V., Mitts, B.A., Sauer, J.S., Sultana, C.M., Cappa, C.D., and Prather, K.A. (2020). Secondary Marine Aerosol Plays a Dominant Role

over Primary Sea Spray Aerosol in Cloud Formation, *ACS Cent. Sci.* 6, 12, 2259-2266. The dissertation author and Dr. Xiaofei Wang were primary investigators and lead authors of this paper.

Chapter 4 is, in full, currently being prepared for submission to *Environmental Science: Processes and Impacts*. Printed with permission from Mayer, K.J., Sauer, J.S., Lee, C., Alves, M.R., Amiri, S., Bahaveolos, C., Barnes, E.B., Crocker, D.R., Dinasquet, J., Garofalo, L.A., Kaluarachchi, C.P., Dang, D., Kilgour, D., Mael, L., Mitts, B.A., Moon, D.R., Moore, A.N., Morris, C.K., Mullenmeister, C., Ni, C.M., Pendergraft, M.A., Petras, D., Simpson, R., Tumminello, P.R., Walker, J.L., DeMott, P.J., Farmer, D.K., Goldstein, A.H., Grassian, V.H., Jaffe, J.S., Francesca Malfatti, F., Martz, T.R., Slade, J.H., Tivanski, A.V., Bertram, T.H., Cappa, C.D., Prather, K.A. (2021). The Sea Spray Chemistry and Particle Evolution Study (SeaSCAPE): Overview and Experimental Methods. The dissertation author, Dr. Jon Sauer, and Dr. Chris Lee were the primary investigators and lead authors of this paper.

Chapter 5 is, in full, currently being prepared for submission to *Proceedings of the National Academy of Sciences*. Printed with permission from Mayer, K.J., Moon, D.R., Kilgour, D.B., Sauer, J.S., Moore, A.N., Barnes, E.B., Lee, C., Mullenmeister, C.A., Bahaveolos, C.J., Ni, C.M., Goldstein, A.H., Bertram, T.H., Cappa, C.D., Prather, K.A., (2021). Atmospheric Aging Drives Variability in Secondary Marine Aerosol Composition and Cloud-Forming Ability. The dissertation author is the primary investigator and lead author of this paper.

VITA

2013-2015	Undergraduate Research Assistant, College of William and Mary
2015	Bachelor of Science, College of William and Mary
2015-2020	Teaching Assistant, University of California San Diego
2015-2021	Research Assistant, University of California San Diego
2021	Doctor of Philosophy, University of California San Diego

PUBLICATIONS

Mayer, K.J.; Wang, X.; Santander, M.V.; Mitts, B.A.; Sauer, J.S.; Sultana, C.M.; Cappa, C.D.; Prather, K.A.; "Secondary Marine Aerosol Production Strongly Influenced by Biological Activity in Seawater," *ACS Central Science*, **2020**, 6(12), 2259-2266.

Mayer, K.J.; Sauer, J.S.; Dinasquet, J.; Prather, K.A.; "CAICE Studies: Insights from a Decade of Ocean-Atmosphere Experiments in the Laboratory," *Acc. Chem. Res.*, **2020**, 53(11), 2510-2520.

Angle, K.; Crocker, D.R.; Simpson, R.M.; **Mayer, K.J**.; Garofalo, L.A.; Moore, A.N.; Mora Garcia, S.L.; Or, V.W.; Srinivasan, S.; Farhan, M.; Sauer, J.S.; Lee, C.; Pothier, M.; Farmer, D.K.; Martz, T.R.; Bertram, T.H.; Cappa, C.D.; Prather, K.A.; Grassian, V.H.; "Acidity Across the Interface: From the Ocean Surface to Sea Spray Aerosol," *Proc. Nat. Acad. Sci.*, **2021**, 118(2).

E. S. Hasenecz, T. Jayarathne, M. A. Pendergraft, M. V Santander, **K. J. Mayer**, J. Sauer, C. Lee, W. S. Gibson, S. M. Kruse, F. Malfatti, K. A. Prather, E. A. Stone, "Marine Bacteria Affect Saccharide Enrichment in Sea Spray Aerosol during a Phytoplankton Bloom," *ACS Earth and Sp. Chem.* **2020**, 4(9), 1638-1649.

Hartley, C.L.; DiRisio, R.J.; Screen, M.E.; **Mayer, K.J**.; McNamara, W.R.; "Iron Polypyridyl Complexes for Photocatalytic Hydrogen Generation," *Inorg. Chem.*, **2016**, 55(17), 8865-8870.

Wise, C.F.; Liu, D.; **Mayer, K.J**.; Crossland, P.M.; Hartley, C.L.; McNamara, W.R.; "A Nickel Complex of a Conjugated Bis-Dithiocarbazate Schiff Base for the Photocatalytic Production of Hydrogen," *Dalton Trans.*, **2015**, 44(32), 14265.

Connor, G.P.; **Mayer, K.J**.; Tribble, C.S.; McNamara, W.R.; "Hydrogen Evolution Catalyzed by an Iron Polypyridyl Complex in Aqueous Solutions," *Inorg. Chem.*, **2014**, 53(11), 5408-5410.

PRESENTATIONS

Undergraduate Research Symposium, College of William and Mary, Williamsburg,VA, (poster presentation),"Hydrogen Evolution Catalyzed by an Iron Polypyridyl Complex in Aqueous Solutions," (2015).

Honors Colloquium, College of William and Mary, Williamsburg, VA (talk), "Electro- and Photocatalytic Generation of Hydrogen by Iron Polypyridyl Complexes," (2015).

UC Chemical Symposium, UCLA Lake Arrowhead Conference Center, Arrowhead, CA (poster presentation), "Biologically Mediated Changes in the Chemistry of Secondary Marine Aerosol," (2018). *Best Analytical Poster Award*.

Student Research Seminar, University of California, San Diego, La Jolla, CA (talk), "The Influence of Biological Activity in Seawater on the Production and Properties Secondary Marine Aerosol" (2018).

AGU Fall Meeting, Washington D.C. (poster presentation), "Influence of Biological Activity in Seawater on the Formation of Secondary Marine Aerosol," (2018).

AGU Fall Meeting, San Francisco, CA (poster presentation), "Production, Composition, and CCN Activity of Secondary Marine Aerosol Observed During SeaSCAPE," (2019).

AWARDS

Graduate Assistance in Areas of National Need (GAANN) Fellow, UCSD, 2017-2018

FIELDS OF STUDY

Major Field of Study: Chemistry (Atmospheric and Analytical Chemistry)

ABSTRACT OF THE DISSERTATION

Secondary Marine Aerosol: A Chemical Link Between Oceans and Clouds

By

Kathryn J. Mayer

Doctor of Philosophy in Chemistry

University of California San Diego, 2021

Professor Kimberly Prather, Chair

Aerosol-cloud interactions are one of the largest sources of uncertainty in our understanding of the Earth's climate system. In order to develop better predictive models and understand how the climate will respond to future changes in atmospheric composition, we must determine the sources and nature of aerosols which serve as cloud condensation nuclei (CCN), thus influencing the properties of clouds. Oceans cover 70% of the Earth's surface and represent a major source of atmospheric aerosols. Sea spray aerosol (SSA) is formed by the action of breaking waves, whereas secondary marine aerosols (SMA) are formed from the oxidation products of gases emitted from the oceans. Biological activity in seawater (i.e. the life, death, and interactions of marine phytoplankton, bacteria, and viruses) can significantly affect the chemical composition of SSA through processing of dissolved organic matter and SMA through the emission of volatile gases. This dissertation investigates the cloud-relevant properties of SSA and

SMA generated using ocean-atmosphere simulators in the laboratory, with a specific emphasis on the influence of biological activity in seawater on the properties of these aerosols. For the first time, SMA was produced from the oxidation of the headspace gases of a phytoplankton bloom grown in natural seawater, enabling measurements of its chemical composition and CCN activity. Overall, these studies show that the formation and properties of SMA are much more sensitive to biological activity in seawater than SSA. In addition, the chemical composition of SMA is highly dependent on the extent of photochemical oxidation, with a distinct shift from organic-rich to sulfate-rich composition in response to increased atmospheric aging. This change in SMA composition leads to a significant change in its hygroscopicity. These results suggest that the properties of SMA evolve temporally in the atmosphere, which has implications for CCN concentrations and cloud properties over the oceans.

Chapter 1 Introduction

Aerosols are solid or liquid particles suspended in the atmosphere. Examples include dust blown from the desert, sea spray from breaking ocean waves, smoke from fires, and smog from urban pollution. These particles range in size over several orders of magnitude, with diameters ranging from 1 nm up to 100 μm. Aerosols can affect climate directly by absorbing or reflecting sunlight (Satheesh and Krishna Moorthy, 2005), and indirectly by influencing the radiative properties of clouds (Lohmann and Feichter, 2005). Cloud condensation nuclei (CCN) are aerosols which provide surfaces for water vapor to condense on, forming cloud droplets (Köhler, 1936). The number of CCN controls both the size and number of droplets in a cloud, which in turn controls its lifetime, albedo (i.e. reflectivity), and precipitation patterns (Albrecht, 1989; Rosenfeld et al., 2014; Twomey, 1974, 1977).

1.1 Cloud Droplet Nucleation

1.1.1 Köhler Theory

Clouds form when air becomes supersaturated with water vapor, often due to adiabatic cooling as air parcels rise through the atmosphere. Supersaturation occurs when the vapor pressure of water is higher than its equilibrium vapor pressure at a given temperature, resulting in a relative humidity (RH) greater than 100%. If a supersaturated air parcel has an RH = 100.4%, we can describe the percent supersaturation (SS) as SS = 0.4%. Without CCN, it would require a supersaturation of several hundred percent for cloud droplets to form from pure water in the atmosphere (Rogers and Yau, 1996). This is due to the high free energy barrier for the phase transition from vapor to liquid. However, typical supersaturations in the atmosphere rarely exceed SS = 2%. Clouds can only form when CCN are present, providing a surface onto which water

vapor can condense and form liquid droplets. The critical supersaturation (S_c) is the minimum saturation ratio at which a CCN will activate to form a droplet.

The ability of an aerosol to serve as a CCN depends on both its size and composition. The effect of particle size on CCN activity is described by the Kelvin equation (Thomson, 1871). Briefly, the Kelvin effect describes the relationship between saturation vapor pressure and surface curvature. Equilibrium vapor pressure is higher over a curved surface than a flat surface, due to lowered intermolecular forces between neighboring water molecules. Surface curvature is inversely related to particle diameter; thus, smaller particles have more highly curved surfaces, whereas large particles have flatter surfaces and will form cloud droplets at a lower supersaturation. The saturation ratio (S) over a droplet is defined as

$$S = \frac{e_s(D)}{e_s^o}$$

Eq 1.1

where $e_s(D)$ is the water vapor pressure over a droplet with diameter D and $e_s°$ denotes the vapor pressure of pure water over a flat surface. The Kelvin equation can be written as

$$S = \exp\left(\frac{4M_w\sigma_{s/a}}{RT\rho_w D}\right)$$

Eq 1.2

where M_w is the molecular weight of water, ρ_w is the density of water, $\sigma_{s/a}$ is the surface tension of the solution/air interface, R is the universal gas constant, and T is temperature.

The effect of aerosol composition on CCN activity is more complex. Hygroscopic aerosols, which are soluble and have an affinity for water, will activate at lower supersaturations than neutral or hydrophobic particles. This effect is described by Raoult's Law, which states that dissolved

solutes lower the equilibrium vapor pressure of a liquid (Raoult, 1887). Combining the Kelvin equation with Raoult's Law yields the Köhler equation (Köhler, 1936), which is often written as:

$$\ln(S) = \frac{4M_w\sigma_{s/a}}{RT\rho_w D} - \frac{6n_s M_w}{\pi\rho_w D^3}$$

Eq 1.3

where n_s is the moles of solute. The minimum supersaturation at which a particle of a given size and composition can be predicted using the Köhler equation. Köhler curves for $(NH_4)_2SO_4$ particles with different diameters are shown in Figure 1.1. However, a major drawback of this equation is that it only considers soluble aerosol components. The behavior of insoluble residues, such as mineral dust and hydrophobic organic compounds, is not well described by classic Köhler theory.

1.1.2 κ-Köhler Equation

The CCN activity of an aerosol can be parameterized by the single hygroscopicity parameter (κ), which is described by the κ-Köhler equation (Petters and Kreidenweis, 2007):

$$S(D) = \frac{D^3 - D_d^3}{D^3 - D_d^3(1-\kappa)} \exp\left(\frac{4\sigma_{s/a}M_w}{RT\rho_w D}\right)$$

Eq 1.4

where D is the droplet diameter, D_d is the dry diameter, $\sigma_{s/a}$ is the surface tension of the surface-air interface, M_w is the molecular weight of water, and ρ_w is the density of water. The hygroscopicity parameter (κ) can be determined experimentally for different aerosol types by measuring both the diameter and critical supersaturation for the particles of interest. Examples of values of κ for selected compounds are shown in Table 1.1. A higher value of κ indicates a higher CCN activity. The hygroscopicity parameter can be used to predict the critical supersaturation for a particle of a given composition and size; similarly, it can be used to calculate the activation

diameter for a particle at a specific supersaturation. For a multicomponent aerosol, the overall value of κ can be calculated by applying the Zdanovskii-Stokes-Robinson (ZSR) assumption (Stokes and Robinson, 1966). This gives the simple mixing rule:

$$\kappa = \sum_{i} \varepsilon_i \kappa_i$$

Eq 1.5

where ε_i is the dry volume fraction of each component. These features have made the κ-Köhler parametrization useful to climate modelers, as it allows for the effect of aerosol composition on CCN to be incorporated into existing models describing aerosol-cloud interactions (Pringle et al., 2010).

1.2 Marine Aerosols

Oceans cover 71% of the Earth's surface and are a major source of both gases and aerosols to the atmosphere. The two major types of marine aerosol are sea spray aerosol (SSA) and secondary marine aerosol (SMA). SSA is produced by breaking waves, while SMA is formed from the gas-to-particle conversion of volatile gases emitted from the ocean (O'Dowd and de Leeuw, 2007). Biological activity in seawater (i.e., marine phytoplankton, bacteria, and viruses) is a major source of both volatile organic compounds (VOCs) and dissolved organic matter (DOM), both of which influence the properties of marine aerosols.

1.2.1 Sea Spray Aerosol

Sea spray aerosols are produced by the action of breaking waves in the ocean, which entrain bubbles of air beneath the water. When these bubbles rise to the surface, they burst and eject SSA into the atmosphere (Lewis and Schwartz, 2004). The rupturing of the bubble cap produces film drops, which contribute primarily to the submicron particles. The subsequent collapse of the

bubble cavity results in jet drop production, which contribute to both sub- and supermicron SSA (Wang et al., 2017). SSA is comprised of both inorganic sea salts (i.e. NaCl) and organic material, the latter of which is enhanced during periods of high biological activity (O'Dowd et al., 2004). Sea spray is the largest source of atmospheric particulate matter by mass, with estimated annual emissions of 1.01×10^{13} kg yr^{-1} (Gong et al., 2002). However, 98% of this mass is from supermicron particles, resulting in high mass concentrations, but relatively low particle number concentrations.

1.2.2 Secondary Marine Aerosol

Secondary marine aerosols (SMA) are formed from the gas-to-particle conversion of VOCs emitted from seawater. The reactions of VOCs with oxidants such as hydroxyl radical (OH) and ozone (O_3) results in the formation of lower volatility products, which condense to form aerosol-phase products. SMA can form new particles via nucleation processes, or it may condense onto existing particles in the marine atmosphere, such as SSA. Significant attention has been paid to the secondary sulfate aerosol formed from dimethyl sulfide (DMS) oxidation, also called non-sea-salt sulfate (nss-SO_4) (Charlson et al., 1987). However, SMA may also be comprised of organic compounds from secondary organic aerosol formation (SOA). Secondary organic species have been found to play a significant role during coastal nucleation events (Vaattovaara et al., 2006). Marine SOA formation has been observed in the Arctic and was found to significantly influence particle growth and CCN concentrations (Croft et al., 2019; Willis et al., 2016). In addition, hygroscopicity measurements of marine aerosols have observed a suppression of water uptake, attributable to an organic component (Fletcher et al., 2007; Modini et al., 2010).

1.2.3 Marine Volatile Organic Compounds

The oceans are a source of a wide variety of VOCs; however, due to its high abundance, dimethyl sulfide (DMS) has been the most extensively studied. Marine emissions of DMS have been linked to the formation non-sea-salt sulfate (nss-SO_4) aerosol and cloud albedo over the oceans (Charlson et al., 1987). Enzymatic cleavage of the multifunctional phytoplankton osmolyte, dimethylsufoniopropionate (DMSP) is the primary source of DMS in the oceans (Kiene et al., 2000). DMS is the largest natural source of sulfur to the atmosphere, with estimated emissions from the ocean of 28.1 (17.6-34.4) Tg S yr^{-1} (Lana et al., 2011). In the atmosphere, DMS is readily oxidized to form SO_2 and methanesulfonic acid (MSA) (Barnes et al., 2006). SO_2 can undergo gas or aqueous-phase reactions to form H_2SO_4, which may participate in particle nucleation and forms aerosol-phase sulfate (Hoffmann et al., 2016). MSA is formed in the gas-phase and condenses onto existing particles, influencing their size distribution and properties (Davis et al., 1998); however, it has also been suggested that MSA may play a role in nucleation (Dawson et al., 2012).

Due to its high abundance and clear link to secondary aerosol formation, the role of DMS in marine cloud formation has been extensively studied. However, the oceans are a source of many other VOCs which have the potential to influence SMA formation (Carpenter et al., 2012). These include well-known SOA precursors such as isoprene and monoterpenes, which are produced by terrestrial plants as well as marine phytoplankton (Dani and Loreto, 2017; Gantt et al., 2009; Kim et al., 2017; Shaw et al., 2010). Biogenic amines have also been implicated in marine secondary aerosol formation (Facchini et al., 2008).

1.2.4 Biological Activity and Aerosols

Oceanic phytoplankton play a critical role in supplying organic material to marine ecosystems and it has been estimated that they contribute 40-50% of the Earth's total

photosynthetic productivity (Field et al., 1998). Marine phytoplankton are the primary source of the estimated 662 Pg C (1 Pg = 10^{15} g) of dissolved organic matter (DOM) contained in the oceans (Hansell et al., 2009). In addition to phytoplankton, heterotrophic bacteria and viruses also play a key role in the turnover of carbon in the oceans (Azam et al., 1983; Cirri and Pohnert, 2019). The growth, death, and interactions of these marine micro-organisms has been shown to affect the properties of marine aerosols (Prather et al., 2013; Wang et al., 2015), as well as influence VOC production (Halsey et al., 2017). However, significant questions remain regarding the influence of seawater biological activity on the climate-relevant properties of marine aerosols and the ultimate effects on cloud properties.

1.3 Aerosols and Clouds

Aerosol-cloud interactions have been identified the largest single source of uncertainty in our understanding of the Earth's climate system (Boucher et al., 2013). A large contribution to this uncertainty is our understanding of natural aerosols and the pre-industrial climate system (Andreae, 2007; Carslaw et al., 2013; Wilcox et al., 2015). Pristine environments, where there is no influence from human pollution, are extremely rare and difficult to study, with only 12% of the Earth's surface identified as unperturbed aerosol sampling locations (Hamilton et al., 2014). Thus, laboratory experiments in which realistic natural aerosols can be studied under controlled conditions can play an important role towards improving our understanding of aerosol-cloud interactions.

On average, approximately 50% of the sky above the oceans is covered by low-lying marine stratus and stratocumulus clouds (Eastman et al., 2011). These types of clouds have a strong cooling effect on the climate, as their albedo (i.e. the fraction of light reflected from surface) is 30-40%, compared to less than 10% for the dark ocean surface (Randell et al., 1984). It has been

estimated that a mere 6% increase in marine cloud cover could offset the warming caused by a doubling of atmospheric CO_2 (Chen et al., 2014). Marine cloud brightening, through the addition of artificial cloud seeds to the marine atmosphere, has been proposed as a method of geoengineering to offset global warming (Zhao et al., 2020). Thus, understanding the natural sources of marine CCN and their interactions with low-lying clouds is crucial for predicting changes in the climate system.

Correlations have been observed between cloud droplet number concentrations and oceanic phytoplankton blooms, which suggests a link between biological activity in seawater and marine CCN (Lana et al., 2012; McCoy et al., 2015; Meskhidze and Nenes, 2006). However, it remains unclear whether this relationship is driven by changes in the production and properties of primary or secondary marine aerosols. Strong seasonal links have been observed between the emission of biogenic DMS and CCN concentrations in the marine boundary layer (Gras and Keywood, 2017; Korhonen et al., 2008; Sanchez et al., 2018). An overview of the interactions between marine biota, aerosols, and clouds is shown in Figure 1.2.

Due to the significant organic enrichment in submicron SSA (Prather et al., 2013; Quinn et al., 2014), it is expected that this would result in a suppression of its CCN activity, as organic material ($\kappa_{org} < 0.2$) is much less hygroscopic than that of salts ($\kappa_{NaCl} = 1.28$). However, this is not observed in measurements of SSA, both in field studies (Bates et al., 2020) and laboratory experiments (Collins et al., 2016). The apparently high CCN activity of primary marine organics in SSA has been attributed to the formation marine hydrogels (Ovadnevaite et al., 2011), but remains an active area of research (Cravigan et al., 2020).

1.4 Methods for Measuring CCN Activity

The CCN activity of aerosols can be measured experimentally using a continuous-flow streamwise thermal-gradient CCN chamber (CCNc) (Roberts and Nenes, 2005). Briefly, this instrument uses a temperature gradient to produce a stable supersaturation and then measures the number of particles which have activated to form droplets using an optical particle counter. The supersaturation in the instrument can be adjusted by changing the temperature gradient and flow rates, allowing for supersaturation range of 0.04% up to 3%. This effectively covers the range of supersaturations typically observed in the atmosphere. The instrument can be deployed for both laboratory and field measurements of CCN, including ship and aircraft measurements (Martin et al., 2011).

The CCNc can be combined with a differential mobility analyzer (DMA) to size select particles of a specific diameter, enabling size-resolved CCN (SR-CCN) measurements (Moore et al., 2010; Petters et al., 2007). In this technique, the aerosol sample flow is split to a condensation particle counter (CPC), which counts the total number of particles. This allows for the calculation of the activated fraction, i.e. the fraction of particles at each supersaturation-diameter pair which activate to form droplets. This technique can be operated in either diameter-scanning mode, in which CCNc supersaturation is fixed and the DMA scans over a range of particle sizes, or it can be run in supersaturation-scanning mode, in which the DMA particle diameter is fixed and the CCNc scans over a range of supersaturations. Both of these variations allow for the calculation of the hygroscopicity parameter. An SR-CCN activation curve for $(NH_4)_2SO_4$ is shown in Figure 1.3. The critical supersaturation is calculated from 50% activation point, which can in turn be used to calculate the single hygroscopicity parameter (κ) using the κ-Köhler equation.

1.5 Laboratory Studies of Marine Aerosols

Laboratory studies play an important role in improving our understanding of the marine atmosphere by supplementing and contextualizing observations from the field. A key advantage of laboratory ocean-atmosphere experiments is that they allow for the isolation of marine aerosols and gases from other sources, such as terrestrial and anthropogenic emissions, which is not always possible during field studies, except in the most remote sampling locations. In addition, laboratory experiments can be designed to probe effects of specific factors on marine aerosol production and composition, including biological perturbations (Hasenecz et al., 2020), seawater temperature (Forestieri et al., 2018), and photochemical reactions (Trueblood et al., 2019a). However, for these laboratory studies to have relevance to the real environment, they must utilize systems which accurately produce SSA and SMA.

1.5.1 Generating Sea Spray Aerosols

Chapter 2 of this dissertation gives a detailed overview of the development of laboratory ocean-atmosphere simulators, as well as key discoveries facilitated by these systems. As described above, SSA is produced by the bursting of entrained bubbles at the air-sea interface. The bubble size distribution of a breaking ocean wave must be replicated in order to generate realistic SSA in the laboratory (Collins et al., 2014). On the largest scale, this can be accomplished through the use of wave channels, which utilize a mechanical paddle to generate waves which break on an artificial beach (Prather et al., 2013; Wang et al., 2015). However, these systems require thousands of liters of seawater to fill and large support teams to facilitate experiments. Marine aerosol reference tanks (MARTs) have been developed for small-scale experimentation (Stokes et al., 2013, 2016). The MART uses a plunging waterfall, which replicates the action of a breaking wave and produces

bubble size distributions which match those observed in the real ocean. These ocean-atmosphere simulators enable measurements of realistic SSA in the laboratory.

1.5.2 Oxidation Flow Reactors

Hydroxyl radical (OH) is the most important reactive species in the troposphere (Seinfeld and Pandis, 2016). Sometimes called "the detergent" of the atmosphere, reactions with OH radical are the primary removal mechanism for a large number of atmospheric trace gases, including CO and CH_4. OH radical is formed in the troposphere from the photodissociation of O_3 via the following reactions:

$$O_3 + h\nu \rightarrow O_2 + O(^1D)$$

$$O(^1D) + H_2O \rightarrow OH + OH$$

The global mean tropospheric concentration of OH is 1.5×10^6 molecules cm^{-3}. However, as OH radical is highly reactive, its atmospheric lifetime is extremely short, approximately 1-2 seconds (Lelieveld et al., 2016). The gas-phase oxidation of VOCs by OH radical is one of the primary processes which leads to the formation of secondary organic aerosol in the atmosphere (Kroll and Seinfeld, 2008).

Oxidation flow reactors (OFRs) have been developed as an alternative to environmental chambers for studies of atmospheric oxidation and aging processes. The potential aerosol mass oxidation flow reactor (PAM-OFR, Aerodyne Inc) is a commercially available OFR that has been extensively studied and characterized (Kang et al., 2007; Li et al., 2015; Peng et al., 2015). The PAM-OFR is a 13.3 L cylindrical reactor which uses low pressure Hg lamps (λ = 185 nm and 254 nm) to produce high concentrations of OH radical, which can simulate aging timescales ranging from hours to weeks, but with a residence time of only 2-5 minutes. The major reactions in the OFR which form OH radical are summarized in Table 1.1.

OFRs can be used in the laboratory to simulate the atmospheric oxidation processes which lead to secondary aerosol formation (Lambe et al., 2011b; Massoli et al., 2010). While they have been used extensively for studies of terrestrial and anthropogenic aerosols, their application to marine systems has been quite limited thus far. However, OFRs have recently been used in the laboratory to simulate secondary marine aerosol formation (Schneider et al., 2019; Trueblood et al., 2019b). They have a notable advantage over environmental chambers in that the short residence time allows for near real-time measurements, whereas a single chamber experiment can take several hours or even days. This allows for measurements on rapidly changing systems, such as phytoplankton blooms. In addition to secondary aerosol measurements, OFRs can also be used to study the heterogeneous oxidation of primary aerosols (Lambe et al., 2011a).

1.6 Dissertation Objectives

This dissertation focuses on the complex interactions between biological activity in the oceans, marine aerosols, and cloud formation. Despite observations from field studies and remote sensing, the mechanisms through which biological activity in seawater affects marine CCN concentrations remain unclear. Until recently, laboratory ocean-atmosphere experiments have focused almost entirely upon freshly emitted SSA. Similarly, decades of research have focused on the role of DMS in secondary sulfate aerosol formation, while the role of other biogenic VOCs in SMA formation are not well-established. However, the implementation of oxidation flow reactors for studies of marine aerosols have enabled new research on both heterogeneously aged SSA and SMA formed from the headspace gases real phytoplankton blooms.

The main science questions which will be addressed by this thesis are presented below:

1. How can ocean-atmosphere simulators be used to conduct studies of primary and secondary marine aerosols under controlled laboratory conditions?
2. What drives the relationship between oceanic phytoplankton blooms and marine clouds? How does biological activity in seawater influence the flux and CCN activity of sea spray aerosol?
3. How does biological activity influence the formation and properties of laboratory-generated secondary marine aerosol during mesocosm experiments?
4. How important are non-sulfur containing (i.e., non-DMS) VOCs for the formation of secondary marine aerosol and its CCN activity? What is the identity and origin of these gases?
5. How do photochemical aging timescales influence the composition and CCN activity of marine aerosols? Do the properties of SSA and SMA evolve over time in the atmosphere?

1.7 Dissertation Synopsis

Chapter 2 of this dissertation gives an overview of recent innovations in the development of ocean-atmosphere simulators, which enable the study of the marine environment under controlled conditions. Laboratory techniques for the generation of realistic primary and secondary marine aerosols are discussed, as well as a brief review of the recent discoveries these systems have enabled. This chapter also presents results regarding the flux and CCN activity of SSA during four mesocosm bloom experiments, which demonstrate the relative insensitivity of primary marine aerosols to seawater biota.

Chapter 3 of this dissertation investigates the influence of biological activity on the production and properties of both SSA and SMA. This study represents the first use of an oxidation flow reactor to study SMA generated from the headspace gases of a phytoplankton bloom grown

in real seawater. It was found that the formation of SMA was quite sensitive to biological activity in seawater, with changes also observed in its CCN activity related to progression of the bloom. In contrast, both the flux and CCN activity of SSA was relatively insensitive to phytoplankton growth. The measurements suggest that relationships between biological activity in seawater and marine clouds may be driven largely by secondary aerosol formation, as opposed to changes in primary SSA.

Chapter 4 of this dissertation provides an overview of the Sea Spray Chemistry and Particle Evolution (SeaSCAPE) experiment, a two-month study conducted in the Scripps Institution of Oceanography wave channel facility which sought to understand the influence of atmospheric aging on marine aerosol production and properties during a phytoplankton bloom cycle. The experimental methods and wave channel characterization process are described, detailing the key steps necessary for facilitating large-scale ocean-atmosphere experiments in the laboratory. In addition, selected results are presented to demonstrate the broad experimental capabilities during the campaign.

Chapter 5 of this dissertation presents results from the SeaSCAPE experiment, focused specifically upon the formation, chemical composition, and CCN activity of secondary marine aerosol. In addition, an analysis of the VOCs present in the bloom headspace is presented to give context to the aerosol-phase observations. The findings indicate an important role for non-sulfur VOCs in SMA formation. In addition, we observe a strong relationship between SMA properties and the degree of photochemical aging, with a tradeoff between the production of secondary organic species at low aging timescales and secondary sulfate production at high aging timescales. These results suggest that the properties of SMA may evolve over time in the atmosphere.

1.8 Acknowledgements

Brock Mitts and Dr. Jon Sauer are acknowledged for assisting with the editing of this chapter.

1.9 Tables

Table 1.1 Values of the hygroscopicity parameter (κ) for selected compounds (Petters and Kreidenweis, 2007).

Compound	κ
NaCl	1.28
H_2SO_4	0.90
Na_2SO_4	0.80
$(NH_4)_2SO_4$	0.61
Succinic acid	0.23
α-pinene SOA	~0.1

Table 1.2 Primary reactions in the PAM-OFR which lead to the formation of OH radical and ozone (O_3). In OFR254 mode, O_3 is injected into the reactor from an external generator and only reactions 1 and 2 occur. In OFR185 mode, O_3 is generated in the reactor by photolysis of molecular oxygen (reactions 4 and 5), which allows for OH production through reactions 1 and 2. Additional OH is formed from the direct photolysis of water vapor (reaction 5).

(1)	$O_3 + h\nu \rightarrow O_2 + O(^1D)$
(2)	$O(^1D) + H_2O \rightarrow 2OH$
(3)	$O_2 + h\nu(185) \rightarrow 2O$
(4)	$O + O_2 \rightarrow O_3$
(5)	$H_2O + h\nu(185) \rightarrow OH$

1.10 Figures

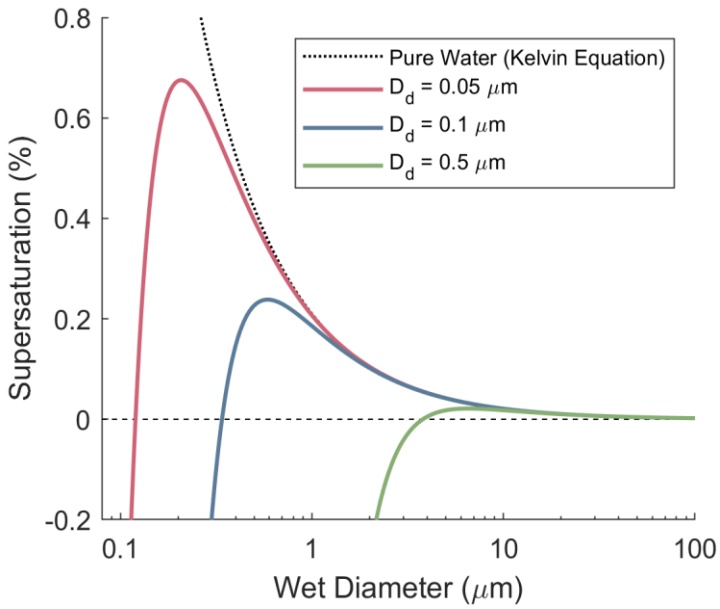

Figure 1.1 Köhler curves for $(NH_4)_2SO_4$ particles with dry diameters of D_d = 0.05, 0.1, and 0.5 μm at 298K. The Kelvin term for pure water is shown for reference.

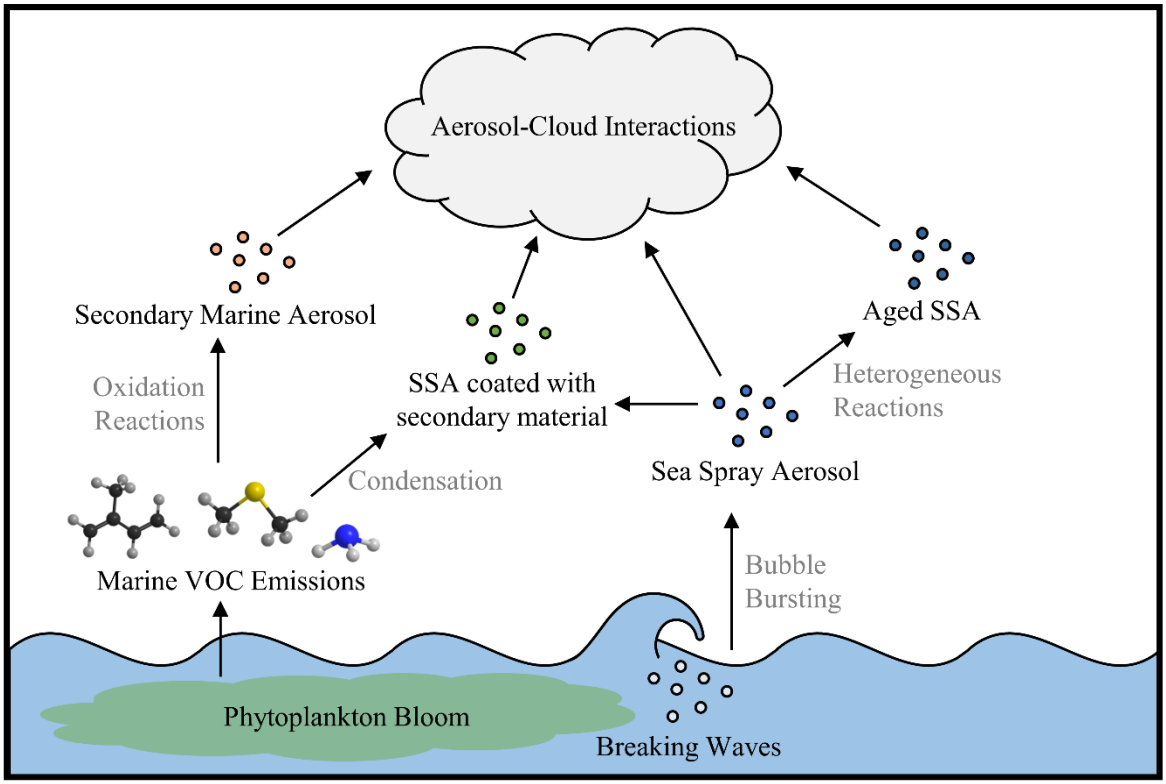

Figure 1.2 Scheme showing the types and transformations of marine aerosols in the atmosphere, and their interactions with clouds.

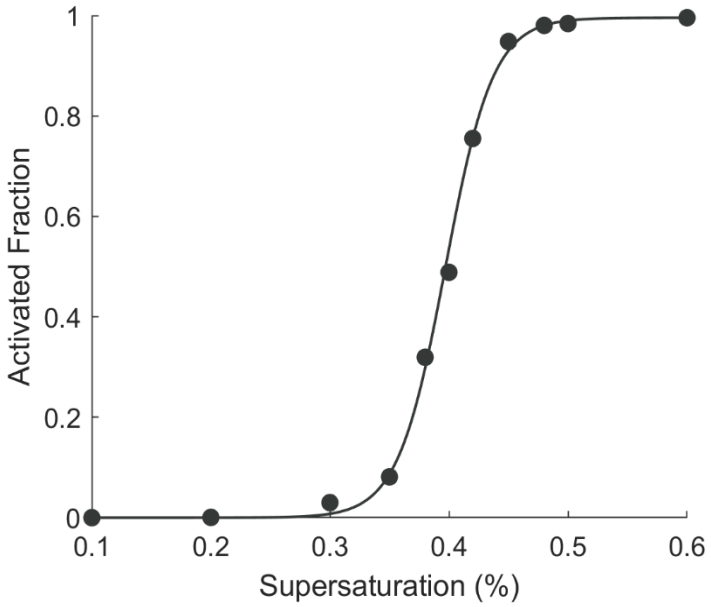

Figure 1.3 SR-CCN activation curve for $(NH_4)_2SO_4$ particles with a dry diameter of D_d = 50 nm. The activated fraction (AF) is ratio of particles which activate to droplets at each supersaturation compared to the total number of particles. An activated fraction of 1 indicates that 100% of particles have activated. The critical supersaturation (S_c) is determined by from the point at which 50% of particles have activated (AF = 0.5).

1.11 References

Albrecht, B. A.: Aerosols, cloud microphysics, and fractional cloudiness, *Science* (80-.)., 245(4923), 1227–1230, doi:10.1126/science.245.4923.1227, 1989.

Andreae, M. O.: Aerosols Before Pollution, *Science* (80-.)., 315(5808), 50-51, doi:10.1126/science.1136529, 2007.

Azam, F., Fenchel, T., Field, J., Gray, J., Meyer-Reil, L. and Thingstad, F.: The Ecological Role of Water-Column Microbes in the Sea, Mar. Ecol. Prog. Ser., 10, 257–263, doi:10.3354/meps010257, 1983.

Barnes, I., Hjorth, J. and Mihalapoulos, N.: Dimethyl sulfide and dimethyl sulfoxide and their oxidation in the atmosphere, *Chem. Rev.*, 106(3), 940–975, doi:10.1021/cr020529+, 2006.

Bates, T. S., Quinn, P. K., Coffman, D. J., Johnson, J. E., Upchurch, L., Saliba, G., Lewis, S., Graff, J., Russell, L. M. and Behrenfeld, M. J.: Variability in Marine Plankton Ecosystems Are Not Observed in Freshly Emitted Sea Spray Aerosol Over the North Atlantic Ocean, *Geophys. Res. Lett.*, 47(1), doi:10.1029/2019GL085938, 2020.

Boucher, O., Randall, D., Artaxo, P., Bretherton, C., Feingold, G., Forster, P., Kerminen, V.-M. V.-M., Kondo, Y., Liao, H., Lohmann, U., Rasch, P., Satheesh, S. K., Sherwood, S., Stevens, B., Zhang, X. Y. and Zhan, X. Y.: Clouds and Aerosols, Clim. Chang. 2013 Phys. Sci. Basis. Contrib. Work. Gr. I to Fifth Assess. Rep. Intergov. Panel Clim. Chang., [Stocker,(Cambridge University Press, Cambridge, United Kingdom and New York, NY, USA), 571–657, doi:10.1017/CBO9781107415324.016, 2013.

Carpenter, L. J., Archer, S. D. and Beale, R.: Ocean-atmosphere trace gas exchange, *Chem. Soc. Rev.*, 41(19), 6473–6506, doi:10.1039/c2cs35121h, 2012.

Carslaw, K. S., Lee, L. a, Reddington, C. L., Pringle, K. J., Rap, a, Forster, P. M., Mann, G. W., Spracklen, D. V, Woodhouse, M. T., Regayre, L. a and Pierce, J. R.: Large contribution of natural aerosols to uncertainty in indirect forcing., *Nature*, 503(7474), 67–71, doi:10.1038/nature12674, 2013.

Charlson, R. J., Lovelock, J. E., Andreae, M. O. and Warren, S. G.: Oceanic phytoplankton, atmospheric sulphur, cloud albedo and climate, *Nature*, 326, 655–661, 1987.

Chen, Y.-C., Christensen, M. W., Stephens, G. L. and Seinfeld, J. H.: Satellite-based estimate of global aerosol–cloud radiative forcing by marine warm clouds, *Nat. Geosci.*, 7(9), 643–646, doi:10.1038/ngeo2214, 2014.

Cirri, E. and Pohnert, G.: Algae−bacteria interactions that balance the planktonic microbiome, *New Phytol.*, 223(1), 100–106, doi:https://doi.org/10.1111/nph.15765, 2019.

Collins, D. B., Zhao, D. F., Ruppel, M. J., Laskina, O., Grandquist, J. R., Modini, R. L., Stokes, M. D., Russell, L. M., Bertram, T. H., Grassian, V. H., Deane, G. B. and Prather, K. A.:

Direct aerosol chemical composition measurements to evaluate the physicochemical differences between controlled sea spray aerosol generation schemes, *Atmos. Meas. Tech.*, 7(11), 3667–3683, doi:10.5194/amt-7-3667-2014, 2014.

Collins, D. B., Bertram, T. H., Sultana, C. M., Lee, C., Axson, J. L. and Prather, K. A.: Phytoplankton blooms weakly influence the cloud forming ability of sea spray aerosol, *Geophys. Res. Lett.*, 9975–9983, doi:10.1002/2016GL069922, 2016.

Cravigan, L. T., Mallet, M. D., Vaattovaara, P., Harvey, M. J., Law, C. S., Modini, R. L., Russell, L. M., Stelcer, E., Cohen, D. D., Olsen, G., Safi, K., Burrell, T. J. and Ristovski, Z.: Sea spray aerosol organic enrichment, water uptake and surface tension effects, *Atmos. Chem. Phys.*, 20(13), 7955–7977, doi:10.5194/acp-20-7955-2020, 2020.

Croft, B., Martin, R. V., Richard Leaitch, W., Burkart, J., Chang, R. Y. W., Collins, D. B., Hayes, P. L., Hodshire, A. L., Huang, L., Kodros, J. K., Moravek, A., Mungall, E. L., Murphy, J. G., Sharma, S., Tremblay, S., Wentworth, G. R., D Willis, M., Abbatt, J. P. D. and Pierce, J. R.: Arctic marine secondary organic aerosol contributes significantly to summertime particle size distributions in the Canadian Arctic Archipelago, *Atmos. Chem. Phys.*, 19(5), 2787–2812, doi:10.5194/acp-19-2787-2019, 2019.

Dani, K. G. S. and Loreto, F.: Trade-Off Between Dimethyl Sulfide and Isoprene Emissions from Marine Phytoplankton, *Trends Plant Sci.*, 22(5), 361–372, doi:10.1016/j.tplants.2017.01.006, 2017.

Davis, D., Chen, G., Kasibhatla, P., Jefferson, A., Tanner, D., Eisele, F., Lenschow, D., Neff, W. and Berresheim, H.: DMS oxidation in the Antarctic marine boundary layer: Comparison of model simulations and held observations of DMS, DMSO, DMSO 2 , H 2 SO 4 (g), MSA(g), and MSA(p), *J. Geophys. Res.*, 103(D1), 1657, doi:10.1029/97JD03452, 1998.

Dawson, M. L., Varner, M. E., Perraud, V., Ezell, M. J., Gerber, R. B. and Finlayson-Pitts, B. J.: Simplified mechanism for new particle formation from methanesulfonic acid, amines, and water via experiments and ab initio calculations, *Proc. Natl. Acad. Sci. U. S. A.*, 109(46), 18719–18724, doi:10.1073/pnas.1211878109, 2012.

Eastman, R., Warren, S. G. and Hahn, C. J.: Variations in Cloud Cover and Cloud Types over the Ocean from Surface Observations, 1954–2008, *J. Clim.*, 24(22), 5914–5934, doi:10.1175/2011JCLI3972.1, 2011.

Facchini, M. C., Decesari, S., Rinaldi, M., Carbone, C., Finessi, E., Mircea, M., Fuzzi, S., Moretti, F., Tagliavini, E., Ceburnis, D. and O'Dowd, C. D.: Important Source of Marine Secondary Organic Aerosol from Biogenic Amines, *Environ. Sci. Technol.*, 42(24), 9116–9121, doi:10.1021/es8018385, 2008.

Field, C. B., Behrenfeld, M. J., Randerson, J. T. and Falkowski, P.: Primary production of the biosphere: Integrating terrestrial and oceanic components, *Science* (80-.)., 281(5374), 237–240, doi:10.1126/science.281.5374.237, 1998.

Fletcher, C. A., Johnson, G. R., Ristovski, Z. D. and Harvey, M.: Hygroscopic and volatile

properties of marine aerosol observed at Cape Grim during the P2P campaign, *Environ. Chem.*, 4(3), 162–171, doi:10.1071/EN07011, 2007.

Forestieri, S. D., Moore, K. A., Martinez Borrero, R., Wang, A., Stokes, M. D. and Cappa, C. D.: Temperature and Composition Dependence of Sea Spray Aerosol Production, *Geophys. Res. Lett.*, 45(14), 7218–7225, doi:10.1029/2018GL078193, 2018.

Gantt, B., Meskhidze, N., and Kamykowski, D.: A new physically-based quantification of marine isoprene and primary organic aerosol emissions, *Atmos. Chem. Phys*., 9, 4915–4927, https://doi.org/10.5194/acp-9-4915-2009, 2009.

Gong, S. L., Barrie, L. A. and Lazare, M.: Canadian Aerosol Module (CAM): A size-segregated simulation of atmospheric aerosol processes for climate and air quality models 2. Global sea-salt aerosol and its budgets, *J. Geophys. Res. Atmos.*, 107(24), 1–14, doi:10.1029/2001JD002004, 2002.

Gras, L. J. and Keywood, M.: Cloud condensation nuclei over the Southern Ocean: Wind dependence and seasonal cycles, *Atmos. Chem. Phys.*, 17(7), 4419–4432, doi:10.5194/acp-17-4419-2017, 2017.

Halsey, K. H., Giovannoni, S. J., Graus, M., Zhao, Y., Landry, Z., Thrash, J. C., Vergin, K. L. and de Gouw, J.: Biological cycling of volatile organic carbon by phytoplankton and bacterioplankton, *Limnol. Oceanogr*., (2013), doi:10.1002/lno.10596, 2017.

Hamilton, D. S., Lee, L. A., Pringle, K. J., Reddington, C. L., Spracklen, D. V and Carslaw, K. S.: Occurrence of pristine aerosol environments on a polluted planet, *Proc. Natl. Acad. Sci.*, 111(52), 18466–18471, doi:10.1073/pnas.1415440111, 2014.

Hansell, D. A., Carlson, C. A., Repeta, D. J. and Schlitzer, R.: Dissolved organic matter in the ocean a controversy stim ulates new insights, Oceanography, 22(SPL.ISS. 4), 202–211, doi:10.5670/oceanog.2009.109, 2009.

Hasenecz, E. S., Jayarathne, T., Pendergraft, M. A., Santander, M. V., Mayer, K. J., Sauer, J., Lee, C., Gibson, W. S., Kruse, S. M., Malfatti, F., Prather, K. A. and Stone, E. A.: Marine Bacteria Affect Saccharide Enrichment in Sea Spray Aerosol during a Phytoplankton Bloom, *ACS Earth Sp. Chem.*, 4(9), 1638–1649, doi:10.1021/acsearthspacechem.0c00167, 2020.

Hoffmann, E. H., Tilgner, A., Schrödner, R., Bräuer, P., Wolke, R. and Herrmann, H.: An advanced modeling study on the impacts and atmospheric implications of multiphase dimethyl sulfide chemistry, *Proc. Natl. Acad. Sci.*, 113(42), 11776–11781, doi:10.1073/pnas.1606320113, 2016.

Kang, E., Root, M. J. and Brune, W. H.: Introducing the concept of Potential Aerosol Mass (PAM), *Atmos. Chem. Phys*., 7, 5727–5744, https://doi.org/10.5194/acp-7-5727-2007, 2007.

Kiene, R. P., Linn, L. J. and Bruton, J. A.: New and important roles for DMSP in marine microbial communities, *J. Sea Res.*, 43(3–4), 209–224, doi:10.1016/S1385-1101(00)00023-X, 2000.

Kim, M. J., Novak, G. A., Zoerb, M. C., Yang, M., Blomquist, B. W., Huebert, B. J., Cappa, C. D. and Bertram, T. H.: Air-Sea exchange of biogenic volatile organic compounds and the impact on aerosol particle size distributions, *Geophys. Res. Lett.*, 44(8), 3887–3896, doi:10.1002/2017GL072975, 2017.

Köhler, H.: The nucleus in and the growth of hygroscopic droplets, *Trans. Faraday Soc.*, 32(0), 1152–1161, doi:10.1039/TF9363201152, 1936.

Korhonen, H., Carslaw, K. S., Spracklen, D. V., Mann, G. W. and Woodhouse, M. T.: Influence of oceanic dimethyl sulfide emissions on cloud condensation nuclei concentrations and seasonality over the remote Southern Hemisphere oceans: A global model study, *J. Geophys. Res. Atmos.*, 113(15), 1–16, doi:10.1029/2007JD009718, 2008.

Kroll, J. H. and Seinfeld, J. H.: Chemistry of secondary organic aerosol: Formation and evolution of low-volatility organics in the atmosphere, *Atmos. Environ.*, 42(16), 3593–3624, doi:10.1016/j.atmosenv.2008.01.003, 2008.

Lambe, A. T., Ahern, A. T., Williams, L. R., Slowik, J. G., Wong, J. P. S., Abbatt, J. P. D., Brune, W. H., Ng, N. L., Wright, J. P., Croasdale, D. R., Worsnop, D. R., Davidovits, P. and Onasch, T. B.: Characterization of aerosol photooxidation flow reactors: Heterogeneous oxidation, secondary organic aerosol formation and cloud condensation nuclei activity measurements, *Atmos. Meas. Tech.*, 4(3), 445–461, doi:10.5194/amt-4-445-2011, 2011a.

Lambe, A. T., Onasch, T. B., Massoli, P., Croasdale, D. R., Wright, J. P., Ahern, A. T., Williams, L. R., Worsnop, D. R., Brune, W. H. and Davidovits, P.: Laboratory studies of the chemical composition and cloud condensation nuclei (CCN) activity of secondary organic aerosol (SOA) and oxidized primary organic aerosol (OPOA), *Atmos. Chem. Phys.*, 11(17), 8913–8928, doi:10.5194/acp-11-8913-2011, 2011b.

Lana, A., Bell, T. G., Simó, R., Vallina, S. M., Ballabrera-Poy, J., Kettle, A. J., Dachs, J., Bopp, L., Saltzman, E. S., Stefels, J., Johnson, J. E. and Liss, P. S.: An updated climatology of surface dimethlysulfide concentrations and emission fluxes in the global ocean, *Global Biogeochem. Cycles*, 25, 1–17, doi:10.1029/2010GB003850, 2011.

Lana, A., Simó, R., Vallina, S. M. and Dachs, J.: Potential for a biogenic influence on cloud microphysics over the ocean: A correlation study with satellite-derived data, *Atmos. Chem. Phys.*, 12(17), 7977–7993, doi:10.5194/acp-12-7977-2012, 2012.

Lelieveld, J., Gromov, S., Pozzer, A. and Taraborrelli, D.: Global tropospheric hydroxyl distribution, budget and reactivity, *Atmos. Chem. Phys.*, 16(19), 12477–12493, doi:10.5194/acp-16-12477-2016, 2016.

Lewis, E. R. and Schwartz, S. E.: Sea Salt Aerosol Production: Mechanisms, Methods, Measurements, and Models--A Critical Review, American Geophysical Union, Washington D.C., 2004.

Li, R., B. Palm, B., M. Ortega, A., Hlywiak, J., Hu, W., Peng, Z., A. Day, D., Knote, C., H. Brune, W., A. de Gouw, J. and L. Jimenez, J.: Modeling the Radical Chemistry in an Oxidation

Flow Reactor: Radical Formation and Recycling, Sensitivities, and the OH Exposure Estimation Equation, *J. Phys. Chem. A.*, 119(19), 4418–4432, doi:10.1021/jp509534k, 2015.

Lohmann, U. and Feichter, J.: Global indirect aerosol effects: a review, *Atmos. Chem. Phys.*, 4(6), 7561–7614, doi:10.5194/acpd-4-7561-2004, 2005.

Martin, M., Chang, R. Y. W., Sierau, B., Sjogren, S., Swietlicki, E., Abbatt, J. P. D., Leck, C. and Lohmann, U.: Cloud condensation nuclei closure study on summer arctic aerosol, *Atmos. Chem. Phys.*, 11(22), 11335–11350, doi:10.5194/acp-11-11335-2011, 2011.

Massoli, P., Lambe, A. T., Ahern, A. T., Williams, L. R., Ehn, M., Mikkilä, J., Canagaratna, M. R., Brune, W. H., Onasch, T. B., Jayne, J. T., Petäjä, T., Kulmala, M., Laaksonen, A., Kolb, C. E., Davidovits, P. and Worsnop, D. R.: Relationship between aerosol oxidation level and hygroscopic properties of laboratory generated secondary organic aerosol (SOA) particles, *Geophys. Res. Lett.*, 37(24), 1–5, doi:10.1029/2010GL045258, 2010.

McCoy, D. T., Burrows, S. M., Wood, R., Grosvenor, D. P., Elliott, S. M., Ma, P.-L., Rasch, P. J. and Hartmann, D. L.: Natural aerosols explain seasonal and spatial patterns of Southern Ocean cloud albedo., *Sci. Adv.*, 1(6), e1500157, doi:10.1126/sciadv.1500157, 2015.

Meskhidze, N. and Nenes, A.: Phytoplankton and Cloudiness in the Southern Ocean, *Science* (80-.)., 314(5804), 1419–1423, 2006.

Modini, R. L., Johnson, G. R., He, C. and Ristovski, Z. D.: Observation of the suppression of water uptake by marine particles, *Atmos. Res.*, 98(2–4), 219–228, doi:10.1016/j.atmosres.2010.03.025, 2010.

Moore, R. H., Nenes, A. and Medina, J.: Scanning Mobility CCN Analysis—A Method for Fast Measurements of Size-Resolved CCN Distributions and Activation Kinetics, *Aerosol Sci. Technol.*, 44(10), 861–871, doi:10.1080/02786826.2010.498715, 2010.

O'Dowd, C. D. and de Leeuw, G.: Marine aerosol production: a review of the current knowledge, *Philos. Trans. R. Soc. A Math. Phys. Eng. Sci.*, 365(1856), 1753–1774, doi:10.1098/rsta.2007.2043, 2007.

O'Dowd, C. D., Facchini, M. C., Cavalli, F., Ceburnis, D., Mircea, M., Decesari, S., Fuzzi, S., Young, J. Y. and Putaud, J. P.: Biogenically driven organic contribution to marine aerosol, *Nature*, 431(7009), 676–680, doi:10.1038/nature02959, 2004.

Ovadnevaite, J., Ceburnis, D., Martucci, G., Bialek, J., Monahan, C., Rinaldi, M., Facchini, M. C., Berresheim, H., Worsnop, D. R. and O'Dowd, C.: Primary marine organic aerosol: A dichotomy of low hygroscopicity and high CCN activity, *Geophys. Res. Lett.*, 38, 1–5, doi:10.1029/2011GL048869, 2011.

Peng, Z., Day, D. A., Stark, H., Li, R., Lee-Taylor, J., Palm, B. B., Brune, W. H. and Jimenez, J. L.: HOx radical chemistry in oxidation flow reactors with low-pressure mercury lamps systematically examined by modeling, *Atmos. Meas. Tech.*, 8(11), 4863–4890,

doi:10.5194/amt-8-4863-2015, 2015.

Petters, M. D. and Kreidenweis, S. M.: A single parameter representation of hygroscopic growth and cloud condensation nucleus activity, *Atmos. Chem. Phys.*, 7, 1961–1971, doi:10.5194/acp-7-1961-2007, 2007.

Petters, M. D., Prenni, A. J., Kreidenweis, S. M. and DeMott, P. J.: On Measuring the Critical Diameter of Cloud Condensation Nuclei Using Mobility Selected Aerosol, *Aerosol Sci. Technol.*, 41(10), 907–913, doi:10.1080/02786820701557214, 2007.

Prather, K. A., Bertram, T. H., Grassian, V. H., Deane, G. B., Stokes, M. D., Demott, P. J., Aluwihare, L. I., Palenik, B. P., Azam, F., Seinfeld, J. H., Moffet, R. C., Molina, M. J., Cappa, C. D., Geiger, F. M., Roberts, G. C., Russell, L. M., Ault, A. P., Baltrusaitis, J., Collins, D. B., Corrigan, C. E., Cuadra-Rodriguez, L. a, Ebben, C. J., Forestieri, S. D., Guasco, T. L., Hersey, S. P., Kim, M. J., Lambert, W. F., Modini, R. L., Mui, W., Pedler, B. E., Ruppel, M. J., Ryder, O. S., Schoepp, N. G., Sullivan, R. C. and Zhao, D.: Bringing the ocean into the laboratory to probe the chemical complexity of sea spray aerosol., *Proc. Natl. Acad. Sci. U. S. A.*, 110(19), 7550–5, doi:10.1073/pnas.1300262110, 2013.

Pringle, K. J., Tost, H., Pozzer, A., Pöschl, U. and Lelieveld, J.: Global distribution of the effective aerosol hygroscopicity parameter for CCN activation, *Atmos. Chem. Phys.*, 10(12), 5241–5255, doi:10.5194/acp-10-5241-2010, 2010.

Quinn, P. K., Bates, T. S., Schulz, K. S., Coffman, D. J., Frossard, A. A., Russell, L. M., Keene, W. C. and Kieber, D. J.: Contribution of sea surface carbon pool to organic matter enrichment in sea spray aerosol, *Nat. Geosci.*, 7(3), 228–232, doi:10.1038/ngeo2092, 2014.

Randell, D. A., Coakley, J. A., Fairall, C. W., Kropfli, R. A. and Lenschow, D. H.: Outlook for research on subtropical marine stratiform clouds., *Bull. - Am. Meteorol. Soc.*, 65(12), 1290–1301, doi:10.1175/1520-0477(1984)0652.0.CO;2, 1984.

Raoult, F.-M.: Loi générale des tensions de vapeur des dissolvants, *CR Hebd. Seances Acad. Sci*, 104, 1430–1433, 1887.

Roberts, G. C. and Nenes, a.: A Continuous-Flow Streamwise Thermal-Gradient CCN Chamber for Atmospheric Measurements, *Aerosol Sci. Technol.*, 39(3), 206–221, doi:10.1080/027868290913988, 2005.

Rogers, R. R. and Yau, M. K.: A short course in cloud physics., 1996.

Rosenfeld, D., Rosenfeld, D., Lohmann, U., Raga, G. B., Dowd, C. D. O., Kulmala, M., Fuzzi, S., Reissell, A. and Andreae, M. O.: Flood or Drought : How Do Aerosols Affect Precipitation ?, *Science* (80-.)., 1309(2008), 1309–1314, doi:10.1126/science.1160606, 2014.

Sanchez, K. J., Chen, C. L., Russell, L. M., Betha, R., Liu, J., Price, D. J., Massoli, P., Ziemba, L. D., Crosbie, E. C., Moore, R. H., Müller, M., Schiller, S. A., Wisthaler, A., Lee, A. K. Y., Quinn, P. K., Bates, T. S., Porter, J., Bell, T. G., Saltzman, E. S., Vaillancourt, R. D. and

Behrenfeld, M. J.: Substantial Seasonal Contribution of Observed Biogenic Sulfate Particles to Cloud Condensation Nuclei, *Sci. Rep.*, 8(1), 1–14, doi:10.1038/s41598-018-21590-9, 2018.

Satheesh, S. K. and Krishna Moorthy, K.: Radiative effects of natural aerosols: A review, *Atmos. Environ.*, 39(11), 2089–2110, doi:https://doi.org/10.1016/j.atmosenv.2004.12.029, 2005.

Schneider, S. R., Collins, D. B., Lim, C. Y., Zhu, L. and Abbatt, J. P. D.: Formation of Secondary Organic Aerosol from the Heterogeneous Oxidation by Ozone of a Phytoplankton Culture, *ACS Earth Sp. Chem.*, 3(10), 2298–2306, doi:10.1021/acsearthspacechem.9b00201, 2019.

Seinfeld, J. H. and Pandis, S. N.: Atmospheric Chemistry and Physics: From Air Pollution to Climate Change, Third Ed., John Wiley & Sons, Inc., Hoboken, New Jersey., 2016.

Shaw, S. L., Gantt, B. and Meskhidze, N.: Production and Emissions of Marine Isoprene and Monoterpenes: A Review, edited by O. Stetzer, *Adv. Meteorol.*, 2010, 408696, doi:10.1155/2010/408696, 2010.

Stokes, M. D., Deane, G. B., Prather, K., Bertram, T. H., Ruppel, M. J., Ryder, O. S., Brady, J. M. and Zhao, D.: A Marine Aerosol Reference Tank system as a breaking wave analogue for the production of foam and sea-spray aerosols, *Atmos. Meas. Tech.*, 6(4), 1085–1094, doi:10.5194/amt-6-1085-2013, 2013.

Stokes, M. D., Deane, G., Collins, D. B., Cappa, C., Bertram, T., Dommer, A., Schill, S., Forestieri, S. and Survilo, M.: A miniature Marine Aerosol Reference Tank (miniMART) as a compact breaking wave analogue, *Atmos. Meas. Tech.*, 9(9), 4257–4267, doi:10.5194/amt-9-4257-2016, 2016.

Stokes, R. H. and Robinson, R. A.: Interactions in Aqueous Nonelectrolyte Solutions. I. Solute-Solvent Equilibria, *J. Phys. Chem.*, 70(7), 2126–2131, doi:10.1021/j100879a010, 1966.

Thomson, W.: LX. On the equilibrium of vapour at a curved surface of liquid, London, Edinburgh, *Dublin Philos. Mag. J. Sci.*, 42(282), 448–452, doi:10.1080/14786447108640606, 1871.

Trueblood, J. V., Alves, M. R., Power, D., Santander, M. V., Cochran, R. E., Prather, K. A. and Grassian, V. H.: Shedding Light on Photosensitized Reactions within Marine-Relevant Organic Thin Films, *ACS Earth Sp. Chem.*, 3(8), 1614–1623, doi:10.1021/acsearthspacechem.9b00066, 2019a.

Trueblood, J. V., Wang, X., Or, V. W., Alves, M. R., Santander, M. V., Prather, K. A. and Grassian, V. H.: The Old and the New: Aging of Sea Spray Aerosol and Formation of Secondary Marine Aerosol through OH Oxidation Reactions, *ACS Earth Sp. Chem.*, 3(10), 2307–2314, doi:10.1021/acsearthspacechem.9b00087, 2019b.

Twomey, S.: Pollution and the planetary albedo, *Atmos. Environ.*, 8(12), 1251–1256, doi:10.1016/0004-6981(74)90004-3, 1974.

Twomey, S.: The influence of pollution on the shortwave albedo of clouds, *J. Atmos. Sci.*, 34(7),

1149–1152, 1977.

Vaattovaara, P., Huttunen, P. E., Yoon, Y. J., Joutsensaari, J., Lehtinen, K. E. J., O'Dowd, C. D., and Laaksonen, A.: The composition of nucleation and Aitken modes particles during coastal nucleation events: evidence for marine secondary organic contribution, *Atmos. Chem. Phys.*, 6, 4601–4616, https://doi.org/10.5194/acp-6-4601-2006, 2006.

Wang, X., Sultana, C. M., Trueblood, J., Hill, T. C. J., Malfatti, F., Lee, C., Laskina, O., Moore, K. A., Beall, C. M., McCluskey, C. S., Cornwell, G. C., Zhou, Y., Cox, J. L., Pendergraft, M. A., Santander, M. V., Bertram, T. H., Cappa, C. D., Azam, F., DeMott, P. J., Grassian, V. H. and Prather, K. A.: Microbial Control of Sea Spray Aerosol Composition: A Tale of Two Blooms, *ACS Cent. Sci*., 1(3), 124–131, doi:10.1021/acscentsci.5b00148, 2015.

Wang, X., Deane, G. B., Moore, K. A., Ryder, O. S., Stokes, M. D., Beall, C. M., Collins, D. B., Santander, M. V., Burrows, S. M., Sultana, C. M. and Prather, K. A.: The role of jet and film drops in controlling the mixing state of submicron sea spray aerosol particles, *Proc. Natl. Acad. Sci. U. S. A.*, 114(27), 6978–6983, doi:10.1073/pnas.1702420114, 2017.

Wilcox, L. J., Highwood, E. J., Booth, B. B. B. and Carslaw, K. S.: Quantifying sources of inter-model diversity in the cloud albedo effect, *Geophys. Res. Lett.*, 42(5), 1568–1575, doi:https://doi.org/10.1002/2015GL063301, 2015.

Willis, M. D., Burkart, J., Thomas, J. L., Köllner, F., Schneider, J., Bozem, H., Hoor, P. M., Aliabadi, A. A., Schulz, H., Herber, A. B., Leaitch, W. R. and Abbatt, J. P. D.: Growth of nucleation mode particles in the summertime Arctic: A case study, *Atmos. Chem. Phys.*, 16(12), 7663–7679, doi:10.5194/acp-16-7663-2016, 2016.

Zhao, M., Cao, L., Duan, L., Bala, G. and Caldeira, K.: Climate more responsive to marine cloud brightening than ocean albedo modification: A model study, *J. Geophys. Res. Atmos.*, doi:10.1029/2020jd033256, 2020.

Chapter 2 CAICE Studies: Insights from a Decade of Ocean-Atmosphere Experiments in the Laboratory

2.1 Conspectus

Ocean-atmosphere interactions control the composition of the atmosphere, hydrological cycle, and temperature of our planet, as well as affect human and ecosystem health. Our understanding of the impact of ocean emissions on atmospheric chemistry and climate is limited relative to terrestrial systems, despite the fact oceans cover the majority (71%) of the Earth. As a result, the impact of marine aerosols on clouds represents one of the largest uncertainties in our understanding of climate, which is limiting our ability to accurately predict the future temperatures of our planet. The emission of gases and particles from the ocean surface constitutes an important chemical link between the ocean and atmosphere, and is mediated by marine biological, physical and chemical processes. It is challenging to isolate the role of biological ocean processes on atmospheric chemistry in the real world, which contains a mixture of terrestrial and anthropogenic emissions. One decade ago, the NSF Center for Aerosol Impacts on Chemistry of the Environment (CAICE) took a unique ocean-in-the-laboratory approach to study the factors controlling the chemical composition of marine aerosols and their effects on clouds and climate. CAICE studies have demonstrated that the complex interplay of phytoplankton, bacteria, and viruses exerts significant control over sea spray aerosol composition and the production of volatile organic compounds. In addition, CAICE experiments have explored the physical production mechanisms and their impact on the properties of marine cloud condensation nuclei and ice nucleating particles, thus shedding light on connections between the oceans and cloud formation. As these ocean-in-the-laboratory experiments become more sophisticated, they allow for further exploration of the complexity of the processes that control atmospheric emissions from the ocean, as well as

incorporating the effects of atmospheric aging and secondary oxidation processes. In the face of unprecedented global climate change, these results provide key insights into how our oceans and atmosphere are responding to human-induced changes to our planet.

This account presents results from a decade of research by chemists in the NSF Center for Aerosol Impacts on Chemistry of the Environment. The mission of CAICE involves taking a multidisciplinary approach to transform the ability to accurately predict the impact of marine aerosols on our environment by bringing the full real-world chemical complexity of the ocean/atmosphere into the laboratory. Towards this end, CAICE has successfully advanced the study of the ocean-atmosphere system under controlled laboratory settings through the stepwise simulation of physical production mechanisms and incorporation of marine microorganisms, building to systems which replicate real-world chemical complexity. This powerful approach has already made substantial progress in advancing our understanding of how ocean biology and physical processes affect the composition of nascent SSA, as well as yielded insights that help explain longstanding discrepancies in field observations in the marine environment. CAICE research is now using laboratory studies to assess how real-world complexity, such as warming temperatures, ocean acidification, wind speed, biology, and anthropogenic perturbations, impacts the evolution of sea spray aerosol properties, as well as shapes the composition of the marine atmosphere.

2.2 Introduction

Marine aerosols constitute an important chemical link between the oceans and the atmosphere. Aerosols affect climate directly by scattering incoming solar radiation and indirectly by affecting cloud properties (Carslaw et al., 2010). Aerosols can serve as cloud condensation

nuclei (CCN), which influences the size and number of droplets in a cloud, thus affecting precipitation and interactions with radiation (Andreae et al., 2005; Rosenfeld et al., 2014). In addition, some aerosols may serve as ice nuclei (IN), facilitating the formation of ice crystals in mixed-phase clouds (Kanji et al., 2017; Wilson et al., 2015). Aerosol-cloud interactions constitute the largest source of uncertainty in our understanding of the Earth's radiative budget (Boucher et al., 2013), with a large contribution from the understanding of natural aerosols (Carslaw et al., 2013).

The climate impacts of marine aerosols are of particular interest, as oceans cover 71% of the Earth's surface. Primary sea spray aerosol (SSA) is generated by bubble-bursting at the ocean surface as a result of breaking waves. Secondary marine aerosol (SMA) is formed from the oxidation of volatile gases emitted from the oceans (O'Dowd and de Leeuw, 2007), which can result in the formation of new particles through nucleation processes (Covert et al., 1992; Vaattovaara et al., 2006). Alternatively, secondary species can condense onto existing particles in the marine atmosphere, such as SSA, influencing their chemical composition and properties (Fitzgerald, 1991). Biological activity in seawater exerts significant control over the chemical composition of SSA (O'Dowd et al., 2004; Wang et al., 2015), as well as the emission of gas-phase precursors which form SMA (Andreae and Raemdonck, 1983; Arnold et al., 2009).

A major challenge in the study of marine aerosols and gases is disentangling the multitude of factors which influence their composition and properties: biological activity in seawater; transport of terrestrial and anthropogenic aerosols and gases to marine regions; heterogeneous and photochemical aging processes; physical parameters such as wind speed, temperature, and relative humidity; and secondary aerosol formation and growth processes. These numerous confounding variables make it challenging to disentangle the individual contributions from each of these

processes, which impedes our ability to model and predict the properties of marine aerosols. Ocean-atmosphere experiments conducted in the laboratory have the significant advantage of allowing for the isolated study of individual processes which control marine aerosol composition, properties, and production flux. Here, we discuss ocean-atmosphere experiments addressing the aforementioned challenges. Through the implementation of technologies designed to produce marine aerosols as naturally as possible, we outline the various directions of new inquiry opened by the ocean-atmosphere experimental approach as well as the successes already achieved (Figure 2.2). Lastly, we introduce the future of ocean-atmosphere experiments through the lens of an under-development facility which seeks to improve upon previous designs and allows for the study of external perturbations on the natural marine environment including high speed winds and cold ocean temperatures.

2.3 Making Waves: Sea Spray Aerosol Generation

Multiple CAICE innovations have advanced our understanding of atmospheric chemistry through ocean-in-the-laboratory approaches. Initial experiments focused on using accurate production methods to generate realistic SSA in controlled laboratory settings. In the past, many studies have used sintered glass filters to produce SSA by forcing air through the filters to produce bubbles, which rise to the surface and burst, producing SSA (Quinn et al., 2015; Sellegri et al., 2006). However, a major drawback of these methods is that they produce a very narrow range of bubble sizes, which skews the resulting SSA size distribution and produces a persistent surface foam (Collins et al., 2014). In order to produce realistic SSA, it is necessary to simulate the action of real breaking ocean waves, which intermittently entrain air beneath the ocean surface via the action of plunging sheets of water, producing a wide range of bubble sizes. To accurately capture

this process in the laboratory, CAICE has pioneered the use of wave channels for laboratory studies of marine aerosols (Prather et al., 2013). Traditionally used for experiments in physical oceanography, these large channels often hold over 10,000 L of seawater and produce waves using computer-controlled reciprocating paddles (Figure 2.3A), which send artificial waves to break on an artificial beach. To facilitate studies of marine aerosols, CAICE researchers transformed an existing wave channel into an ocean-atmosphere simulator by sealing it with lids to create an enclosed headspace along the full length of the channel. Clean, particle-free air is provided to the headspace by a specialized filtration system. These modifications have enabled the study of sea spray aerosol generated by real breaking waves in natural seawater under the cleanest possible conditions, isolated from anthropogenic and terrestrial influences. An advantage of their large size, wave channels allow for many analytical instruments in the same location to sample both seawater properties as well as gases and aerosols in the headspace. These large-scale experiments have discovered numerous processes which govern and contribute to the transfer of molecules from the ocean to the atmosphere (Cochran et al., 2017; Wang et al., 2015).

Despite serving as the "gold standard" for ocean/atmosphere experiments, drawbacks of the use of wave channels are the size and cost, which limit widespread usage. This has been addressed by the development of smaller SSA generation devices which produce realistic bubble and aerosol size distributions without requiring the use of a full-sized wave channel. The Marine Aerosol Reference Tank (MART) is a CAICE-developed 210 L acrylic tank which generates an intermittent plunging sheet of water to produce a bubble plume which replicates the size distribution and has a temporal evolution similar to bubble plumes measured in the ocean and in wave tanks (Figure 2.3B) (Stokes et al., 2013). These bubbles rupture at the water surface, producing SSA closely matching the size distribution produced by breaking waves in wave

channels and the natural environment (Figure 2.3D). The enclosed MART headspace, containing both aerosols and gases, can then be sampled by various offline and online methods at particle concentrations (~500 #/cm^3) needed for most measurement techniques. Replication of the proper SSA size distribution has been a crucial advancement in answering questions such as the impact of changing biology on SSA flux and hygroscopicity (Collins et al., 2016a). Other questions, difficult to study in the field, such as the influence of seawater temperature on SSA production, have also been investigated using the MART (Forestieri et al., 2018). Natural or artificial seawater added to the MART can be biologically stimulated through nutrient and culture additions to grow a representative range of natural marine microorganisms. The versatility of the MART as an accurate SSA production device make it useful not only for investigations of the influences of ocean biology, but the physiochemical properties of aerosols as well (Ault et al., 2013; Lee et al., 2015; Ryder et al., 2015a). The MART has been widely adopted as the *de facto* method for generating realistic SSA size distributions and has been utilized by researchers outside of CAICE for studies on physical production mechanisms (Harb and Foroutan, 2019), health effects (van Acker et al., 2020; Asselman et al., 2019), and ship-based measurements of marine aerosols (Bates et al., 2020).

An undesirable side-effect of the centrifugal pump currently used in the MART is potential physical damage to the marine microorganisms via pump shear, which distorts the biological communities towards the most hardy species. To facilitate smaller scale experiments and preserve fragile microorganisms, a smaller MART which uses a gentler plunging mechanism was developed. The miniMART features a 19 L acrylic tank where a small plunging waterfall is generated through the action of a water wheel (Figure 2.3C) (Stokes et al., 2016). Similarly, bubble plumes and short-lived foams are generated which produce bubble size distributions and sea spray

aerosol closely matching the size distribution found in the natural ocean. Through the miniMART, multiple findings regarding the behavior of surface partitioned organics, marine enzymes, and ice nuclei have been obtained (Hasenecz et al., 2019). The wave channel, MART, and miniMART represent the ability to perform ocean-atmosphere experiments across four orders of magnitude of water volume, giving massive flexibility towards the design of experiments which vary in scale, expense, and complexity. Tradeoffs in constraints involving the air flow, number of SSA produced, ease of cleaning, experimental footprint, transport of water, and other logistical factors must be considered. At the wave channel level, the operational environment and level of effort is similar to that of a field campaign, whereas the miniMART can be easily used to conduct smaller scale experiments by a single investigator in the laboratory.

2.4 Building the Biological Complexity of Ocean-Atmosphere-Simulations:

The initial ocean-atmosphere experiments conducted in CAICE focused on accurately producing SSA in the laboratory, both with regards to size distributions and chemical complexity. This was accomplished initially using a wave channel to generate realistic SSA from natural seawater, and later by the development of the MART and miniMART. Following the development of physical production methods, the next goal of CAICE was to understand how biological activity in the oceans modulates and controls the properties of SSA. To this end, a novel mesocosm experiment was conducted in the wave channel to simulate the biological and chemical complexity of the real ocean (Prather et al., 2013). During this 5-day mesocosm, cultures of marine phytoplankton and bacteria were added to the seawater in the wave channel. The major findings of this study in 2011 were that biogenic organic species have profound impacts on the chemical composition and properties of SSA. However, as the cultures were added to the seawater

sequentially, this experiment did not adequately simulate the full progression of a real oceanic phytoplankton bloom. The next major ocean-atmosphere experiment within CAICE was the Investigation into Marine Particle Chemistry and Transfer Science (IMPACTS) experiment in 2014. During this campaign, a phytoplankton bloom was induced in natural seawater by adding nutrients to the wave channel and measuring the evolution of SSA composition and properties over the full bloom life cycle. A major goal was to replicate the microbial loop—a process which occurs naturally in the oceans wherein marine phytoplankton, bacteria, and viruses interact dynamically over the course of a bloom cycle (Azam et al., 1983).

During IMPACTS, marked differences were observed in SSA properties over two subsequent blooms, including the aerosol composition, organic speciation, and INP production, which has been attributed to differences in the phytoplankton and bacterial dynamics in the system (Wang et al., 2015). The role of enzymes, specifically lipase, produced by marine microorganisms was found to transform the available pool of aqueous organic carbon to a more soluble state. The effects of the microbial transformation of the marine organic carbon were later observed in the composition of aerosols produced through wave breaking. Specifically, the fraction of aliphatic-rich SSA was observed to be enhanced during periods of high phytoplankton productivity and low bacterial activity. This trend was found to be reversed in cases where phytoplankton activity was high with commensurately high bacterial activity. This discovery stimulated further research into the role of lipase as an effector of aerosol composition inside individual droplets, uncovering a new mechanism for the transformation of organic compounds after aerosolization (Malfatti et al., 2019). These results together advance an important narrative that the competition between phytoplankton production and bacterial degradation exert control on the composition of marine

aerosols which contrasts with attempts to predict aerosol composition using chlorophyll-a (chl-a) alone (Quinn et al., 2014; Rinaldi et al., 2013).

Beyond their influence on the array of organic matter, the diversity of marine bacteria and viruses aerosolized from IMPACTS seawater was characterized using state-of-the-art sequencing approaches.(Michaud et al., 2018) This research uncovered new information about specific microorganisms that are preferentially transferred from seawater to aerosols, while also connecting the physiochemical structure of the microorganisms to their efficiency of aerosolization. Aerosolized taxa also included notable species of infectious concern such as *Legionella*, *E. coli*, *Corynebacterium*, and *Mycobacterium*. The implications of taxon-specific aerosolization from marine environments are multifold: where ice nucleation efficiency of different marine organisms can influence cloud formation, and certain taxa may have significant impacts on human health. These findings highlight how biological complexity in the oceans affects marine aerosol composition and atmospheric chemistry.

Further experiments simulating the influence of biological complexity on SSA properties have been conducted using MARTs. The Biological Effects on Air-Sea Transfer (BEAST) experiment investigated the influence of marine bacteria and viruses on SSA composition and organosulfur gas production. Results from BEAST have shed insight on the bacterial turnover of marine saccharides and their transfer to the aerosol phase (S. Hasenecz et al., 2020). In the same experiment, the production of non-dimethyl sulfide organosulfur gases, methanethiol and dimethyl disulfide was found to be significantly enhanced, with flux ratios of (MeSH+DMDS/DMS) which ranged from 0.2-35, significantly higher than those observed in field studies (Sauer et al., 2020). The unexpected production of these reactive gases was connected to both the turnover in bacterial assemblages as well as possible changes in metabolic pathways influencing the transformation of

these dissolved gases. These findings have further reinforced the importance of accounting for the community structure and activity of marine microorganisms.

2.5 Probing the Chemical Complexity of Sea Spray Aerosol

The ability to produce realistic SSA in the laboratory from natural seawater across a wide range of biological conditions, with no contamination from terrestrial gases and aerosols, has greatly expanded our understanding of the chemical complexity of SSA. Studies have investigated the chemical composition of freshly emitted SSA including, morphology and structure, individual particle mixing state, and reactivity with atmospheric trace gases. Early results from wave channel experiments indicated that SSA is an external mixture, made up of four distinct particle types including sea salt, mixed sea salt/organic, organic, and biological particles. In a landmark study on the composition of SSA, the presence of whole bacteria, viruses, phytoplankton, and marine vesicles was discovered using cryo-electron microscopy performed on MART and wave channel generated aerosols (Patterson et al., 2016). The molecular diversity of SSA has also been shown to be sensitive to biological activity and vary over time in response to the dynamics of phytoplankton and heterotrophic bacteria in seawater (Cochran et al., 2017).

Results from laboratory ocean-atmosphere experiments within CAICE have shown that nascent SSA is enriched with organic compounds relative to both bulk seawater and the sea surface microlayer (SSML). For example, saccharides were observed to be enriched in submicron SSA from 14 to 1314-fold relative to seawater (Jayarathne et al., 2016). Analysis of SSA by high resolution mass spectrometry has shown that the molecular composition of nascent SSA is size dependent, and that organic surfactants such as fatty acids are selectively transferred to smaller particles.(Cochran et al., 2016) Further studies have shown that the size-selective transfer of

organic material from seawater to the aerosol phase is largely driven by the mechanics of bubble bursting. Briefly, the bursting of the bubble cap produces film drops, which are enriched with hydrophobic materials which partition to the air-water interface, while jet drops are produced by the collapse of the bubble cavity. These two different SSA production mechanisms result in an externally mixed aerosol population, with two distinct chemical compositions.[1] While it was previously believed that film drops contributed primarily to the submicron aerosol and jet drops contributed to the supermicron mode, CAICE experiments have shown that jet drops can produce up to 43% of submicron SSA (Wang et al., 2017).

The mixing state and chemical complexity of SSA has been shown to have a significant influence over heterogenous reactions with atmospheric trace gases. These findings have significant implications for atmospheric chemistry and climate models, as many currently approximate the properties of SSA as that of pure NaCl. The reactions of SSA with reactive nitrogen species (i.e. N_2O_5, HNO_3) have been of particular interest, given their impact on the global NO_x budget. CAICE laboratory studies of the reaction between individual nascent SSA particles with nitric acid have shown a wide range of behavior, from no reaction to complete reaction, due to both particle type and heterogeneity within individual particles (Ault et al., 2014). The analysis of individual SSA particles using transmission electron microscopy (TEM) has shown that particles undergo ion redistribution after reaction with nitric acid, which indicates particle structure plays an important role in controlling heterogeneous reactivity (Ault et al., 2013).

In addition, studies on the reactive uptake of N_2O_5 by laboratory-generated SSA have also been conducted within CAICE.(Ryder et al., 2015a) These experiments used a MART to generate SSA from both natural ocean water and artificial seawater, which was sequentially doped with molecular mimics of seawater organics, and found that organic films do not impede the reactive

uptake of N_2O_5 at high relative humidity. Studies on the uptake N_2O_5 at the air-sea interface have found that aromatic compounds (i.e. phenol and humic acid) present at an air-liquid interface can suppress the yield of $ClNO_2$ by acting as competitive reactants with chloride (Ryder et al., 2015b). Notably, the usage of low-complexity seawater mimics failed to reproduce the uptake properties observed both in the field and with MART generated aerosols, showing the need for experiments that maintain the high complexity of the marine environment. These results highlight the utility of ocean-atmosphere simulators, which can be used to generate model SSA containing selected compounds in order to simplify and understand the specific variables which contribute to the full complexity of the real environment.

2.6 Climate-Relevant Properties of Marine Aerosols

Aerosol-cloud interactions are the largest source of uncertainty in our understanding of the climate system (Boucher et al., 2013). The oceans have been identified as a major source of ice nucleating particles (INP), however, terrestrial contributions from dust and other sources dominate in regions where there is long-range transport of these aerosols, including over the oceans (McCluskey et al., 2018b, 2018a). Marine INP are now known, partially due to findings by CAICE, to be excellent ice nucleators, however the rarity of marine INPs (about 5 in 10^5 particles at -30˚C) makes understanding their composition very difficult (DeMott et al., 2015) In order to study marine INP, measurements must be conducted in extremely remote sampling locations. By isolating ocean from terrestrial influences in the laboratory, it was possible to definitively identify and measure the properties of INP emitted from the oceans (DeMott et al., 2015; McCluskey et al., 2017). The usage of more representative SSA production techniques like the MART and wave channel have shown that the production method is important to INP release (DeMott et al., 2015)

Further studies on marine INP have focused on developing a molecular-level understanding of the sources of these particles and how they are influenced by the activity of different marine microorganisms such as phytoplankton and bacteria (DeMott et al., 2018; Mccluskey et al., 2018).

Laboratory ocean-atmosphere experiments have lent clarity to the debate over what drives the correlations between cloud droplet number and seawater chlorophyll-a concentrations observed in remote sensing studies (McCoy et al., 2015). It was hypothesized that biological activity in seawater could either affect the CCN activity and production flux of SSA, or it could result in increased SMA formation. Research within CAICE has shown that biological activity in seawater has a weak effect on the CCN activity of freshly emitted SSA, and that the observed changes cannot account for the observed influence on cloud properties (Collins et al., 2016b). Using a miniMART, Forestieri and coworkers observed a strong relationship between SSA production and water temperature for artificial seawater, which is consistent with parameterizations in the literature (Forestieri et al., 2018). However, for natural seawater, they observed seemingly random, irreproducible variability in SSA production, which evolved over the course of several days. This variability was attributed to temporal changes in the water composition, possibly related to organic or biological components of the natural seawater not present in the artificial mimics. While some conflicting data regarding SSA flux has been reported,(Alpert et al., 2015; Christiansen et al., 2019; Forestieri et al., 2018),(Collins et al., 2013) recently Bates and coworkers utilized a MART deployed during a ship-based study in the North Atlantic and concluded that variability in the flux of SSA was not linked to the activity of marine phytoplankton (Bates et al., 2020). In summary, influence of biological activity on SSA flux, and by extension CCN concentrations, remains highly uncertain.

Further experiments within CAICE have shown that the changes in SSA flux and hygroscopicity during a phytoplankton bloom cycle cannot explain the observed correlations between chl-a and cloud properties. During four subsequent phytoplankton bloom cycles, we found a weakly negative correlation between the flux of SSA from a MART (as evidenced by the integrated number concentrations) and the seawater chl-a concentrations, a proxy for biological activity (Figure 2.4a). In addition, the shape of the size distribution remained relatively constant throughout the experiments (Figure 2.6). While some variability is observed in the production of SSA during these experiments, it does not appear to be driven by phytoplankton alone. In addition, no correlation was observed between chl-a and the apparent hygroscopicity parameter, which remained relatively unchanged the course of all four bloom cycles (κ_{app}= 1.02 ± 0.04, Figure 2.4b). In summary, while there appears to be some degree of natural variability in both the flux and hygroscopicity of SSA, ocean-atmosphere experiments using MARTs have conclusively shown that this variability is not directly related to marine phytoplankton concentrations, as indicated by the chl-a concentrations. The relative insensitivity of SSA flux and hygroscopicity to biological activity suggests that the observed correlations between cloud properties and phytoplankton blooms is driven by secondary aerosol formation, either through the formation of new SMA particles or the condensation of secondary species onto existing particles, thus increasing their size and ability to act as CCN.

2.7 Beyond Primary SSA: Marine Gas Emissions and Atmospheric Reactions

CAICE ocean-atmosphere experiments have, in the past, primarily focused on the factors controlling the properties of freshly emitted SSA; however, in the real marine atmosphere, SSA particles are transformed by aging processes, such as photochemistry, oxidation, and reactions

with trace gases. Understanding how the composition and properties of SSA transform over hours, days, or even weeks of atmospheric processing is critical for accurately representing them within climate models. In addition, the oceans are a source of volatile organic compounds (VOCs), which may lead to the formation of secondary marine aerosol. While a great deal of attention has been paid to the formation of sulfate aerosols from dimethyl sulfide oxidation, the role of other reactive trace gases which may contribute to secondary aerosol formation in the marine atmosphere have not been fully explored. Currently, a major research focus within CAICE is determining the biotic and abiotic factors which control the production of marine VOCs, as well as the properties and composition of secondary aerosols formed from their oxidation, and their potential impacts on cloud properties and climate.

Future steps towards replicating the real marine atmosphere in the laboratory have been the incorporation of oxidation and atmospheric aging processes. To accomplish this, Potential Aerosol Mass Oxidative Flow Reactors (PAM-OFRs) have been coupled with both MARTs and the wave channel to generate secondary marine aerosol and simulate the aging of primary SSA. The PAM-OFR system has been described elsewhere (Kang et al., 2007; Lambe et al., 2011). Briefly, the OFR uses UV lamps (λ = 185 nm and 254 nm) to generate high concentrations of OH radical, which react with the sampled air as it flows through the reactor. This results in the formation of new particles, as well as the oxidation of primary aerosols. In contrast to environmental chambers, the short residence time (~100-300 sec) allows for the near real-time measurements of secondary aerosol formation and aged SSA on a dynamic system such as a phytoplankton bloom, which can evolve and change rapidly. Previously, the PAM-OFR has been primarily used to study terrestrial and anthropogenic systems (Palm et al., 2016); however, results from CAICE have shown the utility of this technique for the study of marine systems (Mayer et al., 2020; Trueblood et al.,

2019). The adoption of OFRs for marine aerosol research has pushed the boundaries of ocean-in-the-laboratory experiments and allowed us to further probe the links between biological activity in the ocean and atmospheric chemistry.

As CAICE research has shown the controlling influence of biological activity on marine aerosol formation involves secondary processes, new ways to understand the production of marine gases have become essential. A particular advantage of ocean-atmosphere experiments is the lack of solar flux and oxidants which can break down volatile gases very quickly. For example, during BEAST, the lack of these factors in the MART allowed for effective measurement of methanethiol and dimethyl disulfide; gaseous species which have high absorption and •OH reactive cross sections which keep their steady state concentrations low in the natural environment. Future CAICE ocean-atmosphere experiments will continue to take advantage of this property to better understand the production of labile volatile species far more difficult to observe in the natural environment. Additionally, community structure, stress, solar irradiation, signaling, grazing, nutrient availability, and other factors are relevant and important to the production of gases by microorganisms in the marine environment (Achyuthan et al., 2017; Carpenter et al., 2012). The role of bacteria in the formation of marine alkyl nitrate production was a significant CAICE finding enabled by the usage of ocean-atmosphere analogs (Kim et al., 2015). By eliminating solar flux, this production was narrowed down to the marine organisms present, something not yet demonstrated in field studies. The role of metabolic partitioning along multiple pathways which lead to the production of marine gases, especially organosulfur species, is a central focus of CAICE, as the production of these gases in the marine environment is both highly variable and poorly understood (Kettle et al., 2001). Building a comprehensive list of marine VOCs and their relative fluxes at different biological states is a key CAICE focus which is currently under

investigation. Furthermore, given the vast wealth of biological speciation data obtained during large mesocosm experiments, connecting the production of marine gases to specific biological actors is a new research area within CAICE.

2.8 Outlook

Over the past decade, CAICE studies of isolated ocean-atmosphere interactions have greatly expanded our understanding of marine aerosols and their complex chemical properties. These experiments bridge the gap between field observations and traditional laboratory studies by building up real-world complexity under controlled conditions. New directions in marine aerosol research have been opened by findings using the unique ocean-atmosphere in the laboratory approach, including investigations into enzyme-aerosol activity, formation of unique vesicle macrostructures, heterogenous reactions, and detection of previously under-appreciated reactive biogenic gas phase species (Ault et al., 2013; Kim et al., 2015; Malfatti et al., 2019; Patterson et al., 2016).

The Sea Spray Chemistry and Particle Evolution (SeaSCAPE) campaign was the most recent CAICE study conducted using a wave channel. This campaign focused on simulating atmospheric oxidation processes on both SSA and gases emitted from seawater during a phytoplankton bloom cycle. In addition to the oxidation experiments, comprehensive measurements were made of nascent SSA. Briefly, these measurements include aerosol chemical composition, size distributions, phase and morphology, hygroscopicity, IN activity, and trace gas speciation. The SeaSCAPE campaign will directly measure how rapid atmospheric processing transforms the properties of marine aerosols, enabled by laboratory ocean-atmosphere experiments. While significant progress has been made, critical gaps remain in our ability to fully simulate the marine environment, such as capturing the full temporal scale of oxidation and aging

processes. These challenges must be addressed by modeling and the development of new innovative experimental proxies.

Future ocean-atmosphere experiments in CAICE will take the next step and center around the development of the Scripps Ocean Atmosphere Research Simulator (SOARS), shown in Figure 2.5. Once completed (planned by summer 2021), this first-of-its-kind facility will enable unique multidisciplinary experiments simulating a wide range of biological, physical, and chemical factors which influence the marine atmosphere. As a fully temperature-controlled wind-wave channel, SOARS will provide control of waves, windspeed (up to gale force winds), diurnal light cycling, and both water and air temperature (from polar to tropical conditions). An integrated environmental reaction chamber will allow for the simulation of atmospheric oxidation and aging of particles and gases under both pristine and polluted conditions. The ability to simulate these different physical and chemical processes under controlled conditions in the laboratory will allow for experiments which simulate the full complexity of the real marine environment. Experiments using the SOARS facility will explore the full extent of biological influence on marine aerosol production and properties under past and future climate scenarios. In addition, this facility will allow for studies of how anthropogenic air and water pollution, climate change, and ocean acidification affect ocean biology and the marine atmosphere.

It is critical to develop tools for improving our understanding of the impacts of natural ecosystems as the Earth undergoes unprecedented change. Over the past decade, CAICE has developed unique infrastructure and positioned itself at the forefront in innovating a range of ocean-atmosphere experimental systems and analytical methods to directly unravel the impacts of humans and natural emissions on the marine atmosphere.

2.8.1 Future research challenges and priorities:

- Integrative approach: Use CAICE lab observations to explain field study results
- Understanding how a changing ocean microbiome will lead to changes in atmospheric composition and climate
- Addressing how future changes in ocean temperatures and climate will impact ocean biology emissions and in turn atmospheric composition and climate
- Using CAICE findings to improve air quality and climate model predictions

2.9 Acknowledgements

This material is based upon work supported by the National Science Foundation through the Center for Aerosol Impacts on the Chemistry of the Environment, an NSF Center for Chemical Innovation (CHE-1801971).

Chapter 2 is, in full, a reprint of material as it appears in *Accounts of Chemical Research.* Reprinted with permission from Mayer, K.J., Sauer, J.S., Dinasquet, J., and Prather, K.A. (2020). CAICE Studies: Insights from a Decade of Ocean–Atmosphere Experiments in the Laboratory, *Acc. Chem. Res.*, 53, 11, 2510-2520. The dissertation author and Dr. Jon Sauer were lead authors of this paper.

2.10 Figures

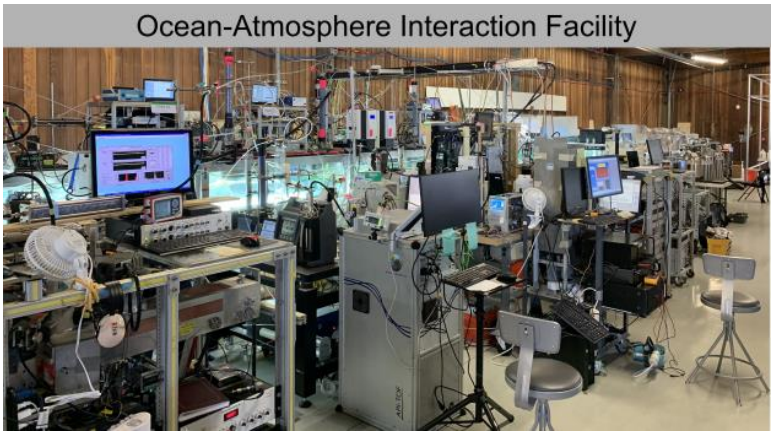

Figure 2.1 Photograph depicting the CAICE Ocean-Atmosphere Interaction Facility

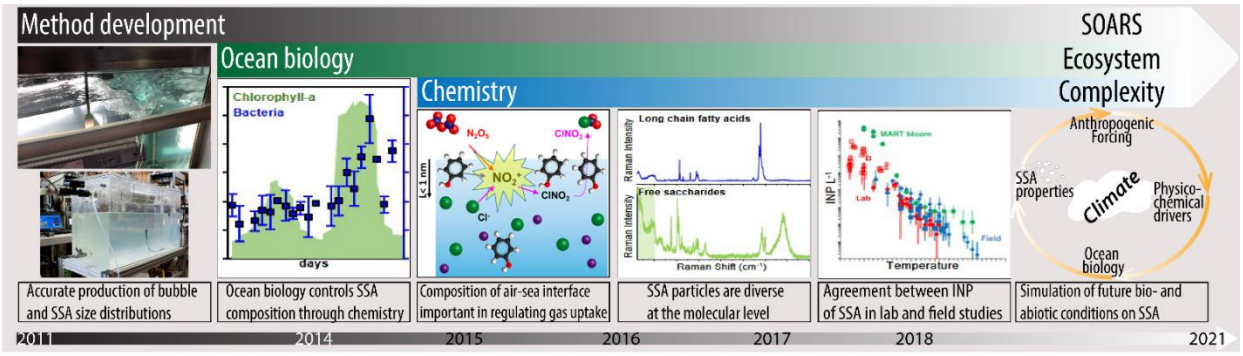

Figure 2.2 Timeline of CAICE achievements, through the innovation and development of a new ocean-atmosphere interaction facility and major experimental results obtained using these systems. CAICE seeks to accurately predict the impact of marine aerosols on our environment by bringing the full real-world chemical complexity to the laboratory. Towards this end, the team has successfully replicated the complexity of the ocean-atmosphere, by accurately reproducing bubble and SSA size distribution and the microbiology of the system. The CAICE in-development SOARS simulator will assess the impact of the full system complexity on atmospheric chemistry. Adapted with permission from Ref. 2 and Ref. 20. Copyright 2015 American Chemical Society. (SSA: Sea spray aerosols, IN: Ice nucleation, SOARS: Scripps Ocean Atmosphere Research Simulator).

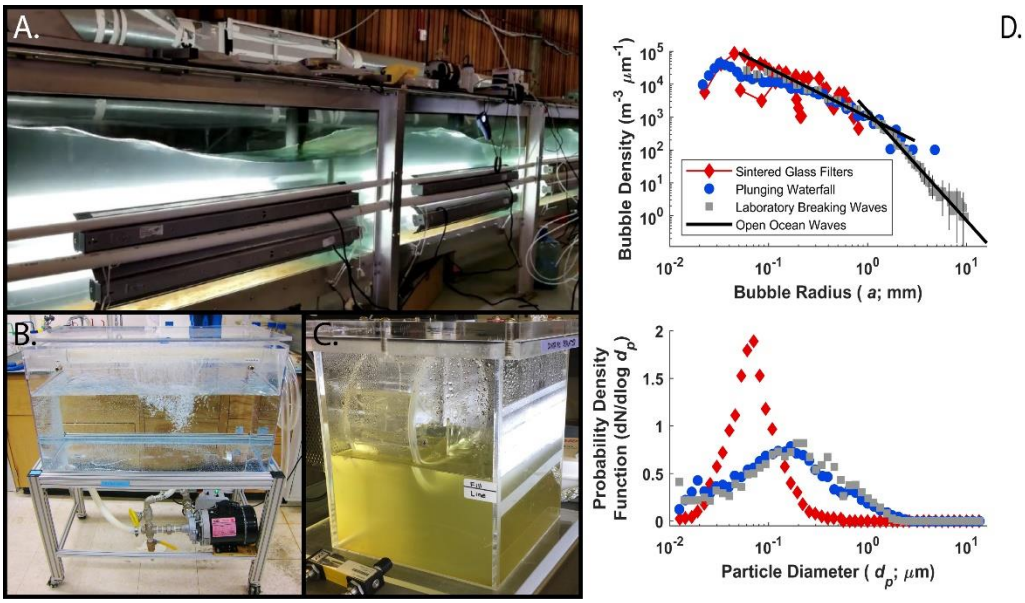

Figure 2.3 CAICE's ocean-atmosphere simulators: 13,000 L wave channel (A), 210 L Marine Aerosol Reference Tank - MART (B) and 19 L miniMART (C). Panel (D) shows the bubble size distributions and normalized aerosol size distributions with laboratory and plunging waterfall in reference to open ocean waves. Reproduced with permission from Quinn et al., 2015. Copyright 2015 American Chemical Society.

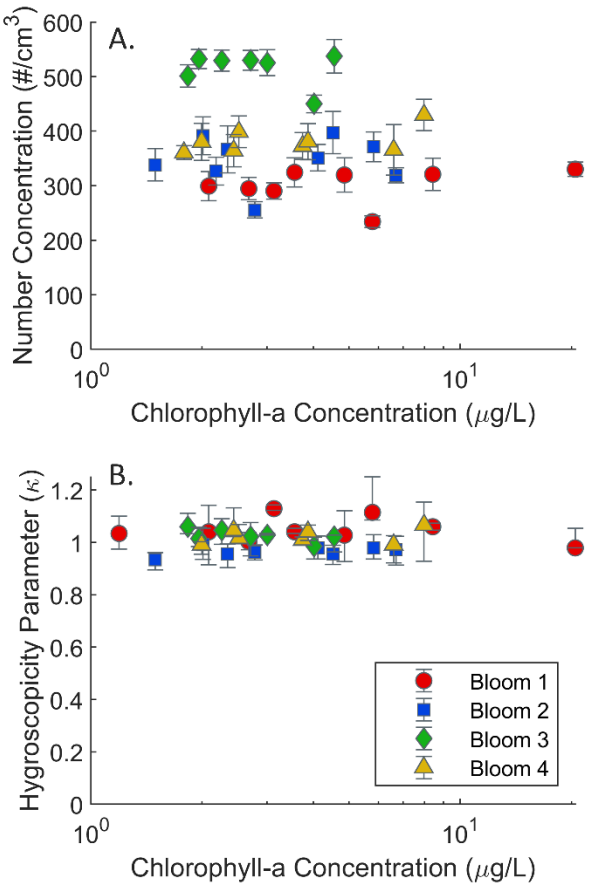

Figure 2.4 a) Number concentrations of MART-generated SSA versus seawater chl-a concentrations during four phytoplankton bloom experiments. As the air flowrate through the MART headspace is kept constant, the number concentration is directly proportional to the flux of SSA. b) Apparent hygroscopicity parameters (k_{app}) of MART-generated SSA during the four phytoplankton bloom experiments. These results show the relative insensitivity of both SSA flux and CCN activity with regards to biological activity in seawater, as represented by the chl-a concentrations. Detailed methods and experimental details are reported in the supplemental, as well as the daily data (Figures 2.7 and 2.9), aerosol size distributions (Figure 2.6) and CCN activation curves (Figure 2.9).

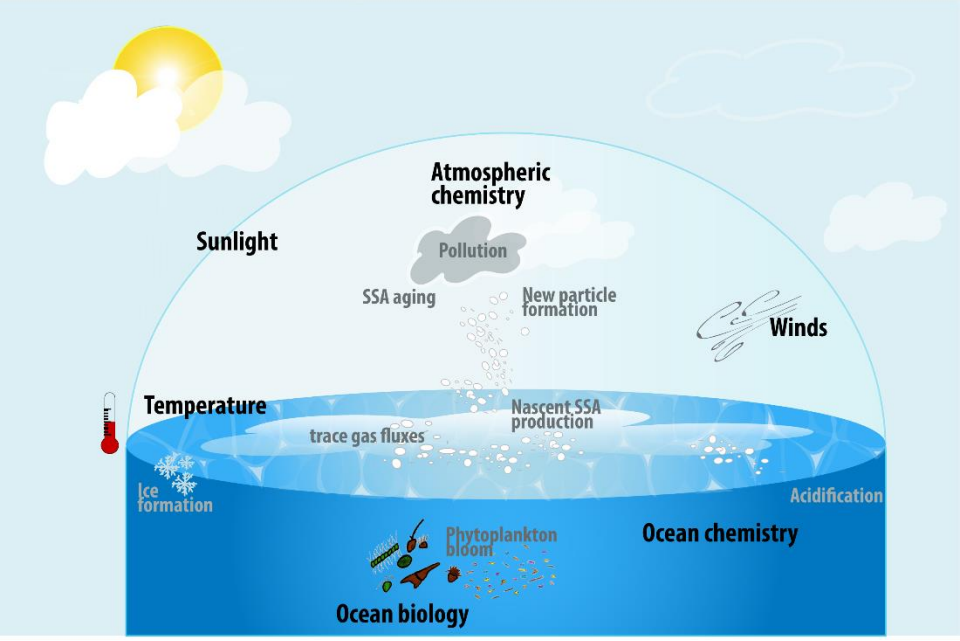

Figure 2.5 Representation of the Scripps Ocean Atmosphere Research Simulator (SOARS) which enables the ability to simulate biotic, as well as physical and non-biotic chemical processes of the marine environment within the laboratory. The facility will provide the possibility to modulate the light intensity (through artificial lights and natural lights), temperature of the atmosphere and water (with the ability to form sea-ice), wind and waves, ocean biology (e.g. inducing a phytoplankton bloom, manipulating bacterial and viral populations), ocean chemistry (e.g. ocean acidification), as well as the atmospheric composition through aging of sea spray aerosol and trace gases in the smog chamber.

2.11 Supporting Information

2.11.1 Description of Mesocosm Experiments

Sea spray aerosol (SSA) was generated using a marine aerosol reference tank (MART) during four mesocosm bloom experiments. The blooms were grown in natural seawater collected from Scripps Pier (32.86 N, -117.25 W) in a 2,400 L outdoor tank, which received natural sunlight. Algae growth media (Guillard's f/2) was added to the seawater to induce a phytoplankton bloom (Guillard and Ryther, 1962). Silicates were added to Blooms 1,2, and 4, but were omitted from Bloom 3 to encourage the growth of non-diatom species. Chlorophyll-A (chl-a) concentrations were measured daily to track the progress of the bloom cycle using a handheld fluorometer (AquaFluor, Turner Designs Inc.). During each day of the bloom experiments, 120 L of seawater was transferred to the MART for SSA measurements. Afterwards, the seawater was returned to the outdoor tank.

Aerosols were dried prior to measurement using a silica diffusion dryer. SSA size distributions were measured using a scanning mobility particle sizer (SMPS 3398, TSI Inc.) and an aerodynamic particle sizer (APS 3321, TSI Inc.). The aerodynamic diameters measured by the APS were converted to physical diameters using an effective density of $\rho = 1.8\ g \cdot cm^{-3}$. The SMPS mobility diameter is assumed to be equivalent to the physical diameter.

Size-resolved CCN measurements were made using a continuous flow stream-wise thermal gradient cloud condensation nuclei counter (CCN-100, Droplet Measurement Technologies, Inc). Briefly, SSA was size selected using a differential mobility analyzer (DMA 3081, TSI Inc) and the flow split evenly between the CCN counter and condensation particle counter (W-CPC 3787, TSI Inc). The size-selected diameter was kept constant at $D_d = 50$ nm and the CCN counter scanned over a range of supersaturations. The apparent hygroscopicity parameter (κ_{app}) was calculated

using the κ-Köhler equation (Petters and Kreidenweis, 2007). The surface tension of the air-surface interface was assumed to be that of pure water, $\sigma_{s/a} = 0.072$ J·m.

2.11.2 Supplementary Tables

Table 2.1 Summary nutrient additions to mesocosm experiments

Experiment	Nutrient Addition	Silicates	Maximum chl-a concentration
Bloom 1	f/20	Yes	20.5 μg/L
Bloom 2	f/100	Yes	6.7 μg/L
Bloom 3	f/100	No	4.6 μg/L
Bloom 4	f/100	Yes	8.0 μg/L

2.11.3 Supplementary Figures

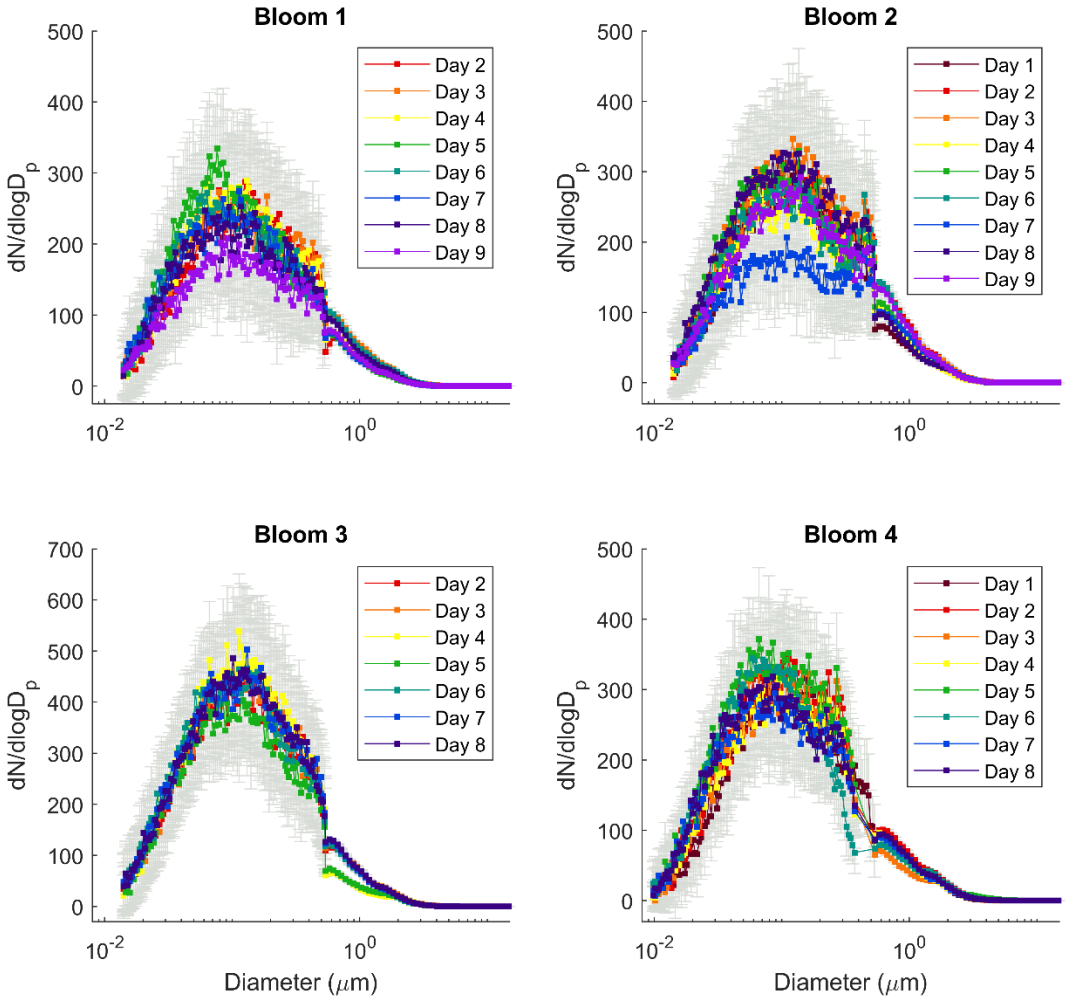

Figure 2.6 Size distributions of MART-generated SSA during each day of the four mesocosm experiments. Error bars are shown in grey and represent ± 1σ.

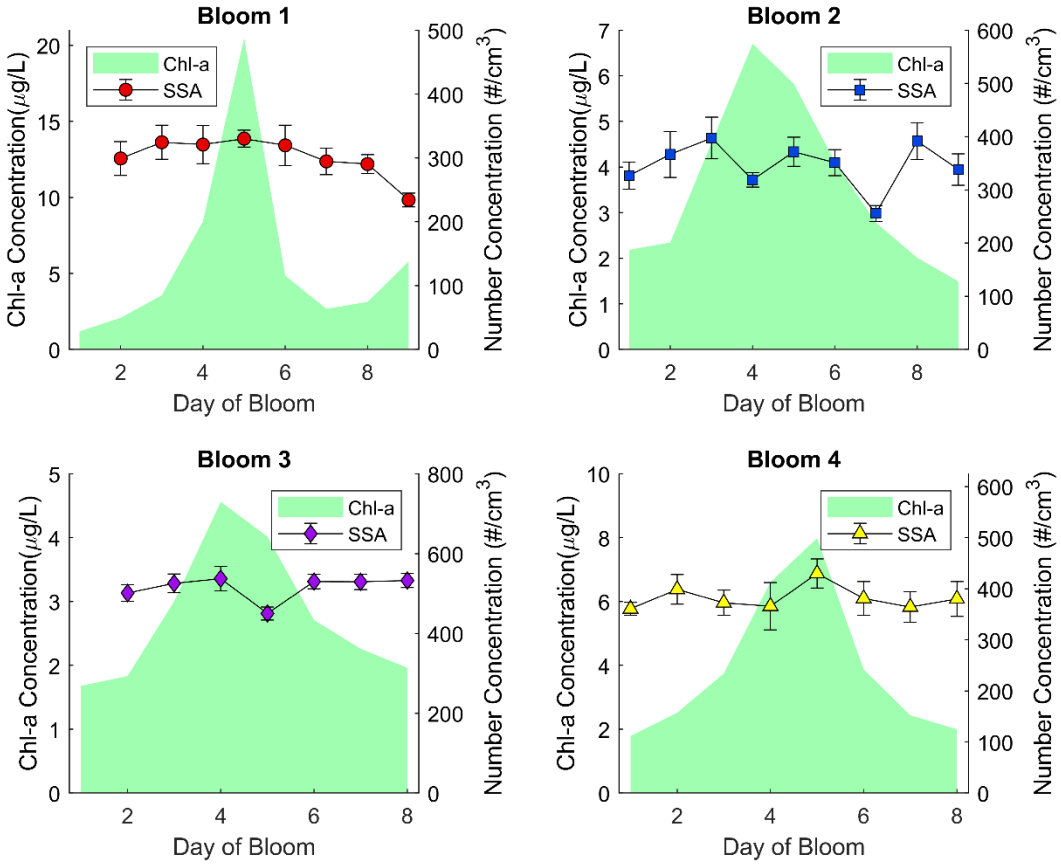

Figure 2.7 Time series of seawater chlorophyll-a concentrations and SSA number concentrations over the course of each bloom experiment. The number concentrations were calculated from the aerosol size distributions shown in Figure 2.6. Error bars represent ± 1σ.

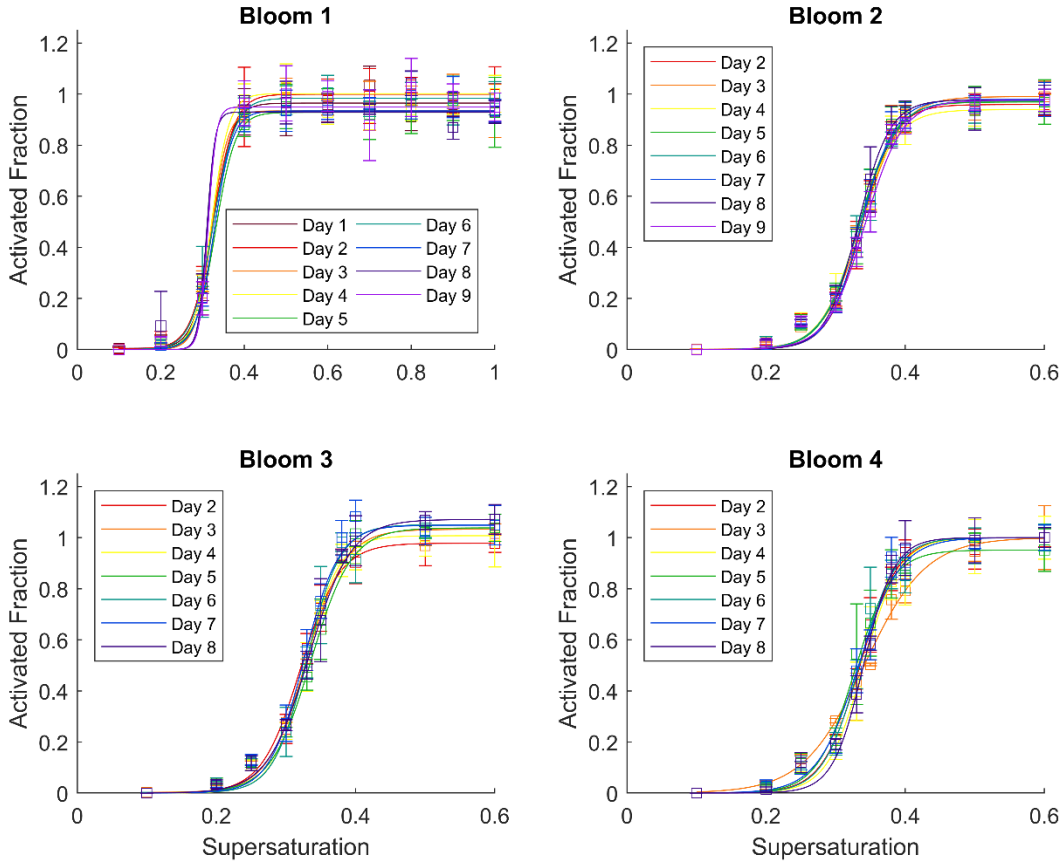

Figure 2.8 Daily SR-CCN activation curves for SSA (D_d = 50 nm) from each day of the bloom experiments. The activated fraction is the ratio of CCN/CN, as measured by the CCN-counter and CPC respectively. Sigmoid curves were fitted to the data and are shown as solid lines. Error bars represent ± 1σ.

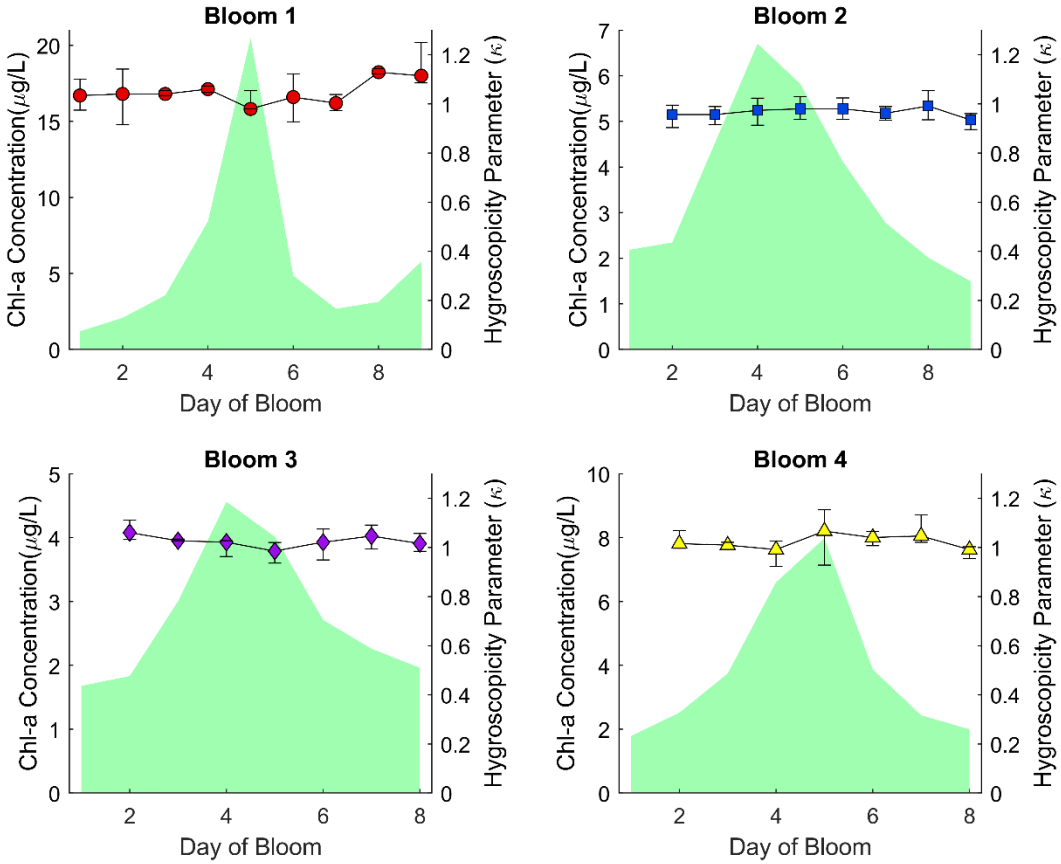

Figure 2.9 Time series of the apparent hygroscopicity parameter (κ_{app}) for SSA (D_d = 50 nm) measured during each day of the bloom. Error bars were calculated from the uncertainty in the measured activated fractions (± 1σ). The observed changes in SSA CCN activity were quite small over the course off all bloom experiments and the mean hygroscopicity parameter was κ_{app}= 1.02 ± 0.04. These results demonstrate the insensitivity of the CCN activity of small SSA to biological activity in seawater, as represented by the chl-a concentrations.

2.12 References

Achyuthan, K. E., Harper, J. C., Manginell, R. P. and Moorman, M. W.: Volatile metabolites emission by in vivo microalgae—an overlooked opportunity?, Metabolites, 7(3), doi:10.3390/metabo7030039, 2017.

van Acker, E., de Rijcke, M., Asselman, J., Beck, I. M., Huysman, S., Vanhaecke, L., de Schamphelaere, K. A. C. and Janssen, C. R.: Aerosolizable marine phycotoxins and human health effects: In vitro support for the biogenics hypothesis, Mar. Drugs, 18(1), doi:10.3390/md18010046, 2020.

Alpert, P. A., Kilthau, W. P., Bothe, D. W., Radway, J. C., Aller, J. Y. and Knopf, D. A.: The influence of marine microbial activities on aerosol production: A laboratory mesocosm study, *J. Geophys. Res. Atmos.*, 120(17), 8841–8860, doi:10.1002/2015JD023469, 2015.

Andreae, M. O. and Raemdonck, H.: Dimethyl Sulfide in the Surface Ocean and the Marine Atmosphere: A Global View, *Science* (80), 221(4612), 744 LP – 747, doi:10.1126/science.221.4612.744, 1983.

Andreae, M. O., Jones, C. D. and Cox, P. M.: Strong present-day aerosol cooling implies a hot future., *Nature*, 435(7046), 1187–90, doi:10.1038/nature03671, 2005.

Arnold, S. R., Spracklen, D. V., Williams, J., Yassaa, N., Sciare, J., Bonsang, B., Gros, V., Peeken, I., Lewis, a. C., Alvain, S. and Moulin, C.: Evaluation of the global oceanic isoprene source and its impacts on marine organic carbon aerosol, *Atmos. Chem. Phys.*, 9(4), 1253–1262, doi:10.5194/acpd-8-16445-2008, 2009.

Asselman, J., Van Acker, E., De Rijcke, M., Tilleman, L., Van Nieuwerburgh, F., Mees, J., De Schamphelaere, K. A. C. and Janssen, C. R.: Marine biogenics in sea spray aerosols interact with the mTOR signaling pathway, *Sci. Rep.*, 9(1), 1–10, doi:10.1038/s41598-018-36866-3, 2019.

Ault, A. P., Guasco, T. L., Ryder, O. S., Baltrusaitis, J., Cuadra-Rodriguez, L. A., Collins, D. B., Ruppel, M. J., Bertram, T. H., Prather, K. A. and Grassian, V. H.: Inside versus outside: Ion redistribution in nitric acid reacted sea spray aerosol particles as determined by single particle analysis, *J. Am. Chem. Soc.*, 135(39), 14528–14531, doi:10.1021/ja407117x, 2013.

Ault, A. P., Guasco, T. L., Baltrusaitis, J., Ryder, O. S., Trueblood, J. V., Collins, D. B., Ruppel, M. J., Cuadra-Rodriguez, L. A., Prather, K. A. and Grassian, V. H.: Heterogeneous reactivity of nitric acid with nascent sea spray aerosol: Large differences observed between and within individual particles, *J. Phys. Chem. Lett.*, 5(15), 2493–2500, doi:10.1021/jz5008802, 2014.

Azam, F., Fenchel, T., Field, J., Gray, J., Meyer-Reil, L. and Thingstad, F.: The Ecological Role of Water-Column Microbes in the Sea, Mar. Ecol. Prog. Ser., 10, 257–263, doi:10.3354/meps010257, 1983.

Bates, T. S., Quinn, P. K., Coffman, D. J., Johnson, J. E., Upchurch, L., Saliba, G., Lewis, S., Graff, J., Russell, L. M. and Behrenfeld, M. J.: Variability in Marine Plankton Ecosystems Are Not Observed in Freshly Emitted Sea Spray Aerosol Over the North Atlantic Ocean, *Geophys. Res. Lett.*, 47(1), doi:10.1029/2019GL085938, 2020.

Boucher, O., Randall, D., Artaxo, P., Bretherton, C., Feingold, G., Forster, P., Kerminen, V.-M. V.-M., Kondo, Y., Liao, H., Lohmann, U., Rasch, P., Satheesh, S. K., Sherwood, S., Stevens, B., Zhang, X. Y. and Zhan, X. Y.: Clouds and Aerosols, Climate Change 2013: The Physical Science Basis. Contribution of Working Group I to Fifth Assessment Report, IPCC., 571–657, doi:10.1017/CBO9781107415324.016, 2013.

Carpenter, L. J., Archer, S. D. and Beale, R.: Ocean-atmosphere trace gas exchange, *Chem. Soc. Rev.*, 41(19), 6473–6506, doi:10.1039/c2cs35121h, 2012.

Carslaw, K. S., Boucher, O., Spracklen, D. V., Mann, G. W., Rae, J. G. L., Woodward, S., and Kulmala, M.: A review of natural aerosol interactions and feedbacks within the Earth system, *Atmos. Chem. Phys.*, 10, 1701–1737, https://doi.org/10.5194/acp-10-1701-2010, 2010.

Carslaw, K. S., Lee, L. a, Reddington, C. L., Pringle, K. J., Rap, a, Forster, P. M., Mann, G. W., Spracklen, D. V, Woodhouse, M. T., Regayre, L. a and Pierce, J. R.: Large contribution of natural aerosols to uncertainty in indirect forcing., *Nature*, 503(7474), 67–71, doi:10.1038/nature12674, 2013.

Christiansen, S., Salter, M. E., Gorokhova, E., Nguyen, Q. T. and Bilde, M.: Sea Spray Aerosol Formation: Laboratory Results on the Role of Air Entrainment, Water Temperature, and Phytoplankton Biomass, *Environ. Sci. Technol.*, doi:10.1021/acs.est.9b04078, 2019.

Cochran, R. E., Laskina, O., Jayarathne, T., Laskin, A., Laskin, J., Lin, P., Sultana, C., Lee, C., Moore, K. A., Cappa, C. D., Bertram, T. H., Prather, K. A., Grassian, V. H. and Stone, E. A.: Analysis of Organic Anionic Surfactants in Fine and Coarse Fractions of Freshly Emitted Sea Spray Aerosol, *Environ. Sci. Technol.*, 50(5), 2477–2486, doi:10.1021/acs.est.5b04053, 2016.

Cochran, R. E., Laskina, O., Trueblood, J. V., Estillore, A. D., Morris, H. S., Jayarathne, T., Sultana, C. M., Lee, C., Lin, P., Laskin, J., Laskin, A., Dowling, J. A., Qin, Z., Cappa, C. D., Bertram, T. H., Tivanski, A. V., Stone, E. A., Prather, K. A. and Grassian, V. H.: Molecular Diversity of Sea Spray Aerosol Particles: Impact of Ocean Biology on Particle Composition and Hygroscopicity, Chem, 2(5), 655–667, doi:10.1016/j.chempr.2017.03.007, 2017.

Collins, D. B., Ault, A. P., Moffet, R. C., Ruppel, M. J., Cuadra-Rodriguez, L. A., Guasco, T. L., Corrigan, C. E., Pedler, B. E., Azam, F., Aluwihare, L. I., Bertram, T. H., Roberts, G. C., Grassian, V. H. and Prather, K. A.: Impact of marine biogeochemistry on the chemical mixing state and cloud forming ability of nascent sea spray aerosol, *J. Geophys. Res. Atmos.*, 118(15), 8553–8565, doi:10.1002/jgrd.50598, 2013.

Collins, D. B., Zhao, D. F., Ruppel, M. J., Laskina, O., Grandquist, J. R., Modini, R. L., Stokes,

M. D., Russell, L. M., Bertram, T. H., Grassian, V. H., Deane, G. B. and Prather, K. A.: Direct aerosol chemical composition measurements to evaluate the physicochemical differences between controlled sea spray aerosol generation schemes, *Atmos. Meas. Tech.*, 7(11), 3667–3683, doi:10.5194/amt-7-3667-2014, 2014.

Collins, D. B., Bertram, T. H., Sultana, C. M., Lee, C., Axson, J. L. and Prather, K. A.: Phytoplankton blooms weakly influence the cloud forming ability of sea spray aerosol, *Geophys. Res. Lett.*, 9975–9983, doi:10.1002/2016GL069922, 2016a.

Collins, D. B., Bertram, T. H., Sultana, C. M., Lee, C., Axson, J. L. and Prather, K. A.: Phytoplankton blooms weakly influence the cloud forming ability of sea spray aerosol, *Geophys. Res. Lett.*, 9975–9983, doi:10.1002/2016GL069922, 2016b.

Covert, D. S., Kapustin, V. N., Quinn, P. K. and Bates, T. S.: New particle formation in the marine boundary layer, *J. Geophys. Res.*, 97(D18), 20581, doi:10.1029/92JD02074, 1992.

DeMott, P. J., Hill, T. C. J., McCluskey, C. S., Prather, K. A., Collins, D. B., Sullivan, R. C., Ruppel, M. J., Mason, R. H., Irish, V. E., Lee, T., Hwang, C. Y., Rhee, T. S., Snider, J. R., McMeeking, G. R., Dhaniyala, S., Lewis, E. R., Wentzell, J. J. B., Abbatt, J., Lee, C., Sultana, C. M., Ault, A. P., Axson, J. L., Diaz Martinez, M., Venero, I., Santos-Figueroa, G., Stokes, M. D., Deane, G. B., Mayol-Bracero, O. L., Grassian, V. H., Bertram, T. H., Bertram, A. K., Moffett, B. F. and Franc, G. D.: Sea spray aerosol as a unique source of ice nucleating particles, *Proc. Natl. Acad. Sci.*, 113(21), 201514034, doi:10.1073/pnas.1514034112, 2015.

DeMott, P. J., Mason, R. H., McCluskey, C. S., Hill, T. C. J., Perkins, R. J., Desyaterik, Y., Bertram, A. K., Trueblood, J. V., Grassian, V. H., Qiu, Y., Molinero, V., Tobo, Y., Sultana, C. M., Lee, C. and Prather, K. A.: Ice nucleation by particles containing long-chain fatty acids of relevance to freezing by sea spray aerosols, *Environ. Sci. Process. Impacts*, 20(11), 1559–1569, doi:10.1039/c8em00386f, 2018.

Fitzgerald, J. W.: Marine aerosols: A review, *Atmos. Environ.* Part A, Gen. Top., 25(3–4), 533–545, doi:10.1016/0960-1686(91)90050-H, 1991.

Forestieri, S. D., Moore, K. A., Martinez Borrero, R., Wang, A., Stokes, M. D. and Cappa, C. D.: Temperature and Composition Dependence of Sea Spray Aerosol Production, *Geophys. Res. Lett.*, 45(14), 7218–7225, doi:10.1029/2018GL078193, 2018.

Guillard, R. R. L. and Ryther, J. H.: Studies of Marine Planktonic Diatoms: I. Cyclotella Nana Hustedt, and Detonula Confervacea (Cleve) Gran, Can. J. Microbiol., 8(2), 229–238, 1962.

Harb, C. and Foroutan, H.: A Systematic Analysis of the Salinity Effect on Air Bubbles Evolution: Laboratory Experiments in a Breaking Wave Analog, J. Geophys. Res. Ocean., 124(11), 7355–7374, doi:10.1029/2019JC015337, 2019.

Hasenecz, E. S., Kaluarachchi, C. P., Lee, H. D., Tivanski, A. V. and Stone, E. A.: Saccharide Transfer to Sea Spray Aerosol Enhanced by Surface Activity, Calcium, and Protein Interactions, *ACS Earth Sp. Chem.*, 3(11), 2539–2548,

doi:10.1021/acsearthspacechem.9b00197, 2019.

Jayarathne, T., Sultana, C. M., Lee, C., Malfatti, F., Cox, J. L., Pendergraft, M. A., Moore, K. A., Azam, F., Tivanski, A. V., Cappa, C. D., Bertram, T. H., Grassian, V. H., Prather, K. A. and Stone, E. A.: Enrichment of Saccharides and Divalent Cations in Sea Spray Aerosol during Two Phytoplankton Blooms, *Environ. Sci. Technol.*, 50(21), 11511–11520, doi:10.1021/acs.est.6b02988, 2016.

Kang, E., Root, M. J. and Brune, W. H.: Introducing the concept of Potential Aerosol Mass (PAM), *Atmos. Chem. Phys*., 7, 5727–5744, https://doi.org/10.5194/acp-7-5727-2007, 2007.

Kanji, Z. A., Ladino, L. A., Wex, H., Boose, Y., Burkert-Kohn, M., Cziczo, D. J. and Krämer, M.: Overview of Ice Nucleating Particles, Meteorol. Monogr., 58, 1.1-1.33, doi:10.1175/AMSMONOGRAPHS-D-16-0006.1, 2017.

Kettle, A. J., Rhee, T. S., Von Hobe, M., Poulton, A., Aiken, J. and Andreae, M. O.: Assessing the flux of different volatile sulfur gases from the ocean to the atmosphere, *J. Geophys. Res. Atmos.*, 106(D11), 12193–12209, doi:10.1029/2000JD900630, 2001.

Kim, M. J., Michaud, J. M., Williams, R., Sherwood, B. P., Pomeroy, R., Azam, F., Burkart, M. and Bertram, T. H.: Bacterial-driven production of nitrates in seawater, *Geophys. Res. Lett.*, 42(2), 1–8, doi:10.1002/2014GL062865.Received, 2015.

Lambe, A. T., Onasch, T. B., Massoli, P., Croasdale, D. R., Wright, J. P., Ahern, A. T., Williams, L. R., Worsnop, D. R., Brune, W. H. and Davidovits, P.: Laboratory studies of the chemical composition and cloud condensation nuclei (CCN) activity of secondary organic aerosol (SOA) and oxidized primary organic aerosol (OPOA), *Atmos. Chem. Phys.*, 11(17), 8913–8928, doi:10.5194/acp-11-8913-2011, 2011.

Lee, C., Sultana, C. M., Collins, D. B., Santander, M. V., Axson, J. L., Malfatti, F., Cornwell, G. C., Grandquist, J. R., Deane, G. B., Stokes, M. D., Azam, F., Grassian, V. H. and Prather, K. A.: Advancing Model Systems for Fundamental Laboratory Studies of Sea Spray Aerosol Using the Microbial Loop, *J. Phys. Chem. A.*, 119(33), 8860–8870, doi:10.1021/acs.jpca.5b03488, 2015.

Malfatti, F., Lee, C., Tinta, T., Pendergraft, M. A., Celussi, M., Zhou, Y., Sultana, C. M., Rotter, A., Axson, J. L., Collins, D. B., Santander, M. V., Anides Morales, A. L., Aluwihare, L. I., Riemer, N., Grassian, V. H., Azam, F. and Prather, K. A.: Detection of Active Microbial Enzymes in Nascent Sea Spray Aerosol: Implications for Atmospheric Chemistry and Climate, *Environ. Sci. Technol. Lett*., 6(3), 171–177, doi:10.1021/acs.estlett.8b00699, 2019.

Mayer, K. J., Wang, X., Santander, M. V, Mitts, B. A., Sauer, J. S., Sultana, C. M., Cappa, C. D. and Prather, K. A.: Secondary Marine Aerosol Production Strongly Influenced by Biological Activity in Seawater, *ACS Cent. Sci*., (1), 2020.

Mccluskey, C. S., Hill, E. T. C. J., Sultana, C. M., Laskina, O., Trueblood, J., Santander, M. V., Beall, C. M., Michaud, J. M., Kreidenweis, S. M., Prather, K. A., Grassian, V. and Demott,

P. J.: A mesocosm double feature: Insights into the chemical makeup of marine ice nucleating particles, *J. Atmos. Sci*., 75(7), 2405–2423, doi:10.1175/JAS-D-17-0155.1, 2018.

McCluskey, C. S., Hill, T. C. J., Malfatti, F., Sultana, C. M., Lee, C., Santander, M. V., Beall, C. M., Moore, K. A., Cornwell, G. C., Collins, D. B., Prather, K. A., Jayarathne, T., Stone, E. A., Azam, F., Kreidenweis, S. M. and DeMott, P. J.: A dynamic link between ice nucleating particles released in nascent sea spray aerosol and oceanic biological activity during two mesocosm experiments, *J. Atmos. Sci.*, 74(1), 151–166, doi:10.1175/JAS-D-16-0087.1, 2017.

McCluskey, C. S., Ovadnevaite, J., Rinaldi, M., Atkinson, J., Belosi, F., Ceburnis, D., Marullo, S., Hill, T. C. J., Lohmann, U., Kanji, Z. A., O'Dowd, C., Kreidenweis, S. M. and DeMott, P. J.: Marine and Terrestrial Organic Ice-Nucleating Particles in Pristine Marine to Continentally Influenced Northeast Atlantic Air Masses, *J. Geophys. Res. Atmos.*, 123(11), 6196–6212, doi:10.1029/2017JD028033, 2018a.

McCluskey, C. S., Hill, T. C. J., Humphries, R. S., Rauker, A. M., Moreau, S., Strutton, P. G., Chambers, S. D., Williams, A. G., McRobert, I., Ward, J., Keywood, M. D., Harnwell, J., Ponsonby, W., Loh, Z. M., Krummel, P. B., Protat, A., Kreidenweis, S. M. and DeMott, P. J.: Observations of Ice Nucleating Particles Over Southern Ocean Waters, *Geophys. Res. Lett.*, 45(21), 11,989-11,997, doi:10.1029/2018GL079981, 2018b.

McCoy, D. T., Burrows, S. M., Wood, R., Grosvenor, D. P., Elliott, S. M., Ma, P.-L., Rasch, P. J. and Hartmann, D. L.: Natural aerosols explain seasonal and spatial patterns of Southern Ocean cloud albedo., *Sci. Adv.*, 1(6), e1500157, doi:10.1126/sciadv.1500157, 2015.

Michaud, J. M., Thompson, L. R., Kaul, D., Espinoza, J. L., Richter, R. A., Xu, Z. Z., Lee, C., Pham, K. M., Beall, C. M., Malfatti, F., Azam, F., Knight, R., Burkart, M. D., Dupont, C. L. and Prather, K. A.: Taxon-specific aerosolization of bacteria and viruses in an experimental ocean-atmosphere mesocosm, *Nat. Commun.*, 9(1), doi:10.1038/s41467-018-04409-z, 2018.

O'Dowd, C. D. and de Leeuw, G.: Marine aerosol production: a review of the current knowledge, *Philos. Trans. R. Soc. A Math. Phys. Eng. Sci.*, 365(1856), 1753–1774, doi:10.1098/rsta.2007.2043, 2007.

O'Dowd, C. D., Facchini, M. C., Cavalli, F., Ceburnis, D., Mircea, M., Decesari, S., Fuzzi, S., Young, J. Y. and Putaud, J. P.: Biogenically driven organic contribution to marine aerosol, *Nature*, 431(7009), 676–680, doi:10.1038/nature02959, 2004.

Palm, B. B., Campuzano-Jost, P., Ortega, A. M., Day, D. A., Kaser, L., Jud, W., Karl, T., Hansel, A., Hunter, J. F., Cross, E. S., Kroll, J. H., Peng, Z., Brune, W. H. and Jimenez, J. L.: In situ secondary organic aerosol formation from ambient pine forest air using an oxidation flow reactor, *Atmos. Chem. Phys.*, 16(5), 2943–2970, doi:10.5194/acp-16-2943-2016, 2016.

Patterson, J. P., Collins, D. B., Michaud, J. M., Axson, J. L., Sultana, C. M., Moser, T., Dommer,

A. C., Conner, J., Grassian, V. H., Stokes, M. D., Deane, G. B., Evans, J. E., Burkart, M. D., Prather, K. A. and Gianneschi, N. C.: Sea spray aerosol structure and composition using cryogenic transmission electron microscopy, *ACS Cent. Sci.*, 2(1), 40–47, doi:10.1021/acscentsci.5b00344, 2016.

Petters, M. D. and Kreidenweis, S. M.: A single parameter representation of hygroscopic growth and cloud condensation nucleus activity, *Atmos. Chem. Phys.*, 7, 1961–1971, doi:10.5194/acp-7-1961-2007, 2007.

Prather, K. a, Bertram, T. H., Grassian, V. H., Deane, G. B., Stokes, M. D., Demott, P. J., Aluwihare, L. I., Palenik, B. P., Azam, F., Seinfeld, J. H., Moffet, R. C., Molina, M. J., Cappa, C. D., Geiger, F. M., Roberts, G. C., Russell, L. M., Ault, A. P., Baltrusaitis, J., Collins, D. B., Corrigan, C. E., Cuadra-Rodriguez, L. a, Ebben, C. J., Forestieri, S. D., Guasco, T. L., Hersey, S. P., Kim, M. J., Lambert, W. F., Modini, R. L., Mui, W., Pedler, B. E., Ruppel, M. J., Ryder, O. S., Schoepp, N. G., Sullivan, R. C. and Zhao, D.: Bringing the ocean into the laboratory to probe the chemical complexity of sea spray aerosol., *Proc. Natl. Acad. Sci. U. S. A.*, 110(19), 7550–5, doi:10.1073/pnas.1300262110, 2013.

Quinn, P. K., Bates, T. S., Schulz, K. S., Coffman, D. J., Frossard, A. A., Russell, L. M., Keene, W. C. and Kieber, D. J.: Contribution of sea surface carbon pool to organic matter enrichment in sea spray aerosol, *Nat. Geosci.*, 7(3), 228–232, doi:10.1038/ngeo2092, 2014.

Quinn, P. K., Collins, D. B., Grassian, V. H., Prather, K. A. and Bates, T. S.: Chemistry and Related Properties of Freshly Emitted Sea Spray Aerosol, *Chem. Rev.*, 115(10), 4383–4399, doi:10.1021/cr500713g, 2015.

Rinaldi, M., Fuzzi, S., Decesari, S., Marullo, S., Santoleri, R., Provenzale, A., Von Hardenberg, J., Ceburnis, D., Vaishya, A., O'Dowd, C. D. and Facchini, M. C.: Is chlorophyll-a the best surrogate for organic matter enrichment in submicron primary marine aerosol?, *J. Geophys. Res. Atmos.*, 118(10), 4964–4973, doi:10.1002/jgrd.50417, 2013.

Rosenfeld, D., Sherwood, S., Wood, R. and Donner, L.: Climate Effects of Aerosol-Cloud Interactions, *Science* (80-.)., 343(January), 379–380, doi:10.1126/science.1247490, 2014.

Ryder, O. S., Campbell, N. R., Morris, H., Forestieri, S., Ruppel, M. J., Cappa, C., Tivanski, A., Prather, K. and Bertram, T. H.: Role of Organic Coatings in Regulating N2O5 Reactive Uptake to Sea Spray Aerosol, *J. Phys. Chem. A.*, 119(48), 11683–11692, doi:10.1021/acs.jpca.5b08892, 2015a.

Ryder, O. S., Campbell, N. R., Shaloski, M., Al-Mashat, H., Nathanson, G. M. and Bertram, T. H.: Role of Organics in Regulating ClNO2 Production at the Air-Sea Interface, *J. Phys. Chem. A.*, 119(31), 8519–8526, doi:10.1021/jp5129673, 2015b.

S. Hasenecz, E., Jayarathne, T., A. Pendergraft, M., V. Santander, M., J. Mayer, K., Sauer, J., Lee, C., S. Gibson, W., M. Kruse, S., Malfatti, F., A. Prather, K. and A. Stone, E.: Marine Bacteria Affect Saccharide Enrichment in Sea Spray Aerosol during a Phytoplankton Bloom, *ACS Earth Sp. Chem.*, 4(9), 1638–1649, doi:10.1021/acsearthspacechem.0c00167, 2020.

Sauer, J. S., Minich, J. J., Dinasquet, J., Malfatti, F., Mayer, K. J., Santander, M. V, Pendergraft, M., Mitts, B. A., Lee, C., Wang, X., Rico, B., Knight, R., Bertram, T. H. and Prather, K. A.: Production of Dimethyl Sulfide , Methanethiol , and Dimethyl Disulfide During Controlled Phytoplankton - Bacterial Mesocosm Experiments, *J. Geophys. Res. Biogeoscience*, Submitted, 2020.

Sellegri, K., O'Dowd, C. D., Yoon, Y. J., Jennings, S. G. and de Leeuw, G.: Surfactants and submicron sea spray generation, *J. Geophys. Res. Atmos.*, 111(22), 1–12, doi:10.1029/2005JD006658, 2006.

Stokes, M. D., Deane, G. B., Prather, K., Bertram, T. H., Ruppel, M. J., Ryder, O. S., Brady, J. M. and Zhao, D.: A Marine Aerosol Reference Tank system as a breaking wave analogue for the production of foam and sea-spray aerosols, *Atmos. Meas. Tech.*, 6(4), 1085–1094, doi:10.5194/amt-6-1085-2013, 2013.

Stokes, M. D., Deane, G., Collins, D. B., Cappa, C., Bertram, T., Dommer, A., Schill, S., Forestieri, S. and Survilo, M.: A miniature Marine Aerosol Reference Tank (miniMART) as a compact breaking wave analogue, *Atmos. Meas. Tech.*, 9(9), 4257–4267, doi:10.5194/amt-9-4257-2016, 2016.

Trueblood, J. V., Wang, X., Or, V. W., Alves, M. R., Santander, M. V., Prather, K. A. and Grassian, V. H.: The Old and the New: Aging of Sea Spray Aerosol and Formation of Secondary Marine Aerosol through OH Oxidation Reactions, *ACS Earth Sp. Chem.*, 3(10), 2307–2314, doi:10.1021/acsearthspacechem.9b00087, 2019.

Vaattovaara, P., Huttunen, P. E., Yoon, Y. J., Joutsensaari, J., Lehtinen, K. E. J., O'Dowd, C. D., and Laaksonen, A.: The composition of nucleation and Aitken modes particles during coastal nucleation events: evidence for marine secondary organic contribution, *Atmos. Chem. Phys.*, 6, 4601–4616, https://doi.org/10.5194/acp-6-4601-2006, 2006.

Wang, X., Sultana, C. M., Trueblood, J., Hill, T. C. J., Malfatti, F., Lee, C., Laskina, O., Moore, K. A., Beall, C. M., McCluskey, C. S., Cornwell, G. C., Zhou, Y., Cox, J. L., Pendergraft, M. A., Santander, M. V., Bertram, T. H., Cappa, C. D., Azam, F., DeMott, P. J., Grassian, V. H. and Prather, K. A.: Microbial Control of Sea Spray Aerosol Composition: A Tale of Two Blooms, *ACS Cent. Sci*., 1(3), 124–131, doi:10.1021/acscentsci.5b00148, 2015.

Wang, X., Deane, G. B., Moore, K. A., Ryder, O. S., Stokes, M. D., Beall, C. M., Collins, D. B., Santander, M. V., Burrows, S. M., Sultana, C. M. and Prather, K. A.: The role of jet and film drops in controlling the mixing state of submicron sea spray aerosol particles, *Proc. Natl. Acad. Sci. U. S. A.*, 114(27), 6978–6983, doi:10.1073/pnas.1702420114, 2017.

Wilson, T. W., Ladino, L. A., Alpert, P. A., Breckels, M. N., Brooks, I. M., Browse, J., Burrows, S. M., Carslaw, K. S., Huffman, J. A., Judd, C., Kilthau, W. P., Mason, R. H., McFiggans, G., Miller, L. A., Nájera, J. J., Polishchuk, E., Rae, S., Schiller, C. L., Si, M., Temprado, J. V., Whale, T. F., Wong, J. P. S., Wurl, O., Yakobi-Hancock, J. D., Abbatt, J. P. D., Aller, J. Y., Bertram, A. K., Knopf, D. A. and Murray, B. J.: A marine biogenic source of atmospheric ice-nucleating particles, *Nature*, 525(7568), 234–238.

Chapter 3 Secondary Marine Aerosol Plays a Dominant Role over Primary Sea Spray Aerosol in Cloud Formation

3.1 Abstract

Marine aerosols play a critical role in impacting our climate by seeding clouds over the oceans. Despite decades of research, key questions remain regarding how ocean biological activity changes the composition and cloud-forming ability of marine aerosols. This uncertainty largely stems from an inability to independently determine the cloud-forming potential of primary versus secondary marine aerosols in complex marine environments. Here, we present results from a unique 6-day mesocosm experiment where we isolated and studied the cloud forming potential of primary and secondary marine aerosols over the course of a phytoplankton bloom. The results from this controlled laboratory approach can finally explain the long-observed changes in the hygroscopic properties of marine aerosols observed in previous field studies. We find that secondary marine aerosols, comprised of sulfate, ammonium, and organic species, correlate with phytoplankton biomass (i.e. chlorophyll-a concentrations), whereas primary sea spray aerosol does not. Importantly, the measured CCN activity ($\kappa_{app} = 0.59 \pm 0.04$) of the resulting secondary marine aerosol matches the values observed in previous field studies, suggesting secondary marine aerosols play the dominant role in affecting marine cloud properties. Given these findings, future studies must address the physical, chemical, and biological factors controlling the emissions of volatile organic compounds that form secondary marine aerosol, with the goal of improving model predictions of ocean biology on atmospheric chemistry, clouds, and climate.

3.2 Introduction

Aerosol-cloud interactions have been identified as the single largest source of uncertainty in estimating changes in the Earth's radiative budget (Boucher et al., 2013; Carslaw et al., 2013). The concentrations of particles that serve as cloud condensation nuclei (CCN) impact both the number and size of cloud droplets, which in turn affect precipitation and albedo (Lohmann and Feichter, 2005; Rosenfeld et al., 2014; Twomey, 1974). Oceans cover nearly three quarters of the Earth's surface and represent an important source of atmospheric aerosols. Marine aerosols can dominate in remote regions, especially over the Southern Ocean where continental influences are low (Murphy et al., 1998).

The two major types of marine aerosol are primary sea spray aerosol (SSA) and secondary marine aerosol (SMA). SSA are directly introduced into the atmosphere by breaking waves. In contrast, SMA are produced via gas-to-particle conversion of the oxidation products of gas phase species emitted from the ocean, including dimethyl sulfide (DMS) and other biogenic volatile organic compounds (VOCs) (Fitzgerald, 1991; O'Dowd and de Leeuw, 2007). These lower volatility oxidation products (i.e. secondary species) can either condense onto pre-existing particles or form new particles via nucleation (Kroll and Seinfeld, 2008). A major focus has been placed on the oxidation of DMS which leads to production of SO_2, among other species, which is further oxidized to form particulate sulfate. To distinguish from the natural seawater sulfur species in SSA, sulfate from the secondary oxidation of DMS and other sulfur-containing gases has traditionally been referred to as non-sea-salt sulfate (nss-SO_4^-). Many studies have shown that secondary organic species can be internally mixed with nss-SO_4^- and represent a significant fraction of submicron marine aerosol mass (Asmi et al., 2010; Facchini et al., 2008; O'Dowd et al., 2004; Virkkula et al., 2006).

Marine aerosols strongly influence cloud properties over oceans. A recent climate modelling study suggested that natural aerosols resulting from biological activity in the ocean account for over half of the spatiotemporal variability in cloud droplet number concentrations over the Southern Ocean (McCoy et al., 2015). However, the specific mechanisms by which biological activity in seawater affects the composition and size of marine aerosols, and hence their ability to form clouds, remain highly uncertain. Several hypotheses have been proposed. Biological activity in seawater can: (1) affect SSA size and production fluxes; (2) change the chemical composition of nascent SSA and thus its CCN activity and (3) produce volatile gases that are released into the atmosphere and undergo chemical reactions, leading to the formation of SMA that can serve as an additional source of CCN.

Over the past several decades, many studies have attempted to determine which of these mechanisms is occurring in the marine environment under different conditions. Alpert et al. reported that seawater chemistry can significantly alter primary SSA production flux during a mesocosm bloom (Alpert et al., 2015). Forestieri et al. also observed that the amount of SSA produced from isolated natural seawater varies over time, most likely driven by changes in biology (Forestieri et al., 2018). However, neither study reports the chlorophyll-a (chl-a) concentrations in seawater, which is useful for understanding the relative amount of biological activity. Chl-a is produced by marine phytoplankton and its concentrations are widely used to calculate photosynthetic rates and primary productivity in surface waters, making it an important metric of biological activity in the oceans (Antoine and Morel, 1996; Behrenfeld and Falkowski, 1997). Thus, these prior studies have been unable to directly associate the observed changes in SSA with specific changes in biological activity under realistic ocean conditions. Collins et al. performed numerous mesocosm blooms, measuring the CCN activity of primary SSA, and concluded that

changes in the CCN activity of SSA show only a weak dependence on phytoplankton biomass (i.e. chl-a) (Collins et al., 2016).

In addition to studies on primary SSA, other studies have attempted to link variability in the emissions of biogenic VOCs to variability in CCN concentrations and cloud properties. Notably, several decades ago, Charlson et al. proposed the well-known CLAW hypothesis that nss-SO_4^- aerosol produced from the oxidation of DMS released by phytoplankton could exert significant control over cloud albedo and thus regulate climate through both positive and negative feedback mechanisms (Charlson et al., 1987). Numerous field studies have established a positive correlation between CCN concentrations and DMS flux, a gas-phase species known to be emitted during periods of high biological activity (Ayers et al., 1991; Berresheim et al., 1993; Pandis et al., 1994). However, other studies have shown that DMS alone does not fully explain both field observations and modelling results of CCN, suggesting there are other sources of cloud seeds in the marine environment, such as nascent SSA and continental aerosols (Quinn and Bates, 2011). Using a global aerosol microphysics model, Merikanto et al. estimated that 55% of CCN (0.2%) in the marine boundary layer are new particles formed by nucleation processes (Merikanto et al., 2009). Recently, Gras and Keywood reported that CCN concentrations over the Southern Ocean show a strong seasonal dependence and that during the summer months CCN are directly correlated with biogenic sulfur compounds (Gras and Keywood, 2017).

The critical challenge involves disentangling and measuring the properties of primary versus secondary marine aerosols formed from the same seawater over the course of a phytoplankton bloom. In this study, we investigate the processes forming marine aerosol under clean conditions in an isolated ocean/atmosphere system, free from anthropogenic and terrestrial influences, enabling the direct measurement of how primary and secondary aerosols impact cloud

formation over an evolving phytoplankton bloom. We initiated the phytoplankton bloom in Pacific Ocean seawater and generated sea spray aerosols in a marine aerosol reference tank (MART). Concurrently, secondary marine aerosol (SMA) was produced by oxidizing the complete mixture of headspace gases from the MART in an oxidative flow reactor (OFR, ~3.3 days equivalent aging). While OFRs have been used extensively for studies of anthropogenic and terrestrial aerosols, this study represents one of the first applications of an OFR to marine systems (Peng and Jimenez, 2020). This novel approach allows for direct determination of how variations in biological activity affect the flux and CCN activity of marine aerosols. By separately producing and measuring primary and secondary marine aerosols, we unambiguously show the strongest correlation exists between seawater chl-a levels and the production of secondary marine aerosols. Furthermore, the CCN activity of the secondary marine aerosols produced at the peak of the phytoplankton bloom is remarkably consistent with decades of field measurements made over the oceans.

3.3 Results and Discussion

3.3.1 Changes in Aerosol Production Over the Course of the Bloom

During each day of the experiment, 120 L of seawater was transferred to a marine aerosol reference tank (MART) for aerosol generation (Figure 3.6). The number concentrations of primary SSA were calculated from the aerosol size distributions measured during each day of the bloom (Figure 3.7). The measured number concentrations are directly proportional to the SSA flux, as the air flow rate through the MART remained constant throughout the experiment. The observed flux at the peak of the bloom, as indicated by the chl-a concentration, was slightly elevated, but after the peak, the flux exhibited a general downward trend over time. At the peak, the maximum

observed change in flux for this bloom was approximately 16%, providing an upper limit for changes in SSA flux during the course of a phytoplankton bloom.

In addition to SSA, the size distributions of the OFR-generated SMA were also measured. These size distributions were converted from number distributions to volume distributions assuming spherical particles (Figure 3.1). The SMPS scanned to a maximum diameter of d_p = 0.43 μm, and thus the volume concentration estimate excludes contributions from much larger particles, which dominate the total volume. Submicron SSA typically dominate in terms of number concentration and have longer lifetimes than supermicron particles, so they are expected to have the largest influence on CCN numbers (Lewis and Schwartz, 2004). In addition, larger particles are primarily composed of sea salt while smaller particles generally have increased fractions of organic compounds (O'Dowd et al., 2004; Prather et al., 2013). Thus, by focusing on variability in the small particles we isolate those particles most likely to be influenced by changes in seawater composition, as well as affect cloud properties. For simplicity, we refer to the measured particles as submicron particles.

Over the duration of the mesocosm bloom, the aged submicron aerosol volume concentrations after the OFR were 3 to 14 times higher than those of primary SSA (Figure 3.1), indicating that nascent SSA only accounts for a small fraction of the total submicron aerosol volume concentration. Thus, secondary species dominate the submicron aerosol produced from the OFR and the properties of the measured aerosol largely reflect the properties of SMA. The volume concentration of SMA specifically was determined by taking the difference between the total volume concentration (SMA + SSA) and that for the SSA alone.

The submicron SMA volume concentrations showed a strong linear relationship with chl-a (r^2 = 0.78), whereas the primary SSA concentrations remained relatively constant over the course of the

bloom (r^2 = 0.33) (Figure 3.2). Moreover, the absolute changes in the SMA volume concentrations were much greater than those for SSA. At the peak of the bloom (9/1), the SMA concentration was 6 times higher than at the end of the bloom (9/5). The specific relationship between SMA volume concentration and chl-a varied somewhat over time, with notable differences during the growth and death stages. This reflects time dependent differences in the gas-phase emissions resulting from changes in the microbe communities and biological processing of organic species in the seawater. These results show that biological activity in seawater has a much larger effect on the emission of gases which lead to SMA production, rather than changes in SSA flux. Thus, we conclude that under these conditions, SMA would play a more important role than SSA in seeding marine clouds.

Similar to the volume concentrations, the particle number concentrations for SMA were also correlated with chl-a. However, nucleation is strongly favored over condensation in the OFR, due to the high OH concentrations and fast oxidation rates. While the OFR system can provide an estimate of secondary aerosol mass yield (Bruns et al., 2015), these experiments do not directly establish the extent to which new particle formation will compete with condensation of oxidized vapors in the marine atmosphere. Indeed, the size distributions of the secondary aerosol indicate that the partitioning of gas-phase compounds into the particle phase was occurring primarily via new particle formation, with a much smaller contribution from coating pre-existing primary SSA particles (Figure 3.8). Nonetheless, these data clearly show that overall, SMA production exhibits a stronger link with chl-a than SSA.

3.3.2 Chemical Composition of Secondary Marine Aerosol

To better understand the relationship between bloom growth and aerosol properties, we measured the chemical composition of SMA using an HR-TOF-AMS. The secondary aerosol

formed during these experiments was primarily composed of sulfate, ammonium and organic compounds, with a small amount of nitrate (Figure 3.3, CE = 0.6). Sulfate made the largest contribution to the secondary aerosol mass (53-71%). We hypothesize that most of this sulfate was formed from dimethyl sulfide (DMS) oxidation. DMS is the most abundant biogenic sulfur-containing gas in the marine atmosphere, with annual emissions from the oceans of ~28.1 (17.6-34.4) Tg S yr^{-1} (Lana et al., 2011). Other methylated sulfur gases, such as methanethiol (MeSH) and dimethyl disulfide (DMDS) are also emitted from the oceans, however the flux of these compounds is believed to be significantly lower than that of DMS, and the role they play in secondary aerosol formation remains largely unexplored (Lee and Brimblecombe, 2016). DMS is produced from the enzymatic cleavage of dimethylsulfoniopropionate (DMSP), an osmolyte produced by many species of marine phytoplankton (Keller et al., 1989).

The flux of DMS from biologically active surface waters can be as high as 14 $\mu mol \cdot m^{-2} day^{-1}$ (Erickson et al., 1990), resulting in mixing ratios of up to ~1 ppbv in the marine atmosphere (Koga et al., 2014). DMS is readily oxidized by OH radical, producing several products including, ultimately, sulfuric acid and methanesulfonic acid (MSA) (Hoffmann et al., 2016). MSA is frequently used in field measurements to distinguish between biogenic and anthropogenic sulfate aerosols (Gaston et al., 2010; Saltzman et al., 1983). We observed an ion at *m/z* 78.99 ($CH_3SO_2^+$) in the AMS spectrum (Figure 3.10), which is a known fragment ion of methanesulfonic acid in the AMS (Huang et al., 2017). The observation of MSA in the secondary marine aerosol during this experiment serves as direct evidence of DMS oxidation in the OFR.

Although the absolute concentrations of both sulfate and ammonium changed significantly during the bloom, the molar ratio of ammonium to sulfate remained relatively constant throughout the experiment ($[NH_4]/[SO_4]$ = 1.31±0.03, Figure 3.11). Notably, the mass fraction of organic

compounds (f_{org}), decreased during the peak of the bloom and increased during the death phase ($f_{org} \approx 0.10$-0.30). This variability in the ratio of organic compounds to inorganic species (sulfate, ammonium, and nitrate) represented the largest overall change in the SMA chemical composition during bloom (Figure 3.12). The average mass-concentration weighted AMS spectrum for secondary organic species in SMA is shown in Figure 3.10. Most of the organic ion signals were from oxygen-containing and sulfur-containing organic fragment ions. The CO^+ (m/z = 28) and CO_2^+ (m/z = 44) peaks dominated the spectrum, indicating that carboxylic acids were likely a major organic component of the secondary aerosol (Canagaratna et al., 2007). The observed O:C elemental ratio values for the secondary organic aerosol ranged from 0.7 to 1.2, and the H:C elemental ratios ranged from 1.0 to 1.9 (Figure 3.13). Both elemental ratios changed throughout the bloom. Changes in the organic aerosol composition reflect changes in the gas-phase VOCs being emitted from the seawater over the course of the bloom. Specifically, this suggests that non-DMS VOCs can be important contributors to SMA formation and the overall chemical composition, and thus CCN activity. The variability in the f_{org} and organic composition can be explained by the phytoplankton releasing different VOCs during different stages of their life cycle (Zuo, 2019), as well as the production of VOCs by heterotrophic bacteria, which increase and become extremely active during the death phase of phytoplankton blooms (Azam et al., 1983).

3.3.3 CCN Activity of Nascent SSA

The CCN activity, characterized by the hygroscopicity parameter, of nascent SSA (D_d = 50 nm) is relatively constant over the course of the bloom (κ_{app} = 1.02 ± 0.02, Figure 3.4). This result is consistent with previous measurements of MART-generated SSA (Collins et al., 2016; Schill et al., 2015). Collins and coworkers measured an average value of κ_{app} = 0.95 ± 0.15 for SSA sampled from numerous mesocosm experiments, with even less intra-experiment variability

observed during individual mesocosms (Collins et al., 2016). The number of CCN that will activate at a supersaturation of 0.2% was calculated from the measured size distributions using the measured κ_{app} and assumed to be the same for particles of all sizes. The number concentrations of CCN(0.2%) for SSA exhibited only modest changes during the bloom, with CCN(0.2%) = 251±18 $\#\cdot cm^{-3}$ (Figure 3.7). Most of the variation can be explained by small changes in the flux of SSA, rather than changes in composition and hygroscopicity. While the flux and CCN activity of primary SSA may be sensitive to variability in ocean composition, these observations suggest that chl-a, specifically, is a weak predictor of both.

3.3.4 CCN activity of Secondary Marine Aerosol

To assess the degree to which SMA could influence cloud formation, the hygroscopicity of OFR-aged particles was also measured. Given that the number concentration of SMA is much larger than that of SSA at 50 nm for these experiments, the properties of the OFR-aged marine aerosol are representative of SMA. The mean SMA hygroscopicity parameter was κ_{app} = 0.59 ± 0.04 (1σ) during the bloom, with values ranging from κ_{app} = 0.52-0.64 (Figure 3.4). The SMA hygroscopicity parameters were significantly lower than those of nascent SSA (κ_{app} = 1.02 ± 0.02) and overall exhibited slightly greater variability across the bloom, suggesting that the CCN activity of SMA is more sensitive to biologically mediated changes in seawater chemistry than SSA. Importantly, the range of OFR-generated SMA hygroscopicity parameters (κ_{app} = 0.52-0.64) is consistent with real-world field measurements of marine aerosol, particularly in remote marine environments. Swietlicki and coworkers compiled the results of several field studies that measured the hygroscopicity of aerosols in marine environments using hygroscopic tandem differential mobility analyzer (HTDMA) (Swietlicki et al., 2008). The hygroscopicity parameter can be calculated from the growth factor (*gf*) as:

$$\frac{RH}{exp\left(\frac{A}{D_d gf}\right)} = \frac{gf^3 - 1}{gf^3 - (1 - \kappa)}$$

Eq 3.1

The authors identified a class of particles, referred to as more-hygroscopic (MH) that was ubiquitous and distinct from sea salt. For particles with a dry diameter of 50 nm, the reported growth factors of these MH particles ranged from *gf* = 1.50-1.71, which corresponds to values of κ = 0.43-0.77. Asmi et al. (2010) reported HTDMA measurements of aerosols from the coast of Antarctica with back-trajectories originating over the Southern Ocean (Asmi et al., 2010). They found an average growth factor of *gf* = 1.67 for 50 nm particles, which corresponds to a single hygroscopicity parameter of κ = 0.70. Measurements of aerosol composition showed that it was mainly composed of ammonium sulfate, un-neutralized sulfuric acid and organic compounds, which is consistent with the composition of SMA measured in this study.

3.3.5 κ-Closure Model

To investigate whether the observed changes in aerosol composition quantitatively explain the changes in SMA hygroscopicity, we calculated the theoretical values of κ using the compositional data measured by the AMS. The predicted κ value is derived from the volume mixing equation (Eq 3.2), where κ_i and ε_i are the hygroscopicity parameter and volume ratio of the i^{th} component of the aerosol respectively (Petters and Kreidenweis, 2007).

$$\kappa = \sum_i \varepsilon_i \kappa_i$$

Eq 3.2

This equation does not account for the potential effects of organics on the aerosol surface tension, which was assumed to be that of pure water for this study (σ = 0.072 J·m). Since there was an excess of sulfate, we assumed that all the NH_4^+ was in the form of ammonium sulfate (κ = 0.61)

and ammonium nitrate ($\kappa = 0.67$) and that the remaining sulfate signal arose from sulfuric acid ($\kappa = 0.70$) (Ovadnevaite et al., 2017). Due to the complexity of organic species contributing to SMA, it was not feasible to calculate the relative contribution from each species, so this value was estimated using parameterizations based on the AMS elemental ratios (Kuwata et al., 2012; Lambe et al., 2011). The values obtained from this parameterization ranged from $\kappa_{org} = 0.15\text{-}0.24$ during the experiment, which is consistent with values of pure organic compounds (Petters and Kreidenweis, 2007). The calculated κ values agree well with the observed values of κ_{app} (Figure 3.4). This agreement indicates that changes in SMA hygroscopicity during the bloom are being driven primarily by changes in aerosol composition, which is influenced by VOCs produced by biological activity in seawater.

3.4 Atmospheric Implications

This study clearly shows a strong correlation between chlorophyll-a concentrations in seawater and secondary marine aerosols produced via OH radical oxidation (Figure 3.2A). In contrast, only a weak correlation is observed between nascent SSA volume and chl-a (Figure 3.2B). The SMA volume concentrations exhibited much larger changes over the course of the bloom than SSA, indicating that gas-phase VOCs, the SMA precursors, are more sensitive to biological activity in seawater than the factors controlling primary SSA flux. Through the use of a unique ocean-atmosphere laboratory approach, we have isolated the influence of biology from other environmental factors such as wind speed and temperature, which may affect marine aerosol production. These results suggest that the observed correlations between cloud properties and biological activity in the oceans is primarily driven by the emission of gas-phase VOCs and

subsequent formation of secondary aerosols, as opposed to changes in the concentration and composition of nascent SSA (Collins et al., 2016).

This study demonstrates that during periods of high biological activity, gas-phase precursors are emitted from seawater, leading to the formation of significant quantities of secondary marine aerosol (Sinha et al., 2007). While the SMA concentration produced in these experiments greatly exceeds the SSA concentration, the balance between emission of VOCs versus SSA in marine environments will additionally depend on atmospheric conditions such as wind speeds and temperature. Nonetheless, the oxidation of gases produces products that can condense onto pre-existing particles or, potentially, nucleate new particles, producing SMA. Here, sulfate, sulfur-containing organic species, ammonium, and other secondary organic species are the main chemical constituents of the SMA formed. The molar ratio between sulfate and ammonium was relatively constant over the bloom, while the ratio of sulfate to organic species varied significantly (Figure 3.11, Figure 3.12). This suggests that the organic components of secondary marine aerosol are playing an important role in controlling aerosol composition and the resulting CCN activity. We hypothesize that SMA properties may be quite sensitive to the presence of non-DMS species, and more generally non-sulfur containing SOA precursors such as isoprene and monoterpenes which may be produced in different regions of the ocean (Kim et al., 2017). In addition, organosulfur compounds such as methanesulfonic acid appear to be an important component of SMA under the conditions of these experiments.

This study shows a weak relationship between chl-a concentrations in seawater and both the production flux and hygroscopicity parameter of primary SSA, consistent with previous studies (Collins et al., 2016). Our findings support the growing body of evidence that correlations between CCN concentrations and biological activity in seawater are largely driven by the emission of

biogenic VOCs that ultimately lead to secondary aerosol production (Sanchez et al., 2018; Vallina et al., 2006; Willis et al., 2017). This is supported by the measured hygroscopicity parameter for the SMA in this study, which is consistent with measurements in previous marine field studies. By separating primary and secondary marine aerosols, the results here strongly suggest that under realistic phytoplankton bloom conditions secondary, not primary, marine aerosols are controlling cloud properties in marine environments. Future work will expand the range of biological conditions to study the impact on the types and concentrations of VOCs produced over the course of a bloom to directly determine how much ocean biology contributes to the variability in SMA composition and the resulting cloud properties in marine environments.

3.5 Methods

3.5.1 Aerosol Generation.

A phytoplankton bloom was grown outdoors in a 2,400 L tank filled with natural seawater from the Pacific Ocean, collected at Scripps Pier (32.86 N, -117.25 W). The bloom was initiated by adding algae growth media (Guillard and Ryther, 1962) (concentration: *f*/50) to the tank, which was placed outside under direct sunlight. The chl-a concentration was measured daily using a handheld fluorometer (AquaFluor, Turner Designs). During the bloom, the chl-a concentration ranged from 0.5 to 8 µg/L, which is within the typical range of oceanic bloom conditions (O'Reilly et al., 1998). During each day of the experiment, 120 L of seawater was transferred to a marine aerosol reference tank (MART) for aerosol generation (Figure 3.6). Importantly, by introducing new water samples each day from a larger reservoir material, physically degraded through SSA production does not build up over time. The MART produces SSA by using an intermittent plunging waterfall to generate bubbles with a size distribution that is similar to that produced by

breaking waves in the ocean (Stokes et al., 2013). The MART was equipped with 5700 K fluorescent lights (Full Spectrum Solutions, Model 205457) to provide light during the indoor sampling periods (Lee et al., 2015). The headspace air, including SSA, was sampled into a Potential Aerosol Mass Oxidation Flow Reactor (PAM-OFR) by pushing a stream of 5 liter-per-minute (LPM) air from a zero air generator (Sabio, Model 1001) through the MART. After completing the aerosol measurements each day, the seawater was transferred back to the large outdoor tank.

The PAM-OFR uses UV lamps with wavelengths of λ = 185 nm and 254 nm (OFR185 mode) to produce a high concentration of OH radicals (Kang et al., 2007). The OH exposure in the OFR was determined by introducing SO_2 (initial concentration ~ 30 ppb) to the OFR at the same air flow rate and relative humidity used during the MART-OFR experiments. The change in SO_2 concentration yielded the OH exposure versus light intensity relationship using the known SO_2 + OH rate coefficient ($k_{OH+SO2} \sim 9.4\times10^{-13}$ cm^3 $molec^{-1}$ sec^{-1}). The residence time of gases in the OFR was 2.67 min. The experiments here used a single OH exposure of $4.3(\pm1.3)\times10^{11}$ molecules·sec/cm^3, which is equivalent to ~ 3.3(±0.5) days of equivalent aging under typical tropospheric conditions ([OH] = 1.5 x 10^6 molec·cm^{-3}). Notably, the plunging waterfall was also active during this experiment, introducing SSA to the OFR that can act as seed particles for secondary aerosol formation (Lambe et al., 2015). While these operating conditions were used to approximate the marine atmosphere, which contains both primary SSA and secondary marine aerosol, the high OH concentrations in the PAM-OFR favor nucleation over condensation.

3.5.2 Aerosol Sampling

All aerosols were dried using silica diffusion dryers before measurement. Aerosol size distributions were measured using a Scanning Mobility Particle Sizer (SMPS 3398, TSI Inc.) and

an Aerodynamic Particle Sizer (APS 3321, TSI Inc.). Aerosol composition was measured using an Aerodyne high-resolution time-of-flight aerosol mass spectrometer (HR-ToF-AMS), which characterizes non-refractory submicron aerosol components (Decarlo et al., 2006). A capture vaporizer was used in the AMS and its temperature was set to 650ºC to vaporize the non-refractory aerosol species.

The hygroscopicity of size-selected aerosol particles was characterized using a continuous flow stream-wise thermal gradient cloud condensation nuclei counter (CCN-100, Droplet Measurement Technologies, Inc.). Dry particles having mobility diameters of 50 nm were size-selected using a differential mobility analyzer (DMA 3081, TSI Inc.) and the flow was split isokinetically between the CCN counter and a condensation particle counter (W-CPC 3787, TSI Inc.). The CCN counter scanned through supersaturations (S_c) over the range 0.1-1.0%. The effective hygroscopicity parameter (κ) for the dry, monodisperse aerosols was calculated from κ-Köhler theory, using Equation 3.3 (Petters and Kreidenweis, 2007),

$$\kappa_{app} = \frac{4A^3\sigma_{s/a}^3}{27D_d^3 \ln^2 S_c}$$

Eq 3.3

where A is a constant, $\sigma_{s/a}$ is the surface tension of the surface-air interface, D_d is the dry particle mobility diameter, and S_c is the critical supersaturation. The surface tension was assumed the same as that of pure water, $\sigma_{s/a}$ = 0.072 J·m. The critical supersaturation (s_{crit}) was determined by fitting a sigmoidal curve to a plot of the fraction of particles that activated versus the instrument supersaturations. The s_{crit} is the point where 50% of the particles had activated.

3.5.3 κ-Closure Model

The density and hygroscopicity parameters for the organic fraction of SMA were calculated from the AMS composition data for each day of the bloom. The density of the organic components

was estimated from the O:C and H:C ratios measured by the AMS using the method described by Kuwata et al. (2011) and ranged from 1.3-1.9 g/cm^3 during the experiment (Kuwata et al., 2012). This density was used to convert the AMS organic mass fraction to a volume fraction. The hygroscopicity parameters of the organic fraction were calculated from the O:C ratios using the linear parameterization from Lambe et al. (2011) for pure SOA produced in an OFR, where κ_{org} = (0.18 ± 0.04) × O:C + 0.03 (Lambe et al., 2011). The resulting values of κ_{org} ranged from 0.15-0.24.

3.6 Acknowledgements

This material is based upon work supported by the National Science Foundation through the Center for Aerosol Impacts on Chemistry of the Environment, an NSF Center for Chemical Innovation (CHE-1801971). We thank Vicki Grassian, Timothy Bertram, Richard Cochran, Armando Estillore, Matthew Pendergraft, Jon Trueblood, Olivia Ryder, Luis Camarda, Jordan Watt, Joey Manson, Mona Shrestha, Charlotte Beall, and Joseph Mayer for their assistance with experiments and many helpful discussions. We would like to thank Paul DeMott and the Colorado State University Department of Atmospheric Science for providing the AMS, as well as William Brune (Penn State) for providing the PAM-OFR used in this experiment. We also thank Delphine Farmer and Lauren Garofalo (Colorado State University) for their advice and assistance with interpretation of the AMS data.

Chapter 3 is, in full, a reprint of material as it appears in *ACS Central Science.* Reprinted with permission from Mayer, K.J., Wang, X., Santander, M.V., Mitts, B.A., Sauer, J.S., Sultana, C.M., Cappa, C.D., and Prather, K.A. (2020). Secondary Marine Aerosol Plays a Dominant Role

over Primary Sea Spray Aerosol in Cloud Formation, *ACS Cent. Sci.* 6, 12, 2259-2266. The dissertation author and Dr. Xiaofei Wang were primary investigators and lead authors of this paper.

3.7 Figures

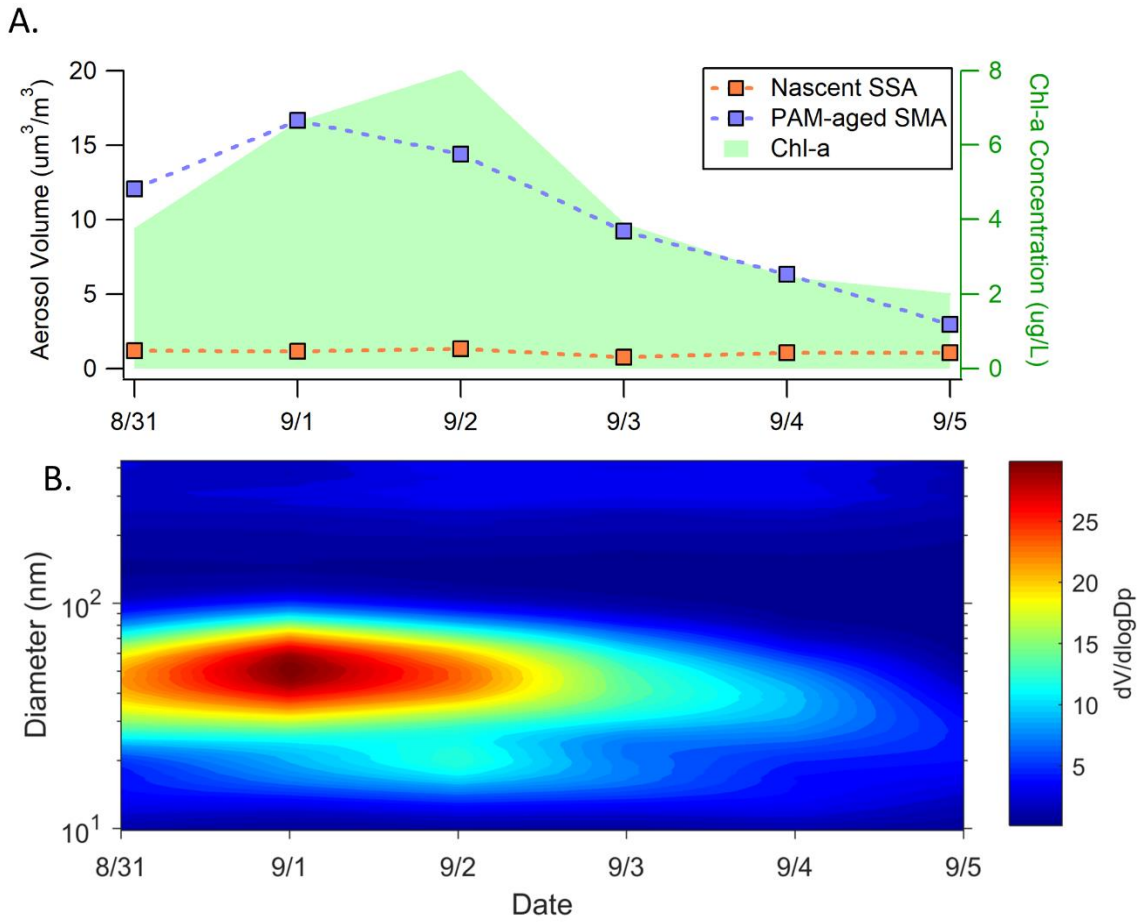

Figure 3.1 a) Daily aerosol volume concentrations (dp < 0.43 um) for OFR-aged SMA and nascent SSA. b) OFR-generated SMA volume size distribution over the course of the bloom.

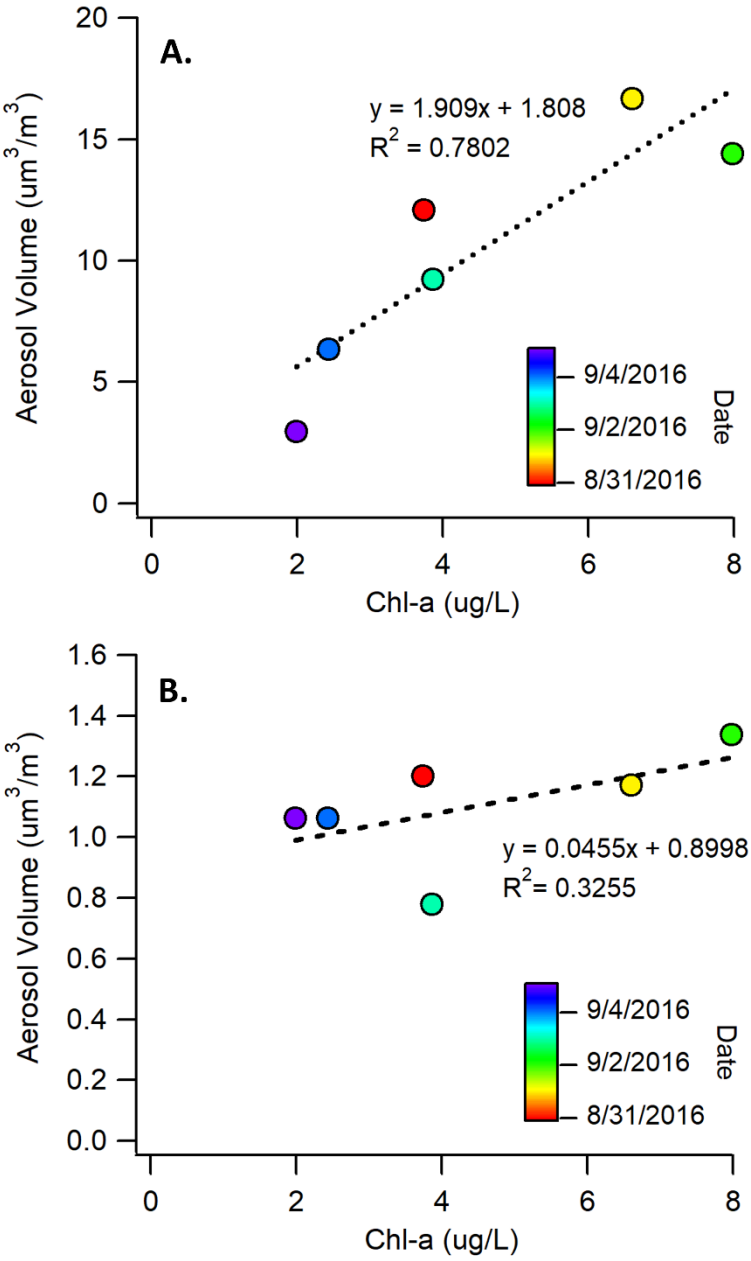

Figure 3.2 a) Correlation between chl-a concentrations and total aerosol volume concentrations for OFR-generated SMA (R2 = 0.78). b) correlation of chl-a with primary SSA total aerosol volume (R2 = 0.37) during the bloom.

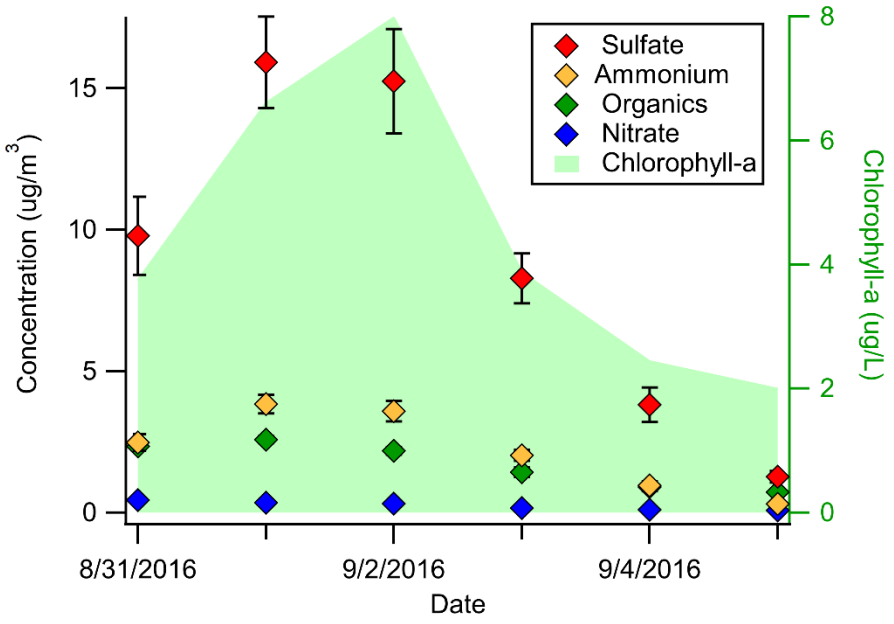

Figure 3.3 Time series of the chemical composition of SMA generated in the OFR measured with the HR-TOF-AMS (CE = 0.6). The seawater chlorophyll-a concentration is shown for reference. Error bars represent ± 1σ.

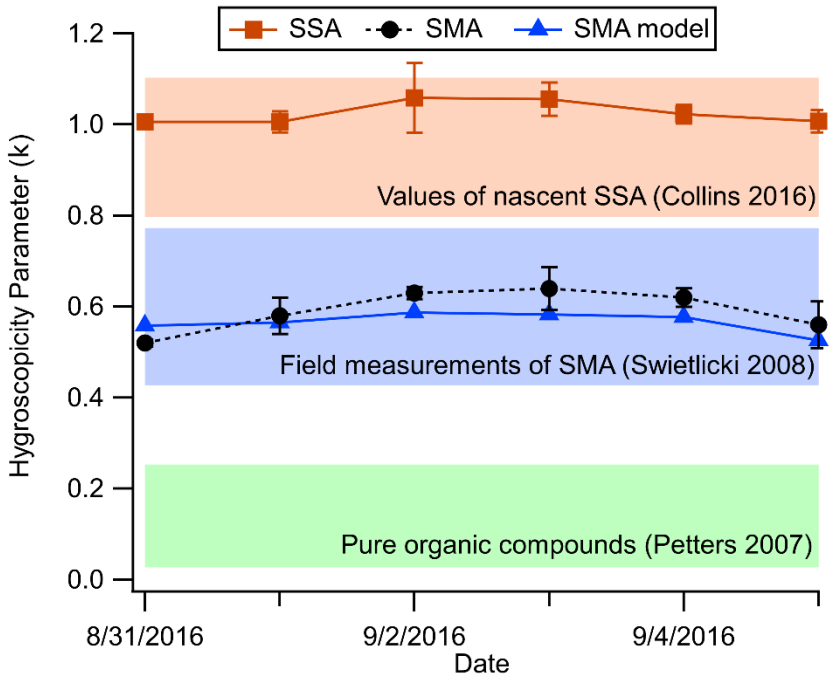

Figure 3.4 Daily hygroscopicity parameters (κ) measured for nascent SSA and OFR-generated SMA during phytoplankton bloom. Values of κ calculated for SMA based on the composition model are also shown. The range of κ for lab-generated SSA (Collins et al., 2016), field measurements of marine aerosols (Swietlicki et al., 2008), and typical values of organic compounds (Petters and Kreidenweis, 2007) are shown in the background for reference.

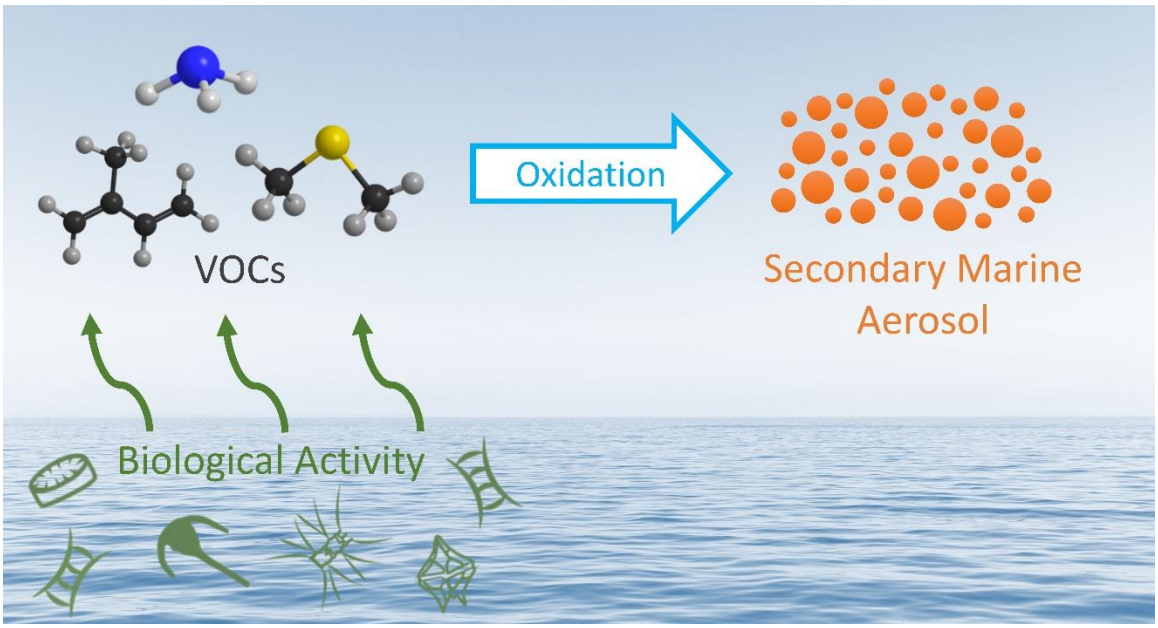

Figure 3.5 Biological activity in the oceans produces volatile gases which undergo atmospheric oxidation to form secondary marine aerosol. These particles have profound impacts on cloud formation and climate.

3.8 Supporting Information

3.8.1 Control Experiment for MART-OFR Study

A control experiment was conducted to determine whether the majority of the AMS signal originated from seawater emissions, rather than background contamination. A brief description follows: the MART tank was filled with ultrapure water (18 MΩ), instead of seawater. Other experiment conditions, OFR settings and aerosol sampling instruments were kept the same with all other SMA experiments. The AMS was used to monitor the background aerosol chemical compositions from the OFR for this control experiment. The concentration of background concentrations of sulfate, nitrate, ammonium and organic aerosol concentrations were 0.015±0.003, 0.004±0.003, -0.002±0.015 and 0.121±0.041 μg/m^3, respectively, which corresponds to 1%, 4%, 0.5%, and 14% of the minimum concentration of each analyte measured during the bloom. The low background concentration of the inorganic ions indicate that background aerosols were not a significant source of the AMS signals during the SMA experiments. However, the background comprises a larger fraction of the organic aerosol, which could have affected our experimental results.

3.8.2 Gas-Phase Measurements

Ammonia can partition to the particle phase and form a major component of SMA particles. The following analysis was done to make sure that our experiment system was not contaminated with ammonia. The input air source is a zero-air generator (ZAG, Model 1001, Sabio) which was used to scrub contaminants from the air before it was introduced to the MART tank; however, it does not completely remove all trace gases, including ammonia. To ensure trace amounts of ammonia transmitted by the ZAG were not skewing the experimental results, we compared the ammonia signal measured by chemical ionization time-of-flight mass spectrometry (CI-TOFMS)

during the bloom to the ZAG baseline. The operating principles of the instrument are described elsewhere (Bertram et al., 2011). The CI-TOFMS was operated with a high pressure inlet at 12 mTorr using $H_3O(H_2O)n^+$ ions generated by passing humidified N_2 through a Po-210 source (20mCi, NRD). The normalized counts per second (ncps) were calculated using the intensity of the reagent water cluster at m/z 37. The signal at m/z = 18, corresponding to NH_4, was used as a proxy for NH_3 concentration. To establish a baseline for the ZAG, zero air was pushed through the headspace of a clean MART tank filled with milliQ H_2O and sampled by the CI-TOFMS. During the bloom, the instrument sampled the gases from the MART headspace after they had passed through OFR. The ammonia signal (Fig. S8) from the bloom was significantly higher than the baseline throughout the experiment, with the normalized counts ranging from 20-40 times higher. This result indicates that that the most of ammonia in the MART headspace gases, and thus the ammonium in the OFR-generated SMA, were derived from the seawater itself and that the contribution from the ZAG were minimal.

3.8.3 CCN Measurements of SSA and SMA

The DMA sample-to-sheath flow ratio used during the experiments was 1:5 for nascent sea spray aerosol and 1:10 for SMA produced in the OFR. A smaller sheath flow ratio was used for the nascent sea spray due to its low particle concentration. Decreasing the sheath flow ratio affects activation behavior by broadening the DMA transfer function, and thus allowing a wider range of particle diameters to pass through the DMA. Assuming an ideal, triangular-shaped transfer function, decreasing the sheath flow ratio from 1:10 to 1:5 has the effect of broadening the width of the transfer function for 50nm particles at half height from $\Delta Z_p = 5$ nm to $\Delta Z_p = 10$ nm (Knutson and Whitby, 1975). This difference is not expected to significantly affect the SR-CCN measurement.

3.8.4 Supplementary Figures

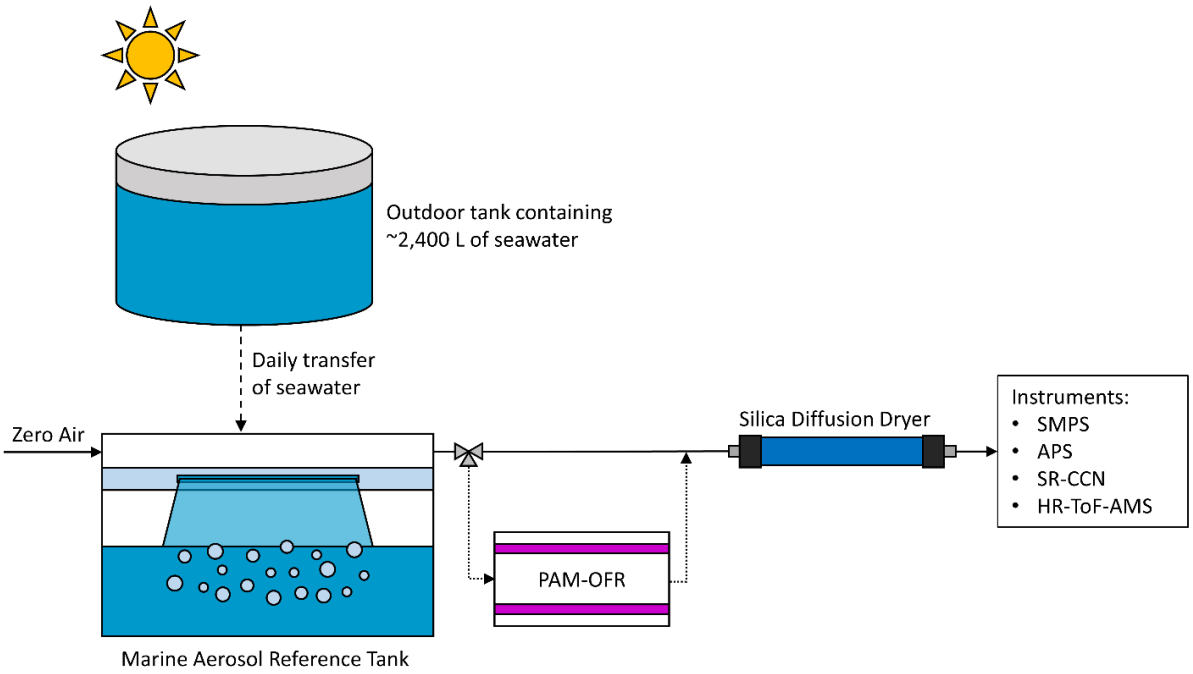

Figure 3.6 Schematic drawing of experimental setup. The phytoplankton bloom was grown in a 2,400 L outdoor tank. Each day, 120 L of seawater were transferred to the MART for aerosol generation, and then returned to the outdoor tank after sampling. Primary sea spray aerosol was generated using a plunging waterfall, while secondary marine aerosols were generated using a PAM-OFR to oxidize the headspace gases.

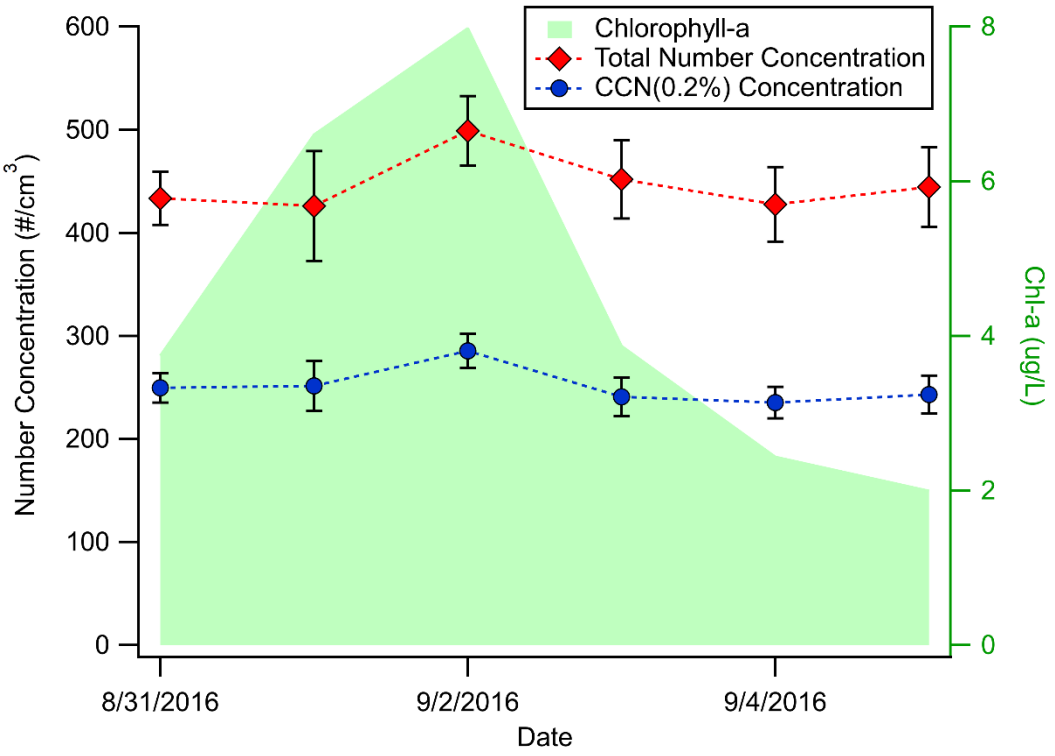

Figure 3.7 Time series of the average number concentrations and CCN (0.2%) concentrations for primary SSA during a mesocosm experiment. The CCN (0.2%) concentration was calculated from the aerosol size distributions and the measured hygroscopicity parameters, which were used to calculate the activation diameter of SSA at a supersaturation of SS = 0.2%. The seawater chlorophyll-a concentration is shown for reference. Error bars represent ± 1σ.

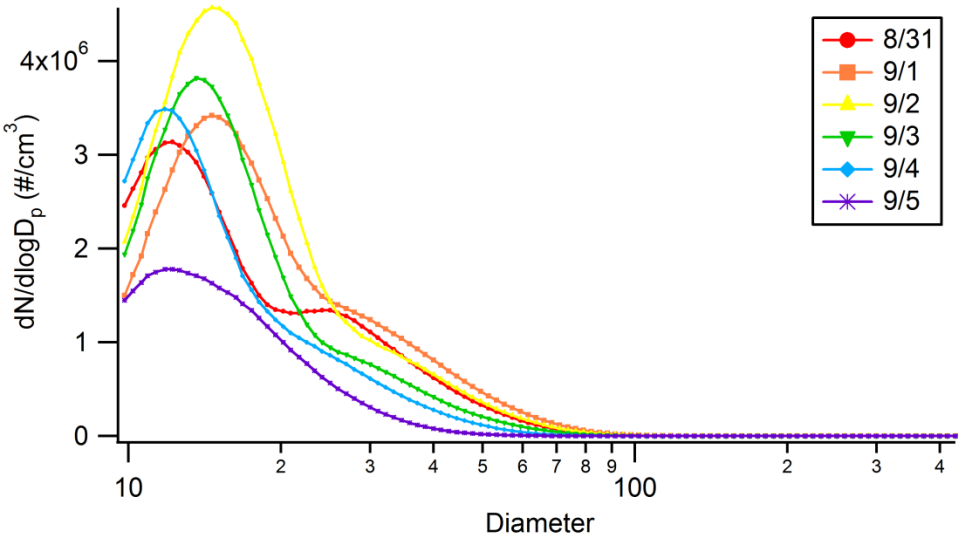

Figure 3.8 SMPS number size distributions of SMA generated in the PAM-OFR

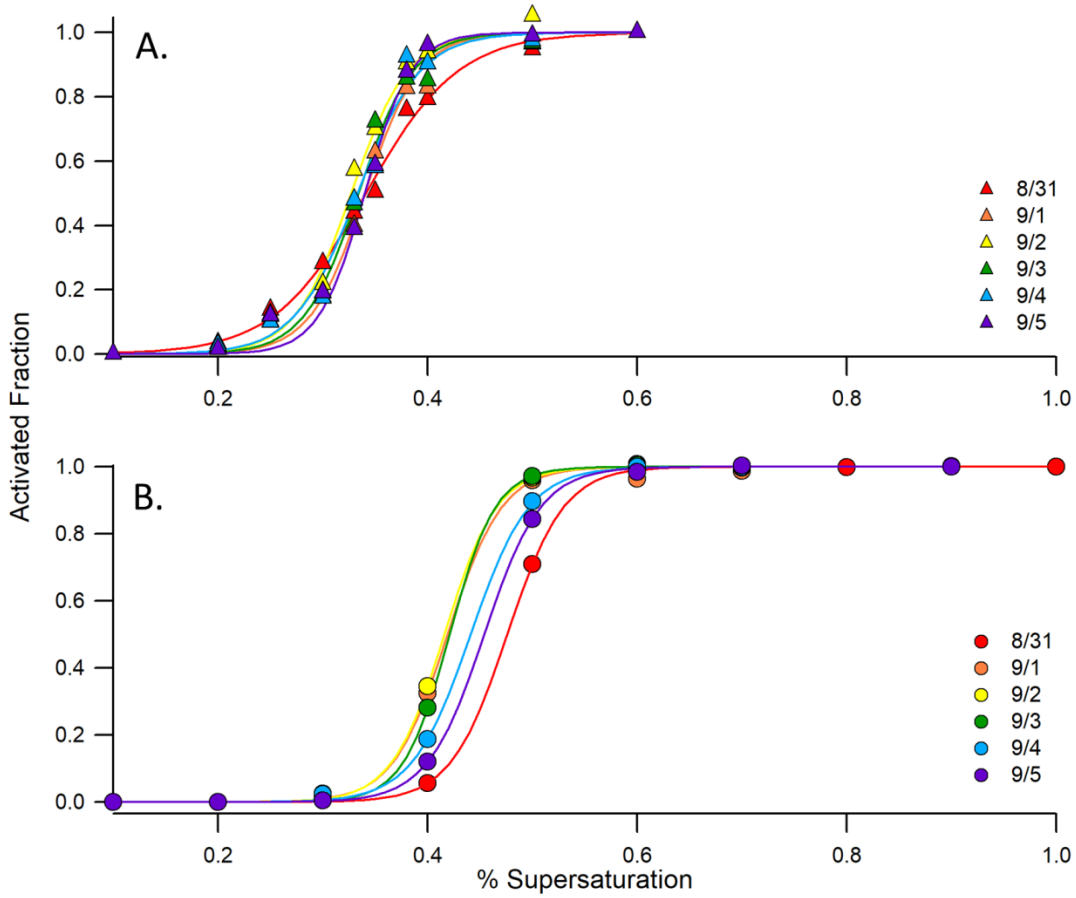

Figure 3.9 a) SR-CCN activation curve for 50 nm nascent SSA particles. b) SR-CCN activation curves for 50 nm OFR-generated SMA particles.

A. SMA

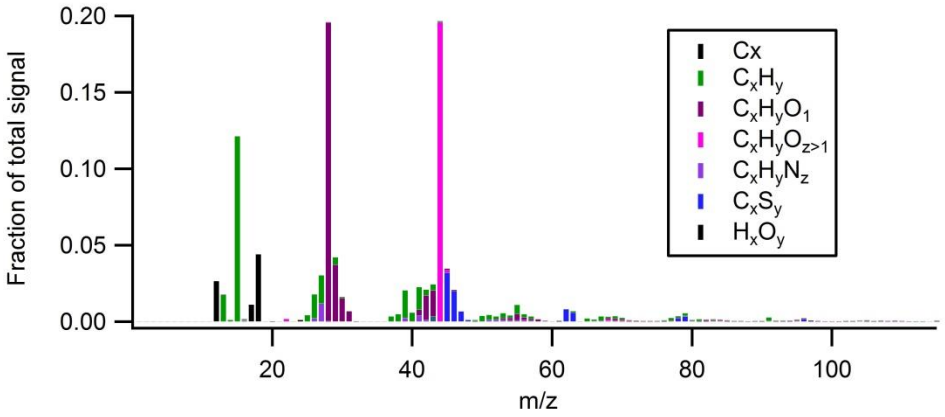

B. SSA

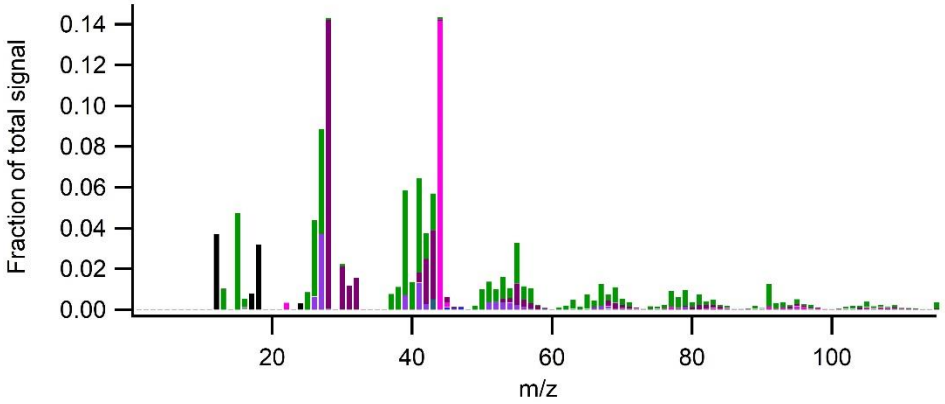

Figure 3.10 Average AMS spectra for organic species in (a) SMA and (b) SSA during bloom.

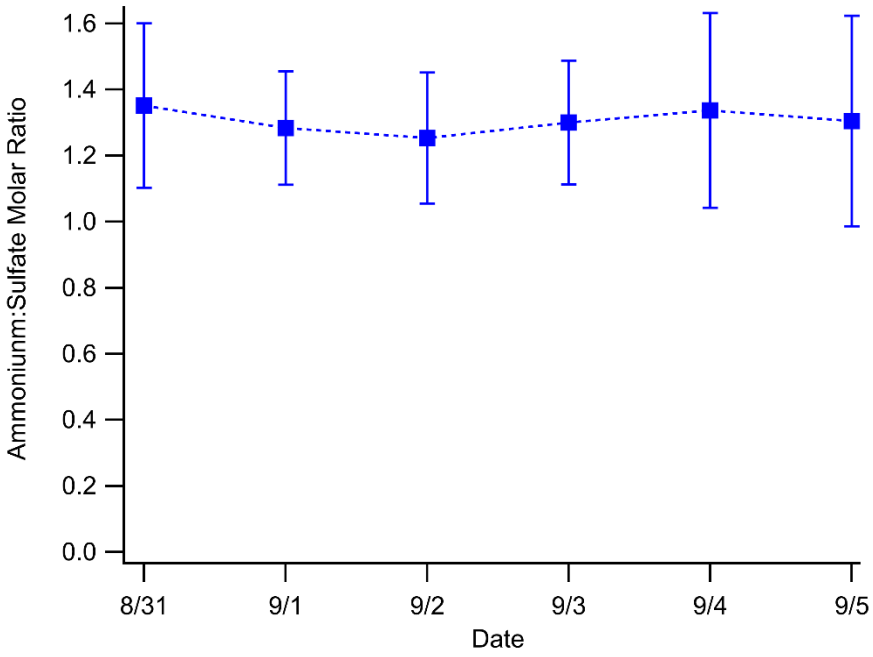

Figure 3.11 The molar ratio of ammonium to sulfate in SMA during the bloom, as measured by the HR-ToF-AMS. Error bars represent ± 1σ.

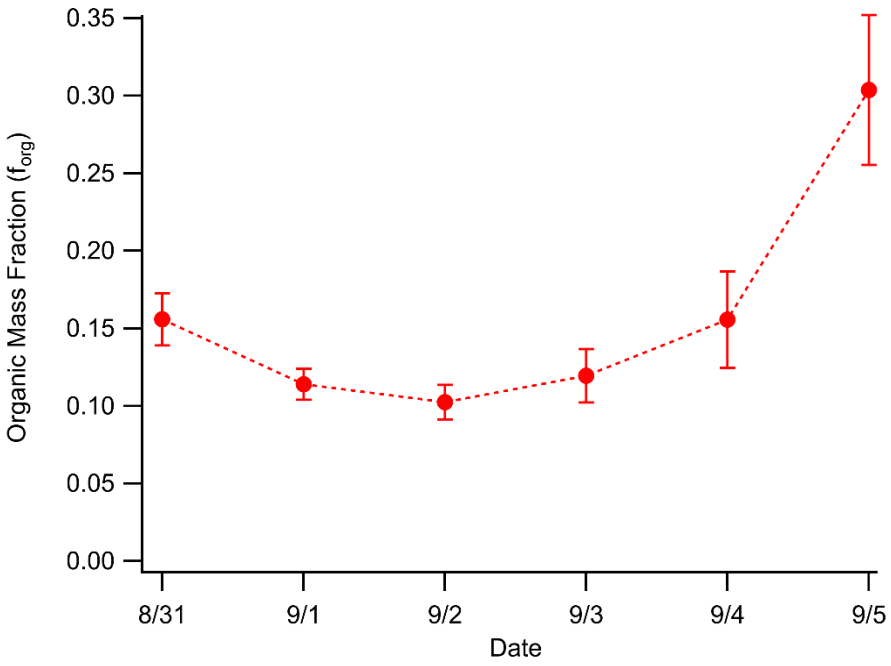

Figure 3.12 Organic mass fraction (f_{org}) of SMA over the course of the phytoplankton bloom, measured by the HR-TOF-AMS. The mass fraction of organics decreases during the peak of the bloom and then increases during the death phase.

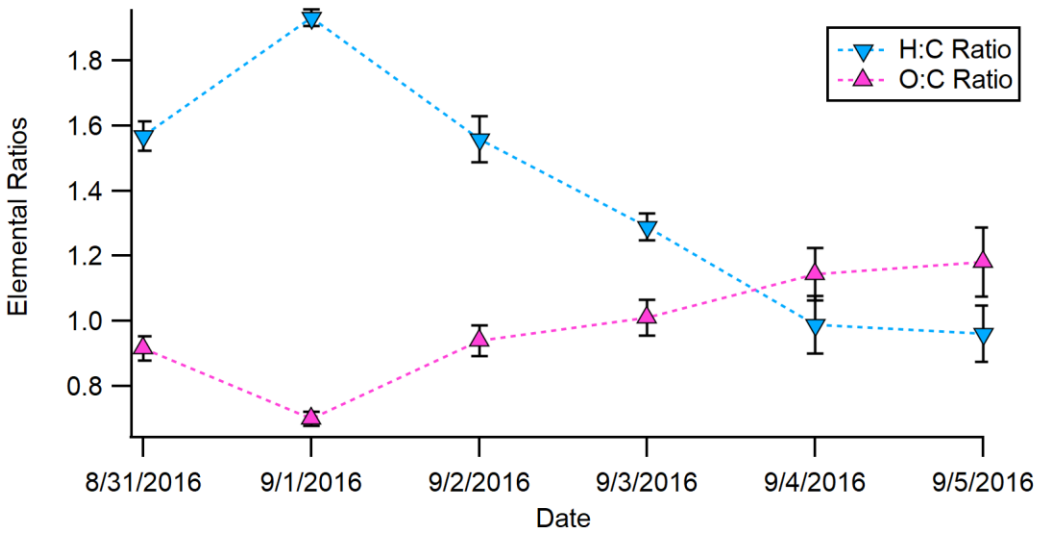

Figure 3.13 Elemental ratios (H/C and O/C) of the organic species in secondary marine aerosol, as measured by HR-TOF-AMS.

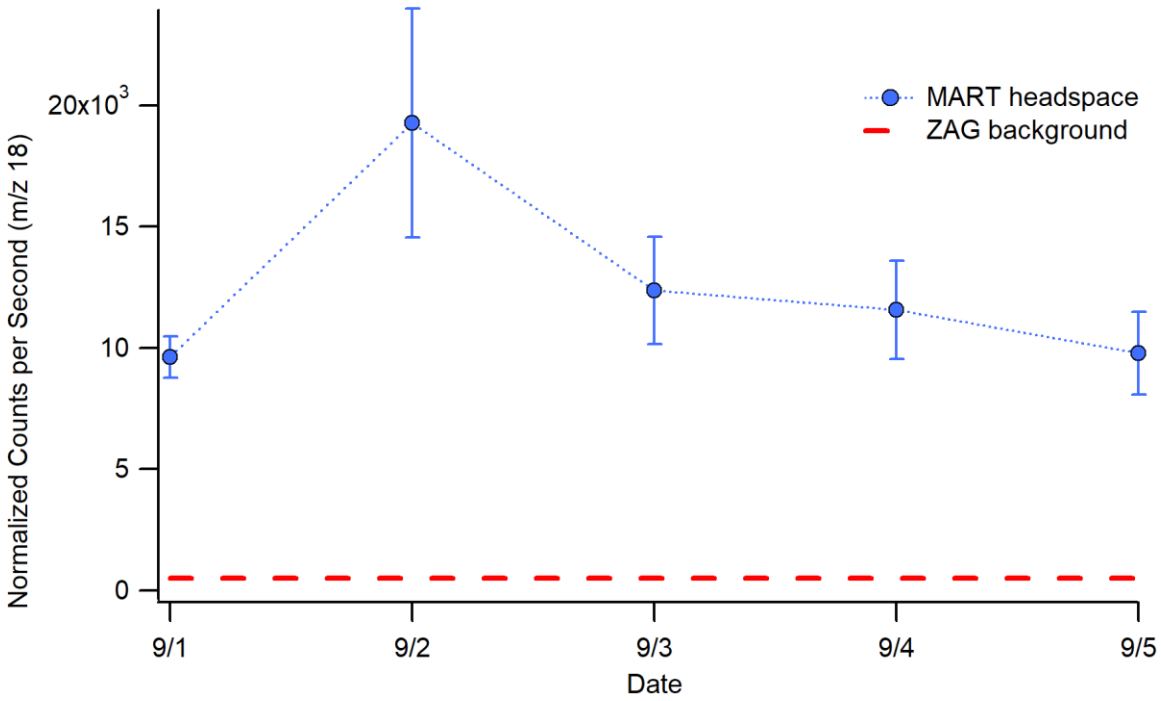

Figure 3.14 Ammonia measurement by CI-TOFMS from the headspace of the MART. The background was measured once prior to the start of the experiment and is shown here as the dashed

3.9 References

Alpert, P. A., Kilthau, W. P., Bothe, D. W., Radway, J. C., Aller, J. Y. and Knopf, D. A.: The influence of marine microbial activities on aerosol production: A laboratory mesocosm study, *J. Geophys. Res. Atmos.*, 120(17), 8841–8860, doi:10.1002/2015JD023469, 2015.

Antoine, D. and Morel, A.: Oceanic primary production: 1. Adaptation of a spectral light-photosynthesis model in view of application to satellite chlorophyll observations, *Global Biogeochem. Cycles*, 10(1), 43–55, doi:10.1029/95GB02831, 1996.

Asmi, E., Frey, A., Virkkula, A., Ehn, M., Manninen, H. E., Timonen, H., Tolonen-Kivimaki, O., Aurela, M., Hillamo, R. and Kulmala, M.: Hygroscopicity and chemical composition of antarctic sub-micrometre aerosol particles and observations of new particle formation, *Atmos. Chem. Phys.*, 10(9), 4253–4271, doi:10.5194/acp-10-4253-2010, 2010.

Ayers, G. P., Ivey, J. P. and Gillett, R. W.: Coherence between seasonal cycles of dimethyl sulphide, methanesulphonate and sulphate in marine air, *Nature*, 349, 404–406, 1991.

Azam, F., Fenchel, T., Field, J., Gray, J., Meyer-Reil, L. and Thingstad, F.: The Ecological Role of Water-Column Microbes in the Sea, Mar. Ecol. Prog. Ser., 10, 257–263, doi:10.3354/meps010257, 1983.

Behrenfeld, M. J. and Falkowski, P. G.: Photosynthetic rates derived from satellite-based chlorophyll concentration, *Limnol. Oceanogr.*, 42(1), 1–20, doi:10.4319/lo.1997.42.1.0001, 1997.

Berresheim, H., Eisele, F. L., Tanner, D. J., McInnes, L. M., Ramseybell, D. C. and Covert, D. S.: Atmospheric Sulfur Chemistry and Cloud Condensation Nuclei (Ccn) Concentrations Over the Northeastern Pacific Coast, *J. Geophys. Res.*, 98(D7), 12701–12711, doi:10.1029/93jd00815, 1993.

Bertram, T. H., Kimmel, J. R., Crisp, T. A., Ryder, O. S., Yatavelli, R. L. N., Thornton, J. A., Cubison, M. J., Gonin, M. and Worsnop, D. R.: A field-deployable, chemical ionization time-of-flight mass spectrometer, *Atmos. Meas. Tech.*, 4(7), 1471–1479, doi:10.5194/amt-4-1471-2011, 2011.

Boucher, O., Randall, D., Artaxo, P., Bretherton, C., Feingold, G., Forster, P., Kerminen, V.-M. V.-M., Kondo, Y., Liao, H., Lohmann, U., Rasch, P., Satheesh, S. K., Sherwood, S., Stevens, B., Zhang, X. Y. and Zhan, X. Y.: Clouds and Aerosols, Clim. Chang. 2013 Phys. Sci. Basis. Contrib. Work. Gr. I to Fifth Assess. Rep. Intergov. Panel Clim. Chang., [Stocker,(Cambridge University Press, Cambridge, United Kingdom and New York, NY, USA), 571–657, doi:10.1017/CBO9781107415324.016, 2013.

Bruns, E. A., El Haddad, I., Keller, A., Klein, F., Kumar, N. K., Pieber, S. M., Corbin, J. C., Slowik, J. G., Brune, W. H., Baltensperger, U. and Prévôt, A. S. H.: Inter-comparison of laboratory smog chamber and flow reactor systems on organic aerosol yield and composition, *Atmos. Meas. Tech.*, 8(6), 2315–2332, doi:10.5194/amt-8-2315-2015, 2015.

Canagaratna, M. R., Jayne, J. T., Jimenez, J. L., Allan, J. D., Alfarra, M. R., Zhang, Q., Onasch, T. B., Drewnick, F., Coe, H., Middlebrook, A., Delia, A., Williams, L. R., Trimborn, A. M., Northway, M. J., DeCarlo, P. F., Kolb, C. E., Davidovits, P. and Worsnop, D. R.: Chemical and microphysical characterization of ambient aerosols with the aerodyne aerosol mass spectrometer, *Mass Spectrom. Rev.*, 26(2), 185–222, doi:10.1002/mas.20115, 2007.

Carslaw, K. S., Lee, L. a, Reddington, C. L., Pringle, K. J., Rap, a, Forster, P. M., Mann, G. W., Spracklen, D. V, Woodhouse, M. T., Regayre, L. a and Pierce, J. R.: Large contribution of natural aerosols to uncertainty in indirect forcing., *Nature*, 503(7474), 67–71, doi:10.1038/nature12674, 2013.

Charlson, R. J., Lovelock, J. E., Andreae, M. O. and Warren, S. G.: Oceanic phytoplankton, atmospheric sulphur, cloud albedo and climate, *Nature*, 326, 655–661, 1987.

Collins, D. B., Bertram, T. H., Sultana, C. M., Lee, C., Axson, J. L. and Prather, K. A.: Phytoplankton blooms weakly influence the cloud forming ability of sea spray aerosol, *Geophys. Res. Lett.*, 9975–9983, doi:10.1002/2016GL069922, 2016.

Decarlo, P. F., Kimmel, J. R., Trimborn, A., Northway, M. J., Jayne, J. T., Aiken, A. C., Gonin, M., Fuhrer, K., Horvath, T., Docherty, K. S., Worsnop, D. R. and Jimenez, J. L.: Field-Deployable, High-Resolution, Time-of-Flight Aerosol Mass Spectrometer, *Anal. Chem.*, 78(24), 8281–8289, doi:8410.1029/2001JD001213.Analytical, 2006.

Erickson, D. J., Ghan, S. J. and Penner, J. E.: Global Ocean-to-Atmosphere Dimethyl Sulfide Flux, *J. Geophys. Res.*, 95(D6), 7543–7552, 1990.

Facchini, M. C., Rinaldi, M., Decesari, S., Carbone, C., Finessi, E., Mircea, M., Fuzzi, S., Ceburnis, D., Flanagan, R., Nilsson, E. D., de Leeuw, G., Martino, M., Woeltjen, J. and O'Dowd, C. D.: Primary submicron marine aerosol dominated by insoluble organic colloids and aggregates, *Geophys. Res. Lett.*, 35(17), 1–5, doi:10.1029/2008GL034210, 2008.

Fitzgerald, J. W.: Marine aerosols: A review, *Atmos. Environ.* Part A, Gen. Top., 25(3–4), 533–545, doi:10.1016/0960-1686(91)90050-H, 1991.

Forestieri, S. D., Moore, K. A., Martinez Borrero, R., Wang, A., Stokes, M. D. and Cappa, C. D.: Temperature and Composition Dependence of Sea Spray Aerosol Production, *Geophys. Res. Lett.*, 45(14), 7218–7225, doi:10.1029/2018GL078193, 2018.

Gaston, C. J., Pratt, K. A., Qin, X. and Prather, K. A.: Real-time detection and mixing state of methanesulfonate in single particles at an inland urban location during a phytoplankton bloom, *Environ. Sci. Technol.*, 44(5), 1566–1572, doi:10.1021/es902069d, 2010.

Gras, L. J. and Keywood, M.: Cloud condensation nuclei over the Southern Ocean: Wind dependence and seasonal cycles, *Atmos. Chem. Phys.*, 17(7), 4419–4432, doi:10.5194/acp-17-4419-2017, 2017.

Guillard, R. R. L. and Ryther, J. H.: Studies of Marine Planktonic Diatoms: I. Cyclotella Nana Hustedt, and Detonula Confervacea (Cleve) Gran, Can. J. Microbiol., 8(2), 229–238, 1962.

Hoffmann, E. H., Tilgner, A., Schrödner, R., Bräuer, P., Wolke, R. and Herrmann, H.: An advanced modeling study on the impacts and atmospheric implications of multiphase dimethyl sulfide chemistry, *Proc. Natl. Acad. Sci.*, 113(42), 11776–11781, doi:10.1073/pnas.1606320113, 2016.

Huang, S., Poulain, L., Van Pinxteren, D., Van Pinxteren, M., Wu, Z., Herrmann, H. and Wiedensohler, A.: Latitudinal and Seasonal Distribution of Particulate MSA over the Atlantic using a Validated Quantification Method with HR-ToF-AMS, *Environ. Sci. Technol.*, 51(1), 418–426, doi:10.1021/acs.est.6b03186, 2017.

Kang, E., Root, M. J. and Brune, W. H.: Introducing the concept of Potential Aerosol Mass (PAM), *Atmos. Chem. Phys*., 7, 5727–5744, https://doi.org/10.5194/acp-7-5727-2007, 2007.

Keller, M. D., Bellows, W. K. and Guillard, R. R. L.: Dimethyl sulfide production in marine phytoplankton., *Biog. Sulfur Environ*., 393, 167–182, 1989.

Kim, M. J., Novak, G. A., Zoerb, M. C., Yang, M., Blomquist, B. W., Huebert, B. J., Cappa, C. D. and Bertram, T. H.: Air-Sea exchange of biogenic volatile organic compounds and the impact on aerosol particle size distributions, *Geophys. Res. Lett.*, 44(8), 3887–3896, doi:10.1002/2017GL072975, 2017.

Knutson, E. O. and Whitby, K. T.: Aerosol classification by electric mobility: apparatus, theory, and applications, J. *Aerosol Sci.*, 6(6), 443–451, doi:10.1016/0021-8502(75)90060-9, 1975.

Koga, S., Nomura, D. and Wada, M.: Variation of dimethylsulfide mixing ratio over the Southern Ocean from 36 S to 70 S, *Polar Sci*., 8(3), 306–313, doi:10.1016/j.polar.2014.04.002, 2014.

Kroll, J. H. and Seinfeld, J. H.: Chemistry of secondary organic aerosol: Formation and evolution of low-volatility organics in the atmosphere, *Atmos. Environ.*, 42(16), 3593–3624, doi:10.1016/j.atmosenv.2008.01.003, 2008.

Kuwata, M., Zorn, S. R. and Martin, S. T.: Using elemental ratios to predict the density of organic material composed of carbon, hydrogen, and oxygen, *Environ. Sci. Technol.*, 46(2), 787–794, doi:10.1021/es202525q, 2012.

Lambe, A. T., Onasch, T. B., Massoli, P., Croasdale, D. R., Wright, J. P., Ahern, A. T., Williams, L. R., Worsnop, D. R., Brune, W. H. and Davidovits, P.: Laboratory studies of the chemical composition and cloud condensation nuclei (CCN) activity of secondary organic aerosol (SOA) and oxidized primary organic aerosol (OPOA), *Atmos. Chem. Phys.*, 11(17), 8913–8928, doi:10.5194/acp-11-8913-2011, 2011.

Lambe, A. T., Chhabra, P. S., Onasch, T. B., Brune, W. H., Hunter, J. F., Kroll, J. H., Cummings, M. J., Brogan, J. F., Parmar, Y., Worsnop, D. R., Kolb, C. E. and Davidovits, P.: Effect of oxidant concentration, exposure time, and seed particles on secondary organic aerosol

chemical composition and yield, *Atmos. Chem. Phys.*, 15(6), 3063–3075, doi:10.5194/acp-15-3063-2015, 2015.

Lana, A., Bell, T. G., Simó, R., Vallina, S. M., Ballabrera-Poy, J., Kettle, A. J., Dachs, J., Bopp, L., Saltzman, E. S., Stefels, J., Johnson, J. E. and Liss, P. S.: An updated climatology of surface dimethlysulfide concentrations and emission fluxes in the global ocean, *Global Biogeochem. Cycles*, 25, 1–17, doi:10.1029/2010GB003850, 2011.

Lee, C., Sultana, C. M., Collins, D. B., Santander, M. V., Axson, J. L., Malfatti, F., Cornwell, G. C., Grandquist, J. R., Deane, G. B., Stokes, M. D., Azam, F., Grassian, V. H. and Prather, K. A.: Advancing Model Systems for Fundamental Laboratory Studies of Sea Spray Aerosol Using the Microbial Loop, *J. Phys. Chem. A.*, 119(33), 8860–8870, doi:10.1021/acs.jpca.5b03488, 2015.

Lee, C. L. and Brimblecombe, P.: Anthropogenic contributions to global carbonyl sulfide, carbon disulfide and organosulfides fluxes, *Earth-Science Rev.*, 160, 1–18, doi:10.1016/j.earscirev.2016.06.005, 2016.

Lewis, E. R. and Schwartz, S. E.: Sea Salt Aerosol Production: Mechanisms, Methods, Measurements, and Models--A Critical Review, American Geophysical Union, Washington D.C., 2004.

Lohmann, U. and Feichter, J.: Global indirect aerosol effects: a review, *Atmos. Chem. Phys.*, 4(6), 7561–7614, doi:10.5194/acpd-4-7561-2004, 2005.

McCoy, D. T., Burrows, S. M., Wood, R., Grosvenor, D. P., Elliott, S. M., Ma, P.-L., Rasch, P. J. and Hartmann, D. L.: Natural aerosols explain seasonal and spatial patterns of Southern Ocean cloud albedo., *Sci. Adv.*, 1(6), e1500157, doi:10.1126/sciadv.1500157, 2015.

Merikanto, J., Spracklen, D. V., Mann, G. W., Pickering, S. J. and Carslaw, K. S.: Impact of nucleation on global CCN, *Atmos. Chem. Phys.*, 9, 8601–8616, doi:10.5194/acpd-9-12999-2009, 2009.

Murphy, D. M., Anderson, J. R., Quinn, P. K., McInnes, L. M., Brechtel, F. J., Kreidenweis, S. M., Middlebrook, A. M., Pósfai, M., Thomson, D. S. and Buseck, P. R.: Influence of sea-salt on aerosol radiative properties in the Southern Ocean marine boundary layer, *Nature*, 392(6671), 62–65, doi:10.1038/32138, 1998.

O'Dowd, C. D. and de Leeuw, G.: Marine aerosol production: a review of the current knowledge, *Philos. Trans. R. Soc. A Math. Phys. Eng. Sci.*, 365(1856), 1753–1774, doi:10.1098/rsta.2007.2043, 2007.

O'Dowd, C. D., Facchini, M. C., Cavalli, F., Ceburnis, D., Mircea, M., Decesari, S., Fuzzi, S., Young, J. Y. and Putaud, J. P.: Biogenically driven organic contribution to marine aerosol, *Nature*, 431(7009), 676–680, doi:10.1038/nature02959, 2004.

O'Reilly, J. E., Maritorena, S., Mitchell, B. G., Siegel, D. A., Carder, K. L., Garver, S. A., Kahru, M. and McClain, C. R.: Ocean color chlorophyll algorithm for SeaWiFS, *J. Geophys. Res.*,

103(Cll), 24937–24953, 1998.

Ovadnevaite, J., Zuend, A., Laaksonen, A., Sanchez, K. J., Roberts, G., Ceburnis, D., Decesari, S., Rinaldi, M., Hodas, N., Facchini, M. C., Seinfeld, J. H. and O' Dowd, C.: Surface tension prevails over solute effect in organic-influenced cloud droplet activation, *Nature*, 546(7660), 637–641, doi:10.1038/nature22806, 2017.

Pandis, S. N., Russell, L. M. and Seinfeld, J. H.: The relationship between DMS flux and CCN concentration in remote marine regions, *J. Geophys. Res.*, 99(D8), 16,945-16,957, 1994.

Peng, Z. and Jimenez, J. L.: Radical chemistry in oxidation flow reactors for atmospheric chemistry research, *Chem. Soc. Rev.*, 49(9), 2570–2616, doi:10.1039/C9CS00766K, 2020.

Petters, M. D. and Kreidenweis, S. M.: A single parameter representation of hygroscopic growth and cloud condensation nucleus activity, *Atmos. Chem. Phys.*, 7, 1961–1971, doi:10.5194/acp-7-1961-2007, 2007.

Prather, K. A, Bertram, T. H., Grassian, V. H., Deane, G. B., Stokes, M. D., Demott, P. J., Aluwihare, L. I., Palenik, B. P., Azam, F., Seinfeld, J. H., Moffet, R. C., Molina, M. J., Cappa, C. D., Geiger, F. M., Roberts, G. C., Russell, L. M., Ault, A. P., Baltrusaitis, J., Collins, D. B., Corrigan, C. E., Cuadra-Rodriguez, L. a, Ebben, C. J., Forestieri, S. D., Guasco, T. L., Hersey, S. P., Kim, M. J., Lambert, W. F., Modini, R. L., Mui, W., Pedler, B. E., Ruppel, M. J., Ryder, O. S., Schoepp, N. G., Sullivan, R. C. and Zhao, D.: Bringing the ocean into the laboratory to probe the chemical complexity of sea spray aerosol., *Proc. Natl. Acad. Sci. U. S. A.*, 110(19), 7550–5, doi:10.1073/pnas.1300262110, 2013.

Quinn, P. K. and Bates, T. S.: The case against climate regulation via oceanic phytoplankton sulphur emissions, *Nature*, 480(7375), 51–56, doi:10.1038/nature10580, 2011.

Rosenfeld, D., Lohmann, U., Raga, G. B., Dowd, C. D. O., Kulmala, M., Fuzzi, S., Reissell, A. and Andreae, M. O.: Flood or Drought : How Do Aerosols Affect Precipitation ?, *Science* (80-.)., 1309(2008), 1309–1314, doi:10.1126/science.1160606, 2014.

Saltzman, E. S., Savoie, D. L., Zika, R. G. and Prospero, J. M.: Methane sulfonic acid in the marine atmosphere (Pacific, Indian Ocean, Miami, Florida)., *J. Geophys. Res.*, 88(C15), 10897–10902, doi:10.1029/JC088iC15p10897, 1983.

Sanchez, K. J., Chen, C. L., Russell, L. M., Betha, R., Liu, J., Price, D. J., Massoli, P., Ziemba, L. D., Crosbie, E. C., Moore, R. H., Müller, M., Schiller, S. A., Wisthaler, A., Lee, A. K. Y., Quinn, P. K., Bates, T. S., Porter, J., Bell, T. G., Saltzman, E. S., Vaillancourt, R. D. and Behrenfeld, M. J.: Substantial Seasonal Contribution of Observed Biogenic Sulfate Particles to Cloud Condensation Nuclei, *Sci. Rep.*, 8(1), 1–14, doi:10.1038/s41598-018-21590-9, 2018.

Schill, S. R., Collins, D. B., Lee, C., Morris, H. S., Novak, G. A., Prather, K. A., Quinn, P. K., Sultana, C. M., Tivanski, A. V., Zimmermann, K., Cappa, C. D. and Bertram, T. H.: The Impact of Aerosol Particle Mixing State on the Hygroscopicity of Sea Spray Aerosol, *ACS Cent. Sci.*, 1(3), 132–141, doi:10.1021/acscentsci.5b00174, 2015.

Sinha, V., Williams, J., Meyerhofer, M., Riebesell, U., Paulino, A. I. and Larsen, A.: Air-sea fluxes of methanol , acetone , acetaldehyde , isoprene and DMS from a Norwegianfjord following a phytoplankton bloom in a mesocosm experiment, *Atmos. Chem. Phys.*, 7, 739–755, 2007.

Stokes, M. D., Deane, G. B., Prather, K., Bertram, T. H., Ruppel, M. J., Ryder, O. S., Brady, J. M. and Zhao, D.: A Marine Aerosol Reference Tank system as a breaking wave analogue for the production of foam and sea-spray aerosols, *Atmos. Meas. Tech.*, 6(4), 1085–1094, doi:10.5194/amt-6-1085-2013, 2013.

Swietlicki, E., Hansson, H. C., Hämeri, K., Svenningsson, B., Massling, A., Mcfiggans, G., Mcmurry, P. H., Petäjä, T., Tunved, P., Gysel, M., Topping, D., Weingartner, E., Baltensperger, U., Rissler, J., Wiedensohler, A. and Kulmala, M.: Hygroscopic properties of submicrometer atmospheric aerosol particles measured with H-TDMA instruments in various environments - A review, *Tellus, Ser. B Chem. Phys. Meteorol*., 60 B(3), 432–469, doi:10.1111/j.1600-0889.2008.00350.x, 2008.

Twomey, S.: Pollution and the planetary albedo, *Atmos. Environ.*, 8(12), 1251–1256, doi:10.1016/0004-6981(74)90004-3, 1974.

Vallina, S. M., Simó, R. and Gassó, S.: What controls CCN seasonality in the Southern Ocean? A statistical analysis based on satellite-derived chlorophyll and CCN and model-estimated OH radical and rainfall, *Global Biogeochem. Cycles*, 20(1), 1–13, doi:10.1029/2005GB002597, 2006.

Virkkula, A., Teinilä, K., Hillamo, R., Kerminen, V. M., Saarikoski, S., Aurela, M., Koponen, I. K. and Kulmala, M.: Chemical size distributions of boundary layer aerosol over the Atlantic Ocean and at an Antarctic site, *J. Geophys. Res. Atmos.*, 111(5), 1–14, doi:10.1029/2004JD004958, 2006.

Willis, M. D., Köllner, F., Burkart, J., Bozem, H., Thomas, J. L., Schneider, J., Aliabadi, A. A., Hoor, P. M., Schulz, H., Herber, A. B., Leaitch, W. R. and Abbatt, J. P. D.: Evidence for marine biogenic influence on summertime Arctic aerosol, *Geophys. Res. Lett.*, 44(12), 6460–6470, doi:10.1002/2017GL073359, 2017.

Zuo, Z.: Why Algae Release Volatile Organic Compounds—The Emission and Roles, *Front. Microbiol*., 10, 491, 2019.

Chapter 4 The Sea Spray Chemistry and Particle Evolution Study (SeaSCAPE): Overview and Experimental Methods

4.1 Abstract

Marine aerosols strongly influence climate through their interactions with solar radiation and clouds. However, the influence of biological activity and seawater chemistry on the flux, chemical composition, and climate-relevant properties of marine aerosols and gases remain poorly constrained. Wave channels, a traditional tool of physical oceanography, have been adapted for large-scale ocean-atmosphere mesocosm experiments in the laboratory. These experiments enable the study of aerosols under controlled conditions which isolate the marine system from anthropogenic and terrestrial influences. Here, we present an overview of the 2019 Sea Spray Chemistry and Particle Evolution (SeaSCAPE) study, which was conducted in an 11,800 L wave channel which has been modified to facilitate atmospheric measurements. The SeaSCAPE campaign sought to understand the influence of biological activity in seawater on the production of primary sea spray aerosols, volatile organic compounds (VOCs), and secondary marine aerosols. Notably, the SeaSCAPE experiment also focused specifically on understanding how photooxidative aging processes transform the marine atmosphere. In addition to a full inventory of aerosol, gas, and seawater measurements, we present key results which highlight the experimental capabilities during the campaign, including the phytoplankton bloom dynamics, VOC production, and the effects of photochemical aging on aerosol production, morphology, and chemical composition. Additionally, we discuss the modifications made to the wave channel and subsequent characterization experiments. The SeaSCAPE experiment provides unique insight into the connections between marine biology, atmospheric chemistry, and climate, and demonstrates

the ocean atmosphere interaction facility's capability to bring the full complexity of the marine atmosphere into the laboratory.

4.1.1 Environmental Significance Statement

The ocean-atmosphere environment is a highly complex system that influences the Earth's radiative balance, cloud formation and precipitation, and air quality, all of which directly impact human health and well-being. Attempts to simulate this system in the laboratory strive to reduce the numerous complicating factors which make understanding this system difficult. Here, we describe the process of utilizing a 11,800 L wave channel towards replicating the ocean atmosphere environment with specific detail paid towards the representative production of sea spray aerosols, marine microbiology, biogenic gases, and secondary marine aerosols. The findings presented herein demonstrate best experimentation practices and uncover new challenges towards replicating and ultimately, understanding the ocean-atmosphere environment.

4.2 Introduction

Oceans cover 71% of the Earth's surface and represent a major source of both aerosols and trace gases, which affect climate, air quality, and human health. Aerosols influence climate directly by absorbing and scattering solar radiation, and indirectly by serving as cloud condensation nuclei (CCN) and ice nucleating particles (INPs), thus controlling the properties of clouds. The interactions between aerosols and clouds represent one of the largest sources of uncertainty in estimates of the Earth's radiative budget (Boucher et al., 2013). Constraining the flux, composition, and cloud-relevant properties of marine aerosols is crucial for understanding their influence on atmospheric processes and predicting future changes in the climate system.

Sea spray aerosol (SSA) is the largest source of atmospheric particles by mass, with a global emission flux of 10.1 $Tg \cdot yr^{-1}$, 98% of which is attributed to supermicron particles (Gong et al., 2002). SSA is produced when breaking waves entrain air bubbles beneath the ocean surface, which rise to the surface and burst. This process produces two types of droplets: film drops from the bursting of the bubble cap and jet drops from the collapse of the bubble cavity (Wang et al., 2017). Measurements of authentic marine aerosols have been traditionally limited to studies performed on research cruises or at remote field stations. More recently, usage of ocean-atmosphere simulators such as wave channels and Marine Aerosol Reference Tanks (MARTs) have brought the complexity of the marine environment into the laboratory (Prather et al., 2013; Stokes et al., 2013, 2016). These experimental systems use breaking waves or plunging waterfalls to produce bubble plumes with the correct size and surface residence time to match bubbles in the real ocean. Subsequent rupturing of these bubbles at the air-sea interface produces SSA that closely resemble the size distribution of SSA observed in the marine environment.

These ocean-atmosphere simulators have been contrasted against other laboratory SSA production devices such as fritted bubblers and found to have several key advantages. While simple in design and application, fritted bubblers tend to produce less accurate aerosol size distributions, resulting in physiochemical discrepancies in morphology and composition (Collins et al., 2014). The utilization of ocean-atmosphere simulators to generate realistic marine aerosols has revealed a large breadth of information (Mayer et al., 2020a). This includes the production of marine ice nucleating particles (INPs); the aerosolization of marine microorganisms; biochemical control of SSA composition by enzymes; biogenic volatile gas production; physical and chemical heterogeneity of SSA; and SSA surface reactivity and uptake properties (Ault et al., 2013a; DeMott et al., 2015; Kim et al., 2015; Michaud et al., 2018; Patterson et al., 2016; Prather et al., 2013;

Ryder et al., 2015; Wang et al., 2015). The further use of these simulators to disentangle the highly complex mechanisms present in the marine environment is being advanced by improvements in their construction and understanding the factors which are relevant for ideal operation.

While many past ocean-atmosphere studies have focused solely on the composition and properties of freshly emitted nascent SSA (nSSA), atmospheric aging processes can transform SSA through reactions with trace gases, oxidants, and sunlight. For example, heterogenous reactions of SSA with HNO_3 has been shown to result in the displacement of HCl, forming $NaNO_3$ (Ault et al., 2013a). In addition to SSA, the oceans are a source of secondary marine aerosol (SMA), which is formed from the reactions of VOCs emitted from seawater. SMA can either form as new particles via nucleation or it can condense onto existing particles in the marine atmosphere, such as SSA, changing their size and chemical composition (O'Dowd and de Leeuw, 2007). However, in field studies, it is extremely difficult to constrain the biological and chemical processes which lead to SMA formation and control its properties. Recently, oxidation flow reactors (OFRs) have been used in the laboratory to simulate both the heterogeneous oxidation of SSA (Trueblood et al., 2019b) and the formation of SMA (Mayer et al., 2020b; Schneider et al., 2019) in laboratory studies of marine mesocosms.

Here we detail the features and usage of a newly constructed wave channel located at the Scripps Institution of Oceanography during a two-month experimental campaign with over 90 participants which focused on the production and measurement of marine aerosols. The Sea Spray Chemistry and Particle Evolution (SeaSCAPE) experiment sought to provide an environment where marine chemistry, microbiology, VOCs, and aerosols could be studied across the ocean-atmosphere interface, under clean, isolated conditions. To enable this, the wave channel was thoroughly studied to optimize the production and collection of SSA and minimize anthropogenic

contamination. These studies informed various modifications to wave channel construction and insights into best practices for operation, while also giving context to future analyses of data collected using this platform. We further outline the scope and scale of the SeaSCAPE experiment, including selected results that demonstrate the types of new discoveries enabled by the mesocosm experiments discussed herein, with an emphasis on the incorporation of atmospheric oxidation processes.

4.3 Methods and Materials

4.3.1 Description of Wave Channel

The Scripps Institution of Oceanography (SIO) wave channel is a 33 m x 0.5 m x 0.8 m (L x W x H) glass channel located inside the Hydraulics Laboratory. When filled to a depth of 0.56 m with seawater, it holds a total water volume of 11,800 L (Figure 4.1). An electromagnetically driven paddle with a surface area of 0.96 m^2 operating at 0.3 Hz with a stroke length of 73 cm generates waves that break just beyond a submerged fiberglass beach located midway down the channel. This beach (2.4 m in length) is positioned at an angle of approximately 16˚ relative to the bottom of the channel. Each breaking wave generates a plume of entrained bubbles with a similar size distribution and residence time as those in the ocean (Prather et al., 2013; Wang et al., 2015). Sampling ports are located both upstream and downstream from the breaking waves (Figure 4.1). A second beach, located at the downstream end of the channel, serves to dissipate residual wave energy. The top of the channel is sealed with acrylic lids, backed by marine-grade plywood for support. A PTFE sheet was suspended from the last lid section to the water surface to prevent backflow of room air into the channel. In addition, the unlidded section of the channel at the end

was draped with lightweight polyethylene film to prevent dust and debris from settling into the channel.

The paddle assembly, including motors, is enclosed within a tent made of flexible PTFE film (TEKFILM, FEP2000E, 0.127 mm in thickness) to seal the system and prevent contamination from the room air, while accommodating pressure fluctuations caused by the reciprocating paddle. Clean, particle-free air was delivered to the wave channel from the top of the tent (Figure 4.1) using a custom air handling system made with galvanized steel duct pipes and stainless-steel connectors to the PTFE tent and the channel. Ambient air pulled in using a custom fan-blade powered by an induction motor (Marathon Electric 5THW8) was filtered through a four-stage filter system (Hydrosil International), consisting of a pre-filter, activated charcoal pellets, potassium permanganate ($KMnO_4$), and a HEPA filter. The scrubbed air was then directed into the wave channel headspace. A condensation particle counter (CPC) positioned upstream of the wave break (Figure 4.1, position 1) was used to continuously monitor background particle counts in the headspace, indicating breakthrough from the filter system as well as leaks in the paddle tent. Headspace concentrations of NO_x, SO_2, and O_3, as well as air velocity, temperature, and relative humidity were also continuously monitored from the same upstream sampling location (see Section 2.5.1).

The wave channel was equipped with fluorescent lights to provide the light flux necessary for photosynthetic organisms to grow in the seawater. Four light fixtures, two on either side, were attached to the outside of each 2 m glass panel of the channel below the water surface. Each fixture was equipped with two 120 cm fluorescent bulbs (Spectra 5700K F32-T8, Full Spectrum Solutions, Inc), giving a total of 8 bulbs per panel. The lights extended the full length of the channel, except for the paddle tank at the front of the channel and the end tank, which are

constructed stainless steel and thus not transparent to light. The flux of photosynthetically active radiation (PAR) in the channel was measured to be ~80 μE/m^{2}s in the center of the channel, approximately ~30 cm below the water surface (Apogee Instruments, MQ-200). While this is significantly lower than typical daytime PAR levels, which often exceed 1,000 μE/m^{2}s on clear days (Bouvet et al., 2002), it is comparable to PAR levels reported in other studies for the purpose of growing marine phytoplankton (Lee et al., 2015). To simulate day/night light cycles, the lights were operated on a timer and turned on for 14 hours during the daytime and off for 10 hours at nighttime.

4.3.2 Wave Channel Characterization Experiments

Control experiments for characterizing the wave channel can be divided into two main types: 1) obtaining minimum background aerosol levels and 2) optimizing the sampling location and depth into the channel headspace. For the control experiments, the wave channel was filled with sand-filtered coastal seawater. This seawater is continually pumped from Ellen Browning Scripps Memorial Pier (Scripps Pier, 32-52'00" N, 117-15’21" W), filtered, and circulated directly into the research buildings at SIO, including the wave channel. As sand-filtration removes most of the large biological species (>1-2 μm) and results in microbiology that differs significantly from the seawater used in mesocosm experiments, this seawater was only used for wave channel characterization and testing.

4.3.2.1 Background Particle Concentrations

Using the flexible PTFE film mentioned above, a box-shaped tent of 244 cm length x 117 cm height x 80 cm depth was fabricated with double heat-sealed edges and housed in a stainless-steel cage over the paddle. The seam between the tent and the wave channel metal body was sealed

using polyester tape (3M 8403, 5 cm diameter). Air velocity through the wave channel headspace was periodically measured using a hot-wire anemometer (TSI 9545-A), inserted at the upstream sampling location approximately 9 m before wave break and 5 cm below the channel lid to minimize the impact of water droplets affecting the measurements.

Total particle counts in the wave channel were measured before and after the wave break with condensation particle counters (Magic CPC, Aerosol Devices Inc). The purpose of the upstream CPC was to detect particle leaks in the paddle tent and the air handling system. Counts were typically very low (< 5 #/cm^3). The downstream CPC measured the total number of particles after the breaking wave. Thus, we assume that the difference between upstream and downstream particle counts is the total number concentration of SSA generated by the breaking wave. During periods when the upstream counts are negligible, we assumed that all the particles measured are SSA generated by wave breaking.

4.3.2.2 Sampling Location Optimization

Aerosol size distributions of nSSA were measured using an Aerodynamic Particle Sizer (APS 3321, TSI Inc) and a Scanning Mobility Particle Sizer (SMPS 3938, TSI Inc) equipped with an X-ray neutralizer (Model 3088, TSI Inc) at various locations downwind of the wave break (5 locations, 60 cm intervals) at 0-10 cm below the channel lid. The induction motor was tuned between 1250 and 2500 rotations per minute (RPM) to optimize the airflow and the total particle number concentration. Particles were dried prior to measurement with a silica diffusion dryer. The electrical mobility diameters (d_m) measured by the SMPS are assumed to be the same as the physical diameter (d_p). The aerodynamic diameters (d_a) measured by the APS were converted to physical diameter using the effective density of sea spray aerosol (ρ_{eff} = 1.8 g·cm^{-3}) (Stokes et al., 2013).

4.3.2.3 Wave Channel Headspace Velocity

Measurements of the wave channel air velocity were obtained by injecting 50 mL of 45 mM dimethyl sulfide (DMS) in methanol into the wave channel headspace at the upstream sampling port. As DMS was carried along the length of the wave channel by the headspace flow, a custom fabricated chemical ionization time of flight mass spectrometer (CI-ToF-MS) drew headspace at 2 slpm from the primary sampling port. The operation of the CI-ToF-MS instrument is described in detail below (Section 2.6.2).

4.3.3 SeaSCAPE Bloom Initiation

4.3.3.1 Wave Channel Cleaning Procedures

The wave channel was cleaned and sanitized prior to all experiments and induced bloom measurements. The channel was first filled and flushed with fresh tap water to remove any large debris, then the inside walls were sprayed with a 3% acetic acid/water mixture. A combination of soft sponges and brushes were used to manually remove any film or debris from the inner walls. Once completed, the channel was flushed with fresh water to remove all of the cleaning solution. As a final rinse, the channel was filled with sand-filtered seawater, then drained and allowed to dry.

4.3.3.2 Water Collection

Seawater was collected from the Scripps Pier. The water is pumped up from the end of the pier and travels through a gravity flume on the south side of the pier to the pier entrance. During the pumping process, the seawater passed through a rough aluminum screen to collect large marine detritus such as seaweed. A submersible pump (Grundfos UNILIFT AP12.40.04.A1) was placed into the gravity flume, and water was pumped through a hose into 1,135 L plastic tanks and transported to the wave channel by truck immediately after filling at the Scripps Pier. The seawater

was further filtered to remove large particulates and zooplankton using an acid-clean 50-mm Nitex nylon mesh (Flystuff; Cat # 57-106) and pumped into the wave channel. During Blooms 1 and 2, the Nitex mesh was attached directly to the outlet submersible pump, which inadvertently created shear forces which damaged some of the more delicate microorganisms in the seawater. To improve the seawater collection procedure, a gravity filtration system was used during Bloom 3. Briefly, a stainless-steel frame was built to fit over the top of the wave channel, to which a sheet of Nitex mesh with a surface area of ~0.5 m^2 was affixed. Seawater was poured over the frame, allowing it to gently filter through the mesh.

4.3.3.3 Bloom Initiation

Algae growth media and sodium metasilicate was added to the seawater at the beginning of each bloom cycle to promote phytoplankton growth (Guillard and Ryther, 1962). The dates and concentrations of the nutrient additions are summarized in Table 4.1. The growth media was added at two locations: the upstream sampling ports (Figure 4.1, Location 1) and after the end of the lid sections (Figure 4.1, Location 4). Both the growth media and silicates were dissolved into several liters of milliQ H_2O, then slowly added dropwise to the channel using a sterilized separatory funnel or polycarbonate carboy equipped with a spigot over the course of several hours. This slow nutrient addition allows the growth media to mix with the seawater in the channel and prevents compounds from precipitating out of solution due to the high salinity.

During the third bloom cycle, a separate phytoplankton bloom was grown in a 1,135 L cylindrical plastic tank outside of the hydraulics laboratory. The purpose of this was to inoculate the wave channel with healthy phytoplankton biomass grown under natural sunlight to promote a larger bloom. Seawater was collected from Scripps Pier and filtered using 50-μm Nitex mesh, then it was transferred to the 1,135 L outdoor tank, covered with wire mesh to keep out debris, and

placed in partial shade. To stimulate the growth of a phytoplankton bloom, f/2 growth media and sodium metasilicate were added immediately and the seawater was bubbled gently to oxygenate. Once the outdoor tank reached the exponential growth phase as indicated by *in vivo* fluorescence measurements (AquaFluor, Turner Designs), 1,135 L of water were drained from the wave channel, and the contents of the tank were added to the wave channel. Water was transferred gently using sanitized buckets to avoid damaging the phytoplankton during the transfer. Additional nutrients were added to the wave channel immediately following the outdoor tank addition to bring the total concentration of growth media and silicates up to f/2 in the wave channel.

4.3.4 OFR Experiments

4.3.4.1 Description of Isolated Sampling Vessel

Due to challenges associated with removing all trace gases from both the air handler and off-gassing from wave channel materials, an isolated headspace was used to sample VOCs produced from seawater. The isolated sampling vessel (ISV) was constructed from a single cylindrical tube of borosilicate glass (Greatglas, Delaware U.S.A.). The dimensions of the glass tube were as follows: 400 mm outer diameter, 6 mm wall thickness, 74 cm long, resulting in a total volume of 87 L and a water volume of 44 L, when filled halfway with seawater. An annotated schematic of the ISV can be found in Figure 4.12. Each end of the ISV was sealed by a PTFE disk, thickness 1.6 mm, braced against the face of the cylinder by a 9.5 mm acrylic disk and backed by an aluminum frame. Six 6.4 mm stainless steel Swagelok bulkhead ports in the headspace partition were used for the zero air inlet and gas sampling outlets (located on opposite ends), with one 13 mm bulkhead to continuously pump seawater and a 25 mm bulkhead drain port located 13 mm above the center of a PTFE sealing plate opposite of the filling bulkhead.

Seawater was delivered to the ISV via a plunging stream located opposite the sampling ports. The seawater was circulated using a peristaltic pump equipped with Tygon tubing, which withdrew water from the wave channel, ~0.5 m beneath the water surface. In order to maintain a consistent flow rates and prevent leaks, the tubing within the peristaltic pump was adjusted every 6-8 hours and replaced every 3 days. ISV water drained back into the channel through 25 mm tubing attached to the large central port opposite the plunging jet, with the end of the return flow tubing submerged beneath the water level. Zero air flow rate through ISV headspace varied from 8-10 standard liters per minute (slpm), leading to an average air residence time of 5 minutes. The water flow rate was fixed at 1.5 slpm, leading to a water residence time of 29 minutes. The ISV was lit by two fluorescent light fixtures, which extended the length of the vessel on either side.

4.3.4.2 OFR Operation

To study the effect of atmospheric aging processes on marine aerosols, potential aerosol mass oxidation flow reactors (PAM-OFR, Aerodyne Inc) were used to simulate both the heterogeneous oxidation of primary sea spray aerosol and the formation of secondary marine aerosol from the oxidation of VOCs. The PAM-OFR uses UV lamps to produce high concentrations of OH radical, simulating atmospheric aging from days to weeks, with a residence time of 1-3 minutes (Kang et al., 2007; Lambe et al., 2011). Two OFRs (OFR1 and OFR2) sampled from the wave channel headspace at sampling port #2, with the goal of producing heterogeneously aged SSA (hetSSA), although SMA is also produced from the oxidation of VOCs in the wave channel headspace. A third OFR (OFR3) sampled from the ISV (Figure 4.1), for the purpose of producing SMA under the cleanest possible conditions.

All OFRs were operated in OFR185 mode, meaning the UV lamps produce light with wavelengths of both 185 nm and 254 nm. The OH exposure at each lamp intensity was determined

by introducing carbon monoxide to the OFR and measuring the drop in CO concentration due to oxidation using a CO analyzer (APMA-370, Horiba Ltd). The OH exposure is determined using the rate coefficient of CO + OH ($k_{OH + CO, 298K} = 1.5\times10^{-13}$ cm^3 $molec^{-1}$ s^{-1}), assuming pseudo-first order kinetics (Chen and Marcus, 2006). The OH exposure can be converted to "days of equivalent aging" using typical tropospheric OH concentrations ([OH] = 1.0×10^6 molec·cm^{-3}) (Wolfe et al., 2019). O_3 concentrations were monitored downstream of each of the OFRs using an O_3 analyzer (Model 202 and Model 106-L, 2B Technologies). Before aerosol measurements, the sample air was passed through a denuder to remove O_3 (Carulite-200, obtained from Ozone Solutions).

4.3.5 SeaSCAPE – Aerosol Measurements

A large suite of aerosol measurements was conducted during the SeaSCAPE experiment to study the properties of nSSA, hetSSA, and SMA. These include measurements of the size distributions, chemical composition, INP characteristics, CCN activity and water uptake, and phase state and morphology, among other properties. All measurements conducted during the campaign are summarized in Table 4.2 and Table 4.3.

4.3.5.1 Aerosol Number and Size Distributions

Total particle counts in the wave channel were measured before and after the wave break with condensation particle counters. The aerosol size distributions of nSSA after the wave break was measured using the APS and SMPS as described in the control experiment. Size distributions from OFR1 and OFR2, which includes both hetSSA and SMA, were measured using a Scanning Electrical Mobility Spectrometer (SEMS, Brechtel Manufacturing, Inc) and an APS (3321, TSI Inc). SMA size distributions from OFR3 were measured using an SMPS (Model 3938, TSI Inc) equipped with a Nano DMA (DMA 3085, TSI Inc) and a soft X-ray Neutralizer (Model 3088, TSI Inc).

4.3.5.2 Single Particle Atomic Force Microscopy (AFM) Measurements

Nascent and heterogeneously aged sea spray aerosols were collected for AFM measurements of aerosol phase and morphology throughout SeaSCAPE. Here we show a selected analysis of particles collected on 8/3/19, which corresponded to the peak of the phytoplankton growth during Bloom 3 (Figure 4.2). The nSSA were deposited onto hydrophobically treated silicon substrates (Ted Pella, Inc.) using a micro-orifice uniform deposit impactor (MOUDI, MSP, Inc., model 110) at ca. 80% RH (i.e. wet deposition). The hetSSA were deposited onto the hydrophobically treated silicon substrates using a separate MOUDI (MSP, Inc., model 125R) at ca. 20% RH (i.e. dry deposition) (Lee et al., 2019, 2020a). MOUDI stages 6, 7 and 8 were used, which corresponds to an aerosol aerodynamic diameter 50% cut off range of 0.18-1.0 μm. The hetSSA were generated using OFR2, with a UV lamp voltage of 2.0 V which corresponds to approximately 4-5 days of photochemical aging in the atmosphere. The substrate-deposited nascent and hetSSA samples were stored in clean Petri dishes and kept inside a laminar flow hood (NuAire, Inc., NU-425-400) at ambient temperature (20−25°C) and pressure.

AFM height images of individual nascent and hetSSA particles were recorded using the molecular force probe 3D AFM (Asylum Research, Santa Barbara, CA), at ambient temperature (20−25°C) and pressure. Silicon nitride AFM tips (MikroMasch, Model NSC35, tip radius of curvature ~10 nm) were used to image individual particles. A custom-made humidity cell was used to control the RH at 50% for all imaging; the elevated RH was used due to expected lowering of the viscosity for the organic components relative to inorganic that facilitates differentiation of their spatial distribution using AFM. AC mode AFM was used to image individual particles and determine their morphology. A total of 50 individual particles were characterized for each sample type.

4.3.5.3 Aerosol Mass Spectrometry (AMS)

The chemical composition of submicron non-refractory aerosol was determined by high resolution time-of-flight aerosol mass spectrometry (HR-TOF-AMS; Aerodyne, Inc.) (DeCarlo et al., 2006). The AMS was operated in V-mode with standard MS mode (5s open, 5s closed) and PTOF (10s) with typically 5-min sampling averages.

4.3.6 SeaSCAPE – Gas-phase Measurements

In addition to the gas-phase measurements discussed below, Table 4.4 details the full inventory of gas-phase measurements conducted during SeaSCAPE to assess questions regarding VOCs produced from seawater and anthropogenic contaminants.

4.3.6.1 Trace Inorganic Gases

The concentrations of trace gases were monitored at several locations: the air handling system, room air, and the wave channel headspace, upstream of the wave break. A custom-fabricated solenoid valve switching array was used to automatically switch between the different air sampling lines. The concentrations of the oxides of nitrogen (NOx) were continuously monitored using a Model 42C NO-NO_2-NOx analyzer (Thermo Electron Corporation). Ozone concentrations were measured using a UV photometric based O_3 analyzer (Model 49C, Thermo Electron Corporation). The analyzer was calibrated using an ozone calibration source (Model 306, 2B Technologies). Sulfur dioxide concentrations were measured using a pulsed fluorescence SO_2 analyzer (Model 43iQ Trace Level SO_2 Analyzer, Thermo Electron Corporation).

4.3.6.2 Chemical Ionization Time of Flight Mass Spectrometry

CI-ToF-MS has been previously described by others, briefly, ~300 ppm benzene vapor was generated by passing 10 standard cubic centimeters per second (sccm) of N_2 over a cylinder of liquid benzene and diluted to concentration with added N_2 (Kercher et al., 2009; Kim et al., 2016;

Lavi et al., 2018). Benzene vapor was passed through a 20mCi Po-210 α-source, and further drawn through an inline critical orifice at 1.8 slpm into the ion-molecule region (IMR) of the CI-ToF-MS. Sample analyte was similarly drawn into the IMR at the same flow rate as analyte. The IMR pressure was maintained at 60 Torr and 60 V for all analyses. Analyte ions generated through charge transfer and ligand switch reactions with benzene cluster cations were further focused by a radio frequency ion funnel, and subsequently transferred by an RF-only quadrupole into an orthogonal-extraction time of flight analyzer (Tofwerk). Co-summed mass spectra from 5-500 m/z were obtained at 1 Hz, with generated data analyzed using the Tofware plugin for Igor Pro 7 software.

4.3.6.3 Proton Transfer Reaction Mass Spectrometry

A Vocus proton transfer reaction time-of-flight mass spectrometer (PTR-ToF-MS) (TOFWERK, Aerodyne Inc.) measured headspace gas-phase VOCs (Krechmer et al., 2018). The focusing ion-molecule reactor was operated at high reduced field strength (E/N = 143 Td). It was held at a pressure of 1.5 mbar, electric field of 41.5 V cm^{-1}, and temperature of 100 °C. The big segmented quadrupole voltage was 275 V, reducing the transmission of low mass (<35 m/Q) ions. The PTR-ToF-MS mass spectra were saved at 1 Hz time resolution. The headspace of the ISV was sampled at 100 sccm through a roughly 2.5 m, 6.35 mm O.D. PFA tube. The air handling system and wave channel headspace were pulled down a 9.525 mm O.D. PFA tube approximately ~15 m at a flow rate of 8 slpm. The PTR-ToF-MS subsampled 100 sccm of this flow. Room air was sampled intermittently approximately 8 times throughout the day. Instrument background signals were determined about 8 times daily by overflowing the PTR-ToF-MS inlet with zero air from the zero-air generator (Sabio 1001) that provided air to the ISV headspace. Daily average background

signals were used for background correction. Peak fitting and integration were completed in Tofware 3.1.2.

4.3.6.4 Offline Atmospheric Pressure Chemical Ionization for Irradiation Experiments

A high resolution Orbitrap Elite (ThermoFisher) mass spectrometer equipped with a modified gas-phase atmospheric pressure chemical ionization (APCI) source was used to detect VOCs from the surface of collected water during the SeaSCAPE campaign (Roveretto et al., 2019) upon irradiation using an LCS-100 solar simulator (94011A, Oriel). Data was collected solely in positive mode, where needle voltage was set to 4 kV, needle current at 5 mA, and vaporizer temperature at 150 °C. Sheath and auxiliary flow were set to zero. An AM1.5G and water filter were used to simulate the solar spectrum and block infrared radiation, respectively. From the wave channel, 200 mL of surface water was collected and transferred into a 350 mL jacketed custom glass tube (Ace Glass Inc.) with quartz windows on each end. The surface area of the water sample in the tube was approximately 77 cm^2. With a headspace of 150 mL, pure nitrogen gas was used as a carrier at a rate of 200 sccm. Temperature was regulated and measured constantly to ensure minimal thermal variation (± 1°C) during the experiment. The collected water settled for 2 hours before being irradiated to allow a stable surface layer to form. To verify whether the immediate spike in signal was abiotic or biotic in nature when under lighted conditions, a separate experiment using the same water, but filtered with a 0.2 μm GTTP filter (MilliporeSigma), was shown to not be able to remove the signal spike seen in Figure 4.10a.

4.3.7 SeaSCAPE – Water Measurements

The seawater measurements sought to characterize both the biotic and abiotic drivers of marine particles and gases, including nutrient availability, organic chemical composition,

biological speciation, biological productivity, dissolved gas turnover and other important factors. Table 4.5 lists the seawater and sea surface microlayer (SSML) measurements made through the duration of SeaSCAPE.

4.3.7.1 Bulk Seawater Sampling

Bulk seawater was sampled daily for the following analyses: dissolved organic carbon (DOC); inorganic nutrients; extracted chl-a; bacterial and viral abundances; phytoplankton identification; enzyme measurements; 16S and 18S rDNA amplicon sequencing; and tandem mass spectrometry (MS/MS) based metabolomics. Seawater was collected using a ~2 m long siphon constructed from Teflon tubing. Nalgene carboys were used to transport and dispense the collected seawater for analysis. Both the siphon and the carboys were rinsed with methanol, 70% ethanol, 0.1 M HCl solution, and ultra-purified water prior to water collection. The siphon was inserted near the end of the channel before the second beach (Figure 4.1) approximately 20 cm below the surface of the water. Approximately 16 L of bulk seawater were collected daily around 09:30 PST. The volume of collected seawater was replenished by adding a corresponding volume of Milli-Q (Millipore) water (<18 μΩ) every other day to maintain the water level in the flume without introducing any microbiological contaminants.

4.3.7.2 Sea Surface Microlayer Sampling

Sea surface microlayer (SSML) sample collection was conducted using a glass plate, a glass funnel and a Teflon scraper. During the day preceding collection of SSML samples, the glass plate and funnel were cleaned of biological material using Millipore water, methanol, 70% ethanol, and 10% HCl. The collection glassware was placed in a combustion furnace for 5 hours at 500 ˚C to remove organic contaminants. The glass plate with a handle was lowered carefully into the wave channel at a rate of 5-6 cm s^{-1} and withdrawn at the same rate. This withdrawal rate corresponds

to an estimated sampled SSML thickness of around 50 µm (Carlson, 1982; Cunliffe and Wurl, 2015). After removal from the wave channel, the glass plate was suspended for 20 seconds to allow any bulk seawater to drain off the plate and back into the channel, ensuring that the majority of remaining material was SSML. The remaining liquid was scraped from the glass plate into a collection vessel using a Teflon scraper. This process was repeated until approximately 200 mL of sample was collected.

4.3.7.3 DOM Extraction and Compositional Analysis

Dissolved organic matter (DOM) extracted from samples collected from the wave channel were done using the solid phase extraction method described and characterized by Dittmar and coworkers (Dittmar 2008). At the end of Bloom 3, a large volume of about 2,000 L was extracted over the course of 72 hours using this method. A total of 1.51 ± 0.01 g of marine DOM was collected and stored at –18 °C for future analyses.

Samples of extracted DOM were analyzed by TD-GCxGC-EI-HR-ToF-MS (Worton et al., 2017). DOM samples were reconstituted in methanol immediately prior to analysis and injected onto quartz fiber filter segments, then doped with a custom blend of 23 deuterated internal standard compounds prior to analysis, allowing corrections for instrument condition and matrix effects across samples. Briefly, the instrument thermally desorbs samples from the filter media, then introduces them into the GC oven. The instrument employs online derivatization during thermal desorption with MSTFA (n-methyl-n-trimethylsilyl-trifluoro-acetamide), which replaces OH groups with O-($Si(CH_3)_3$) to enhance recovery of polar organics. Next, analytes are separated by both volatility and polarity by two GC columns in sequence. Separated analytes from are ionized by 70 eV electron ionization (EI) and detected by HR-ToF-MS (Tofwerk), acquired at 100 Hz with a resolving power 4000. This method generates a 2D image of compounds separated in GCxGC

space, with each separated analyte characterized by a 70 eV EI mass spectral "fingerprint" Methodological details and documentation can be found in Worton et al. 2017, and thermal desorption unit and gas chromatography methods, component manufacturers, and column materials for both GCxGC instruments may be found in supplemental information. Six-point calibration curves of custom standard blends containing ~150 representative organic compounds were performed periodically throughout sample analysis for each sample medium class to maximize quantification accuracy.

4.3.7.4 Chlorophyll-a, Dissolved Oxygen, and DOC Measurements

A continuous time series of *in vivo* chl-a and dissolved oxygen was measured throughout all three wave channel experiments using an Environmental Sample Processor (ESP). The ESP was located at the back of the wave channel just behind the seawater sampling section (Figure 4.1). The ESP is a homemade, continuous flow system that pumps seawater through tubing at a flow rate around 1 lpm using a peristaltic pump. The seawater first passed an SBE 37 MicroCAT that measures conductivity, followed by an SBE 63 optical dissolved oxygen sensor before being deposited into a reservoir. In the reservoir, chl-a is quantified through fluorescence measurements using a Sea Bird Scientific ECO-Triplet-BBFL2 sensor at excitation/emission wavelengths of 470/695 nm. After measurement of chl-a, the seawater is circulated out of the ESP and back into the wave channel.

Each morning, the ESP was rinsed by circulating Millipore water through the tubing for 20 minutes, and every fourth day, solutions of 0.1% bleach, 30% ethanol, and Millipore water were sequentially circulated through the tubing for 20 minutes to thoroughly clean the instrument. This helped prevent biological growth in the tubing and biofouling of the optics. Additionally, in between each experiment, the reservoir was removed from the laser optics and both were carefully

wiped with 70% EtOH. Any ESP measurement periods that were affected by instrument maintenance or biofouling were corrected using *in vivo* chl-a measurements made by a hand-held fluorometer (AquaFluor, Turner Designs). AquaFluor chl-a measurements were made every few hours from the seawater sampling section of the wave channel.

To calibrate both the ESP and AquaFluor chl-a measurements, chl-a was extracted from the bulk seawater and analyzed by fluorometric analysis in accordance with CALCOFI methods (Holm-Hansen et al., 1965). The seawater was collected once daily from the wave channel (as described in Section 2.7.1) and filtered on 25 mm Whatman GF/F filters. The filters were then submerged in 8 mL of 90 % acetone for 24 hours at -20 ˚C to extract the chl-a. Concentrations of the extracted chl-a were determined by a calibrated fluorometer (10AU, Turner Designs). The extracted chl-a measurements were separately plotted against both the ESP and AquaFluor data, and each plot was fitted with a least squares regression used to calibrate the ESP and AquaFluor chl-a values. A continuous time series of the calibrated ESP chl-a data for all three experiments is shown in Figure 4.2.

For DOC measurements, two 40 mL aliquots of the bulk seawater (see Section 2.7.1 for details of water collection) were filtered into combusted glass vials through a Whatman GF/F filter with a 0.7 µm pore size. Functionally this implies that the DOC was comprised of OC with diameters <0.7 µm. The vacuum filtration was carried out using a hand pump to minimize cell lysis during filtration. The DOC samples were immediately acidified to pH ~2 with three drops of concentrated HCl and stored in a covered box at room temperature until analysis. All DOC concentration measurements were made on a Shimadzu TOC-V_{CSH} catalytic combustion oxidation instrument.

4.3.7.5 Phytoplankton Enumeration and Photography

In order to determine the taxonomic composition of the mesocosm, two methods were employed: 1) Whole seawater samples were collected and manually counted under confocal microscopy; 2) A dual version of the Scripps Plankton Camera System (SPCS: https://spc.ucsd.edu) was placed on the bottom of the wave channel to continuously image the developing plankton community for *in situ* observations. The SPCS was positioned at the downstream end of the channel, just in front of the dampening beach (Figure 4.1). For the manual counting method, 400 mL of seawater was collected from approximately 30 cm depth at both ends of the wave channel. Samples were taken twice per day with Teflon tubing and poured gently into amber Nalgene bottles. Samples were immediately fixed with a 2% buffered formalin solution and stored at 6 °C to preserve samples for enumeration. From these, 50 mL subsamples were then poured into a settlement chamber and allowed to settle for 24 hrs. The cells were prepared for enumeration using the Utermöhl method under an Olympus IX-71 inverted microscope (Utermöhl, 1931). Samples from the settlement chamber were counted to calculate the cell concentrations per L for each distinct species. Then, the taxa cell counts were binned into functional phytoplankton types, including a microzooplankton group. These bins were used to calculate the relative abundance of the functional groups over time and were then compared to the *in-situ* camera data.

The *in-situ* camera enabled the research team to study the plankton community undisturbed in the mesocosm, monitor the presence of delicate taxa, and observe intra- and inter-species interactions. The goal of the image analysis was to target detritus, aggregates, phytoplankton and zooplankton between 20-1000 µm in major axis length. For this reason, only images collected by the 5x magnification system of the SPCS were considered. Over the course of the 3-week experiment, nearly 1.85×10^6 images of particles were collected within this size range. The system

uses darkfield illumination to image free-floating particles in approximately 3 µL/frame sampling volume with a resolution of 3-5 µm (Orenstein et al., 2020). In order to train a neural net to classify this large amount of data, a subset of the images was manually labelled to serve as a training set.

4.3.7.6 Bacteria, Virus, and Phytoplankton Enumeration

Seawater, SSML and nSSA samples were run with a BD FACSCanto II™ flow cytometer (FCM, bacteria, cyanobacteria and viruses). Samples were prepared according to the protocols for bacteria (heterotrophic and autotrophic) and viral enumeration (Brussaard, 2004; Gasol and Del Giorgio, 2000; Marie et al., 1997). All samples were preserved with glutaraldehyde at 5% final concentration and stored at -80°C after flash freezing (Noble and Fuhrman, 1998). For heterotrophic bacteria staining: water was diluted (1:10) in 1×TE buffer (pH 8), then stained with SYBR Green I at RT for 10 min in the dark (Gasol and Del Giorgio, 2000). For virus staining, water was diluted (1:50) in 1×TE buffer (pH 8) and stained with SYBR Green I at 80°C and incubated for 10 min in the dark (Brussaard, 2004). Aliquots of seawater and SSML samples were analyzed unstained for the counting *Cyanobacteria*, namely *Synechococcus* (Olson et al., 1990).

SSA samples were collected into 0.7 mL 4X PGE (prepared as 4x PBS, 20% glycerol, 20 mM EDTA) buffer using a Liquid Spot Sampler (SS110A, Aerosol Devices Inc), which sampled at 1.8 slpm for 4-6 hours (Hering et al., 2014). The liquid sample was brought to 1 mL by adding 4XPGE, then split into two 0.5 mL aliquots that were processed as described above for FCM counting of heterotrophic bacteria and viruses. SSA blank samples were also collected via Spot Sampler with a HEPA filter on the inlet and processed accordingly. The values counted in the same SSA blank gates were subtracted from the SSA sample runs. For heterotrophic bacteria and viruses, the samples were analyzed at medium rate (60 µL min^{-1}) with a threshold set on green fluorescence. Side scatter versus green fluorescence plots were generated to identify and quantify

heterotrophic bacterial and viral populations (Marie et al., 1997). *Synechococcus* population were identified on forward scatter versus orange fluorescence and red fluorescence (Olson et al., 1990). Samples for nano, picophytoplankton and heterotrophic nanoflagellates were run on a BD Accuri FCM following established protocols (Christaki et al., 2011a; Marie et al., 2014).

4.4 Results: Characterization and Optimization of the Wave Channel

4.4.1 Wave Channel Headspace Gas Composition

Volatile organic compounds were measured in the wave channel headspace, air handling system, ISV, and room air, with PTR-ToF-MS to determine whether they originate from a marine biogenic source or anthropogenic contamination (Figure 4.3). Dimethyl sulfide (DMS) and methanethiol (MeSH) were chosen as proxies for expected marine biogenic VOCs in comparison to benzene and toluene which are more closely associated with anthropogenic pollutants and are not expected to be produced biogenically in large quantities in the marine environment (Wakeham et al., 1986). Figure 4.3 shows that benzene and toluene were most elevated in room air, the air handling system, and the wave channel headspace, but were significantly diminished in the ISV. These results suggest that the primary source of benzene and toluene in the wave channel was not derived from the seawater, but likely as breakthrough of the air handling system and possible off-gassing of building materials in the wave channel. Conversely, the concentrations of DMS and MeSH in the ISV were significantly elevated compared to the wave channel, due to the ratio of water to the renewal rate of the headspace in the ISV which was much higher than that of the wave channel. These results show that the ISV was effective in maintaining a clean headspace that better reflects the emissions of gases present in seawater without including anthropogenic gases introduced into the wave channel headspace.

4.4.2 Wave Channel Headspace Velocity

Given the unique aspects of the wave channel, which features a highly longitudinal construction, with air introduction at one side, and a propagating water wave inside, a short investigation undertaken to determine the headspace flow velocity along the channel length using spikes of injected DMS at the upstream port. Shown in Figure 4.4 is the arrival of DMS spikes at the downstream sampling port measured by CI-ToF-MS. Mean arrival time was 200 seconds, with a standard deviation of 35 seconds (N=3) with the paddle running. Replicate experiments with the paddle stationary did not yield arrival times that significantly differed (Figure 4.4). Given the distance of the upstream sampling port from the downstream ports, the wave channel headspace velocity was calculated to be 4.9-7.0 cm/second. This contrasts with measurements from the hot wire anemometer, which describe a velocity range from 32-35 cm/s. The disagreement between these two measurement techniques may be due to the operation of the hot wire anemometer near the lower boundary of its dynamic range, in combination with gas turbulence induced by the waves as they passed through the channel. In addition, while the CI-ToF-MS measurement obtains a flow velocity that reflects an average of the velocity throughout the wave channel length between the upstream and downstream sampling ports, the velocity measurement by the hot wire anemometer was only performed at the upstream location. These results further suggest that significant variability in flow conditions occur along the length of the wave channel and merit further investigation.

4.4.3 Characterization of Particle Backgrounds and SSA Production

Background particle concentrations were measured in the wave channel headspace at the upstream sampling port (Figure 4.1, Location 1) using a CPC to determine the contribution of non-marine particles from sources such as leaks in the paddle tent or breakthrough in the air handling

system while the waves were being generated. Setting the RPM of the induction motor that supplied clean air to the wave channel to a speed less than 1500 RPM introduced ambient non-marine particles into the wave channel headspace (10-50x more), thus establishing a lower limit of the air handling unit. While increasing the speed of the motor could increase the amount of clean air into the headspace of the wave channel, doing so dilutes the total number of SSA from wave breaking, thus our testing found that 1500 RPM was the optimal setting (Figure 5a).

With the optimized setting of the air handling unit, these background particle concentrations were generally low (~3 #/cm^3, Figure 4.8), indicating that the wave channel headspace was quite clean, with respect to ambient particulate contamination (~10,000 #/ cm^3). In comparison, the average particle concentrations after the breaking wave were significantly higher (242 ± 91 #/ cm^3), indicating that the vast majority (>98%) of the particles sampled downwind of the breaking wave were sea spray aerosols produced in the wave channel.

With the air handling unit and the background optimized, the next step was to optimize the sampling location for SSA downwind of the breaking waves. Five locations at 0 cm, 60 cm, 120 cm, 180 cm, and 240 cm downwind of the breaking wave were tested. The APS and SMPS size distributions were used to calculate the total SSA number at each location. Figure 5b shows that position 4, which corresponds to 180 cm downwind of the breaking waves, had the highest SSA number concentrations. The continuous water and air flows pushed the entrained air bubbles and the generated SSA downwind of the breaking wave (Lewis and Schwartz, 2004; Prather et al., 2013). In addition to sampling location, the sampling port (1.27 cm i.d.) depth was tested from 0 cm to 10 cm into the headspace. While the specific relationship between port depth and SSA number concentration varied with sampling location, at position 4, a port depth of 5 cm yielded the highest values. However, lack of clear trend in the total number concentration as a function of

sampling location and depth indicates that there may be heterogeneous mixing within the wave channel headspace due to flow turbulence. In addition, factors such as wall losses and gravitational deposition of particles may have influenced the variability in particle numbers over time. It was observed during testing that port depths of 10 cm or greater were prone to splashing by the breaking waves, resulting in excess water being pulled into the sampling lines. Similarly, a port depth of 0 cm (flush with the lid surface) resulted in condensation from the lids being pulled into the sampling lines. Thus, from an operational standpoint, it is a sampling port depth of 2-8 cm is ideal to minimize the introduction of water droplets to the sampling lines.

4.5 Results from the SeaSCAPE Experiment

4.5.1 Biological dynamics of phytoplankton blooms

The time series of seawater chl-a, heterotrophic bacteria, and dissolved organic carbon, shown in Figure 4.2, provide an overview of the biological progression of Bloom 3. No significant phytoplankton growth was observed after the first nutrient addition (chl-a < 2 µg/L, Figure 4.2a), possibly due to light limitation. A phytoplankton bloom was induced with natural seawater collected as before and then added to the wave channel on 8/1. After the addition of the outdoor-grown bloom, the phytoplankton growth continued and peaked at 25 µg/L chl-a, and then proceeded through an extended senescent phase (Figure 4.2a). During the senescent phase, chl-a concentrations remained stable around 5 µg/L, higher than the pre-bloom state, suggesting some phytoplankton growth was still occurring. Bacterial and viral dynamic (Figure 4.2a) followed a typical microbial succession generally observed during phytoplankton bloom (Buchan et al., 2014).

The combination of ESP and inverted microscopy with chlorophyll concentrations over time confirmed a distinct natural bloom progression in Bloom 3 (Figure 4.6). Phytoplankton community structure was initially dominated by diatoms (composed mostly of *Skeletonema sp. and Cylindrotheca sp.)* with an overall relative abundance of 55% and 1.9×10^6 cells/L. The community then shifted towards an aggregation of diatoms (composed mostly of *Cylindrotheca sp. and Navicula sp.)* at the end of the bloom with a relative abundance of 33% and 5.0×10^5 cells/L. There was also a proliferation in microzooplankton (composed mostly of tintinnids and copepods) at the end of the bloom with a relative abundance of 25% and 5.452×10^3 cells/L. Phytoplankton physiology across the bloom was screened in both methods, where diatoms and dinoflagellates show signs of pigment loss, broken frustules, and increased aggregation over time.

4.5.2 Temperature, Dissolved Gases, and DOC

Over the course of Bloom 3, dissolved organic carbon steadily increased in concentration, due to both primary production and bacterial production of DOC, which is consistent with previous bloom incubation experiments (Wang et al., 2015) Notably, the addition of the starter tank resulted in a DOC increase of 100 µM compared to the background level of the first week. The dissolved inorganic gases, O_2 and CO_2, varied on a diurnal basis as the phytoplankton utilized light for photosynthesis and produced O_2 as a byproduct during the daytime. During periods of higher chl-a (Figure 4.2a), after the tank amendment, dissolved O_2 concentrations were generally more elevated, except for 8/2 when the heterotrophic bacteria reached a local maximum concentration. The dissolved CO_2 concentration steadily decreased with respect to chl-a due to increased carbon fixation by phytoplankton. After reaching a minimum on 8/5 (Figure 4.2b), the CO_2 concentration began increasing during the senescent phase of the mesocosm probably in response to increased bacterial respiration relative to carbon fixation by phytoplankton.

Lastly, the seawater temperature of the wave channel initially began at the temperature of the ocean (17°C) but equilibrated quickly to the temperature of the hydraulics laboratory within ~24 hours (Figure 4.2b). Daily, temperature varied ~0.75°C day^{-1} with the ambient temperature of the laboratory. Longer term variation in water temperature followed changes in local weather but ranged between 24.5-27°C for the duration of experiment after initial equilibration. Keeping the water at in situ temperature will be one of the key improvements of future setups to mimic microbial growth conditions as in the environment. The air temperature in the wave channel headspace ranged from 21.5-27°C and was inversely correlated with the relative humidity, which had a mean value of 86 ± 5% RH (1σ) (Figure 4.13, Table 4.6).

4.5.3 Impact of Transportation on Seawater Dissolved Organic Matter

While a complete discussion of the analysis of marine dissolved organic matter (DOM) throughout SeaSCAPE is beyond the scope of this manuscript, two selected analyses are shown here to illustrate various factors which influenced the seawater chemistry: the impact of 1) seawater transportation and 2) phytoplankton growth on the DOM composition. In order to fill the wave channel, 11,800 L of seawater must be collected from the ocean and transported into the laboratory facility. There is significant concern that this process may introduce anthropogenic contaminants to the water. Figure 4.16 is a GCxGC ion chromatogram of seawater obtained before addition to the wave channel. Notable in the composition of this seawater is the vast chemical diversity of the sample in addition to a large quantity of anthropogenic contaminants. These species are ubiquitous in the coastal zone and are unavoidable in mesocosm experiments using coastal seawater.

To understand the effect of transport on the chemical composition of the seawater during SeaSCAPE, TD-GCxGC-EI-HRToFMS was performed on DOM samples from seawater gathered

from the SIO pier before and after transfer to the wave channel on 7/23. As a comparison, we also analyzed DOM of the seawater after the addition of the outdoor phytoplankton culture on 8/1 to understand the influence of biological processes on DOM. Figure 4.17 is a spectral comparison plot in which the ion intensity chromatogram obtained after the water transfer was subtracted by the chromatogram obtained before the water was transfer. We found that few compounds were introduced by the transfer process, with 4% of the ion current for species classified as anthropogenic contaminants being added during the water transfer process (Figure 4.7a). In contrast to the small changes made by water transfer, a much larger change was measured in DOM after the addition of the outdoor phytoplankton tank to the wave channel, with over 87% of the GCxGC signal introduced or significantly enhanced after the perturbation (Figure 4.7b). This is likely due to organic material being actively produced by biological activity in the seawater. Thus, we find that transportation of the seawater to the wave channel has a relatively small effect on seawater composition, especially in contrast to the large changes induced by phytoplankton growth.

4.5.4 nSSA Size Distributions and Stability

The shape of the nSSA size distributions is largely consistent with previous studies of SSA generated by breaking waves (Figure 4.14) (Prather et al., 2013). However, there was significant temporal variability in the total concentration of particles observed during the experiment. A strong diurnal trend was observed, with higher, more variable concentrations observed during the daytime (N_{day} = 272 ± 92 #/cm^3) and lower, yet more stable concentrations observed during the nighttime (N_{night} = 199 ± 70 #/cm^3) (Figure 4.8). While seawater temperature can affect the flux of nSSA, the daily changes observed during the SeaSCAPE experiment were likely not large enough to explain the variability in nSSA concentration (Lewis and Schwartz, 2004). Typical daily water

temperature changes were less 1°C (Figure 4.2), which should correspond to a change in SSA flux of only 2-4% (Forestieri et al., 2018), whereas the observed change from night to day is, on average, ~37 %. The diurnal changes also do not appear to be linked to other changes such as the wave channel lights or the chemical composition of the seawater. Rather, we suspect that the changes in SSA production were driven by the opening and closing of the laboratory doors, which resulted in a pressure change, which affected the air flow and mixing dynamics within the channel headspace. These findings, alongside the results of the sampling port location and depth testing (Figure 5), demonstrate the turbulent mixing within the wave channel headspace, resulting in variable nSSA number concentrations. Further testing and modelling of the wave channel is necessary to fully understand these observations.

4.5.5 Characteristics of hetSSA and SMA Produced in the OFRs

OFRs were used to assess the effects of atmospheric aging on gases and particles emitted from the oceans. While the primary goal of the OFR1 and OFR2 experiments was to assess the effects of photooxidative aging on the properties of SSA (referred to as hetSSA herein), the gases present in the wave channel headspace were not removed and thus also reacted in the OFRs. New particle formation events were observed due to the reactions of these gases, as evidenced by the appearance of a large nucleation mode in the aerosol distributions when the OFRs are active (Figure 4.9a). The formation of SMA in OFR1 and OFR2 presents a significant challenge for the measurement of hetSSA; however, size-resolved measurements can overcome this by simply selecting for particle sizes larger than the ultrafine mode (D_p > ~100 nm) and thus presumed to be primary SSA particles. Measurements of the bulk non-refractory aerosol show significant changes in chemical composition due to oxidation processes in the OFR. A more complete analysis, including size-resolved chemical composition, to identify the source of new particle formation is

the subject of a future manuscript. In the bulk chemical speciation shown in Figure 4.9, the relative increase in particulate NO_3, compared to non-refractory particulate Cl, is consistent with heterogeneous reaction of $HNO_3 + NaCl \rightarrow NaNO_3 + HCl$ (Leu et al., 1995). The displacement of Cl for NO_3 has been previously observed in coastal sea spray aerosol (Gard et al., 1998) and explored in laboratory experiments (Ault et al., 2013b, 2014). In our experiment, this anion substitution indicates that HNO_3 is likely produced in the OFR through the oxidation of NO_x to form HNO_3.

4.5.6 Evidence of Abiotic VOC Production from Interfacial Photochemistry

To test whether abiotic VOCs could be produced simply by irradiating the surface species with sunlight, surface water from the wave channel was exposed to light from a solar simulator and analyzed using a modified gas-phase APCI Orbitrap MS. Shown in Figure 4.10a, there were two unique molecular signatures that were immediately sensitive upon irradiation, as well as three others not shown here (isoprene, dimethyl sulfone, and decadienal only in some days during Bloom 3). Several other species also increased during this time but exhibited a more gradual increase, indicating a diffusion limited, and therefore most likely biogenic, process. Two of these abiotically-produced species were able to be putatively annotated using tandem MS, showing fragmentation patterns that clearly indicated the presence of phenol, C_6H_6O, and beta-cyclocitral, $C_{10}H_{16}O$. The signal enhancement of these molecules immediately upon irradiation (within 3 minutes), compared to the background dark signal, are shown in Figure 4.10b and Figure **4.10**c respectively. The fragmentation pattern of $C_{10}H_{16}O$ suggests that beta-cyclocitral was not the only species of the same mass-to-charge ratio. Without an in-depth experiment to constrain the many variables in seawater such as the microbiology or surface tension, it is difficult to make any assumptions about the specific mechanisms. Gas-phase APCI Orbitrap MS was shown to

successfully ionize a variety of molecular signatures off-gassing from the seawater surface as well as detect changes when the sample was exposed to solar light.

4.5.7 Relative Distribution of Morphologies for Nascent and hetSSA

Nascent SSA displayed four unique morphologies including prism-like, core-shell, rounded and aggregates, while hetSSA had two main morphologies: core-shell and rounded (Figure 4.11a). The morphological categorization was performed qualitatively, analogous to previous studies (Lee et al., 2020b; Ray et al., 2019). Next, the relative distribution of morphologies for nSSA and hetSSA samples were compared (Figure 4.11b). For the nSSA sample morphologies, the rounded (47%) was most common, followed by the core-shell (22%), while prism-like (17%) and aggregates (14%) showed similar abundancies. On the other hand, for the hetSSA sample morphologies, core-shell (72%) was most common, followed by the rounded (28%) morphology, while no prism-like and aggregates were observed. Overall, SSA aging results in significant increase of the abundance for core-shell morphology, and concomitant decreases in the other morphologies. Additionally, core-shell hetSSA particles showed a thicker coating compared with similar-size nascent core-shell particles.

4.6 Discussion

4.6.1 Wave Channel Characterization

A key challenge in ocean-atmosphere simulation experiments is maintaining the highest degree of experimental cleanliness while still capturing the complexity of the natural environment. This challenge is further pressed by the massive volumes of seawater that must be collected and transferred without significant perturbation of the biological assemblages and chemical contamination of the water. For the headspace, large airflows are necessary to offset the flow

demand required by online instrumentation and filter sampling. Generating large volumes of high purity air is a significant challenge beyond the removal of particulates. Here we showed that the transfer of seawater from the ocean to the laboratory incurred little contamination. However, the headspace of the wave channel was challenging to keep clean of anthropogenic VOCs with the air handling system. In addition to VOCs, non-negligible concentrations of NO_x and O_3 were present in the wave channel headspace (Figure 4.15, Table 4.7), indicating that these trace gases are not effectively removed by the air handling system. Specifically, the presence of NO_x is notable, as it appears to have resulted in significant NO_3 formation in the OFR. The incorporation of the ISV was a critical addition that enabled the measurement of secondary marine aerosol and gases by providing a much cleaner headspace than the wave channel. In the future, advances in economically generating high volumes of particle-free, low VOC, and low NO_x air would be ideal to enable the measurements of secondary aerosols without the incorporation of secondary chambers.

Systematic testing of the wave channel was conducted to determine the optimal sampling conditions for nascent SSA. This testing showed a clear relationship between the air flowrate in the channel headspace and the measured concentrations of SSA particles, with lower air speeds resulting in higher particle concentrations. However, when the effect of both sampling port location and penetration depth into the channel headspace were evaluated, it was apparent that the nSSA concentrations in the headspace were heterogeneous and highly variable, depending on sampling locations. Further observations during the SeaSCAPE experiment showed a strong diurnal trend in the nSSA concentrations, which may have been caused by the opening and closing of the laboratory doors, creating a change in air pressure in the building. Based on these findings, future work is needed to model the fluid dynamics in the wave channel to understand the mixing

and transport of aerosols and gases in the headspace. Additionally, it was observed that nSSA concentrations were typically more stable at night when the laboratory doors were closed, which could have caused higher air pressure in the room. This suggests that future modifications could be made to the wave channel to increase stability in the particle concentrations, such as replacing the open flap at the end of the channel with a sealed vent system. However, despite the variability in total number concentrations, the shape of the SSA size distributions remained consistent throughout the experiment and agrees well with previous wave channel experiments (Prather et al., 2013). This indicates that the variability in the number concentrations was driven by different degrees of dilution, due to uneven mixing in the headspace, as opposed to variations in the SSA production mechanism or bubble sizes generated by the breaking wave.

4.6.2 Biological dynamics during the mesocosm experiment

One of the most crucial elements of mesocosm experiments to study ocean-atmosphere processes is the stimulation of a phytoplankton bloom involving all the trophic interactions in the microbial loop (Azam et al., 1983; Buchan et al., 2014) between phytoplankton, protozoans, heterotrophic bacteria, and viruses (Lee et al., 2015; Pomeroy et al., 2007). Recent efforts have sought to better reproduce the complexity of marine biology while also accurately measuring the turnover of assemblages to better ascribe changes in seawater, SSA composition and properties, and VOC production. An ongoing challenge is the successful stimulation of authentic mesocosms using natural seawater, which varies in biological composition and may not respond immediately to nutrient amendments. During Bloom 3, the addition of the outdoor tank grown in elevated nutrient conditions and natural sunlight provided a richer starter culture for further growth in the wave channel. In the future, enhanced lighting intensity, possibly the usage of actinic flux, will be implemented to allow bloom formation without this added intervention.

The combination of SPCS and microscopy provided a detailed observation of the phytoplankton and microzooplankton dynamic and trophic interactions during the experiment. The phytoplankton assemblages showed a natural succession throughout the course of the experiment, from a diatom-dominated community at the peak of the bloom during the growth phase towards a diatom-aggregate and zooplankton-populated senescent phase. Observation of potential grazing on phytoplankton by microzooplankton and aggregate formation towards the end of the bloom provided insight on the physiological state of the phytoplankton bloom across the experiment (Figure 4.6). These types of stressors upon phytoplankton may lead to released exudates containing carbon and sulfur that will supply microbial metabolisms, which in turn may influence the production and composition of climate relevant trace gases and the composition of biogenic aerosol (Ksionzek et al., 2016). Future work will compare phytoplankton and VOC concentrations across this study to screen for specific taxa that may influence VOC production and transformation. The connections between the biological species and the chemical composition of DOM and aerosol will also be the focus of forthcoming SeaSCAPE studies. Further analysis of the functional (e.g. production, enzymes) and community (16S and 18S rDNA amplicon sequencing) adaptation of the marine microbes over the course of the bloom in the water, SML and aerosols will help address some of the chemical changes observed during SeaSCAPE.

4.6.3 Photochemical VOC Production

The abiotic production of VOCs from seawater via reactions of surface-present organics with light and oxidants has been recently discussed as a possible source of atmospheric VOCs competitive in emission quantity with marine biology (Novak and Bertram, 2020). Currently, only laboratory measurements of abiotic VOC production have been undertaken, with most utilizing SSML or synthetic organic films doped with terrestrially relevant photosensitizers to enhance

yields of irradiation-initiated VOC emission (Ciuraru et al., 2015; Trueblood et al., 2019a). Here, using unadulterated seawater from our mesocosm experiments, we show small quantities of abiotic VOC generation, including cyclic species, but do not maintain sustained emission compared to other laboratory investigations. Lack of sustained emission is likely due to the limited pool of volatile organic species in seawater, which may have been lost through emission and chemical transformation. While the complex mechanisms that control photoinitiated VOC production are poorly understood, mesocosm experiments serve as a valuable bridge between field and laboratory work towards determining the relative contributions of biotic and abiotic VOC production in the marine environment and will be further pursued.

4.6.4 Influence of Photochemical Aging on SSA Composition and Secondary Aerosol Formation

Heterogeneous aging of SSA by OH radical led to significant changes in its morphology, with the total loss of prism-like and aggregate type particles and a large enhancement in core-shell particles. Increased oxidation of organic aerosol has been shown to increase its viscosity, potentially affecting its phase state (Athanasiadis et al., 2016; Saukko et al., 2012). This process may have contributed to the change in SSA morphologies observed here. An alternative explanation is that coating of secondary organic species onto the SSA altered its morphology. Future studies are necessary to understand how both of these processes influence SSA phase and morphology, and the potential influence on the climate relevant properties of SSA, such as ice nucleation, water uptake, and light scattering.

4.7 Conclusions

In summary, wave channels represent an important method for understanding the production and properties of marine aerosols and gases under controlled laboratory conditions. Optimization of the wave channel system has enabled even more detailed atmospheric measurements over previous experimental campaigns. In addition, major improvements have been made in the capability to simulate complex seawater biology. The incorporation of oxidation flow reactors has, for the first time, enabled the study of secondary aerosol formation and photochemical aging of SSA during a large-scale wave channel experiment. Preliminary findings from the SeaSCAPE campaign have shed light on the photochemical production of VOCs, impact of atmospheric aging on SSA phase and morphology, and the chemical composition of SMA. Future analysis of the SeaSCAPE dataset is expected to give insight to, among other processes, the nature of marine INPs in both freshly-emitted and hetSSA; the potential for both SSA and SMA to serve as CCN in the marine atmosphere; the molecular composition of SSA and its links to biological activity; the identity of unique marine VOCs and possible SOA precursors; and the effect of photochemical aging on the chemical composition of marine aerosols. Oceanic emissions of both gases and particles have profound effects on the climate through their interactions with clouds and solar radiation. Laboratory ocean-atmosphere experiments have and will continue to expand our knowledge of marine aerosols and their influence on a changing climate system.

4.8 Acknowledgements

This material is based upon work supported by the National Science Foundation through the Center for Aerosol Impacts on the Chemistry of the Environment, an NSF Center for Chemical Innovation (CHE-1801971). Thank you to the entire SeaSCAPE team for their hard work

throughout the experimental campaign. A full list of participants can be found online: https://caice.ucsd.edu/experiment-campaigns/. We thank Tran Nguyen and the Aluwihare Lab for analysis of the DOC samples. We would like to acknowledge Betsy Stone, Juan Navea, Mike Tauber, Jim Smith, Pieter Dorrestein, Rob Knight, Pedro Belda-Ferre, and Farooq Azam for their contributions to the experiment. Special thanks Joe Mayer for his assistance with fabricating the ISV and the wave channel paddle system; Mark Young and Kathryn Moore for assisting with the paddle software and maintenance; Grant Deane and Dale Stokes for assistance with wave channel operation; Victor Or for assistance with graphic design; and Rob Klidy and the Hydraulics Laboratory staff for maintaining the facility.

Chapter 4 is, in full, currently being prepared for submission to *Environmental Science: Processes and Impacts*. Printed with permission from Mayer, K.J., Sauer, J.S., Lee, C., Alves, M.R., Amiri, S., Bahaveolos, C., Barnes, E.B., Crocker, D.R., Dinasquet, J., Garofalo, L.A., Kaluarachchi, C.P., Dang, D., Kilgour, D., Mael, L., Mitts, B.A., Moon, D.R., Moore, A.N., Morris, C.K., Mullenmeister, C., Ni, C.M., Pendergraft, M.A., Petras, D., Simpson, R., Tumminello, P.R., Walker, J.L., DeMott, P.J., Farmer, D.K., Goldstein, A.H., Grassian, V.H., Jaffe, J.S., Francesca Malfatti, F., Martz, T.R., Slade, J.H., Tivanski, A.V., Bertram, T.H., Cappa, C.D., Prather, K.A. (2021). The Sea Spray Chemistry and Particle Evolution Study (SeaSCAPE): Overview and Experimental Methods. The dissertation author, Dr. Jon Sauer, and Dr. Chris Lee were primary investigators and lead authors of this paper.

Dr. Jon Sauer, Dr. Chris Lee, Prof. Chris Cappa, Prof. Tim Bertram, and Prof. Kim Prather were responsible for the planning, organization, and leadership of the SeaSCAPE experiment. Dr. Sauer, Alexia Moore, and Delaney Kilgour were responsible for the gas-phase measurements, including the CI-ToF-MS and the PTR-MS. Michael Alves and Duyen Dang conducted the

measurements of photochemical VOC production. Dr. Daniel Moon and Dr. Lauren Garofalo operated the HR-ToF-AMS instruments. Chathuri Kaluarachchi conducted the AFM particle morphology measurements. The dissertation author, Catherine Mullenmeister, Cristina Bahaveolos, and Chi-Min Ni were responsible for aerosol size distribution measurements and OFR operation. Dr. Julie Dinasquet and Prof. Francesca Malfatti supervised the biological measurements. Sarah Amiri and Joe Walker were responsible for phytoplankton enumeration. Clare Morris was responsible for the heterotrophic bacteria measurements. Dan Crocker contributed the chlorophyll-a measurements. Dr. Daniel Petras supervised the seawater chemical measurements. Emily Barnes was responsible for the dissolved organic matter speciation. Brock Mitts, Ryan Tumminello, Liora Mael, and Matthew Pendergraft assisted with day-to-day operations, including cleaning the wave channel, seawater collection, and OFR operation.

4.9 Tables

Table 4.1 Summary of nutrient additions during the three SeaSCAPE bloom cycles.

Bloom Cycle	Water Fill Date	Nutrient Addition Date	Nutrient Concentration
Bloom 1	7/1/2019	7/4/2019	f/2 nutrients + silicates
Bloom 2	7/12/2019	7/14/2019	f/20 nutrients + silicates
Bloom 3	7/23/2019	7/25/2019	f/20 nutrients + f/40 silicates
		7/26/2019	Addition silicates, to f/20 total
		8/1/2019	Additional nutrients and silicates, to total concentration of f/2 for both

Table 4.2 Summary of all online aerosol measurement techniques employed during SeaSCAPE. The sample type is designated by a single letter (N = Nascent SSA, H = Heterogeneously-aged SSA, S = Secondary Marine Aerosol).

Measurement	Technique	Sample type	Sampling Interval	Reference
Dry particle size distributions from 5 nm to 20 μm	Scanning Mobility Particle Sizer (SMPS, TSI Inc)	N,H,S	2-5 min	(Shen et al., 2002)
	Aerodynamic Particle Sizer (APS 3321, TSI inc)	N,H	1 min	(Peters and Leith, 2003)
	Scanning Electrical Mobility Spectrometer (SEMS, Brechtel)	N,H	5 min	(Lopez-Yglesias et al., 2014)
Total particle number	Condensation Particle Counter (CPC)	N	1 s	(Hering et al., 2019)
Single particle composition and size	Aerosol Time-of-Flight Mass Spectrometer (ATOFMS)	N,H	1 min	(Gard et al., 1997)
Size-resolved non-refractory submicron aerosol composition	High Resolution Time-of-Flight Aerosol Mass Spectrometer (HR-ToF-AMS)	N,H,S	5 min	(DeCarlo et al., 2006)
Ultrafine aerosol chemical composition	Thermal Desorption Chemical Ionization Mass Spectrometer (TDCIMS)	N,S	N: 1 h S: 30 min	(Smith et al., 2004; Voisin et al., 2003)
Submicron aerosol chemical composition	Extractive Electrospray Ionization Mass Spectrometry (EESI-MS)	N,H,S	1 s	(Lopez-Hilfiker et al., 2019)
Size-resolved cloud condensation nuclei activity	Continuous-flow streamwise thermal-gradient CCN counter	N,H,S	30-60 min	(Roberts and Nenes, 2005)
Relative humidity-dependent aerosol bounce	Electrical Low Pressure Impactor (ELPI)	N,H,S	1 min	(Jain and Petrucci, 2015)
INP concentration	Continuous-Flow Diffusion Chamber (CFDC)	N,H	5-15 min	(Demott et al., 2015)
Size-resolved fluorescent biological particle number concentrations	Wideband Integrated Bioaerosol Sensor (WIBS)	N,H	1 s	(Gabey et al., 2011)

Table 4.3 Summary of all offline aerosol measurement techniques employed during SeaSCAPE. The sample type is designated by a single letter (N = Nascent SSA, H = Heterogeneously-Aged SSA, S = Secondary Marine Aerosol)

Measurement	Collection Technique	Analysis Technique	Sample type	Sampling Interval	Reference
INP concentration	Poly-carbonate filters	Ice spectrometer	N,H	1-5.5 h	(Perkins et al., 2020)
Size-segregated organic aerosol composition	Sioutas cascade impactor	High resolution mass spectrometry	N,H	6-12 h	(Cochran et al., 2016; Hettiyadura et al., 2017)
Single particle morphology, phase state, organic volume fraction, and water uptake	MOUDI impactor	Atomic Force Microscopy (AFM)	N,H	N: 5-6 h H: 1-2 h	(Lee et al., 2017, 2020a)
		AFM photothermal infrared spectroscopy (AFM-PTIR)	N,H	N: 5-6 h H: 1-2 h	(Or et al., 2018)
Immersion freezing of single particles	MOUDI impactor	Micro-Raman spectroscopy	N,H	1-2h	(Mael et al., 2019)
Aerosol pH	MOUDI impactor	pH paper	N	1-2 h	(Angle et al., 2020)
Chemical and microbial composition	Quarts fiber filters	High-resolution mass spectrometry	N	24 h	(Petras et al., 2017)
		16S/18S rDNA sequencing	N	24 h	(Michaud et al., 2018)
Viral and bacterial abundances	Spot sampler	Flow cytometry	N	4-6h	(Brussaard, 2004; Gasol and Del Giorgio, 2000)
Enzymes activities	Spot sampler	Fluorogenic substrates	N	6 h	(Hering et al., 2014; Hoppe, 1983)
C_{13}-C_{36} n-alkane equivalents chemical speciation	Quartz fiber filters	GCxGC-HRToF-MS	N	14 h /10 h (day/night)	(Jen et al., 2019)
Submicron and Supermicron Isotopic Analysis	Cyclone and quartz fiber filters	MAT 253 Isotope-ratio mass spectrometry (IRMS)	N	48 h	(Crocker et al., 2020)

Table 4.4 Summary of all gas-phase measurement techniques employed during SeaSCAPE. The sample type is designated by a single letter (W = wave channel headspace, I = isolated sampling vessel headspace, D = dissolved gases, A = air handling system, O = OFR, B = bulk seawater, L = SSML)

Measurement	Technique	Sample type	Sampling Interval	Reference
O_3	UV absorption, Thermo Environmental Model 49C	W	1 s	N/A
	UV absorption, 2B Technologies Model 202	A,O	1 s	N/A
$NO\text{-}NO_2\text{-}NO_x$	Chemiluminescence, Thermo Environmental Model 42C	W,A	1 s	N/A
SO_2	Pulsed fluorescence, Thermo Environmental Model 43iQ	W,A	1 s	N/A
VOCs	Vocus Proton Transfer Reaction Mass Spectrometry (PTR-ToF-MS)	W,I,A	1 s	(Krechmer et al., 2018)
Sulfur-containing VOCs	Chemical Ionization Mass Spectrometry (benzene reagent ion, B-CI-ToF-MS)	I,D	1 s	(Kim et al., 2016)
C5-C18 n-alkane equivalents	TD-GCxGC-EI/VUV-HRToF-MS	I	20 min collection, every 1-3 days	(Hatch et al., 2019)
Abiotic photo-enhanced surface products	Gas phase modified-atmospheric pressure chemical ionization Orbitrap mass spectrometry (APCI-MS)	B,L	24 h	(Roveretto et al., 2019)

Table 4.5 Summary of all seawater and SSML measurements collected during SeaSCAPE. The sample type is designated by a single letter (L = SSML, B = bulk seawater).

Measurement	Technique	Sample type	Sampling Interval	Reference
Chlorophyll-a	Continuous fluorescence (ESP)	B	1 min	(Wang et al., 2015)
	Fluorescence (AquaFluor)	B	24 h	(Wang et al., 2015)
	Extracted fluorescence	B	24 h	(Holm-Hansen et al., 1965)
Dissolved O_2	Continuous optical absorption	B	1 min	(Wei et al., 2019)
Bacterial community composition	Amplicon Sequencing	B,L	24 h	(Walters et al., 2016)
Heterotrophic bacteria concentration	Flow Cytometry	B,L	24 h	(Gasol and Del Giorgio, 2000)
Virus concentration		B,L	24 h	(Brussaard, 2004)
Nano-pico-phytoplankton and heterotrophic nanoflagellates concentration		B,L	24 h	(Christaki et al., 2011b; Marie et al., 1997)
Phytoplankton community	*In-situ* camera	B	10 Hz	(Orenstein et al., 2020)
	Microscopy and sequencing	B,L	24 h	(Minich et al., 2018)
Dissolved organic carbon	High temperature catalytic combustion (Shimadzu TOC-V series instrument)	B	Daily	(Stubbins and Dittmar, 2012)
Speciated DOM organic compounds	HR-ESI-MS	B	72 h	(Trueblood et al., 2019a)
	TD-GCxGC-EI/VUV-HRToF-MS	B,L	72 h	(Worton et al., 2017)
Nutrients (NO_3, NO_2, PO_4, SiO_4, NH_4)	Seal Analytical continuous-flow AutoAnalyzer 3	B	24 h	(Becker et al., 2020)

Table 4.5 (continued) Summary of all seawater and SSML measurements collected during SeaSCAPE. The sample type is designated by a single letter (L = SSML, B = bulk seawater).

Measurement	Technique	Sample type	Sampling Interval	Reference
Alkalinity, Bicarbonate, Carbonate, Dissolved Inorganic Carbon, Dissolved CO_2, Salinity, pH	Combined pCO_2/TCO_2 Dual Analyzer	B	1 Hz	(Hales et al., 2004)
Water temperature	Thermocouple (ESP)	B	1 min	(Wang et al., 2015)
Enzyme Activity	Fluorogenic Substrates	B,L	24 h	(Hoppe, 1983)
Bacterial production/Growth rate	H3Leucine incorporation	B,L	24 h	(Smith and Azam, 1992)
Methylotrophy	C14-methanol incorporation	B,L	24 h	(Dinasquet et al., 2018)
DMSPp,DMSPd, [DMS]aq	Cryo Purge and Trap Benzene CI-ToF-MS	B	24 h	(Kim et al., 2016)
Functional genes and transcripts dddP, dmdA	Q-PCR for quantification, and sequencing	B, L	24 h	(Levine et al., 2012)
INP concentration and characteristics	Ice Spectrometer	B,L	24 h	(Perkins et al., 2020)
Fluorescent DOM	Fluorescence excitation emission matrix spectroscopy (EEMS)	B,L	24 h	(Trueblood et al., 2019a)
HONO production from DOM	Incoherent broadband cavity-enhanced absorption spectroscopy (IBBCEAS)	B	End of Bloom 3 only	(Gherman et al., 2008)

4.10 Figures

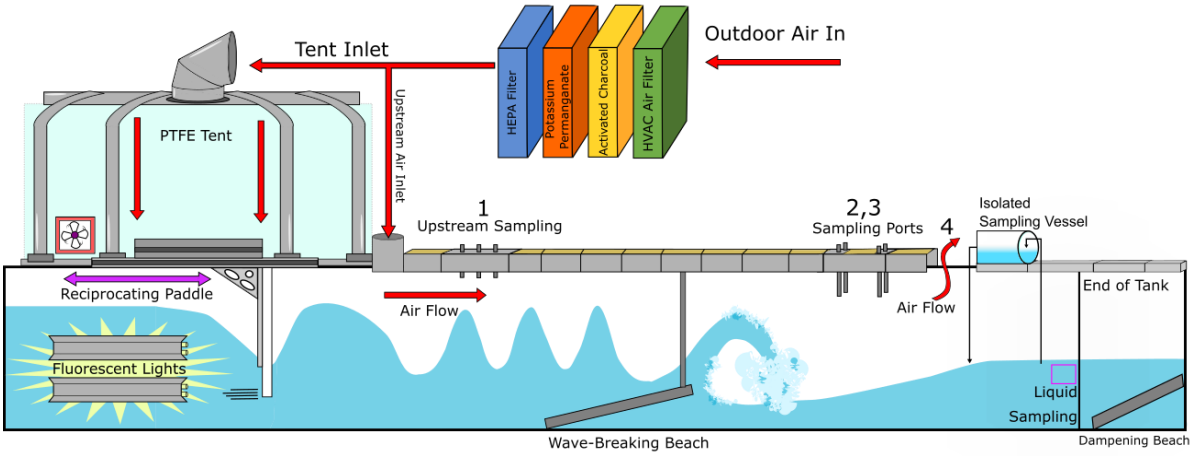

Figure 4.1 Schematic of the SIO Ocean-Atmosphere Interaction Facility (OAIF) Wave Channel: Notable locations for sampling and air outflow are denoted by 1, 2, 3, 4 where the distances of each (from the front of the wave channel): 1 = 6 m , 2 = 16.0 m , 3 = 17.5 m , 4 = 20.6 m. The fluorescent lights extend the full length of the channel; however, they are only shown on the first panel here for clarity.

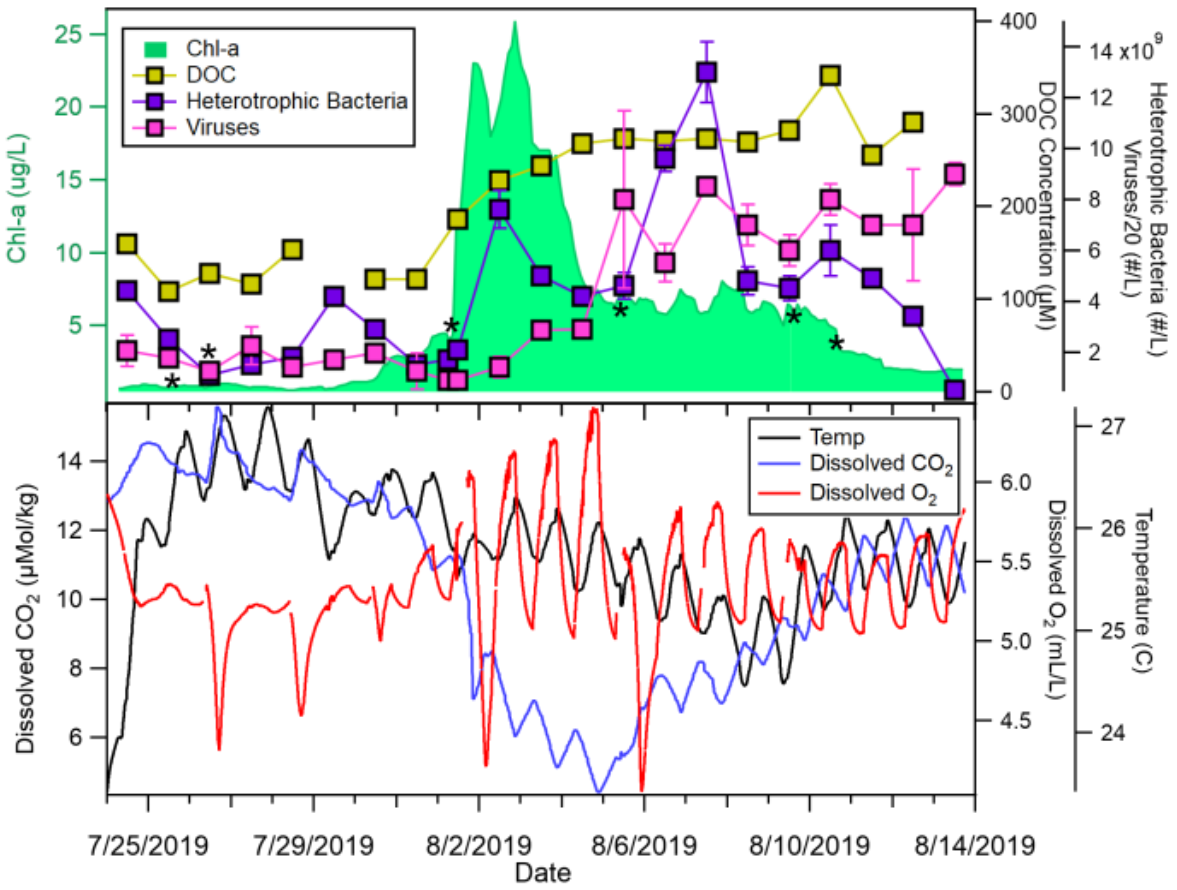

Figure 4.2 a) SeaSCAPE Bloom 3 chl-a, DOC, heterotrophic bacteria, and virus counts over the mesocosm duration. Asterisks indicate notable interventions in mesocosm. Asterisks 1 and 2 correspond to nutrient additions specified in Table 4.1. Asterisk 3 corresponds to the addition of the outdoor tank to the wave channel. Asterisk 4 corresponds to the scraping of wave channel walls to remove light-obstructive detritus. Asterisks 5 and 6 correspond to the addition of circulating pumps to resuspend cellular material aggregated on the wave channel bottom. b) Bloom 3 water temperature, dissolved CO_2, and dissolved O_2.

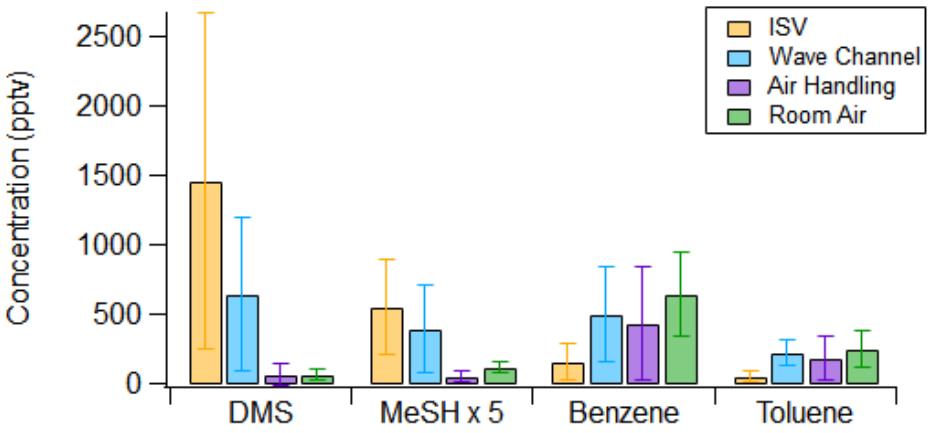

Figure 4.3 Histogram comparing daytime mixing ratios of DMS, MeSH, benzene, and toluene in the ISV, wave channel headspace downstream of wave-breaking, air handling system, and hydraulics laboratory room air. Bars represent the averages over the entire third bloom, and error bars represent the standard deviation over the daily average measurements.

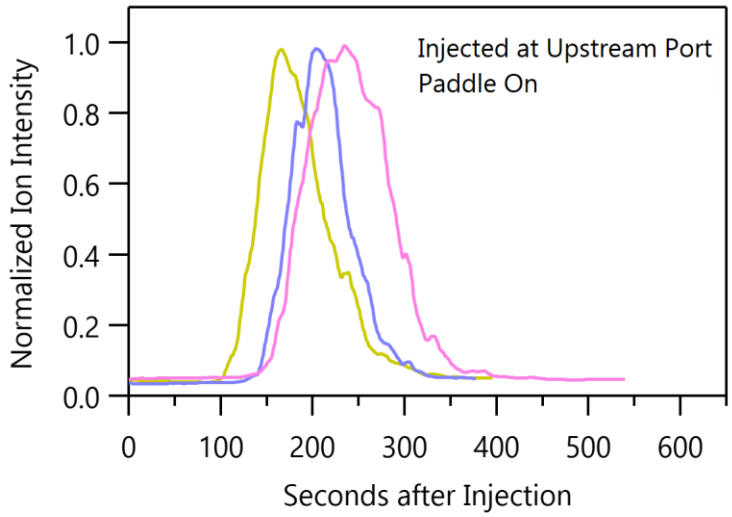

Figure 4.4 Replicate experiments of m/z 62 (dimethyl sulfide) arrival time at sampling port after injection into wave channel headspace at the upstream location. Instrument signal was boxcar smoothed into 10 second bins.

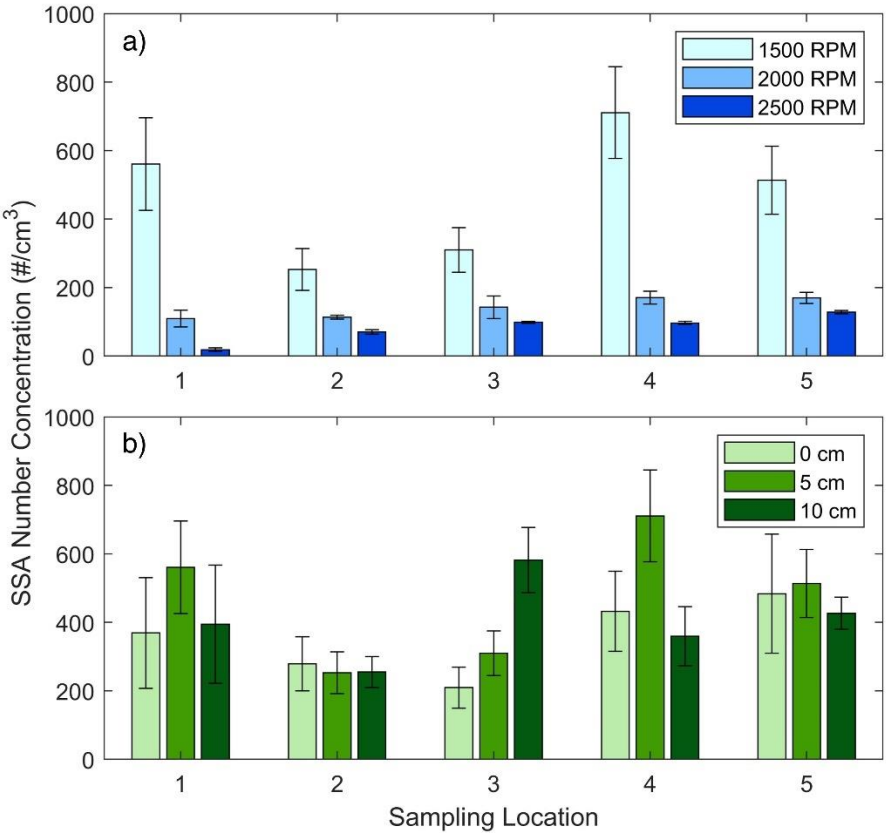

Figure 4.5 a) The SSA number concentration measured at 5 sampling locations with a 5 cm port depth, testing 3 different fan settings, which control the air velocity in the wave channel headspace. The lowest setting (1500 RPM) was determined to yield the highest SSA concentrations at all sampling locations. b) The SSA number concentrations at the different sampling locations with a fan speed of 1500 RPM, showing the effect of sampling port depth (0 cm, 5 cm, and 10 cm below the channel lids). There is no clear relationship between sampling port depth or location and number concentration, indicating heterogeneous particle concentrations in the channel headspace. The sampling port locations are evenly spaced and correspond to 0 cm, 60 cm, 120 cm, 180 cm, and 240 cm from the end of the beach.

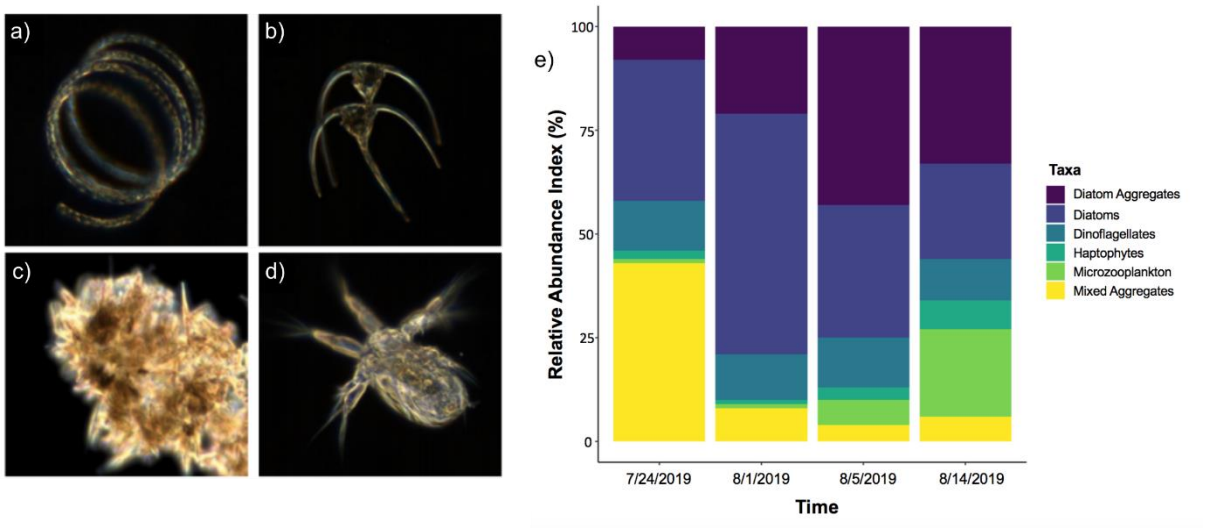

Figure 4.6 Micrographs of representative taxa across a microcosm experiment, a-b) diatoms and dinoflagellates (beginning of bloom), c) mixed aggregates (dominated by diatoms and haptophytes mid bloom), d) microzooplankton (micro zooplankton and ciliates peak at the end of the bloom). e) Time series speciation of phytoplankton taxa across SeaSCAPE.

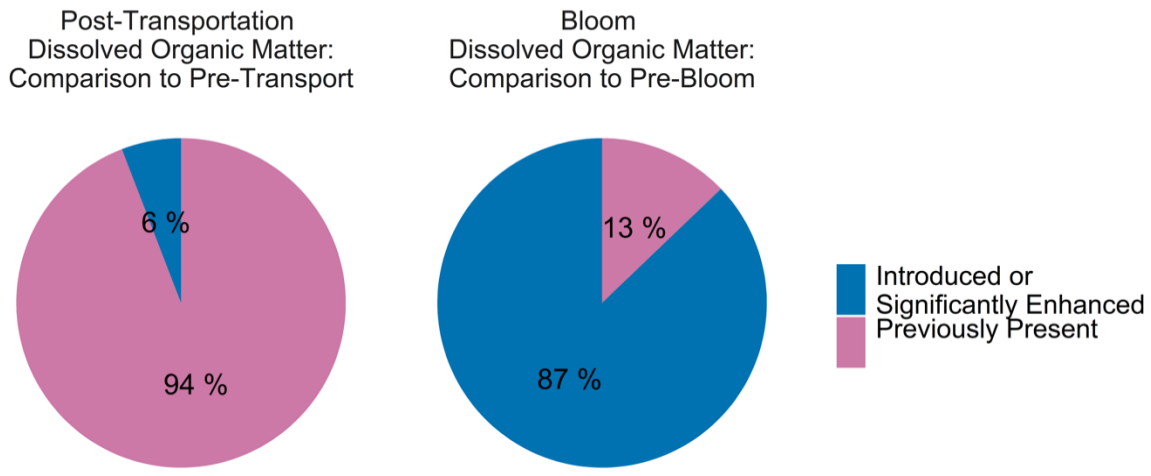

Figure 4.7 Relative changes in GCxGC signal intensity for: a) Comparison of organic signature pre- and post-water transport from pier; b) Comparison of organic signature pre and post concentrated bloom addition (8/1/2019).

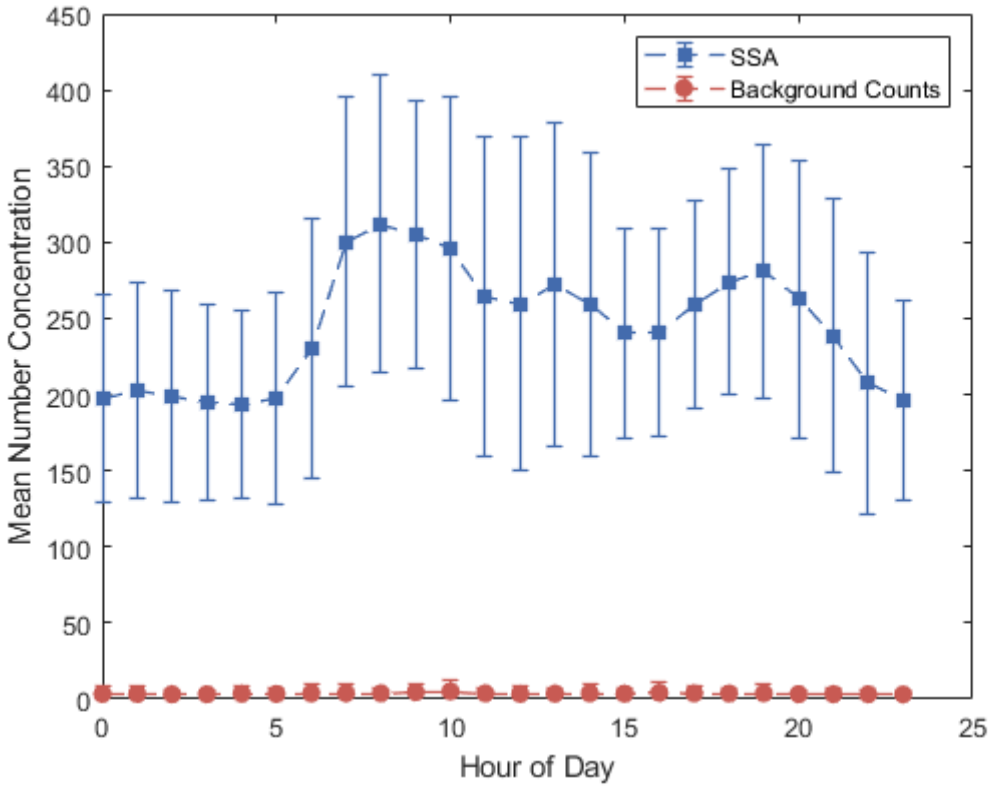

Figure 4.8 Hourly average SSA number concentrations for all of Blooms 2 and 3, demonstrating the large variability in aerosol production as well as differing diurnal behavior. In general, particle concentrations tended to be higher and more variable during the daytime, but lower and more stable overnight. The background particle counts, as measured by the upstream CPC, are also shown. Times reflect local time (PST).

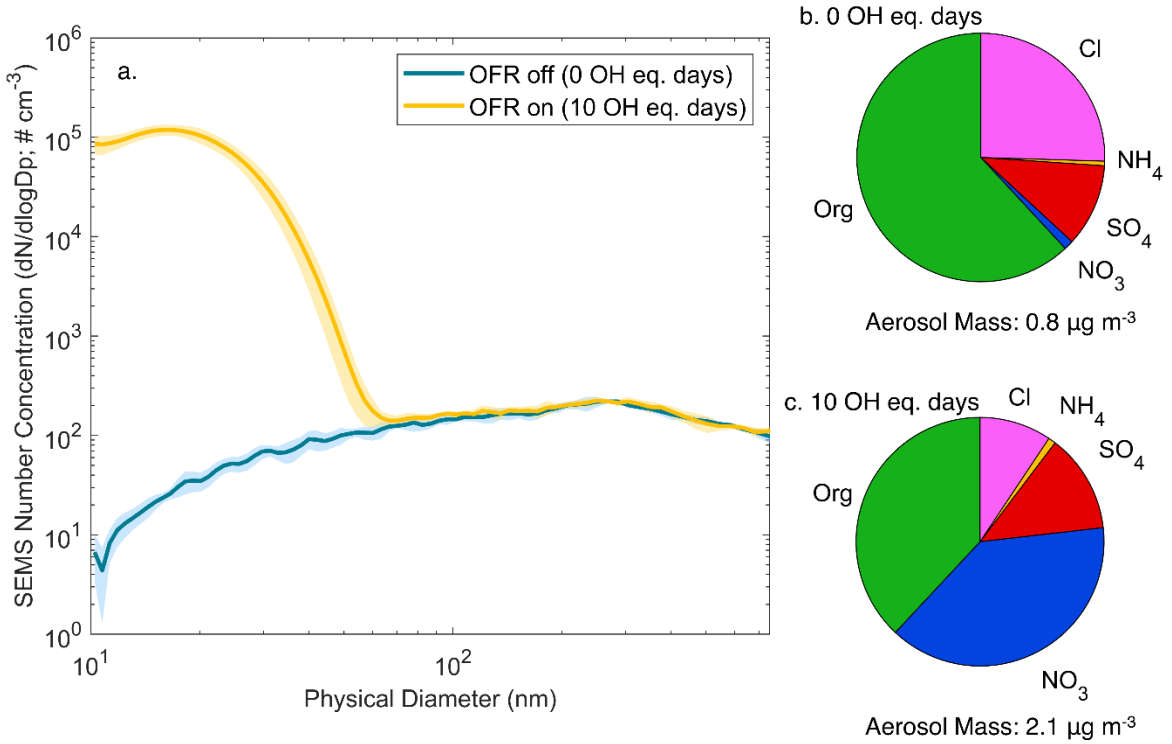

Figure 4.9 A representative aerosol size distribution from OFR1 (a), in which the complete mixture of gases and SSA from the wave channel headspace are oxidized in the OFR. Shading represents uncertainty in the particle concentrations (± 1σ). The large ultrafine mode, which is present only when the lamps are active, is evidence of new particle formation in the reactor. Median fractional bulk chemical composition of submicron non-refractory aerosol for (b) nascent/bypass SSA and (c) SSA aged 10 OH-equivalent days in the OFR.

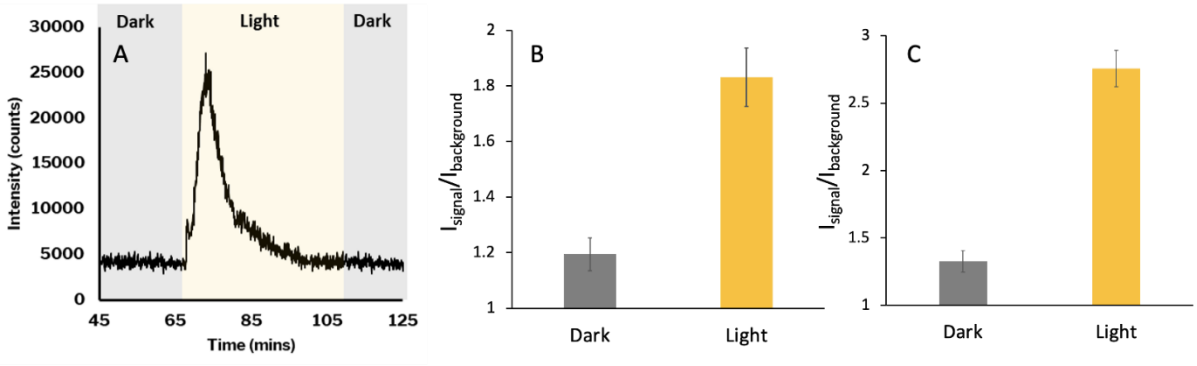

Figure 4.10 Data from gas-phase modified APCI high resolution mass spectrometry showing a) total ion current of summed volatile species found to be sensitive to irradiation, where gray indicates when the sample was kept dark and yellow when the sample was subjected to light; b) the signal enhancement of C_6H_6O, or phenol, immediately upon irradiation, and c) the signal enhancement of $C_{10}H_{16}O$, or beta-cyclocitral, immediately upon irradiation. Error bars represent one standard deviation of the signal averaged over its highest peak.

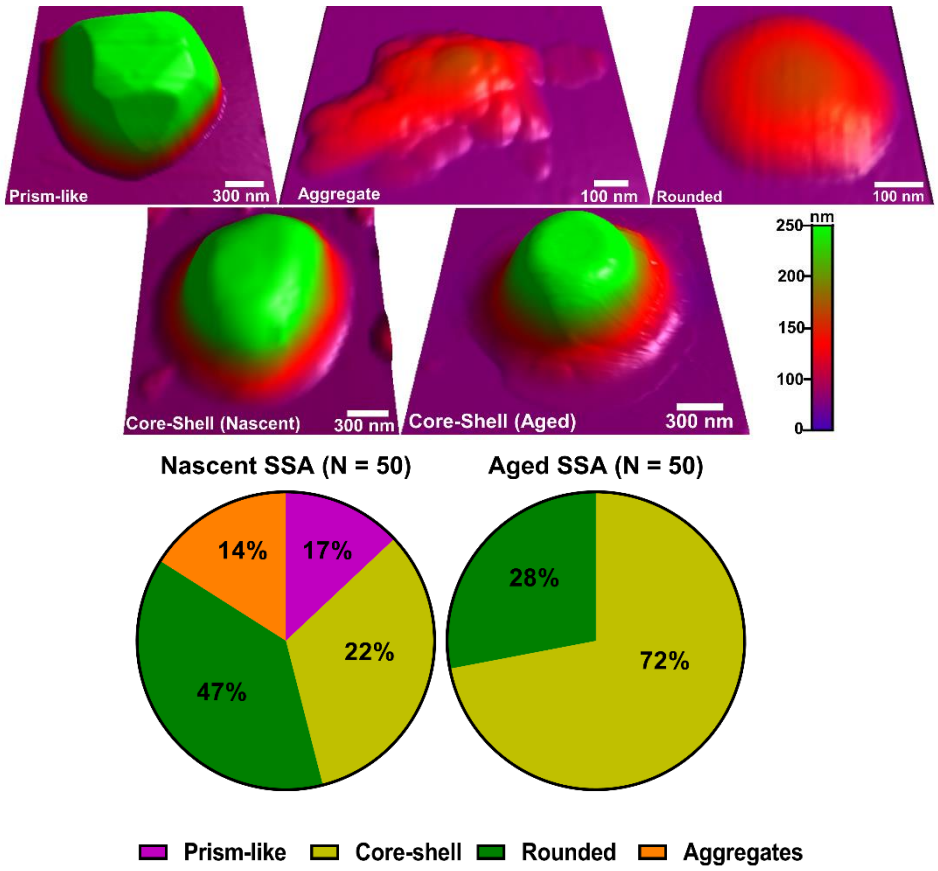

Figure 4.11. a) Representative AFM 3D-height images of individual SSA particles observed during the peak-bloom (Aug 3rd). Color scale shows height difference between the particles. b) Relative distribution of the morphologies in nascent and aged SSA samples. Prism-like, core-shell, rounded, and aggregates particles are represented by purple, yellow, green, and orange colors, respectively.

4.11 Supporting Information

4.11.1 Supplementary Tables

Table 4.6 Statistics describing the distribution of air temperature and relative humidity in the waveflume headspace during SeaSCAPE.

	Temperature (ºC)	**Relative Humidity (%)**
Minimum	21.58	74.15
1st Quartile	23.41	82.77
Median	24.15	86.04
Mean	24.12	86.19
3rd Quartile	24.84	88.89
Maximum	27.18	100
Standard Deviation	1.03	5.22

Table 4.7 Mean, median, and standard deviations of trace gases monitored in the wave channel headspace. All values are in ppb.

Trace Gas	Mean	Standard Deviation	Median
NO	0.41	0.88	0.25
NO_2	0.99	1.51	0.58
NO_x	1.39	2.18	0.88
O_3	15.97	5.55	15.56

4.11.2 Supplementary Figures

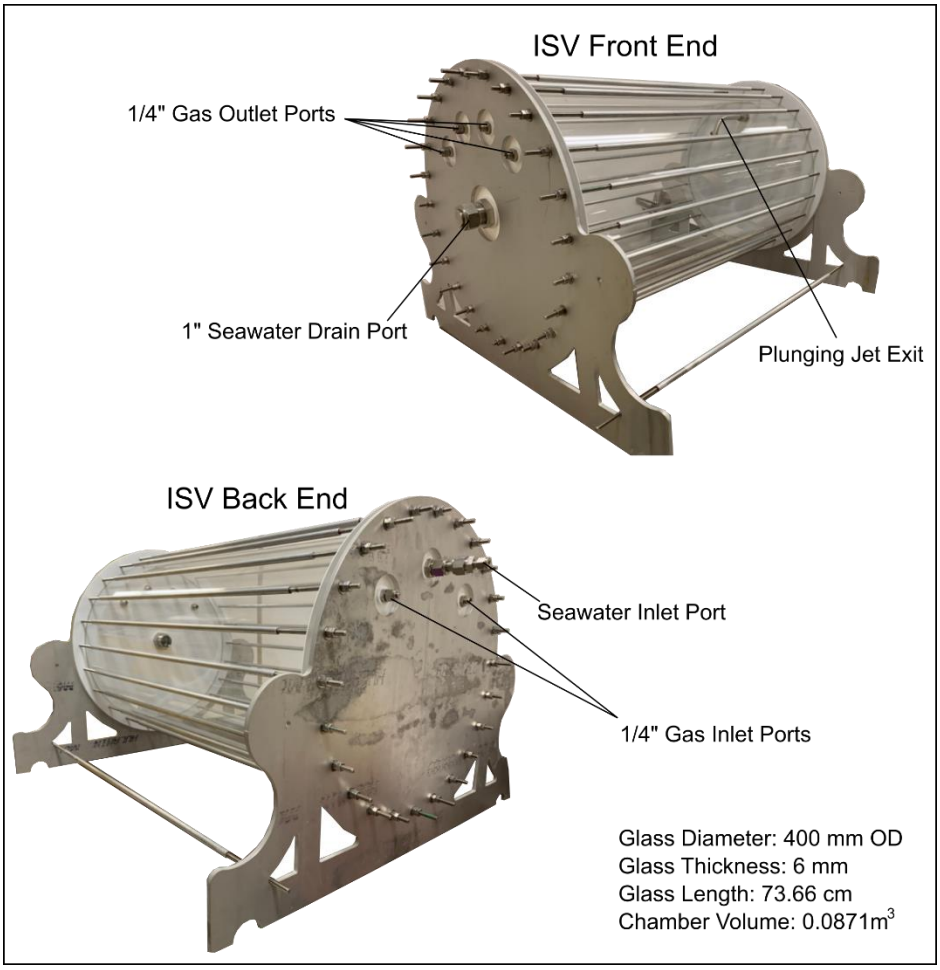

Figure 4.12 Photographs showing the design and dimensions of the isolate sampling vessel (ISV) used for gas-phase and OFR experiments during SeaSCAPE

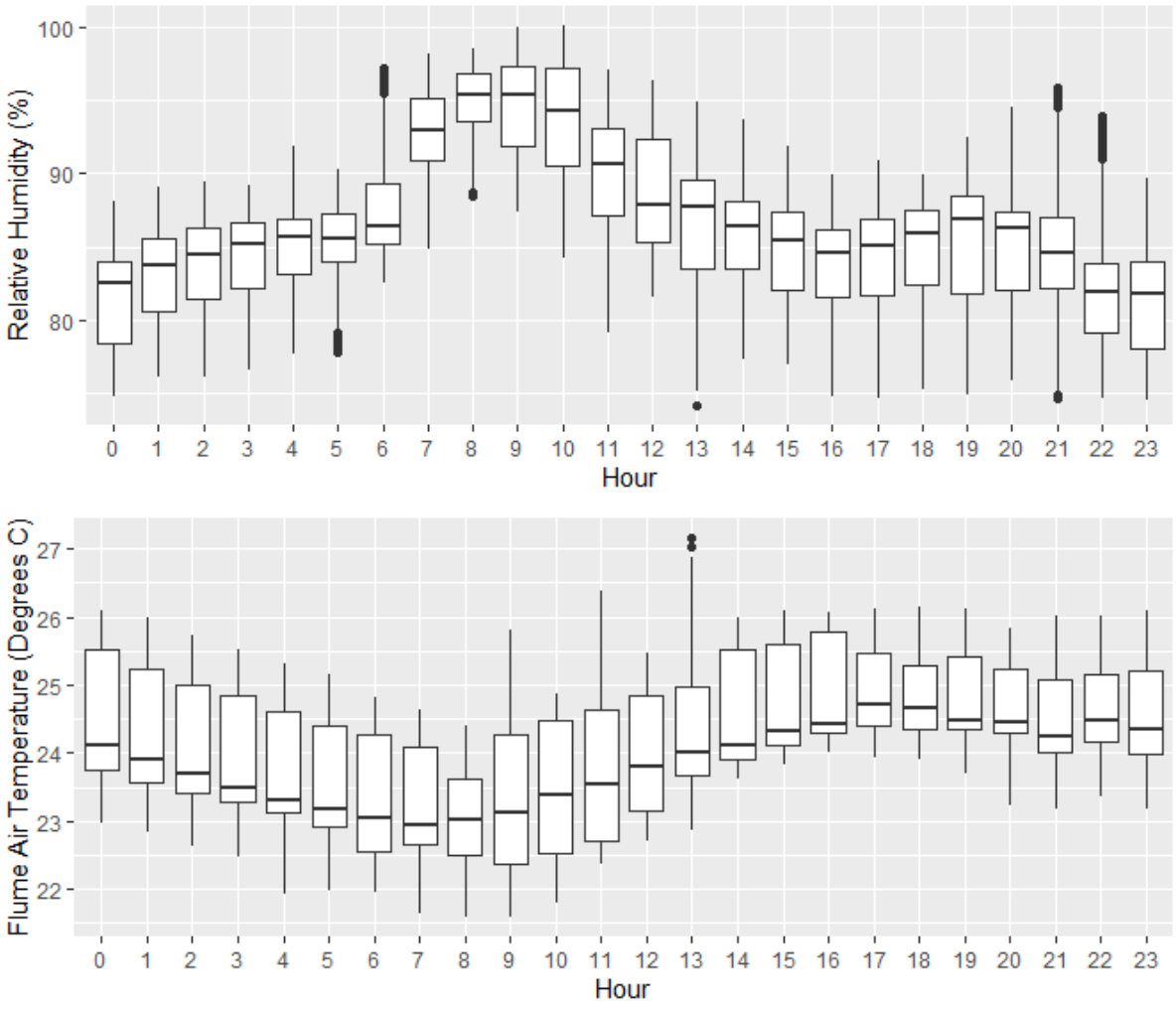

Figure 4.13 Diurnal variability of the a) relative humidity and b) air temperature in the waveflume headspace over time during Bloom 3 of SeaSCAPE.

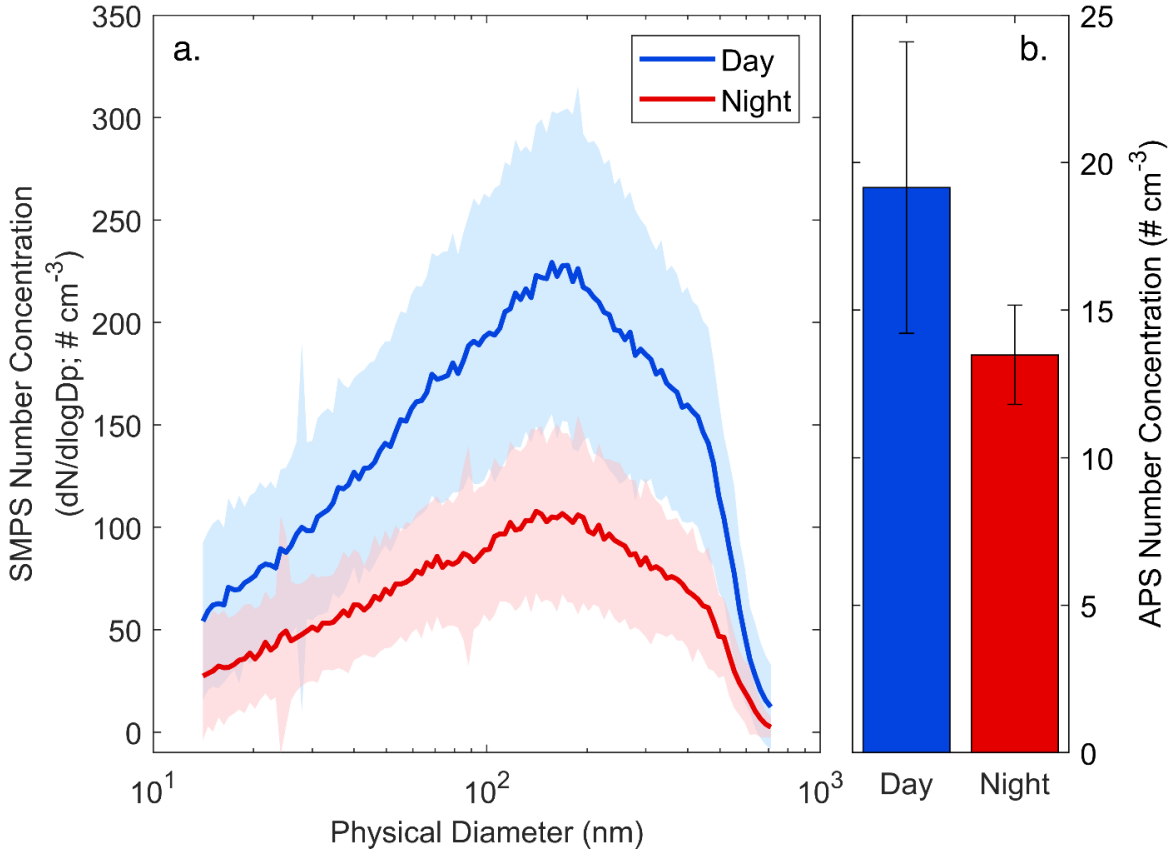

Figure 4.14 SMPS size distributions (a) and APS total number concentrations (D_p = 0.6 – 10 μm) (b) of nascent SSA from the day and night of a representative sampling period during Bloom 3 (8/7/2019). Shaded regions and error bars represent ± 1 σ. Day is defined as local time 07:00-21:59 PST and night is defined as 22:00-06:59 PST. While the number concentrations of SSA exhibit a strong diurnal change, the shape of the size distribution is relatively stable.

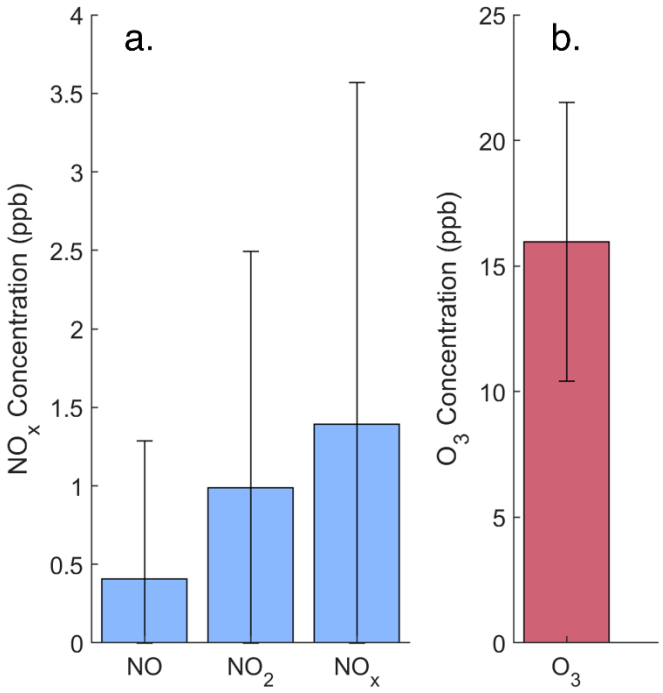

Figure 4.15 Average headspace concentrations of a) NO, NO_2, NO_x and b) O_3, measured from the upstream sampling port on the wave channel. Error bars represent ± σ.

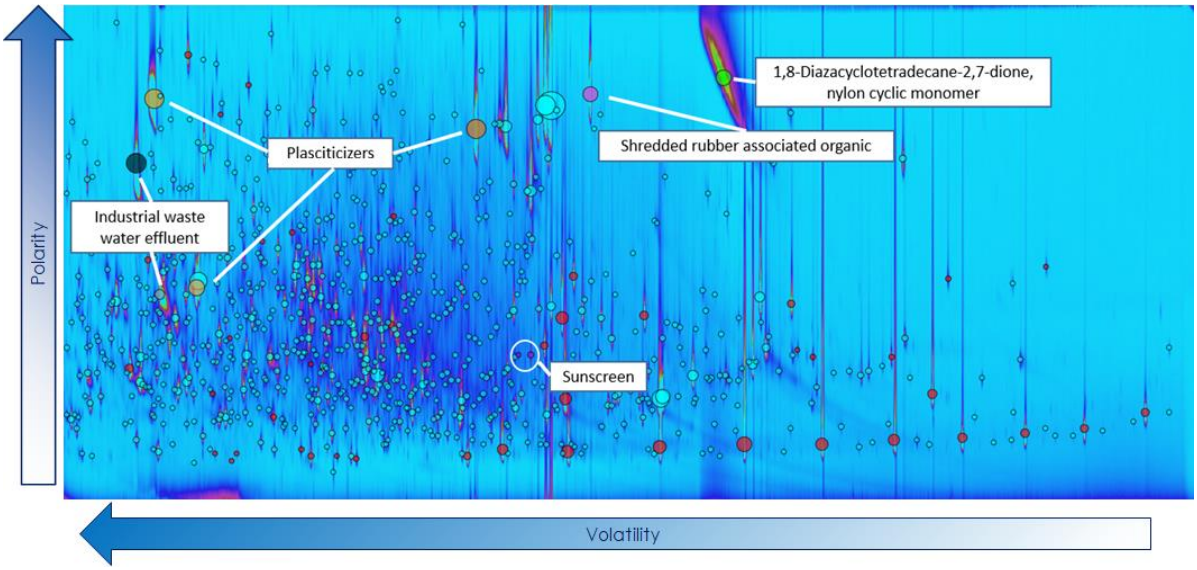

Figure 4.16 GCxGC spectrum of Scripps Pier marine DOM prior to transport. Significant contributions of anthropogenic plasticizers, wastewater effluent products, and personal care products (identified by confident mass spectral match to NIST library complemented by literature review) highlighted.

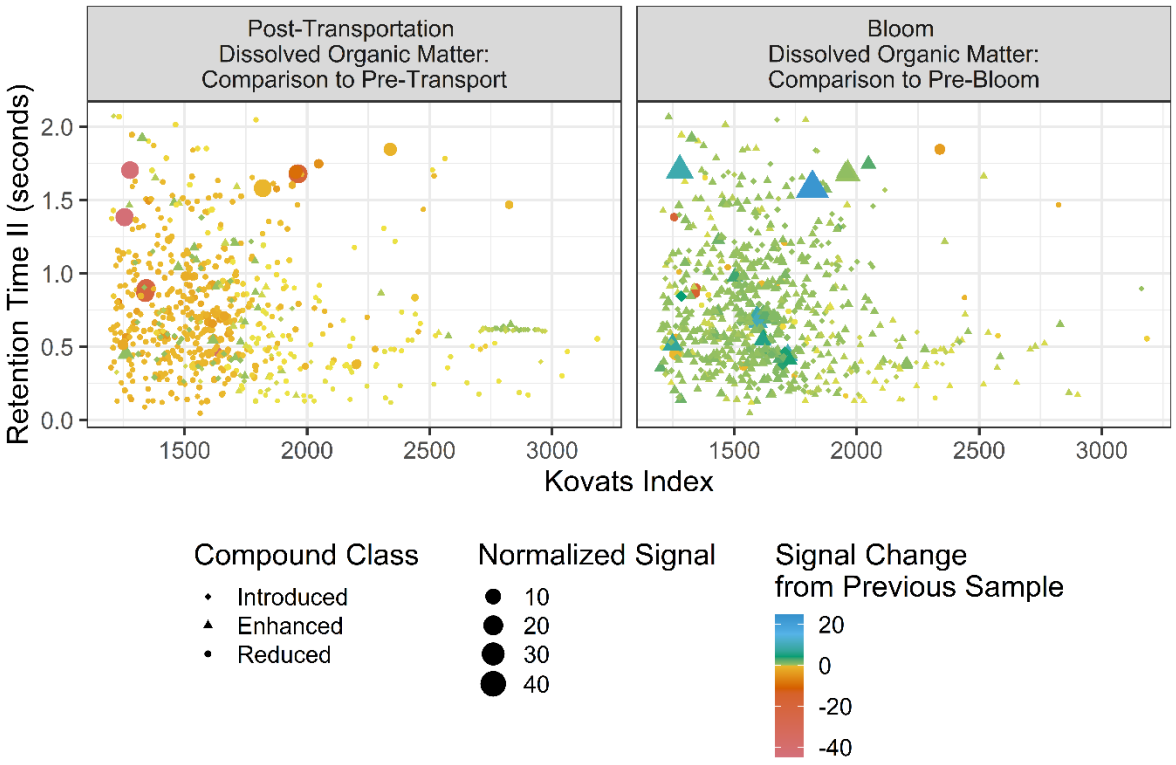

Figure 4.17 GCxGC spectra of DOM from Bloom 3, post-transportation from Scripps Pier into the wave channel (left) and post-bloom addition (right) samples illustrating the relative changes from pre-perturbation conditions.

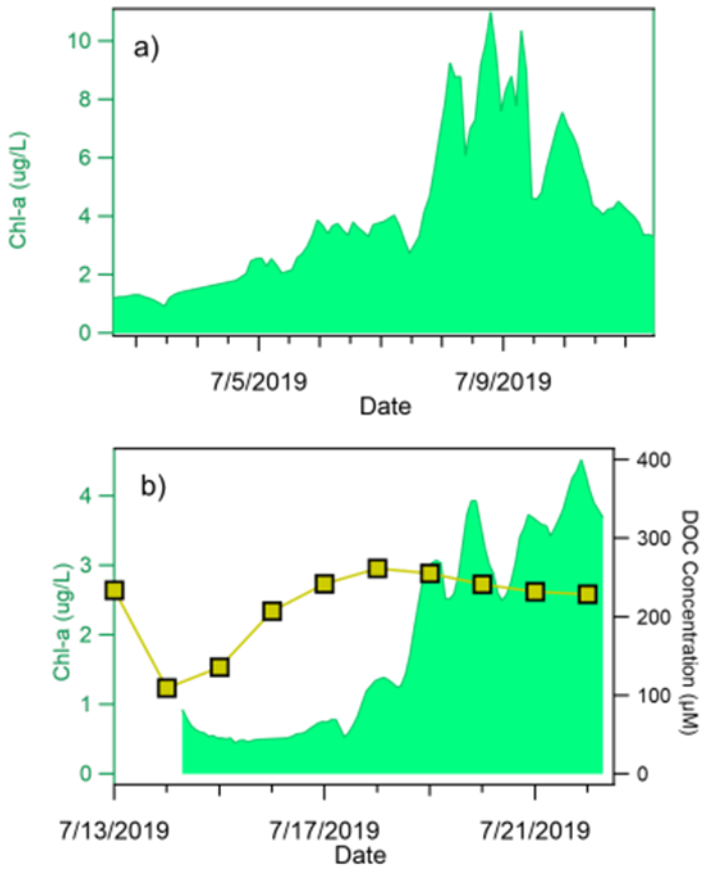

Figure 4.18 Time series chl-a and DOC concentration for a) Bloom 1 and b) Bloom 2.

4.12 References

Angle, K. J., Crocker, D. R., Simpson, R. M. C., Mayer, K. J., Garofalo, L. A., Moore, A. N., Garcia, S. L. M., Or, V. W., Srinivasan, S., Farhan, M., Sauer, J. S., Lee, C., Pothier, M. A., Farmer, D. K., Martz, T. R., Bertram, T. H., Cappa, C. D., Prather, K. A. and Grassian, V. H.: Acidity across the interface: from ocean waters to sea spray aerosol, *Proc. Natl. Acad. Sci.*, Accepted, 2020.

Athanasiadis, A., Fitzgerald, C., Davidson, N. M., Giorio, C., Botchway, S. W., Ward, A. D., Kalberer, M., Pope, F. D. and Kuimova, M. K.: Dynamic viscosity mapping of the oxidation of squalene aerosol particles, , 30385–30393, doi:10.1039/c6cp05674a, 2016.

Ault, A. P., Guasco, T. L., Ryder, O. S., Baltrusaitis, J., Cuadra-Rodriguez, L. A., Collins, D. B., Ruppel, M. J., Bertram, T. H., Prather, K. A. and Grassian, V. H.: Inside versus outside: Ion redistribution in nitric acid reacted sea spray aerosol particles as determined by single particle analysis, *J. Am. Chem. Soc.*, 135(39), 14528–14531, doi:10.1021/ja407117x, 2013a.

Ault, A. P., Guasco, T. L., Ryder, O. S., Baltrusaitis, J., Cuadra-Rodriguez, L. A., Collins, D. B., Ruppel, M. J., Bertram, T. H., Prather, K. A. and Grassian, V. H.: Inside versus outside: Ion redistribution in nitric acid reacted sea spray aerosol particles as determined by single particle analysis, *J. Am. Chem. Soc.*, 135(39), 14528–14531, doi:10.1021/ja407117x, 2013b.

Ault, A. P., Guasco, T. L., Baltrusaitis, J., Ryder, O. S., Trueblood, J. V., Collins, D. B., Ruppel, M. J., Cuadra-Rodriguez, L. A., Prather, K. A. and Grassian, V. H.: Heterogeneous reactivity of nitric acid with nascent sea spray aerosol: Large differences observed between and within individual particles, *J. Phys. Chem. Lett.*, 5(15), 2493–2500, doi:10.1021/jz5008802, 2014.

Azam, F., Fenchel, T., Field, J., Gray, J., Meyer-Reil, L. and Thingstad, F.: The Ecological Role of Water-Column Microbes in the Sea, Mar. Ecol. Prog. Ser., 10, 257–263, doi:10.3354/meps010257, 1983.

Becker, S., Aoyama, M., Woodward, E. M. S., Bakker, K., Coverly, S., Mahaffey, C. and Tanhua, T.: GO-SHIP Repeat Hydrography Nutrient Manual: The Precise and Accurate Determination of Dissolved Inorganic Nutrients in Seawater, Using Continuous Flow Analysis Methods, *Front. Mar. Sci.*, 7, doi:10.3389/fmars.2020.581790, 2020.

Boucher, O., Randall, D., Artaxo, P., Bretherton, C., Feingold, G., Forster, P., Kerminen, V.-M. V.-M., Kondo, Y., Liao, H., Lohmann, U., Rasch, P., Satheesh, S. K., Sherwood, S., Stevens, B., Zhang, X. Y. and Zhan, X. Y.: Clouds and Aerosols, Clim. Chang. 2013 Phys. Sci. Basis. Contrib. Work. Gr. I to Fifth Assess. Rep. Intergov. Panel Clim. Chang., 571–657, doi:10.1017/CBO9781107415324.016, 2013.

Bouvet, M., Hoepffner, N. and Dowell, M. D.: Parameterization of a spectral solar irradiance model for the global ocean using multiple satellite sensors, *J. Geophys. Res.Ocean.*,

107(C12), 8–18, doi:https://doi.org/10.1029/2001JC001126, 2002.

Brussaard, C. P. D.: Optimization of procedures for counting viruses by flow cytometry, *Appl. Environ. Microbiol.*, 70(3), 1506–1513, doi:10.1128/AEM.70.3.1506, 2004.

Buchan, A., LeCleir, G. R., Gulvik, C. A. and González, J. M.: Master recyclers: features and functions of bacteria associated with phytoplankton blooms., *Nat. Rev. Microbiol.*, 12(10), 686–698, doi:10.1038/nrmicro3326, 2014.

Carlson, D. J.: Surface microlayer phenolic enrichments indicate sea surface slicks, *Nature*, 296, 426–429, doi:10.1038/296426a0, 1982.

Chen, W.-C. and Marcus, R. A.: On the theory of the reaction rate of vibrationally excited CO molecules with OH radicals, *J. Chem. Phys.*, 124(2), 024306, doi:10.1063/1.2148408, 2006.

Christaki, U., Courties, C., Massana, R., Catala, P., Lebaron, P., Gasol, J. M. and Zubkov, M. V.: Optimized routine flow cytometric enumeration of heterotrophic flagellates using SYBR Green I, *Limnol. Oceanogr. Methods*, 9(AUG), 329–339, doi:10.4319/lom.2011.9.329, 2011a.

Christaki, U., Courties, C., Massana, R., Catala, P., Lebaron, P., Gasol, J. M. and Zubkov, M. V.: Optimized routine flow cytometric enumeration of heterotrophic flagellates using SYBR Green I, *Limnol. Oceanogr. Methods*, 9, 329–339, doi:10.4319/lom.2011.9.329, 2011b.

Ciuraru, R., Fine, L., Pinxteren, M. Van, D'Anna, B., Herrmann, H. and George, C.: Unravelling New Processes at Interfaces: Photochemical Isoprene Production at the Sea Surface, *Environ. Sci. Technol.*, 49(22), 13199–13205, doi:10.1021/acs.est.5b02388, 2015.

Cochran, R. E., Laskina, O., Jayarathne, T., Laskin, A., Laskin, J., Lin, P., Sultana, C., Lee, C., Moore, K. A., Cappa, C. D., Bertram, T. H., Prather, K. A., Grassian, V. H. and Stone, E. A.: Analysis of Organic Anionic Surfactants in Fine and Coarse Fractions of Freshly Emitted Sea Spray Aerosol, *Environ. Sci. Technol.*, 50(5), 2477–2486, doi:10.1021/acs.est.5b04053, 2016.

Collins, D. B., Zhao, D. F., Ruppel, M. J., Laskina, O., Grandquist, J. R., Modini, R. L., Stokes, M. D., Russell, L. M., Bertram, T. H., Grassian, V. H., Deane, G. B. and Prather, K. A.: Direct aerosol chemical composition measurements to evaluate the physicochemical differences between controlled sea spray aerosol generation schemes, *Atmos. Meas. Tech.*, 7(11), 3667–3683, doi:10.5194/amt-7-3667-2014, 2014.

Crocker, D. R., Hernandez, R. E., Huang, H. D., Pendergraft, M. A., Cao, R., Dai, J., Morris, C. K., Deane, G. B., Prather, K. A. and Thiemens, M. H.: Biological Influence on 13C and Organic Composition of Nascent Sea Spray Aerosol, *ACS Earth Sp. Chem.*, 4(9), 1686–1699, doi:10.1021/acsearthspacechem.0c00072, 2020.

Cunliffe, M. and Wurl, O.: Sampling the Sea Surface Microlayer., 2015.

DeCarlo, P. F., Kimmel, J. R., Trimborn, A., Northway, M. J., Jayne, J. T., Aiken, A. C., Gonin, M., Fuhrer, K., Horvath, T., Docherty, K. S., Worsnop, D. R. and Jimenez, J. L.: Field-deployable, high-resolution, time-of-flight aerosol mass spectrometer, *Anal. Chem.*, 78(24), 8281–8289, doi:10.1021/ac061249n, 2006.

Demott, P. J., Prenni, A. J., McMeeking, G. R., Sullivan, R. C., Petters, M. D., Tobo, Y., Niemand, M., Möhler, O., Snider, J. R., Wang, Z. and Kreidenweis, S. M.: Integrating laboratory and field data to quantify the immersion freezing ice nucleation activity of mineral dust particles, *Atmos. Chem. Phys.*, 15(1), 393–409, doi:10.5194/acp-15-393-2015, 2015.

DeMott, P. J., Hill, T. C. J., McCluskey, C. S., Prather, K. A., Collins, D. B., Sullivan, R. C., Ruppel, M. J., Mason, R. H., Irish, V. E., Lee, T., Hwang, C. Y., Rhee, T. S., Snider, J. R., McMeeking, G. R., Dhaniyala, S., Lewis, E. R., Wentzell, J. J. B., Abbatt, J., Lee, C., Sultana, C. M., Ault, A. P., Axson, J. L., Diaz Martinez, M., Venero, I., Santos-Figueroa, G., Stokes, M. D., Deane, G. B., Mayol-Bracero, O. L., Grassian, V. H., Bertram, T. H., Bertram, A. K., Moffett, B. F. and Franc, G. D.: Sea spray aerosol as a unique source of ice nucleating particles, *Proc. Natl. Acad. Sci.*, 113(21), 201514034, doi:10.1073/pnas.1514034112, 2015.

Dinasquet, J., Tiirola, M. and Azam, F.: Enrichment of Bacterioplankton Able to Utilize One-Carbon and Methylated Compounds in the Coastal Pacific Ocean , *Front. Mar. Sci.*, 5, 307.

Forestieri, S. D., Moore, K. A., Martinez Borrero, R., Wang, A., Stokes, M. D. and Cappa, C. D.: Temperature and Composition Dependence of Sea Spray Aerosol Production, *Geophys. Res. Lett.*, 45(14), 7218–7225, doi:10.1029/2018GL078193, 2018.

Gabey, A. M., Stanley, W. R., Gallagher, M. W. and Kaye, P. H.: The fluorescence properties of aerosol larger than 0.8 μ in urban and tropical rainforest locations, *Atmos. Chem. Phys.*, 11(11), 5491–5504, doi:10.5194/acp-11-5491-2011, 2011.

Gard, E., Mayer, J. E., Morrical, B. D., Dienes, T., Fergenson, D. P. and Prather, K. A: Real-time analysis of individual atmospheric aerosol particles: Design and performance of a portable ATOFMS, *Anal. Chem.*, 69(20), 4083–4091, doi:10.1021/ac970540n, 1997.

Gard, E. E., Kleeman, M. J., Gross, D. S., Hughes, L. S., Allen, J. O., Morrical, B. D., Fergenson, D. P., Dienes, T., Gälli, M. E., Johnson, R. J., Cass, G. R. and Prather, K. A.: Direct observation of heterogeneous chemistry in the atmosphere, *Science* (80-.)., 279(5354), 1184–1187, doi:10.1126/science.279.5354.1184, 1998.

Gasol, J. M. and Del Giorgio, P. A.: Using flow cytometry for counting natural planktonic bacteria and understanding the structure of planktonic bacterial communities, *Sci. Mar.*, 64(2), 197–224, doi:10.3989/scimar.2000.64n2197, 2000.

Gherman, T., Venables, D. S., Vaughan, S., Orphal, J. and Ruth, A. A.: Incoherent Broadband Cavity-Enhanced Absorption Spectroscopy in the near-Ultraviolet: Application to HONO and NO2, *Environ. Sci. Technol.*, 42(3), 890–895, doi:10.1021/es0716913, 2008.

Gong, S. L., Barrie, L. A. and Lazare, M.: Canadian Aerosol Module (CAM): A size-segregated

simulation of atmospheric aerosol processes for climate and air quality models 2. Global sea-salt aerosol and its budgets, *J. Geophys. Res. Atmos.*, 107(24), 1–14, doi:10.1029/2001JD002004, 2002.

Guillard, R. R. L. and Ryther, J. H.: Studies of Marine Planktonic Diatoms, *Can. J. Microbiol*., 8(2), 229–238, 1962.

Hales, B., Chipman, D. and Takahashi, T.: High-frequency measurement of partial pressure and total concentration of carbon dioxide in seawater using microporous hydrophobic membrane contactors, *Limnol. Oceanogr.* Methods, 2(11), 356–364, doi:https://doi.org/10.4319/lom.2004.2.356, 2004.

Hatch, L. E., Jen, C. N., Kreisberg, N. M., Selimovic, V., Yokelson, R. J., Stamatis, C., York, R. A., Foster, D., Stephens, S. L., Goldstein, A. H. and Barsanti, K. C.: Highly Speciated Measurements of Terpenoids Emitted from Laboratory and Mixed-Conifer Forest Prescribed Fires, *Environ. Sci. Technol.*, 53(16), 9418–9428, doi:10.1021/acs.est.9b02612, 2019.

Hering, S. V., Spielman, S. R. and Lewis, G. S.: Moderated, water-based, condensational particle growth in a laminar flow, *Aerosol Sci. Technol*., 48(4), 401–408, doi:10.1080/02786826.2014.881460, 2014.

Hering, S. V., Lewis, G. S., Spielman, S. R. and Eiguren-Fernandez, A.: A MAGIC concept for self-sustained, water-based, ultrafine particle counting, *Aerosol Sci. Technol*., 53(1), 63–72, doi:10.1080/02786826.2018.1538549, 2019.

Hettiyadura, A. P. S., Jayarathne, T., Baumann, K., Goldstein, A. H., De Gouw, J. A., Koss, A., Keutsch, F. N., Skog, K. and Stone, E. A.: Qualitative and quantitative analysis of atmospheric organosulfates in Centreville, Alabama, *Atmos. Chem. Phys.*, 17(2), 1343–1359, doi:10.5194/acp-17-1343-2017, 2017.

Holm-Hansen, O., Lorenzen, C. J., Holmes, R. W. and Strickland, J. D. H.: Fluorometric Determination of Chlorophyll, ICES *J. Mar. Sci*., 30(1), 3–15, doi:10.1093/icesjms/30.1.3, 1965.

Hoppe, H.-G.: Significance of exoenzymatic activities in the ecology of brackish water: measurements by means of methylumbelliferyl-substrates, *Mar. Ecol. Prog. Ser.*, 11(3), 299–308, doi:10.3354/meps011299, 1983.

Jain, S. and Petrucci, G. A.: A new method to measure aerosol particle bounce using a cascade electrical low pressure impactor, *Aerosol Sci. Technol*., 49(6), 390–399, doi:10.1080/02786826.2015.1036393, 2015.

Jen, C. N., Hatch, L. E., Selimovic, V., Yokelson, R. J., Weber, R., Fernandez, A. E., Kreisberg, N. M., Barsanti, K. C. and Goldstein, A. H.: Speciated and total emission factors of particulate organics from burning western US wildland fuels and their dependence on combustion efficiency, *Atmos. Chem. Phys.*, 19(2), 1013–1026, doi:10.5194/acp-19-1013-2019, 2019.

Kang, E., Root, M. J. and Brune, W. H.: Introducing the concept of Potential Aerosol Mass (PAM), *Atmos. Chem. Phys*., 7, 5727–5744, doi:10.5194/acp-7-5727-2007, 2007.

Kercher, J. P., Riedel, T. P. and Thornton, J. A.: Chlorine activation by N2O5: Simultaneous , in situ detection of ClNO2 and N2O5 by chemical ionization mass spectrometry, *Atmos. Meas. Tech.*, 1(2), 193–204, doi:https://dx.doi.org/10.5194/amt-2-193-2009, 2009.

Kim, M. J., Michaud, J. M., Williams, R., Sherwood, B. P., Pomeroy, R., Azam, F., Burkart, M. and Bertram, T. H.: Bacterial-driven production of nitrates in seawater, *Geophys. Res. Lett.*, 42(2), 1–8, doi:10.1002/2014GL062865, 2015.

Kim, M. J., Zoerb, M. C., Campbell, N. R., Zimmermann, K. J., Blomquist, B. W., Huebert, B. J. and Bertram, T. H.: Revisiting benzene cluster cations for the chemical ionization of dimethyl sulfide and select volatile organic compounds, *Atmos. Meas. Tech.*, 9(4), 1473–1484, doi:10.5194/amt-9-1473-2016, 2016.

Krechmer, J., Lopez-Hilfiker, F., Koss, A., Hutterli, M., Stoermer, C., Deming, B., Kimmel, J., Warneke, C., Holzinger, R., Jayne, J., Worsnop, D., Fuhrer, K., Gonin, M. and De Gouw, J.: Evaluation of a New Reagent-Ion Source and Focusing Ion-Molecule Reactor for Use in Proton-Transfer-Reaction Mass Spectrometry, *Anal. Chem.*, 90(20), 12011–12018, doi:10.1021/acs.analchem.8b02641, 2018.

Ksionzek, K. B., Lechtenfeld, O. J., McCallister, S. L., Schmitt-Kopplin, P., Geuer, J. K., Geibert, W. and Koch, B. P.: Dissolved organic sulfur in the ocean: Biogeochemistry of a petagram inventory, *Science* (80-.)., 354(6311), 456 LP – 459, doi:10.1126/science.aaf7796, 2016.

Lambe, A. T., Ahern, A. T., Williams, L. R., Slowik, J. G., Wong, J. P. S., Abbatt, J. P. D., Brune, W. H., Ng, N. L., Wright, J. P., Croasdale, D. R., Worsnop, D. R., Davidovits, P. and Onasch, T. B.: Characterization of aerosol photooxidation flow reactors: Heterogeneous oxidation, secondary organic aerosol formation and cloud condensation nuclei activity measurements, *Atmos. Meas. Tech.*, 4(3), 445–461, doi:10.5194/amt-4-445-2011, 2011.

Lavi, A., Vermeuel, M. P., Novak, G. A. and Bertram, T. H.: The sensitivity of benzene cluster cation chemical ionization mass spectrometry to select biogenic terpenes, *Atmos. Meas. Tech.*., 11, 3251–3262, https://doi.org/10.5194/amt-11-3251-2018, 2018.

Lee, C., Sultana, C. M., Collins, D. B., Santander, M. V., Axson, J. L., Malfatti, F., Cornwell, G. C., Grandquist, J. R., Deane, G. B., Stokes, M. D., Azam, F., Grassian, V. H. and Prather, K. A.: Advancing Model Systems for Fundamental Laboratory Studies of Sea Spray Aerosol Using the Microbial Loop, *J. Phys. Chem. A.*, 119(33), 8860–8870, doi:10.1021/acs.jpca.5b03488, 2015.

Lee, H. D., Ray, K. K. and Tivanski, A. V.: Solid, Semisolid, and Liquid Phase States of Individual Submicrometer Particles Directly Probed Using Atomic Force Microscopy, *Anal. Chem.*, 89(23), 12720–12726, doi:10.1021/acs.analchem.7b02755, 2017.

Lee, H. D., Kaluarachchi, C. P., Hasenecz, E. S., Zhu, J. Z., Popa, E., Stone, E. A. and Tivanski, A. V.: Effect of dry or wet substrate deposition on the organic volume fraction of core-

shell aerosol particles, *Atmos. Meas. Tech.*, 12(3), 2033–2042, doi:10.5194/amt-12-2033-2019, 2019.

Lee, H. D., Morris, H. S., Laskina, O., Sultana, C. M., Lee, C., Jayarathne, T., Cox, J. L., Wang, X., Hasenecz, E. S., Demott, P. J., Bertram, T. H., Cappa, C. D., Stone, E. A., Prather, K. A., Grassian, V. H. and Tivanski, A. V.: Organic Enrichment, Physical Phase State, and Surface Tension Depression of Nascent Core-Shell Sea Spray Aerosols during Two Phytoplankton Blooms, *ACS Earth Sp. Chem.*, 4(4), 650–660, doi:10.1021/acsearthspacechem.0c00032, 2020a.

Lee, H. D., Wigley, S., Lee, C., Or, V. W., Hasenecz, E. S., Stone, E. A., Grassian, V. H., Prather, K. A. and Tivanski, A. V.: Physicochemical Mixing State of Sea Spray Aerosols: Morphologies Exhibit Size Dependence, *ACS Earth Sp. Chem.*, 4(9), 1604–1611, doi:10.1021/acsearthspacechem.0c00153, 2020b.

Leu, M. T., Timonen, R. S., Keyser, L. F. and Yung, Y. L.: Heterogeneous reactions of HNO3(g) + NaCl(s) → HCl(g) + NaNO3(s) and N2O5(g) + NaCl(s) → ClNO2(g) + NaNO3(s), *J. Phys. Chem.*, 99(35), 13203–13212, doi:10.1021/j100035a026, 1995.

Levine, N. M., Varaljay, V. A., Toole, D. A., Dacey, J. W. H., Doney, S. C. and Moran, M. A.: Environmental, biochemical and genetic drivers of DMSP degradation and DMS production in the Sargasso Sea, *Environ. Microbiol.*, 14(5), 1210–1223, https://doi.org/10.1111/j.1462-2920.2012.02700.x, 2012.

Lewis, E. R. and Schwartz, S. E.: Sea Salt Aerosol Production: Mechanisms, Methods, Measurements, and Models--A Critical Review, American Geophysical Union, Washington D.C., 2004.

Lopez-Hilfiker, F. D., Pospisilova, V., Huang, W., Kalberer, M., Mohr, C., Stefenelli, G., Thornton, J. A., Baltensperger, U., Prevot, A. S. H., and Slowik, J. G.: An extractive electrospray ionization time-of-flight mass spectrometer (EESI-TOF) for online measurement of atmospheric aerosol particles, Atmos. Meas. Tech., 12, 4867–4886, https://doi.org/10.5194/amt-12-4867-2019, 2019.

Lopez-Yglesias, X. F., Yeung, M. C., Dey, S. E., Brechtel, F. J. and Chan, C. K.: Performance evaluation of the Brechtel Mfg. Humidified Tandem Differential Mobility Analyzer (BMI HTDMA) for studying hygroscopic properties of aerosol particles, *Aerosol Sci. Technol.*, 48(9), 969–980, doi:10.1080/02786826.2014.952366, 2014.

Mael, L. E., Busse, H. and Grassian, V. H.: Measurements of Immersion Freezing and Heterogeneous Chemistry of Atmospherically Relevant Single Particles with Micro-Raman Spectroscopy, *Anal. Chem.*, 91(17), 11138–11145, doi:10.1021/acs.analchem.9b01819, 2019.

Marie, D., Partensky, F., Jacquet, S. and Vaulot, D.: Enumeration and cell cycle analysis of natural populations of marine picoplankton by flow cytometry using the nucleic acid stain SYBR Green I, Appl. *Environ. Microbiol.*, 63(1), 186–193, doi:10.1128/aem.63.1.186-193.1997, 1997.

Marie, D., Rigaut-Jalabert, F. and Vaulot, D.: An improved protocol for flow cytometry analysis of phytoplankton cultures and natural samples, *Cytom. Part A*, 85(11), 962–968, doi:10.1002/cyto.a.22517, 2014.

Mayer, K. J., Sauer, J. S., Dinasquet, J. and Prather, K. A.: CAICE Studies: Insights from a Decade of Ocean−Atmosphere Experiments in the Laboratory, *Acc. Chem. Res*. 2020, 53, 11, 2510–2520, doi: 10.1021/acs.accounts.0c00504, 2020a.

Mayer, K. J., Wang, X., Santander, M. V, Mitts, B. A., Sauer, J. S., Sultana, C. M., Cappa, C. D. and Prather, K. A.: Secondary Marine Aerosol Plays a Dominant Role over Primary Sea Spray Aerosol in Cloud Formation, *ACS Cent. Sci*., 6, 12, 2259–2266 doi:10.1021/acscentsci.0c00793, 2020b.

Michaud, J. M., Thompson, L. R., Kaul, D., Espinoza, J. L., Richter, R. A., Xu, Z. Z., Lee, C., Pham, K. M., Beall, C. M., Malfatti, F., Azam, F., Knight, R., Burkart, M. D., Dupont, C. L. and Prather, K. A.: Taxon-specific aerosolization of bacteria and viruses in an experimental ocean-atmosphere mesocosm, *Nat. Commun*., 9(1), doi:10.1038/s41467-018-04409-z, 2018.

Minich, J. J., Zhu, Q., Janssen, S., Hendrickson, R., Amir, A., Vetter, R., Hyde, J., Doty, M. M., Stillwell, K., Benardini, J., Kim, J. H., Allen, E. E., Venkateswaran, K. and Knight, R.: KatharoSeq Enables High-Throughput Microbiome Analysis from Low-Biomass Samples, edited by M. J. McFall-Ngai, *mSystems*, 3(3), e00218-17, doi:10.1128/mSystems.00218-17, 2018.

Noble, R. T. and Fuhrman, J. A.: Use of SYBR Green I for rapid epifluorescence counts of marine viruses and bacteria, *Aquat. Microb. Ecol*., 14(2), 113–118, doi:10.3354/ame014113, 1998.

Novak, G. A. and Bertram, T. H.: Reactive VOC Production from Photochemical and Heterogeneous Reactions Occurring at the Air-Ocean Interface, *Acc. Chem. Res.*, 53(5), 1014–1023, doi:10.1021/acs.accounts.0c00095, 2020.

O'Dowd, C. D. and de Leeuw, G.: Marine aerosol production: a review of the current knowledge, *Philos. Trans. R. Soc. A Math. Phys. Eng. Sci.*, 365(1856), 1753–1774, doi:10.1098/rsta.2007.2043, 2007.

Olson, R. J., Chisholm, S. W., Zettler, E. R. and Armbrust, E. V.: Pigments, size, and distributions of Synechococcus in the North Atlantic and Pacific Oceans, *Limnol. Oceanogr.*, 35(1), 45–58, doi:10.4319/lo.1990.35.1.0045, 1990.

Or, V. W., Estillore, A. D., Tivanski, A. V. and Grassian, V. H.: Lab on a tip: Atomic force microscopy-photothermal infrared spectroscopy of atmospherically relevant organic/inorganic aerosol particles in the nanometer to micrometer size range, *Analyst*, 143(12), 2765–2774, doi:10.1039/c8an00171e, 2018.

Orenstein, E. C., Ratelle, D., Briseño-Avena, C., Carter, M., Franks, P. J. S., Jaffe, J. S. and Roberts, P. L. D.: The Scripps Plankton Camera system: a framework and platform for in situ microscopy, *Limnol. Oceanogr. Methods*, submitted, doi:10.1002/lom3.10394, 2020.

Patterson, J. P., Collins, D. B., Michaud, J. M., Axson, J. L., Sultana, C. M., Moser, T., Dommer, A. C., Conner, J., Grassian, V. H., Stokes, M. D., Deane, G. B., Evans, J. E., Burkart, M. D., Prather, K. A. and Gianneschi, N. C.: Sea Spray Aerosol Structure and Composition Using Cryogenic Transmission Electron Microscopy., *ACS Cent. Sci.*, 2(1), 40–47, doi:10.1021/acscentsci.5b00344, 2016.

Perkins, R. J., Gillette, S. M., Hill, T. C. J. and Demott, P. J.: The Labile Nature of Ice Nucleation by Arizona Test Dust, *ACS Earth Sp. Chem.*, 4(1), 133–141, doi:10.1021/acsearthspacechem.9b00304, 2020.

Peters, T. M. and Leith, D.: Concentration measurement and counting efficiency of the aerodynamic particle sizer 3321, *J. Aerosol Sci.*, 34(5), 627–634, doi:10.1016/S0021-8502(03)00030-2, 2003.

Petras, D., Koester, I., Da Silva, R., Stephens, B. M., Haas, A. F., Nelson, C. E., Kelly, L. W., Aluwihare, L. I. and Dorrestein, P. C.: High-Resolution Liquid Chromatography Tandem Mass Spectrometry Enables Large Scale Molecular Characterization of Dissolved Organic Matter, *Front. Mar. Sci.*, 4, 405.

Pomeroy, L. R., Williams, P. J. B., Azam, F. and Hobbie, J. E.: The Microbial Loop, *Oceanography*, 20(2), 28–33, doi:10.5670/oceanog.2007.45, 2007.

Prather, K. A, Bertram, T. H., Grassian, V. H., Deane, G. B., Stokes, M. D., Demott, P. J., Aluwihare, L. I., Palenik, B. P., Azam, F., Seinfeld, J. H., Moffet, R. C., Molina, M. J., Cappa, C. D., Geiger, F. M., Roberts, G. C., Russell, L. M., Ault, A. P., Baltrusaitis, J., Collins, D. B., Corrigan, C. E., Cuadra-Rodriguez, L. a, Ebben, C. J., Forestieri, S. D., Guasco, T. L., Hersey, S. P., Kim, M. J., Lambert, W. F., Modini, R. L., Mui, W., Pedler, B. E., Ruppel, M. J., Ryder, O. S., Schoepp, N. G., Sullivan, R. C. and Zhao, D.: Bringing the ocean into the laboratory to probe the chemical complexity of sea spray aerosol., *Proc. Natl. Acad. Sci. U. S. A.*, 110(19), 7550–5, doi:10.1073/pnas.1300262110, 2013.

Ray, K. K., Lee, H. D., Gutierrez, M. A., Chang, F. J. and Tivanski, A. V.: Correlating 3D Morphology, Phase State, and Viscoelastic Properties of Individual Substrate-Deposited Particles, *Anal. Chem.*, 91(12), 7621–7630, doi:10.1021/acs.analchem.9b00333, 2019.

Roberts, G. C. and Nenes, A.: A Continuous-Flow Streamwise Thermal-Gradient CCN Chamber for Atmospheric Measurements, *Aerosol Sci. Technol.*, 39(3), 206–221, doi:10.1080/027868290913988, 2005.

Roveretto, M., Li, M., Hayeck, N., Brüggemann, M., Emmelin, C., Perrier, S. and George, C.: Real-Time Detection of Gas-Phase Organohalogens from Aqueous Photochemistry Using Orbitrap Mass Spectrometry, *ACS Earth Sp. Chem.*, 3(3), 329–334, doi:10.1021/acsearthspacechem.8b00209, 2019.

Ryder, O. S., Campbell, N. R., Morris, H., Forestieri, S., Ruppel, M. J., Cappa, C., Tivanski, A., Prather, K. and Bertram, T. H.: Role of Organic Coatings in Regulating N2O5 Reactive Uptake to Sea Spray Aerosol, *J. Phys. Chem. A.*, 119(48), 11683–11692, doi:10.1021/acs.jpca.5b08892, 2015.

Saukko, E., Lambe, A. T., Massoli, P., Koop, T., Wright, J. P., Croasdale, D. R., Pedernera, D. A., Onasch, T. B., Laaksonen, A., Davidovits, P., Worsnop, D. R. and Virtanen, A.: Humidity-dependent phase state of SOA particles from biogenic and anthropogenic precursors, *Atmos. Chem. Phys.*, 12(16), 7517–7529, doi:10.5194/acp-12-7517-2012, 2012.

Schneider, S. R., Collins, D. B., Lim, C. Y., Zhu, L. and Abbatt, J. P. D.: Formation of Secondary Organic Aerosol from the Heterogeneous Oxidation by Ozone of a Phytoplankton Culture, *ACS Earth Sp. Chem.*, 3(10), 2298–2306, doi:10.1021/acsearthspacechem.9b00201, 2019.

Shen, S., Jaques, P. A., Zhu, Y., Geller, M. D. and Sioutas, C.: Evaluation of the SMPS-APS system as a continuous monitor for measuring PM2.5, PM10 and coarse (PM2.5-10) concentrations, *Atmos. Environ.*, 36(24), 3939–3950, doi:10.1016/S1352-2310(02)00330-8, 2002.

Smith, D. and Azam, F.: A simple, economical method for measuring bacterial protein synthesis rates in seawater using 3H-leucine, *Mar. Microb. food webs*, 6(2), 107–114, 1992.

Smith, J. N., Moore, K. F., McMurry, P. H. and Eisele, F. L.: Atmospheric Measurements of Sub-20 nm Diameter Particle Chemical Composition by Thermal Desorption Chemical Ionization Mass Spectrometry, *Aerosol Sci. Technol.*, 38(2), 100–110, doi:10.1080/02786820490249036, 2004.

Stokes, M. D., Deane, G. B., Prather, K., Bertram, T. H., Ruppel, M. J., Ryder, O. S., Brady, J. M. and Zhao, D.: A Marine Aerosol Reference Tank system as a breaking wave analogue for the production of foam and sea-spray aerosols, *Atmos. Meas. Tech.*, 6(4), 1085–1094, doi:10.5194/amt-6-1085-2013, 2013.

Stokes, M. D., Deane, G., Collins, D. B., Cappa, C., Bertram, T., Dommer, A., Schill, S., Forestieri, S. and Survilo, M.: A miniature Marine Aerosol Reference Tank (miniMART) as a compact breaking wave analogue, *Atmos. Meas. Tech.*, 9(9), 4257–4267, doi:10.5194/amt-9-4257-2016, 2016.

Stubbins, A. and Dittmar, T.: Low volume quantification of dissolved organic carbon and dissolved nitrogen, *Limnol. Oceanogr. Methods*, 10, 347–352, doi:10.4319/lom.2012.10.347, 2012.

Trueblood, J. V., Alves, M. R., Power, D., Santander, M. V., Cochran, R. E., Prather, K. A. and Grassian, V. H.: Shedding Light on Photosensitized Reactions within Marine-Relevant Organic Thin Films, *ACS Earth Sp. Chem.*, 3(8), 1614–1623, doi:10.1021/acsearthspacechem.9b00066, 2019a.

Trueblood, J. V., Wang, X., Or, V. W., Alves, M. R., Santander, M. V., Prather, K. A. and Grassian, V. H.: The Old and the New: Aging of Sea Spray Aerosol and Formation of Secondary Marine Aerosol through OH Oxidation Reactions, *ACS Earth Sp. Chem.*, 3(10), 2307–2314, doi:10.1021/acsearthspacechem.9b00087, 2019b.

Utermöhl, H.: Neue Wege in der quantitativen Erfassung des Plankton.(Mit besonderer Berücksichtigung des Ultraplanktons.), *SIL Proceedings*, 1922-2010, 5(2), 567–596,

doi:10.1080/03680770.1931.11898492, 1931.

Voisin, D., Smith, J. N., Sakurai, H., McMurry, P. H. and Eisele, F. L.: Thermal desorption chemical ionization mass spectrometer for ultrafine particle chemical composition, *Aerosol Sci. Technol.*, 37(6), 471–475, doi:10.1080/02786820300959, 2003.

Wakeham, S. G., Canuel, E. A. and Doering, P. H.: Geochemistry of volatile organic compounds in seawater: Mesocosm experiments with 14C-model compounds, *Geochim. Cosmochim. Acta*, 50(6), 1163–1172, doi:10.1016/0016-7037(86)90399-6, 1986.

Walters, W., Hyde, E. R., Berg-Lyons, D., Ackermann, G., Humphrey, G., Parada, A., Gilbert, J. A., Jansson, J. K., Caporaso, J. G., Fuhrman, J. A., Apprill, A. and Knight, R.: Improved Bacterial 16S rRNA Gene (V4 and V4-5) and Fungal Internal Transcribed Spacer Marker Gene Primers for Microbial Community Surveys, edited by H. Bik, mSystems, 1(1), e00009-15, doi:10.1128/mSystems.00009-15, 2016.

Wang, X., Sultana, C. M., Trueblood, J., Hill, T. C. J., Malfatti, F., Lee, C., Laskina, O., Moore, K. A., Beall, C. M., McCluskey, C. S., Cornwell, G. C., Zhou, Y., Cox, J. L., Pendergraft, M. A., Santander, M. V., Bertram, T. H., Cappa, C. D., Azam, F., DeMott, P. J., Grassian, V. H. and Prather, K. A.: Microbial Control of Sea Spray Aerosol Composition: A Tale of Two Blooms, *ACS Cent. Sci*., 1(3), 124–131, doi:10.1021/acscentsci.5b00148, 2015.

Wang, X., Deane, G. B., Moore, K. A., Ryder, O. S., Stokes, M. D., Beall, C. M., Collins, D. B., Santander, M. V., Burrows, S. M., Sultana, C. M. and Prather, K. A.: The role of jet and film drops in controlling the mixing state of submicron sea spray aerosol particles, *Proc. Natl. Acad. Sci. U. S. A.*, 114(27), 6978–6983, doi:10.1073/pnas.1702420114, 2017.

Wei, Y., Jiao, Y., An, D., Li, D., Li, W. and Wei, Q.: Review of dissolved oxygen detection technology: From laboratory analysis to online intelligent detection, Sensors (Switzerland), 19(18), doi:10.3390/s19183995, 2019.

Wolfe, G. M., Nicely, J. M., St. Clair, J. M., Hanisco, T. F., Liao, J., Oman, L. D., Brune, W. B., Miller, D., Thames, A., González Abad, G., Ryerson, T. B., Thompson, C. R., Peischl, J., McKain, K., Sweeney, C., Wennberg, P. O., Kim, M., Crounse, J. D., Hall, S. R., Ullmann, K., Diskin, G., Bui, P., Chang, C. and Dean-Day, J.: Mapping hydroxyl variability throughout the global remote troposphere via synthesis of airborne and satellite formaldehyde observations, *Proc. Natl. Acad. Sci.*, 116(23), 11171 LP – 11180, doi:10.1073/pnas.1821661116, 2019.

Worton, D. R., Decker, M., Isaacman-VanWertz, G., Chan, A. W. H., Wilson, K. R. and Goldstein, A. H.: Improved molecular level identification of organic compounds using comprehensive two-dimensional chromatography, dual ionization energies and high resolution mass spectrometry, *Analyst*, 142(13), 2395–2403, doi:10.1039/c7an00625j, 2017.

Chapter 5 Atmospheric Reactions Drive Variability in Secondary Marine Aerosol Composition and Cloud-Forming Ability

5.1 Abstract

The ability of clouds in marine environments to cool the planet by reflecting sunlight has been suggested to be linked to biological processes occurring in the ocean leading to changes in aerosols in marine environments. A major challenge has involved separating the cloud seeding contributions of sea spray aerosol (SSA) emitted directly from the ocean versus secondary marine aerosol (SMA). Here, we induce a phytoplankton bloom in an isolated ocean-atmosphere system to study the cloud forming abilities of marine aerosols. Whereas nascent SSA hygroscopicity is relatively insensitive to biological activity in seawater, the hygroscopicity of SMA depends on both the extent of biological activity and photochemical aging. The observations reveal that differences in photochemical aging timescales of sulfur-containing and non-sulfur organic gases, along with differences in their response to ocean biological activity over the course of the bloom, drive variations in SMA composition, with SMA at short (<1 day) photochemical aging times transitioning to sulfur-rich gases under more extensive aging.

5.2 Introduction

Oceans cover 71% of Earth's surface and are a major source of atmospheric aerosols, which influence cloud formation, weather, and climate. The two major types of ocean-derived aerosols are sea spray aerosol (SSA) produced by breaking waves, and secondary marine aerosol (SMA) formed by condensation of products formed by oxidation of gases emitted from the ocean. SSA and SMA differ in composition, size, and abundance. In addition, their relative sensitivities to ocean conditions and potential effects on low-level marine clouds remain unclear. Nonetheless, correlations between marine cloud droplet number and seawater chlorophyll-a (chl-a)

concentrations have suggested links between marine clouds, aerosols, and oceanic phytoplankton blooms (Lana et al., 2012; McCoy et al., 2015; Meskhidze and Nenes, 2006). Establishing the mechanisms through which ocean biological activity can influence marine aerosol properties and abundances, and thus cloud properties, is crucial for understanding the current and future climate system.

The relative contributions of SSA and SMA to marine cloud condensation nuclei (CCN) vary widely, but recent studies indicate that over much of the ocean only a small fraction of nascent SSA represents only a small fraction of CCN (Gras and Keywood, 2017; Quinn et al., 2017). Furthermore, studies have shown that the flux, size distribution, and CCN activity of SSA are relatively insensitive to biological activity in seawater (Bates et al., 2020; Collins et al., 2016; Forestieri et al., 2018b). In contrast, strong seasonal relationships have been observed between marine phytoplankton, dimethyl sulfide (DMS) emissions, and the production of secondary sulfate aerosols (Ayers and Gras, 1991; Gras and Keywood, 2017; Korhonen et al., 2008; Sanchez et al., 2018). This implicates SMA as a major driver of ocean-cloud interactions in remote regions such as the southern oceans, where marine emissions dominate with little to no contributions from anthropogenic or terrestrial sources.

For several decades, the oxidation products of dimethyl sulfide (DMS) have been the most studied contributors to secondary marine aerosol (Charlson et al., 1987; Clarke et al., 1998). However, the oceans also emit a wide range of other volatile organic compounds (VOCs) (15, and references therein), including isoprene (Palmer and Shaw, 2005), monoterpenes (Kim et al., 2017; Shaw et al., 2010), and amines (Facchini et al., 2008). Photochemical reactions oxidize VOCs, forming products which can condense to form secondary organic aerosol (SOA), thus influencing the properties and chemical composition of SMA. Studies of marine aerosol hygroscopicity have

shown a suppression of water uptake in sub-micron particles, which has been attributed to the presence of organic matter (Fletcher et al., 2007; Modini et al., 2010). In laboratory studies, the formation of SOA has been observed from oxidizing the headspace gases above phytoplankton blooms (Schneider et al., 2019). In addition, VOCs may potentially enhance H_2SO_4 nucleation, with SOA tracers observed in ultrafine particles during coastal nucleation events (Vaattovaara et al., 2006). Yet, the relative importance of non-sulfur containing VOCs (NS-VOCs) compared to DMS for controlling SMA production and properties has not yet been established. This is primarily due to an inability to study the hygroscopicity of SMA without interferences from primary sea spray and terrestrial aerosols in the marine atmosphere.

Despite the potential for NS-VOCs to contribute significantly to SMA formation—and the consequent associated implications for both SMA production rates and CCN activity—targeted studies that elucidate and systematically unravel the relationships between biological conditions in seawater, VOC emissions, and SMA formation over the course of a phytoplankton bloom are generally lacking. Such laboratory ocean-atmosphere experiments will allow for separate characterization of SMA and SSA under clean, isolated conditions, removing the challenges from interferences that impact the interpretation of ambient measurements (Mayer et al., 2020; Trueblood et al., 2019).

Here, we present results from an ocean-atmosphere mesocosm experiment in which both SMA and SSA were characterized concurrently over the course of a phytoplankton bloom, which was initiated in 12,000 L of coastal Pacific Ocean seawater. Throughout the experiment, gases emitted from the seawater were entrained in a clean airflow and oxidized by OH radicals to form SMA in an oxidation flow reactor (OFR), which was operated at multiple OH exposures ranging from 0.5 to 8 days of equivalent aging (see Supplementary Material). We demonstrate that

temporal variability of both non-DMS and DMS gaseous emissions across a phytoplankton bloom controls SMA production and composition, which ultimately determines SMA CCN activity. Notably, seawater chl-a concentrations, a proxy for phytoplankton biomass, only weakly predicts both SMA production and composition. This suggests a complex relationship between VOC emissions and marine microorganism life cycles and community dynamics. Importantly, we observe a strong relationship between OH exposure extent in the OFR and the CCN activity of the resulting aerosol, indicating that atmospheric aging timescales strongly effect the composition and properties of SMA. Together with concurrently produced SSA, the observed CCN activities match the full range of values previously observed in marine environments, and thus can be used to explain previous ocean-cloud relationships that have eluded scientists for decades.

5.3 Results and Discussion

5.3.1 Marine VOC Emissions

Measurements of the gas-phase VOCs evolved from the seawater indicate the presence of a wide range of compounds that are involved in SMA formation. The production and emission of biogenic VOCs from seawater are largely controlled by the growth and death of phytoplankton, as well as by its interactions with bacteria, and viruses (Halsey et al., 2017). Furthermore, abiotic factors such as light flux, temperature, and wind speed can significantly affect the production and emission of gases from seawater (Carpenter et al., 2012). As expected, DMS is one of the more abundant gas phase species observed (Figure 5.1A). The DMS concentration starts relatively low, increases initially until reaching a maximum shortly after the peak of the bloom (indicated by the maximum in the chl-a), remains elevated as the chl-a initially decays, and then decreases. Other notably abundant ions include C_2H_4O (likely acetaldehyde, ethanol, or acetic acid), C_3H_6O

(acetone or propanal), and C_4H_8O (butanone or butyraldehyde). Acetone and acetaldehyde have also been observed in seawater and atmospheric measurements made in the Southern Ocean (Wohl et al., 2020). However, these low molecular weight species are unlikely to contribute to SOA formation and thus we do not discuss them further. We also observed several known biogenic SOA precursors: monoterpenes, oxygenated monoterpenes, and isoprene (Figure 5.5), but their abundances are generally too small to explain the observed SOA formation. However, number of additional NS-VOCs were observed in the headspace, which may have contributed to the SOA formation (Figure 5.6, Figure 5.7).

The source of these other NS-VOCs is unclear. Marine phytoplankton and bacteria have been shown to produce a wide range of VOCs beyond isoprene and monoterpenes (Carpenter et al., 2012). However, in coastal environments, terrestrial runoff could comprise an additional source of VOCs in seawater (Anku et al., 2017). A number of aromatic compounds were observed in the bloom headspace, with notable abundances well in excess of the traditional biogenic species (monoterpenes and isoprene), including benzothiazole (C_7H_5NS), benzoquinone ($C_6H_4O_2$), and various phenolic compounds (Table 5.1). These compounds may be of anthropogenic origin, given the use of coastal seawater collected off the Scripps Pier in La Jolla, CA. Such compounds have previously been identified as surface runoff contaminant in river waters (Fries et al., 2011). However, there are also marine origins for such compounds (Le Bozec and Moody, 2009). Interestingly, the benzothiazole concentration increases continually across the majority of the bloom, decreasing only near the tail end, suggestive of a possible biogenic source. Aromatic compounds are known SOA precursors and thus likely contribute to the observed SMA formation during this experiment.

5.3.2 Production and Chemical Composition of SMA

Photochemical oxidation of the headspace gases emitted during the phytoplankton bloom led to substantial variation in amount of SMA formed, ranging from <0.1 $\mu g/m^3$ to nearly 2.7 $\mu g/m^3$, dependent upon both the OH exposure and progression of the phytoplankton bloom (Figure 5.1B). The SMA was primarily composed of sulfate (47% by mass), organic species (24%), ammonium (15%), nitrate (10%), and chloride (4%), averaged across all conditions. Both the production and composition of the SMA exhibited a strong dependence on photochemical aging timescales. Averaged across all periods, SOA comprised a substantial fraction (40% by mass) of the SMA at low OH exposures (≤ 1 day of equivalent aging). However, as OH exposure increased the contribution from inorganic species increased; at eight days of equivalent aging the average SOA contribution is reduced to only 7%.

Further, the photochemical age dependence of SMA formation differed across the course of the bloom (Figure 5.1, Figure 5.8). During the pre-bloom period (R1), the amount of SMA formed decreases with increasing OH exposure, whereas during other periods of the bloom, it increases. This behavior derives from differences in the gas-phase species emitted over the course of the bloom (Figure 5.1 and Figure 5.2). Independent of which period is considered the evolution in the relative composition and absolute abundance of SMA with photochemical aging shows continual production of secondary inorganic aerosol (SIA), with a steeply declining absolute SOA concentration. During certain periods the long-time SIA production outweighed the SOA decline leading to net increases in total SMA, whereas during other periods SIA production balanced SOA loss (with approximately constant SMA) or was insufficient to offset the entirety of the SOA loss (leading to decreasing SMA with aging) (Figure 5.2).

The observed changes in SMA over the course of the bloom can be explain by less VOCs and more DMS as the bloom progressed. This results in SOA forming from oxidation of the various non-sulfur VOCs at the beginning of the bloom and transitioning more to SIA forming from oxidation of DMS during the peak of the bloom. These processes occur with varying efficiencies and, importantly, varying timescales. The identified VOCs have a range of photochemical lifetimes based on their OH reaction rate coefficients, ranging from about (1 hr to 1.5 days) with SOA formed on similar timescales (Jenkin et al., 2018). The substantial decay in the SOA with photochemical aging results from fragmentation-driven evaporation of aerosol-phase products due to heterogeneous OH oxidation (Lambe et al., 2012). Laboratory experiments using individual VOCs as SOA precursors demonstrate initially strong SOA formation at lower photochemical ages as VOCs react and form lower-volatility products that condense to form SOA. However, after a few VOC photooxidation lifetimes SOA production wanes and direct reaction of OH radicals with the SOA drive mass loss (Lambe et al., 2015). This behavior strongly implicates VOCs with relatively short photochemical lifetimes as the main SOA source and indicates that heterogeneous oxidation is an important SOA loss pathway.

In contrast, DMS has a lifetime about an order of magnitude longer (τ_{OH} ~ 1.1 days) (Burkholder et al., 2019), but forms intermediate species (e.g., hydroperoxymethyl thioformate (HPMTF) and SO_2) that react slowly (τ_{OH} ~ 5 days) to form H_2SO_4, and other products, and subsequently sulfate aerosol. Methanesulfonic acid (MSA) also forms from DMS oxidation, but is primarily detected as sulfate by the aerosol mass spectrometer and is thus primarily included with SIA (Chen et al., 2019). At the highest OH exposure (8 days of equivalent aging), the daily average SMA formed correlated well with the DMS headspace concentration (R^2 = 0.77; Figure 5.9). However, the correlation decreased monotonically with decreasing OH exposure, with R^2 = 0.19

at 0.5 days. In contrast, the NS-VOCs show an extremely weak negative correlation with SMA mass at all OH exposures (R^2 = 0.09-0.12; Figure 5.10). This photochemical age dependence indicates a particular importance for non-DMS gas-phase precursors under short atmospheric aging timescales.

The SMA organic mass fraction (OMF) initially decreases (at all photochemical ages) as the bloom progresses to a minimum about five days after the chl-a peak, after which the OMF increases (Figure 5.1D). This behavior is consistent with the temporal evolution of the DMS and NS-VOCs. Specifically, the OMF correlates strongly with the estimated VOC mass and yield-weighted fraction of the total VOCs and DMS (R^2 = 0.7; Figure 5.11). This provides clear evidence that the NS-VOCs are important for SMA formation, especially at low OH exposures. Further, a simplified model of VOC oxidation and SMA formation and loss, constrained by the observed VOC concentrations, generally reproduces the observed SMA formation and illustrates the influence of the differential gas-phase lifetimes and heterogeneous oxidation on SMA composition (Figure 5.12). A key outcome made possible by this isolated ocean/atmosphere bloom approach, as noted above, is that at shorter aging times, SOA comprises a significant fraction of the SMA, with sulfate becoming more abundant at longer aging timescales. Consequently, we see that variability in SMA composition and abundance depends on the extent of biological activity (or state of the bloom) as well as aging timescales in the atmosphere.

5.3.3 CCN Activity of SMA

The CCN activity of SMA, characterized by the apparent hygroscopicity parameter (κ_{app}), increased with photochemical aging during all bloom periods (Figure 5.2B), varying over the range of κ_{app} = 0.22–0.80 (Table 5.2). The apparent κ_{app} assumes the surface tension of the activating droplets is that of pure water (72 mN m^{-1}). A consistent shift towards higher CCN activity was

observed with increased photochemical aging (Figure 5.3B, Figure 5.13). The κ_{app} averaged 0.43 ± 0.08 at 0.5 days of equivalent aging, increasing to 0.66 ± 0.07 at 8 days (Figure 5.3B). The κ_{app} at a given photochemical age also generally increased across the course of the bloom. This last behavior contrasts notably with the κ_{app} for primary SSA, which exhibits little variability across the bloom (Figure 5.14). Interestingly, κ_{app} for SMA exhibits a moderately positive correlation with the headspace DMS concentration at all OH exposures (Figure 5.15).

The variability in the SMA κ_{app}, both with respect to the bloom stage and photochemical age, is attributable to changes in the chemical composition of the aerosol. Indeed, the SMA κ_{app} inversely correlates with the OMF (R^2 = 0.88, Figure 5.3D), consistent with the generally greater hygroscopicity of inorganic salts compared to organic compounds (Petters and Kreidenweis, 2007). This indicates that the shifting inorganic-to-organic content primarily controls the SMA hygroscopicity, consistent with theoretical κ_{app} from volume mixing rules (Figure 5.16,

Table 5.4). A linear fit to all data yields a κ_{org} = 0.3 for SOA (OMF = 1), consistent with the highly oxidized nature of the SOA. There is, however, some indication of curvature, with the points having high SOA fractions falling slightly below the linear fit but those with low SOA fractions slightly above. This could indicate a slight increase in the SOA hygroscopicity with aging, as observed for SOA formed from individual VOCs and oxidized primary OA (Lambe et al., 2011; Massoli et al., 2010).

Alternatively, the non-linearity at high photochemical ages could indicate an enhancement of the SMA CCN activity by surface-active organic species, which can reduce the surface tension of the growing droplets up to the point of activation (Ruehl et al., 2016). Enhancement of the CCN activity means that the particles can serve as more effective cloud seeds, yet the importance and influence of organic-driven surface tension depression on CCN has been long debated (Ovadnevaite et al., 2017; Ruehl et al., 2016). Here, at the highest photochemical ages the derived theoretical κ_{app} ~ 0.6 (corresponding to 16% OA and 84% H_2SO_4 by volume). If the organics actually reduced the surface tension by only 4-5 mN m-1 the experimentally obtained κ_{app} ~ 0.7, even if completely insoluble. Use of a more realistic film model (Forestieri et al., 2018a; Ruehl et al., 2016), as opposed to assuming a constant surface tension depression, with a gas-like pressure-area isotherm resembling that in (Ovadnevaite et al., 2017) assumed, indicates sustained surface-tension depression to the activation point can plausibly explain the difference between the volume-mixing model results and the observations (Figure 5.17). Altogether, these results indicate that changes in the CCN activity of SMA are primarily driven by a shift from organic-rich particles to sulfate-rich particles with increasing oxidation, and that surface tension depression by the organic components may further enhance the overall CCN activity.

5.4 Conclusions

The SMA hygroscopicity parameters observed here are consistent with values observed during numerous field studies in marine environments (κ = 0.46 - 0.79, Table 5.3 and references therein). Our results provide a rationale for the variability observed within and between different studies and locations for clean marine environments. Specifically, the observed SMA hygroscopicity will depend on particular state of a phytoplankton bloom (affecting the emission of DMS and NS-VOCs) and the extent of photochemical aging, coupled with mixing and transport of the emissions within the marine boundary layer along with entrainment from and export to the free troposphere. We note that our observations focus on what are likely pure SMA particles, as opposed to secondary materials that have condensed onto preexisting particles—including SSA.

This study demonstrates that the production, composition, and hygroscopicity of secondary marine aerosols are controlled by the absolute and relative emission of DMS versus other VOCs, which are strongly influenced by biological activity in seawater. However, there are numerous variables that control the properties of the resulting secondary marine aerosol. The time scales of oxidative aging are extremely important, with SMA becoming more hygroscopic and sulfate-rich with higher OH exposures (Figure 5.4). Increased emission of dimethyl sulfide was linked to both increased SMA production and hygroscopic, primarily due to increased sulfate content in the particles. While DMS is an extremely important precursor of SMA, the oxidation of other VOCs to form secondary organic species is an important source of SMA and strongly influences it's CCN activity, especially at low oxidation timescales. Understanding the nature of the VOC mixtures, their global flux from the oceans, and the resulting aerosol yields is critical for modelling the production of SMA and accurately predicting its composition and properties.

5.5 Methods and Materials

5.5.1 Experimental Setup

A phytoplankton bloom was initiated in 11,800 L of natural seawater in the SIO wave channel during the SeaSCAPE campaign. The wave channel and bloom initiation are described in detail elsewhere (Prather et al., 2013; Wang et al., 2015). Due to the large size of the wave channel, it is difficult to fully remove all trace gases and other contaminants which may affect the results of OFR experiments. To address this, an isolated sampling vessel (ISV) was constructed using only inert materials to facilitate the gas-phase measurements and OFR experiments (Figure 5.18). Seawater is pumped from the wave channel into the ISV using a peristaltic pump. The headspace air is provided by an ultrapure air generator (Sabio Model 1001). Further details on the experimental setup can be found in the Supplementary Text.

5.5.2 OFR Operation

Secondary marine aerosol was generated by flowing the headspace gases from the ISV through a potential aerosol mass oxidative flow reactor (PAM-OFR, Aerodyne Inc) (Kang et al., 2007), operated in OFR185 mode. The OFR was operated on a 4-hour cycle which stepped through 5 OH exposure settings and a control period with the lamps off (Figure 5.19), which was repeated several times daily throughout the bloom cycle. OFR calibration procedures are described in the supplementary information (Figure 5.20).

5.5.3 Size Distribution Measurements

Particles are dried prior to measurements using a silica diffusion dryer. Aerosol size distributions were measured using a Scanning Mobility Particle Sizer (SMPS 3938, TSI Inc) equipped with a Nano DMA (DMA 3085, TSI Inc) and a soft X-ray Neutralizer (Model 3088, TSI

Inc). The size distributions were converted to aerosol mass concentrations assuming spherical particles and a density of $\rho = 1.8\ g \cdot cm^{-3}$.

5.5.4 CCN Measurements

Size-resolved CCN measurements were made using a CCN counter (CCN-100, Droplet Measurement Technologies). Particles are size-selected using a DMA (Model 3081, TSI), then the flow is split between the CCN counter and a CPC (W-CPC 3787, TSI) which measures the total number of particles. The CCN counter scans across a range of supersaturations. The point where 50% of the particles have activated to droplets is defined as the critical supersaturation (S_c) and used to calculate the apparent hygroscopicity parameter (κ_{app}) using the κ-Köhler equation (Petters and Kreidenweis, 2007). The surface tension of the surface-air interface is assumed to be that of water ($\sigma_{s/a} = 0.072\ J \cdot m$).

5.5.5 Aerosol Composition Measurements

Non-refractory aerosol chemical composition was measured using a high-resolution time-of-flight aerosol mass spectrometer (HR-ToF-AMS, Aerodyne Inc). This instrument is described in detail elsewhere (Decarlo et al., 2006). Data analysis methods are described in the supplementary text.

5.5.6 Gas-Phase Measurements

Trace gas measurements were conducted using three complementary techniques. Real time VOC concentrations were measured using a VOCUS proton transfer resonance mass spectrometer (PTR-MS) (Krechmer et al., 2018). Additional measurements of isoprene and organosulfur gas concentrations were conducted using a chemical ionization time-of-flight mass spectrometer, operating with benzene as the reagent ion (b-CI-ToF-MS) (Kim et al., 2016). Additional trace gas measurements were conducted using sorbent tubes, which were analyzed using thermal desorption

2D gas chromatography coupled with high resolution time-of-flight mass spectrometry (TD-GCxGC-EI/VUV-HRTOF-MS) (Hatch et al., 2019).

5.6 Acknowledgements

We thank the entire SeaSCAPE team for their hard work and assistance throughout the experimental campaign. A full list of SeaSCAPE participants can be found online (https://caice.ucsd.edu/experiment-campaigns/). Special thank you to Margaux Winter, Savannah Shaul, Lauren Garofalo, Delphine Farmer, Dan Crocker, and Clare Morris. This material is based upon work supported by the National Science Foundation through the NSF Center for Aerosol Impacts on Chemistry of the Environment, an NSF Center for Chemical Innovation (CHE-1801971).

Chapter 5 is, in full, currently being prepared for submission to *Proceedings of the National Academy of Sciences*. Printed with permission from Mayer, K.J., Moon, D.R., Kilgour, D.B., Sauer, J.S., Moore, A.N., Barnes, E.B., Lee, C., Mullenmeister, C.A., Bahaveolos, C.J., Ni, C.M., Goldstein, A.H., Bertram, T.H., Cappa, C.D., Prather, K.A., (2021). Atmospheric Aging Drives Variability in Secondary Marine Aerosol Composition and Cloud-Forming Ability. The dissertation author is the primary investigator and lead author of this paper.

5.7 Figures

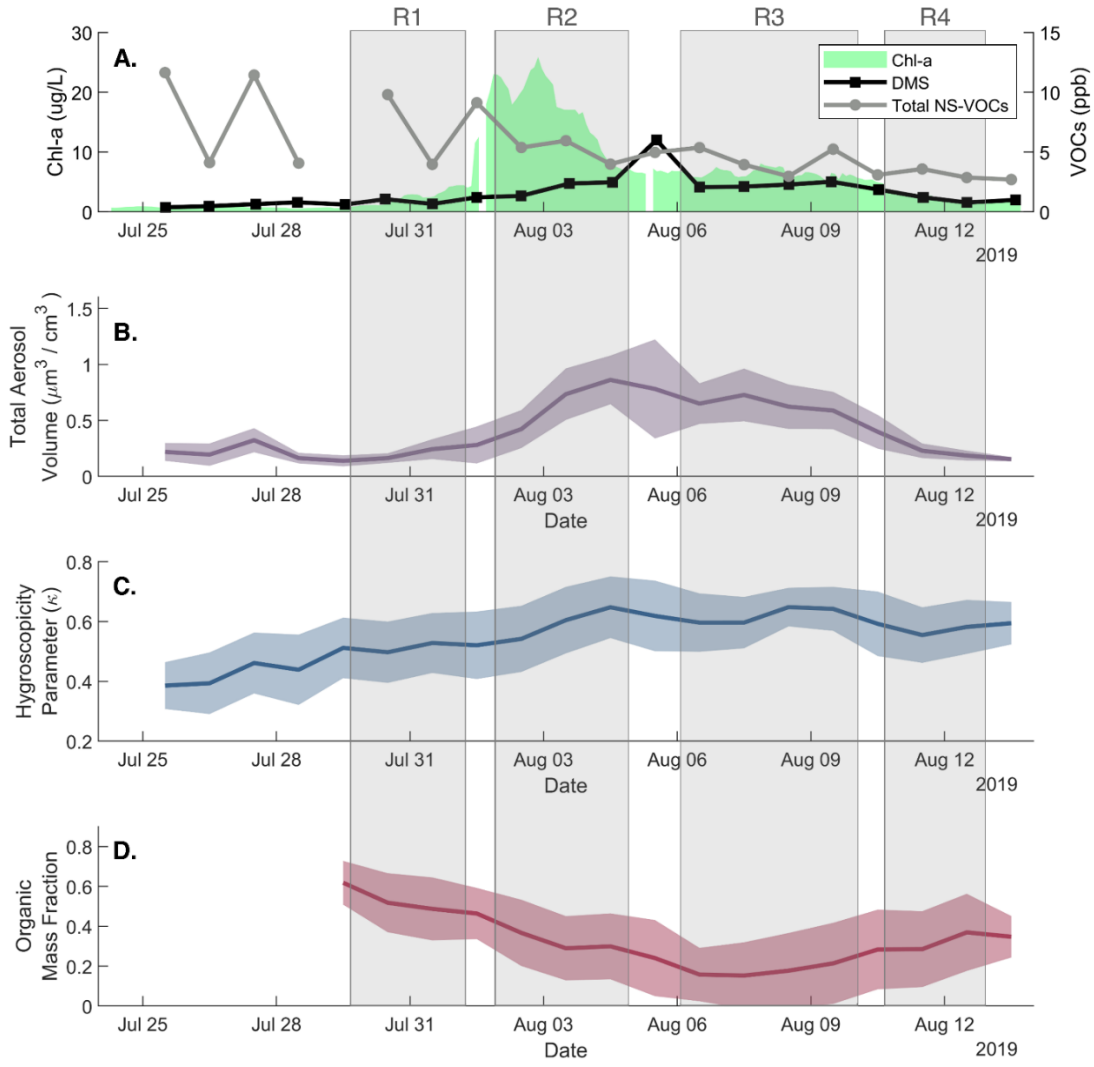

Figure 5.1 Time series of seawater and SMA properties. A) Seawater chl-a concentrations and headspace DMS and total non-sulfur VOC concentrations measured by the PTR-MS. B) Total aerosol volume calculated from the SMPS size distributions. C) Apparent hygroscopicity parameters (κapp) of SMA over the course of the bloom (Dd = 30 nm). D) HR-ToF-AMS organic mass fraction (OMF), which is the ratio of [Org] / [Org + SO4 + NO3 + NH4]. Four periods of interest are highlighted: pre-bloom conditions (R1), peak chl-a concentrations (R2), high DMS (R3), and post-bloom (death phase) conditions (R4). Selected data from these periods is shown in Figure 5.2.

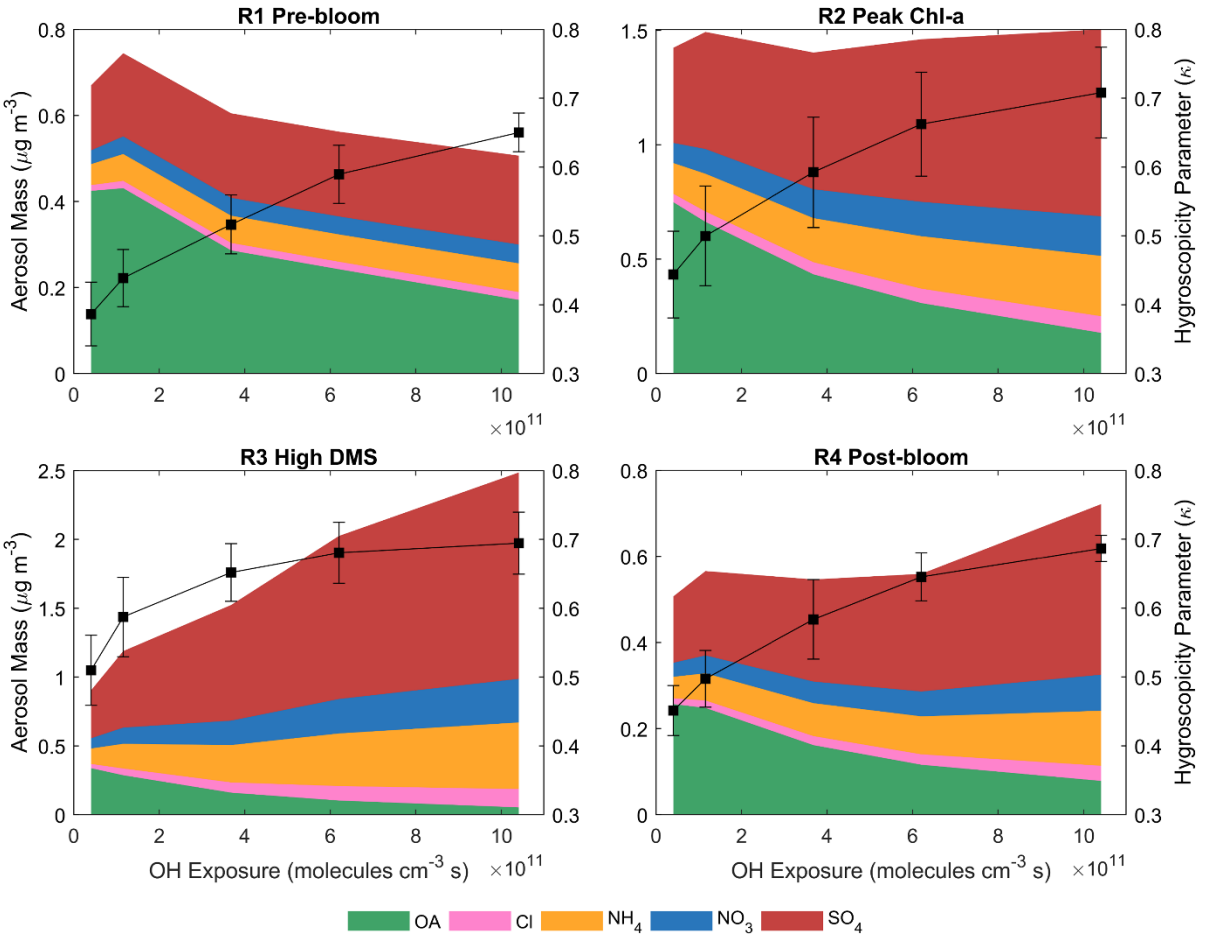

Figure 5.2 Observed SMA composition and hygroscopicity versus OH exposure during four periods of interest: pre-bloom conditions (R1), peak chl-a concentrations (R2), high DMS (R3), and post-bloom (death phase) conditions (R4).

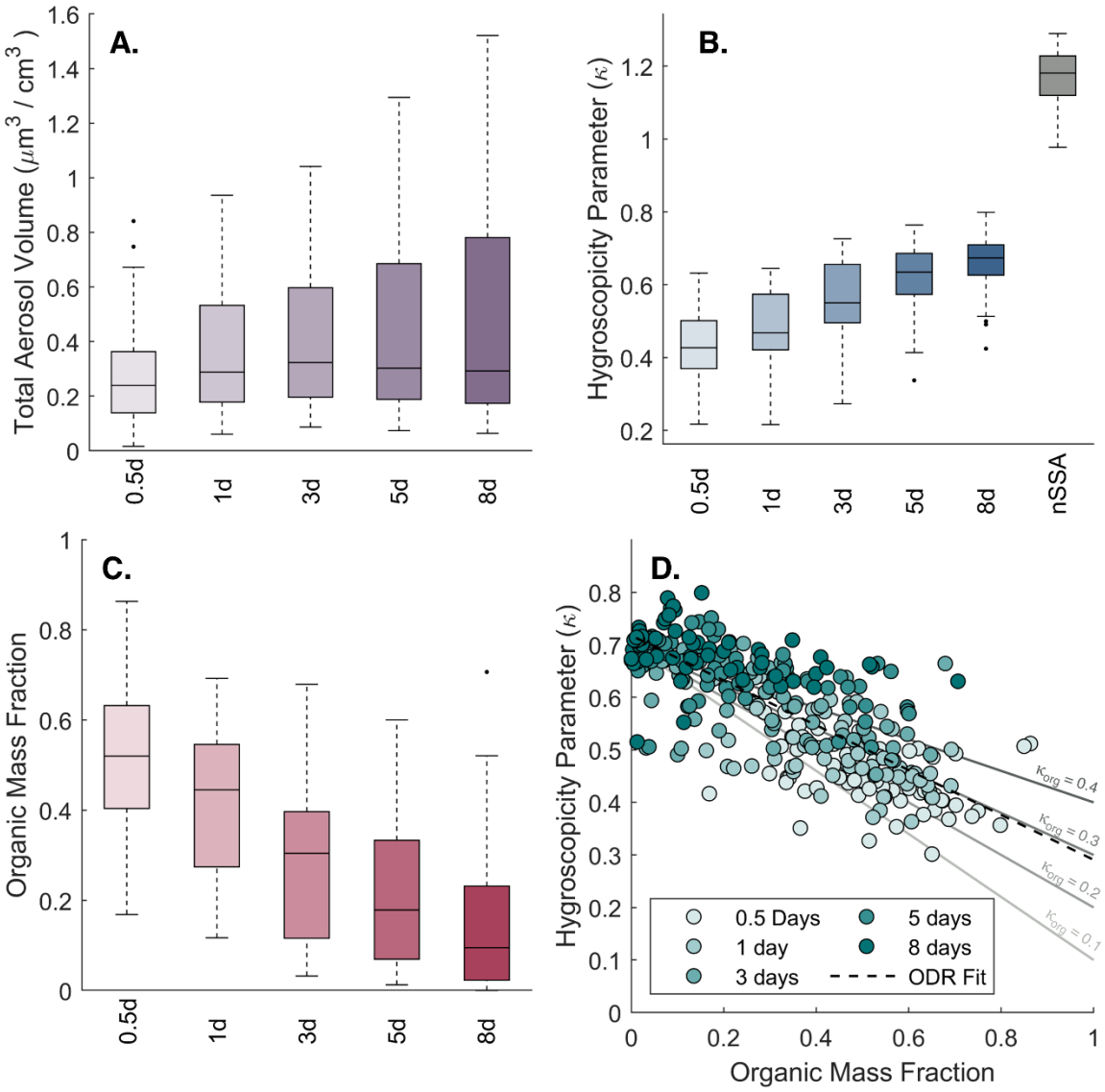

Figure 5.3 Box and whisker plots showing the distribution of SMA properties averaged over the entire bloom at each OFR condition for A) total aerosol volume, B) hygroscopicity parameter, and C) organic mass fraction. D) Organic mass fraction, as measured by the AMS, versus the observed hygroscopicity parameter for SMA at all PAM conditions throughout the bloom cycle. The organic mass fraction is defined as OMF = [Org] / ([Org] + [SO_4] + [NO_3] + [NH_4]).

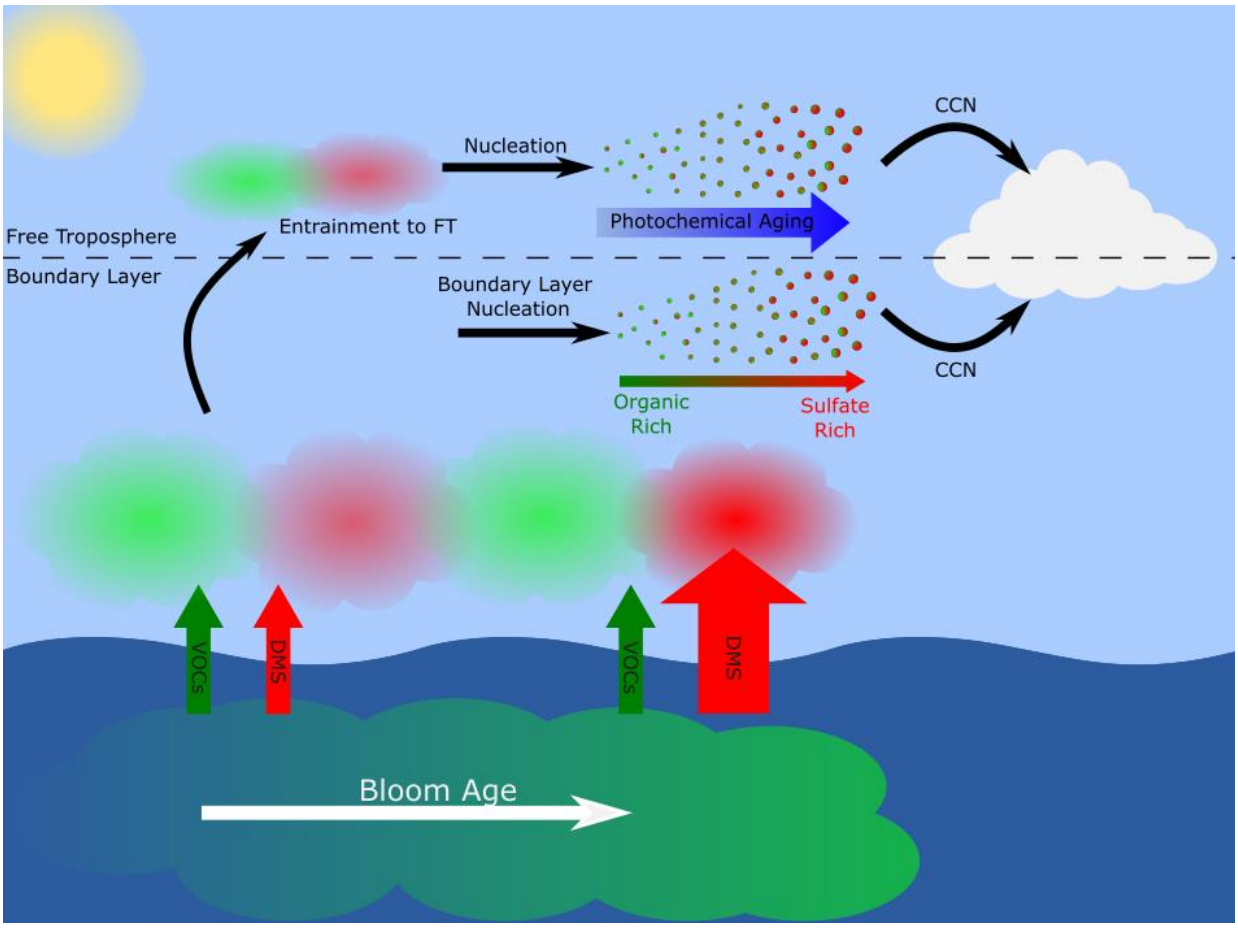

Figure 5.4 Schematic showing the effects of both bloom life cycle and photochemical aging on the properties of SMA and its potential impacts on cloud properties.

5.8 Supporting Information

5.8.1 Methods and Materials

5.8.1.1 Experimental Setup

A phytoplankton bloom was initiated in 11,800 L of natural seawater in the SIO wave channel during the SeaSCAPE campaign. The wave channel and bloom initiation are described in detail elsewhere (Prather et al., 2013). Due to the large size of the wave channel, it is difficult to fully remove all trace gases and other contaminants which may affect the results of OFR experiments. To address this, an isolated sampling vessel (ISV) was constructed using only inert materials (stainless steel, glass, and Teflon) to facilitate the gas-phase measurements and OFR experiments (Figure 5.18). Seawater is pumped from the wave channel into the ISV using a peristaltic pump that produced an ~1 cm diameter water jet that fell ~10 cm to the water surface. The headspace air is provided by an ultrapure air generator (Sabio Model 1001), which carried evolved gases to the oxidation flow reactor and to the gas-phase sampling instrumentation. Owing to the water jet, some background primary sea spray particles were generated in the ISV. These SSA particles were substantially larger than the SMA particles formed from reaction of the evolved gases and did not affect the CCN measurements but did affect the aerosol mass composition measurements. The composition of the SMA and SSA were distinguished using positive matrix factorization (see below).

5.8.1.2 OFR Operation and Calibration

Secondary marine aerosol was generated by flowing the headspace gases from the ISV through a potential aerosol mass oxidative flow reactor (PAM-OFR, Aerodyne Inc) (Kang et al., 2007), operated in OFR185 mode. The OFR uses UV lamps to generate high concentrations of OH radical, simulating oxidative aging equivalent to days or even weeks in the real atmosphere, but

with a residence time of only ~2.66 minutes in the reactor (flow rate = 5 lpm). The OFR was operated on a 4-hour cycle which stepped through 5 OH exposure settings and a control period with the lamps off (Figure 5.19), which was repeated several times daily throughout the bloom cycle. The relationship between the OFR lamp settings and the OH exposure was determined by introducing CO to the reactor and monitoring the loss due to reaction with OH radical at different lamp voltages. The concentration of CO was measured using a commercial gas analyzer (Horiba, APMA-370). The OH exposure is calculated assuming first order kinetics, using the rate coefficient of CO + OH ($k_{OH + CO, 298K} = 1.5\times10^{-13}$ cm^3 $molec^{-1}$ s^{-1}) (Chen and Marcus, 2006). A calibration curve is shown in Figure 5.20.

5.8.1.3 CCN Measurements

Size-resolved CCN measurements were made using a CCN counter (CCN-100, Droplet Measurement Technologies). Particles are size-selected using a DMA (Model 3081, TSI), then the flow is split between the CCN counter and a CPC (W-CPC 3787, TSI) which measures the total number of particles. The CCN counter scans across a range of supersaturations. The point where 50% of the particles have activated to droplets is defined as the critical supersaturation (S_c) and used to calculate the apparent hygroscopicity parameter (κ_{app}) using the κ-Köhler equation (Petters and Kreidenweis, 2007). The surface tension of the surface-air interface is assumed to be that of water ($\sigma_{s/a}$ = 0.072 J·m). Selected CCN activation curves are shown in Figure 5.13.

5.8.1.4 PTR-MS Measurements

A Vocus proton transfer reaction time-of-flight mass spectrometer (PTR-ToF-MS) (TOFWERK, Aerodyne Inc.) was deployed to measure gas-phase volatile organic compounds (VOCs)(Krechmer et al., 2018). The focusing ion-molecule reactor was operated at high reduced field strength (E/N = 143 Td) with a pressure of 1.5 mbar, electric field of 41.5 V cm^{-1}, and heated

to 100 °C. The big segmented quadrupole voltage was set to 275 V, which reduced the transmission of low mass (<35 m/Q) ions. The Vocus mass spectra were saved at 1 Hz time resolution. A typical mass spectrum is shown in Figure 5.21. The headspace of the ISV was sampled at 100 sccm through a roughly 2.5 m 0.25" O.D. PFA tube. Instrument background signals were determined about 8 times daily by overflowing the Vocus inlet with zero air from a zero air generator (Sabio Environmental, Model 1001) that provided air to the ISV headspace. Daily average background signals were used for background correction. Peak fitting and integration were completed in Tofware 3.1.2.

We focus primarily on DMS (measured as $C_2H_6SH^+$) other VOCs having five or greater carbon atoms. This includes monoterpenes (measured as $C_{10}H_{16}H^+$), oxygenated monoterpenes (measured as $C_{10}H_{16}OH^+$), and the $C_5H_8H^+$ ion, the signal ion where isoprene is detected, as these molecules have been previously measured in the marine environment and are known secondary aerosol precursors. Calibration factors for DMS, monoterpenes, and oxygenated monoterpenes are, in order: 3.0, 1.3, and 4.4 cps ppt^{-1}, where the calibration factors for monoterpenes and oxygenated monoterpenes are taken as the sensitivities to α-pinene and β-cyclocitral, respectively. For other VOCs we assume the same sensitivity as for the oxygenated monoterpenes. As such, the reported concentrations of these other VOCs should be taken as approximate.

5.8.1.5 High-resolution Time-of-flight Aerosol Mass Spectrometry (HR-ToF-AMS) Measurements

Throughout the experiment the HR-ToF-AMS was operated in “V” mode to ensure the instrument was operating at the highest possible sensitivity. Before the experiment, the sample flow rate and ion efficiency (IE) calibrations were conducted. The sample flow rate calibration

was performed using a Gilibrator Calibrator (Sensidyne) for accurate determination of the species mass concentration. The average sample flow rate during the experiment was 1.35 ± 0.02 (2σ) cm^3 s^{-1}. The IE calibration was conducted by sampling various concentrations (0-1003 particle cm^{-3}) of dried ammonium nitrate (AN) aerosol generated from a ~5 mmol AN solution and a constant output atomizer (TSI Model 3076) which were size selected with a mobility diameter of 300 nm using a Differential Mobility Analyzer (DMA, TSI Model 3081 with electrostatic classifier Model 3080). Particle concentrations were measured with a Condensation Particle Counter (CPC, TSI Model 3010). The NO_3 mass entering the HR-ToF-AMS was calculated from CPC data using the particle shape factor (0.8) and density (1.725 g cm^{-3}). A plot of the NO_3 HR signal (ions s^{-1}) against the number of molecules of NO_3 entering the instrument yielded an IE calibration factor of 1.39 ± 0.08 (2σ) $\times 10^{-8}$ ions $molecule^{-1}$ with an IE to air-beam ratio of 1.01×10^{-12} ions $molecule^{-1}$. The relative ionization efficiency (RIE) factor for NH_4 was also calculated from the same calibration experiment to be 3.81. The calibration experiment was repeated but with ammonium sulphate aerosol (AS) to yield a RIE for SO4 of 1.07. Default values from the RIE factors for organics and Cl of 1.4 and 1.3, respectively, were applied (Canagaratna et al., 2007). A number of blank measurements were made on a daily basis during the experiment by sampling through a high-efficiency particulate-free air (HEPA, Pall) filter to determine the contribution of the HR signal of CHO^+ and particulate CO_2^+ ions at m/z 29 and 44 respectively.

5.8.1.6 HR-ToF-AMS Data Analysis

HR-ToF-AMS data processing was conducted within the ToF-AMS HR Analysis Toolkit v1.23 (http://tinyurl.com/tofams-analysis) in Igor Pro v6.37 (Wavemetrics). During AMS data processing, a unit mass resolution (UMR) signal at a m/z dominated by air is used to correct for fluctuations in signal due to changes in the filament emission and the sensitivity of the

Microchannel Plate (MCP) detector, known as the air-beam correction. Typically, the N_2^+ UMR signal (m/z = 28) is used as it is the most sensitive to any such fluctuations. However, an intermittent fault with the MCP that occurred twice during the course of the experiment resulted in the saturation of N_2^+ UMR signal, therefore the O_2^+ UMR signal (m/z = 32) was used to conduct the air-beam correction. In addition, to account for any instrumentation changes during the fault, the data was split into three periods and subsequent analysis was conducted separately; the period before the fault occurred (P1, 07/29/19 11:05-08/04/19 08:45), the periods during the fault (P2, 08/04/19 10:50-08/05/19 22:25 and 08/09/19 09:45-08/13/19 18:50) and the period with no fault between the intermittent fault occurring (P3, 08/06/19 22:30-08/09/19 08:25). Within the ToF-AMS HR Toolkit, the CHO^+ and CO_2^+ ion signals are calculated within a fragmentation table (Allan et al., 2004) using the N_2^+ ion signal. During P2, the N_2^+ ion signal was estimated using the O_2^+ ion signal and the known ratio of atmospheric concentrations of N_2 and O_2. The particle collection efficiency (CE) should be applied to the data to account for particle bounce losses on the AMS vaporizer (Canagaratna et al., 2007). Typically a default value of CE of 0.5 is used, however as sulfate comprises a significant component of SMA and upon comparison with Scanning Mobility Particle Sizer (SMPS, see below for details) data, a compositional dependent CE was calculated and applied (Middlebrook et al., 2012).

5.8.1.7 Positive Matrix Factorization (PMF) Analysis

PMF was used to distinguish between the SMA and background SSA. A detailed description of PMF and its application to HR-AMS data is provided elsewhere (Paatero and Tapper, 1994; Ulbrich et al., 2009). PMF analysis was undertaken within PMF Execute Tool (PET) v3.05 (http://tinyurl.com/PMF-guide) in Igor Pro v6.37 (Wavemetrics). Data was input into PET via a combined organic and inorganic HR-AMS ion matrix and a corresponding error matrix

prepared in the ToF-AMS HR Analysis Toolkit. A minimum error value was applied to the error matrix and ions with a Signal-to-Noise Ratio (SNR) <0.2 were removed and 0.2-2 downweighted by increasing their error by a factor of 2. In addition, ion signals for CO_2^+, CO^+, H_2O^+, HO^+ and O^+ were also downweighted. Isotopic ions were also removed as their signals are scaled to the signal of their parent ions, rather than being measured directly. In this study, the solution for six factors was chosen based on detailed evaluation of the mass spectral profiles and temporal trends (Zhang et al., 2011). All three analysis periods gave the same six factors, with P2 giving an additional seventh factor that corrected the CHO^+ and CO_2^+ ion signals associated with error from their estimation from the less sensitive O_2^+ ion signal (CHO Corr.). Four of the factors were associated with larger (>1 μm) primary mode background aerosol created within the ISV, they were: a hydrocarbon dominated factor (Primary Organic Aerosol, POA1), an alternative hydrocarbon dominated factor that accounts for a change in the organic mass within the seawater (POA2), an oxidized organic and inorganic factor believed to be surface active species on the primary aerosol that includes high molecular weight organo-nitrate-chloride ions (POA3), and a factor associated with heterogeneous nitrification (Nitrate). The other two factors are the highly oxidized secondary organic (Secondary Organic Aerosol, SOA) and secondary inorganic (Secondary Inorganic Aerosol, SIA) components of SMA. Only the SMA and SIA factors are discussed in the main text. The mass spectra of the six factors from the PMF solutions for P1, P2 and P3 are presented in Figure 5.22, Figure 5.23, and Figure 5.24.

Several parameters within the PMF diagnostics can support the number of factors used within the solution and the quality of the data. Q represents the total model-measured residual weighted against the error and the ratio of Q and Q expected (Q/Q_{exp}) indicates how well the model fits the data. As the number of factors in a solution increases, the degrees of freedom increase and

Q/Q_{exp} decreases close to 1. The fPeak parameter is used to indicate the rotational stability of the solution. The rotational stability of each of the solution sets were explored with varying fPeak values from -1 to +1, with an increment of 0.1. Figure 5.25, Figure 5.26, and Figure 5.27 present the PMF diagnostic plots for P1, P2 and P3. In the figures, plot (a) shows Q/Q_{exp} of the solutions with a different number of factors tends to around 1, plot (b) presents Q/Q_{exp} for the varying fPeak values showing the solution sets to be rotationally stable, plot (c) shows the relative changes of the mass fraction for the factors as the fPeak value was varied, plot (d) indicates the similarity of the time series and mass spectra of factors to each other with POA1 and POA2 being the most similar, plots (e) and (f) present the model-measured fit for each considered ion and plots (g), (h) and (i) present the model-measured fit for the total time series, all showing the six factor PMF solution fits the measurements well.

5.8.2 Supplementary Text

5.8.2.1 Theoretical Hygroscopicity Model

To assess the degree to which changes in the SMA chemical composition can explain its CCN activity, the simple ZSR mixing rule was used to model the theoretical hygroscopicity parameters (Petters and Kreidenweis, 2007).

$$\kappa_{theor} = \sum_{i} \varepsilon_i \kappa_i$$

where ε_I is the volume fraction and κ_i is the hygroscopicity parameter of each individual component of the mixed aerosol. The following assumptions were used:

1) All NO_3 reacts with NH_4 to form NH_4NO_3
2) All remaining NH_4 reacts with SO_4 to form $(NH_4)_2SO_4$
3) The remaining SO_4 is in the form of H_2SO_4

The organic aerosol mass was converted to a volume fraction using an assumed density of $\rho = 1.3$ g cm^{-3}, which is similar to the value of pure SOA generated from α-pinene and limonene ozonolysis (Saathoff et al., 2009). Similarly, a value of $\kappa_{org} = 0.2$ was assumed based on studies of pure SOA generated in an OFR (Massoli et al., 2010). The other values used in the model are summarized in

Table 5.4. The results of the model are shown in Figure 5.16.

5.8.2.2 HR-ToF-AMS Mass Concentration Verification

Verification of the mass concentration time series for the SMA factors was conducted with SMPS data that provides time-resolved size distributions of SMA from which the total aerosol volume concentration can be calculated, assuming the particles are spherical. The SMA mass concentration was then determined by applying the particle density of 1.77 g cm^{-3} for the SIA factor and 2.09 g cm^{-3} for the SOA factor calculated from H/C and O/C ratios given by the mass spectrum (H/C = 1.33, O/C = 2.08) (Kuwata et al., 2011). Scatter plots of the SMPS derived SMA mass concentration ($[SMA]_{SMPS}$) against the SMA mass concentration measured with the HR-ToF-AMS ($[SMA]_{AMS}$) were used to determined verification factors of 1.729, 2.992 and 1.065 for P1, P2 and P3 respectively (see Figure 5.28 and Figure 5.29). These verification factors were then applied and the data for all periods were then combined. A scatter plot of the verified combined data sets gives a slope of the linear regression of 0.978 with $R^2 = 0.847$, showing that, once verified, HR-ToF-AMS and SMPS measurements give good agreement. This is confirmed by the direct comparison of the SMA mass concentration time series from SMPS derived values and those measured with the HR-ToF-AMS shown in Figure 5.30. The verified SMA, SIA and SOA times series measured with the HR-ToF-AMS are presented in Figure 5.31.

5.8.2.3 Estimation of SMA Organic Fraction Variability

The variability in the SMA composition and abundance across the bloom and as a function of photochemical age were estimated in two distinct ways. The first method used to estimate variability with the bloom state is referred to as the fixed-yield model. For the fixed-yield model, the organic mass fraction of the SMA was calculated as:

$$\mathrm{OMF} = \frac{\sum_i y_i[\mathrm{VOC}_{ns,i}]}{\sum_i y_i[\mathrm{VOC}_{ns,i}] + y_{DMS}[\mathrm{DMS}]} = \frac{\mathrm{SOA}}{\mathrm{SOA+SIA}} \qquad (1)$$

where the sums are over the i non-sulfur-containing VOCs and the y values are assumed OH-independent SOA or SIA yields. For the non-sulfur-containing VOCs we assume that the y_i increase with the molecular weight (MW) of the ions with a functional form of y_i = min[(MW_i/150)^3,1]. Allowing for MW-dependent yields is generally consistent with understanding of SOA formation. We find generally good agreement between the predicted and observed OMF when the $y_{DMS} = 3y_{noS}$, and where the noS subscript indicates the maximum MW-weighted yield for non-sulfur-containing VOCs. We assume that DMS is converted entirely to sulfuric acid and thus assume a constant MW of 96, rather than using the actual MW of DMS. Absolute SOA and SIA abundances can also be derived from the model. If we assume $y_{DMS} = 1$ (and so the maximum $y_{noS} = 0.33$) the predicted SMA (=SOA + SIA) greatly exceeds the observed SMA abundance. If the model SOA and SIA are both scaled down by a factor of 13 there is reasonable agreement between the observed and modeled SMA (Figure 5.11). While the absolute abundances of the non-sulfur-containing VOCs have substantial uncertainties (owing to unknown calibration factors for most of the ions), it seems unlikely that calibration uncertainty drives this difference as the sulfate from DMS strongly influences the temporal variability in the [SMA]. It may be that substantial scavenging of H_2SO_4 and low-volatility gas-phase VOC oxidation products onto the OFR walls suppressed SMA formation or that particle loss through the O_3 denuder and drier that followed the OFR depressed the observed [SMA]. Likely, both contributed. Regardless, the key aspect is that the shape of the modeled [SMA] temporal dependence (Figure 5.11) is quite similar to the observations, with the notable exception of the large amount of predicted SMA on the 5th of August. The large SMA abundance on this day was driven by DMS. We note that the gas-phase sampling occurred only periodically and for a short time each day. In contrast, the SMA measurements were near continuous, with the exception of the 5th when the instrument had to be

taken offline for maintenance and thus only sampled for a small part of that day. It may be that the DMS concentration was large for only a small portion of this day and that a temporal mismatch between the gas-phase and SMA measurements led to the model-measurement discrepancy. Nonetheless, the model-measurement agreement is generally quite good.

The VOC composition was not constant across the bloom. The most notable differences were for the first few days of the bloom, as indicated by the cosine similarity of the daily average MW- and yield-weighted spectra compared to the campaign averaged being smallest (Figure 5.7). The spectral similarity increased when the Chl-a concentration increased, and the spectra remained reasonable similar throughout the remainder of the bloom, although with some differences over time.

The second model considers photooxidation of the VOCs in more detail to examine the dependence on photochemical age. We refer to this model as the photochemical age-dependent model. We consider oxidation of DMS along with the collective oxidation of all VOCs. The chemistry governing the transformation of these species into condensable products, especially for the VOCs, is simplified relative to a detailed reaction scheme, but meant to capture major salient features. Oxidation of DMS generally follows the scheme set forth in Hoffmann et al. (2016), modified to account for formation of hydroperoxymethyl thioformate (HPMTF) (Hoffmann et al., 2016; Veres et al., 2020). We assume that when DMS reacts with OH it can form DMSO via OH addition (k_{OH} = 2.15 x 10^{-12} cm^3 $molecules^1$ s^1) or it can form the methylthioxymethyl-peroxy radical via OH abstraction (k_{OH} = 4.8 x 10^{-12} cm^3 $molecules^1$ s^1) which goes on to form HPMTF (BR = 0.08), MSA (BR = 0.16), or SO_2 (BR = 0.76), and where BR indicates the branching ratio. The BR values are adjusted relative to those reported in Veres et al. (2020) since autoxidation will be less important in the OFR compared to the remote atmosphere. DMSO can react with OH to

form MSIA (k_{OH} = 8.9 x 10^{11} cm^3 $molecules^{-1}$ s^{-1}) which can react further to form SO_2 (k_{OH} = 9 x 10^{-11} cm^3 $molecules^{-1}$ s^{-1}). HPMTF can also react with OH to form SO_2 (k_{OH} = 3.6 x 10^{-11} cm^3 $molecules^{-1}$ s^{-1}) with an assumed 95% yield. SO_2 reacts with OH (k_{OH} = 1.3 x 10^{-12} cm^3 $molecules^{-1}$ s^{-1}) to form H_2SO_4 (BR = 0.7) or $HOSO_2O_2H$ (BR = 0.3). H_2SO_4 and MSA can condense and form SMA or be lost to the OFR walls, with the assumption that both are non-volatile. The assumed condensation rate coefficient is assumed to be 0.025 s^{-1}, generally consistent with the observed particle surface area. The assumed wall-loss rate is 0.03 s^{-1}, slightly higher than that used by Ehn et al. (2014) for losses of very low volatility compounds to the walls of a somewhat larger reaction vessel (Ehn et al., 2014). MSA can react heterogeneously to produce H_2SO_4 with 95% yield (Kwong et al., 2018).

The non-sulfur-containing VOCs react with OH radicals to form condensable (low volatility) first-generation products. All condensable products are assumed to be non-volatile. We assume there are three groups of VOCs based on reaction rate coefficients: those that react very fast (k_{OH} = 2 x 10^{-10} cm^3 $molecules^{-1}$ s^{-1}), fast (k_{OH} = 5 x 10^{-11} cm^3 $molecules^{-1}$ s^{-1}), and slower (k_{OH} = 5 x 10^{-12} cm^3 $molecules^{-1}$ s^{-1}), consistent with estimated rate coefficients for some of the species observed. The concentrations of each of these VOC groups are assumed equal and sum to the total observed VOC The yield of condensable products is assumed 0.035. This represents an average across all of the observed species (with $\geq$ 5 carbon atoms). The MW of the SOA formed is assumed equal to 150 g mol^{-1}. The SOA formed can react heterogeneously with OH radicals with a second-order rate coefficient assumed as 1.5 x 10^{-11} cm^3 $molecules^{-1}$ s^{-1}, consistent with effective reactive uptake coefficients near unity. Upon heterogeneous reaction, it is assumed that volatile products are formed, leading to loss of SOA. The model inputs are constrained by the observed time-varying concentrations of total VOCs and DMS.

For a given set of input conditions the model is run for a total reaction time of 300 seconds with different assumed OH concentrations that correspond to equivalent aging times of 0.5, 1, 3, 5, and 8 days. The species-specific aerosol mass concentrations at the end of each run are stored to determine the aerosol composition and abundance as a function of OH aging (Figure 5.12). The calculations were carried out using KinSim v4.05 (Peng and Jimenez, 2019) in Igor Pro v.8.0.4.2 (Wavemetrics). Results are shown for two bloom conditions, corresponding to Period 1 (lower DMS (700 ppt) and higher total VOCs (6000 ppt)) and to Period 3 (higher DMS (2400 ppt) and lower total VOCs (3900 ppt)).

5.8.2.4 Surface Film Model

We use a modified version of the surface film model (Ruehl et al., 2016) to calculate how κ_{app} might be influenced by surface-active organic species that can depress the surface tension of growing droplets (Figure 5.17). The difference from our model versus Ruehl et al. (2016) is that we assume a different form for the surface pressure isotherm, namely that of Barger and Means (1985) (Barger and Means, 1985). The compressed film model used by Ruehl et al. (2016) is most appropriate for surfactants that form tightly packed, solid or liquid-like films, such as fatty acids. In contrast, naturally-occurring surface active films can exhibit gas-like isotherms for which the surface pressure falls off less steeply with an increase in the molecular-area per molecule (A) compared to solid or liquid-like isotherms. The particular isotherm used here has the functional form:

$$\pi \cdot A = C_0 + C_1 \cdot \pi + C_2 \cdot \pi^2$$

and where π is the surface pressure (equal to 72 mN m^{-1} – σ, where sigma is the surface tension) and the C_i values are constants describing the isotherm behavior. Values to use for the C_i are not known a priori, but can be guided by previous work. For example, Ovadnevaite et al. (2017)

derived a surface pressure isotherm for ambient marine aerosol using a thermodynamic model that can be used as a constraint here (Ovadnevaite et al., 2017). We find that the observed κ_{app} versus OMF relationship (Figure 5.3D) for 30 nm diameter particles is reasonably reproduced for a binary sulfuric acid-organic mixture when $C_0 = 50$, $C_2 = -30$, and C_1 is allowed to vary inversely with the OMF (from 100 to 685), assuming a molecular weight for the soluble organic material of 200 g mol^{-1} and a density of 2 g cm^{-3}. Specifically, under these conditions the calculated κ_{app}-OM F relationship exhibits curvature, similar to the observations. As the C_1 value increases, the surface tension depression at a given wet-particle diameter is greater, and the influence persists out to larger wet diameters. Similarly, the surface pressure remains elevated to larger A values as C_1 increases. It is reasonable to think that the surface activity of the SOA species would vary with photooxidation, as continued photooxidation tends to increase the oxygen content and thus, likely, the solubility of some of the components.

Unlike the compressed film model, the surface tension can remain below that for pure water after activation. This is a result of the different surface pressure-area isotherm shapes of the compressed film model versus the gas-film model. In contrast, if the organic component is assumed soluble but not surface active, the expected linear relationship is obtained with $\kappa_{app} = 0.17$ for OMF = 1. The calculated gas-film model κ_{app} are lower than the κ_{app} with no surface-tension depression when the OMF is greater than 0.85. This is because, for these particular parameters, above this value the exclusion of surface-active material to the surface decreases the amount of soluble material that can contribute to droplet growth. Below this value the decrease in soluble material via exclusion to the surface is offset by the decrease in surface tension, but above this particular OMF this is no longer the case. We note this predicted behavior occurs outside the observed range of OMF values in our study 0-0.7, with most values at OMF <0.6). A linear fit to

the gas-film κ_{app} over the range $0 < OMF < 0.6$ yields $\kappa_{app} = 0.3$ at $OMF = 1$, consistent with the observations.

5.8.3 Supplementary Figures

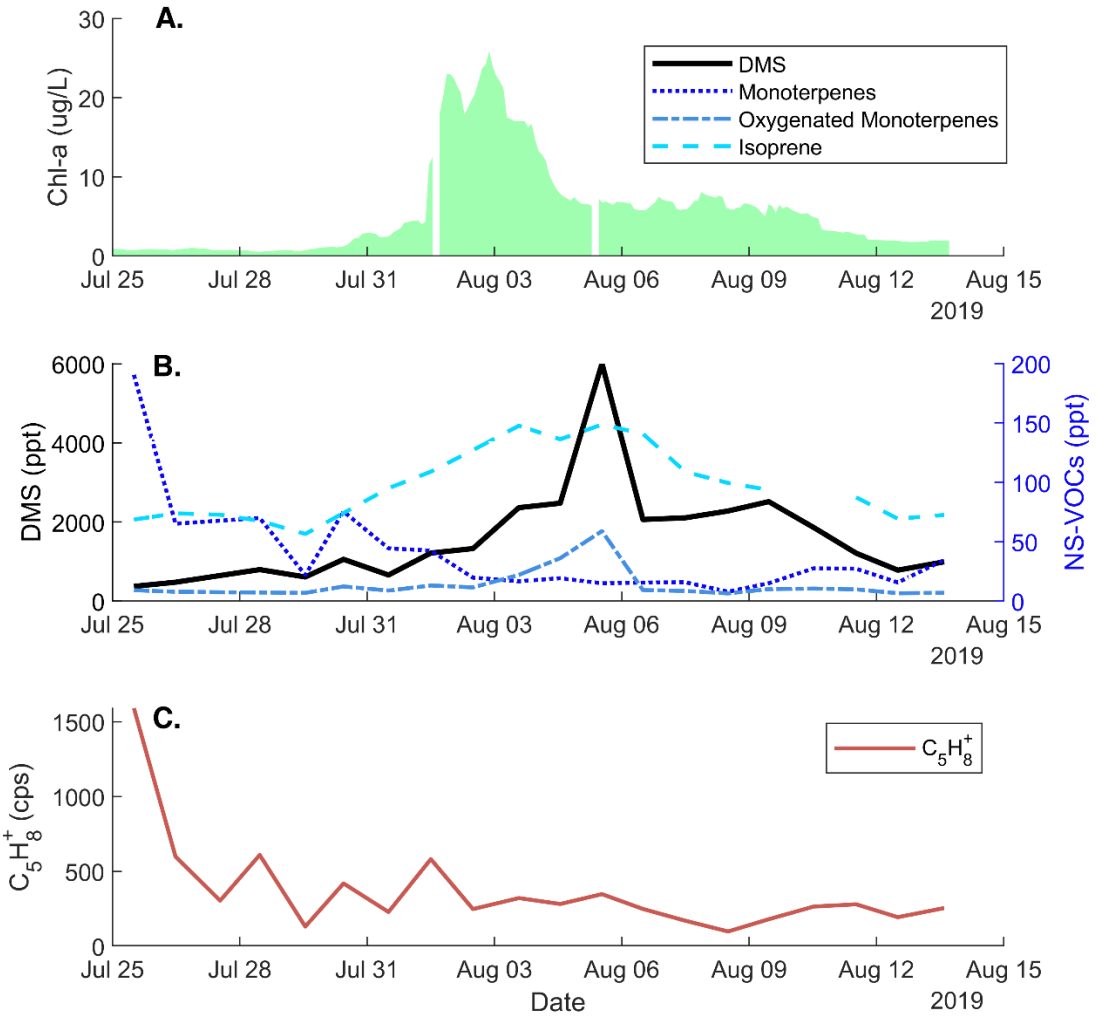

Figure 5.5: Headspace gas concentrations measured throughout the bloom. A) Chl-a concentrations are shown for reference. B) Headspace concentrations of DMS, monoterpenes, and oxygenated monoterpenes as measured by the PTR-MS, while the isoprene concentration was measured by b-CI-ToF-MS. C) The C5H8+ ion signal as measured by the PTR-MS. This ion is isobaric with isoprene, but it is likely influenced by fragmentation products of larger compounds.

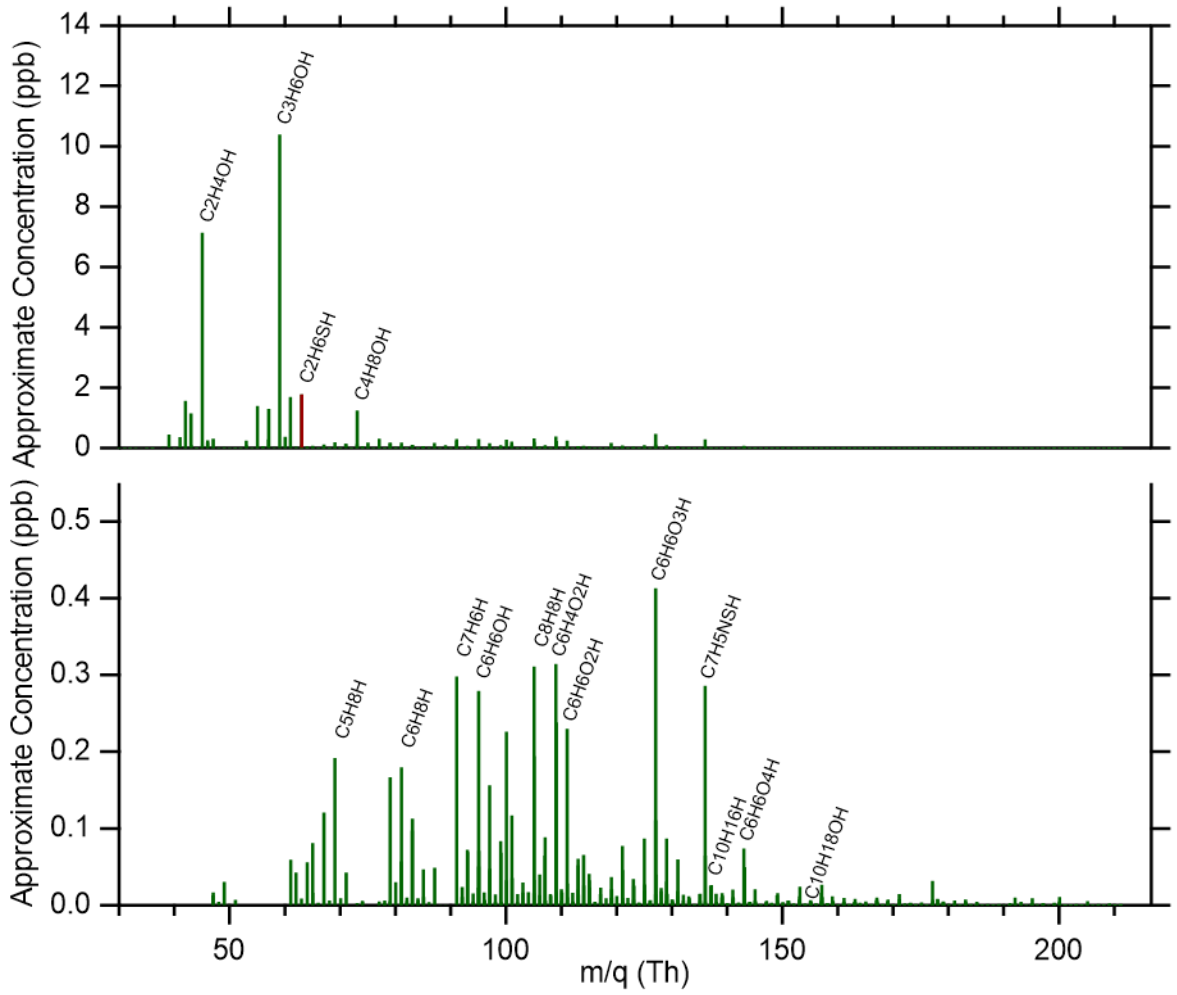

Figure 5.6 The campaign average VOC mass spectra shown for (top) all ions and (bottom) only those ions having 5 or greater carbon atoms, excluding DMS. Notable ions are indicated with the molecular formulas (including the H from proton transfer). The concentrations are in approximate ppb, based on the assumed calibration factor.

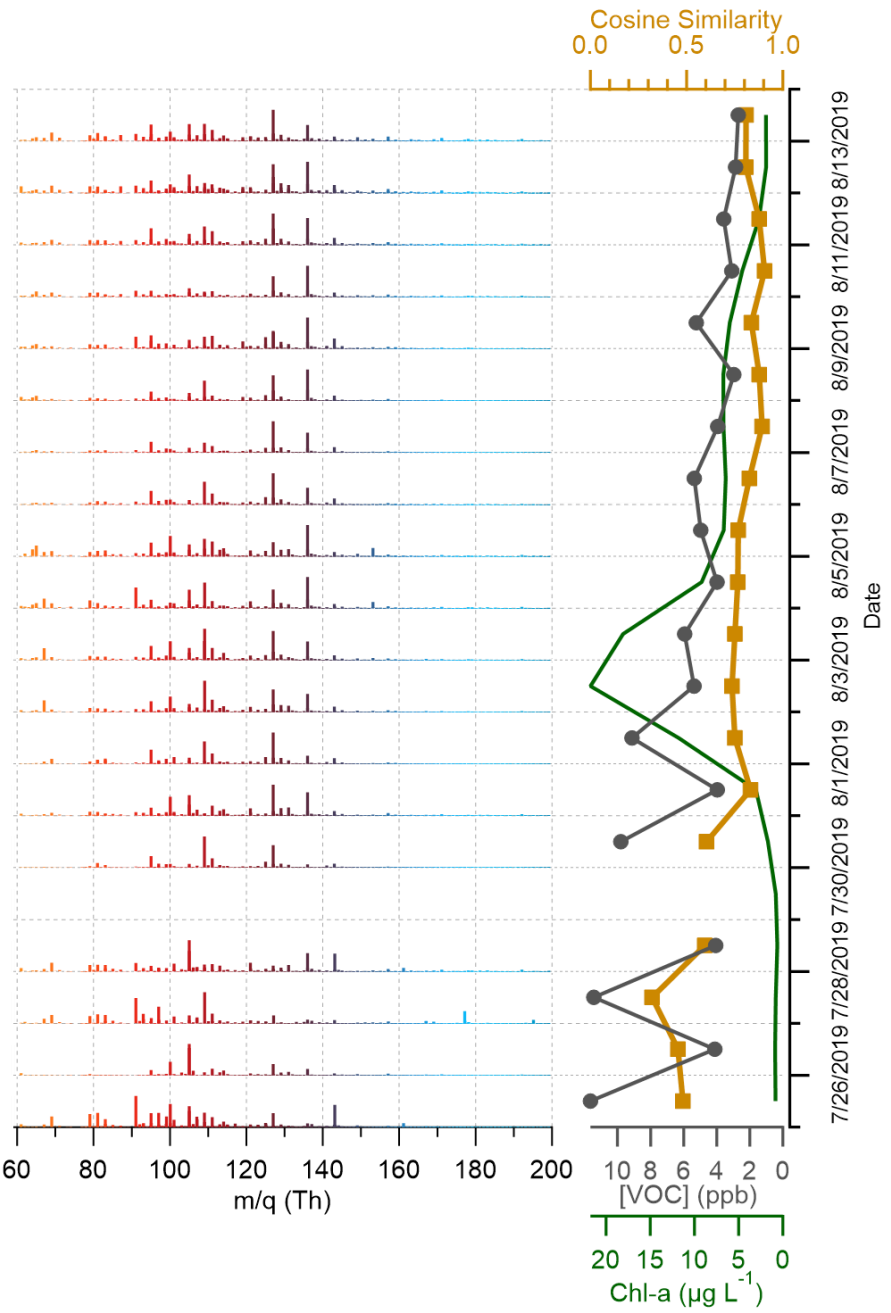

Figure 5.7 Time-series of daily average molecular-weight and SOA-yield weighted VOC mass spectra (excluding DMS) along with the cosine similarity between these spectra and the overall average spectrum (orange), the total approximate VOC concentration (gray), and the Chl-a concentration (green).

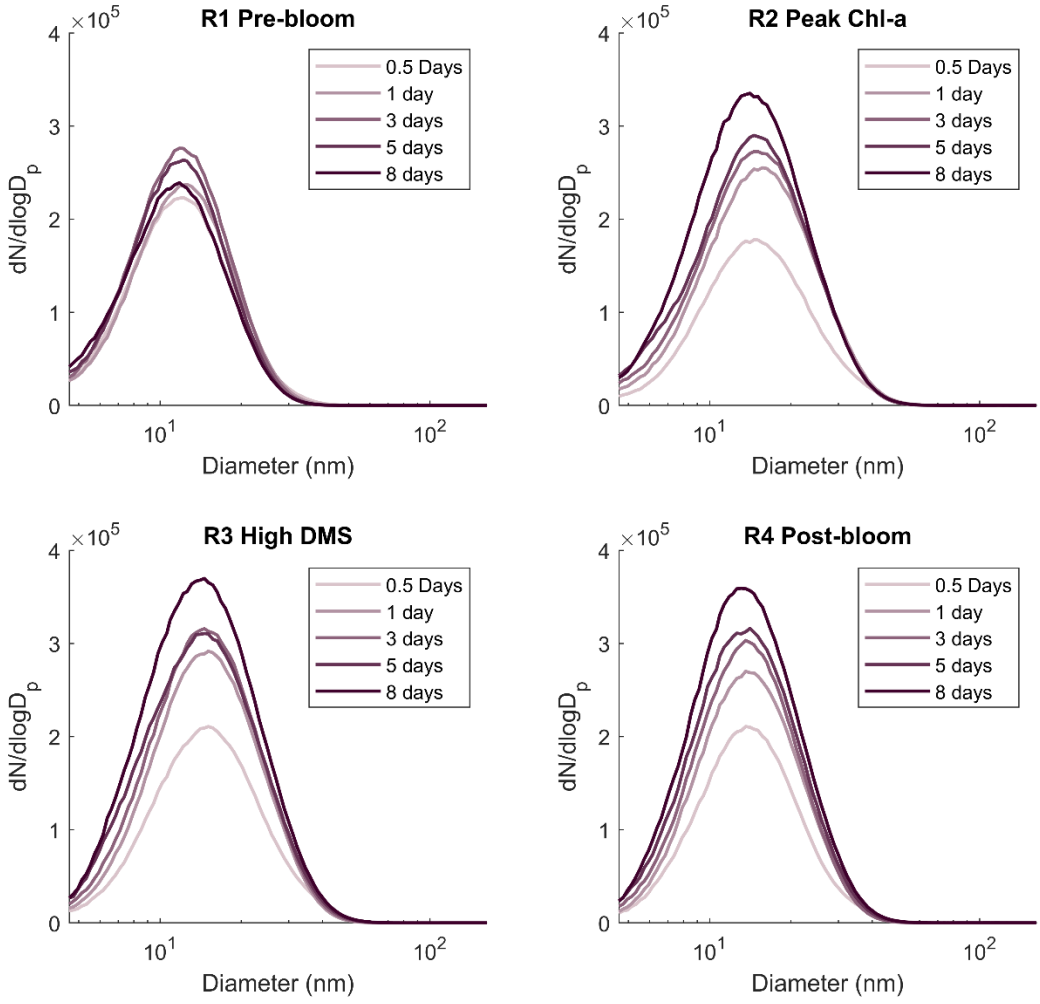

Figure 5.8 SMPS size distributions for SMA at each OFR condition during the four selected bloom periods. Each panel represents data from a single 4-hour OFR cycle, illustrating the typical behavior during these periods.

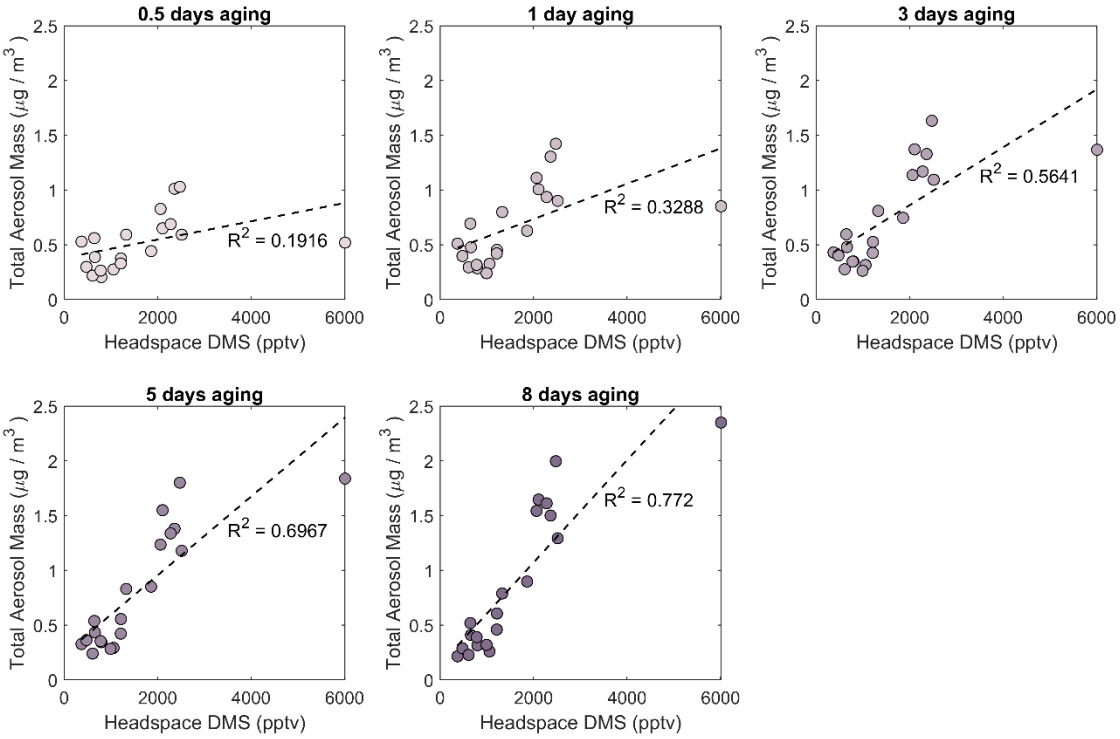

Figure 5.9 Correlation between DMS headspace concentrations and the SMA aerosol mass at each OH exposure.

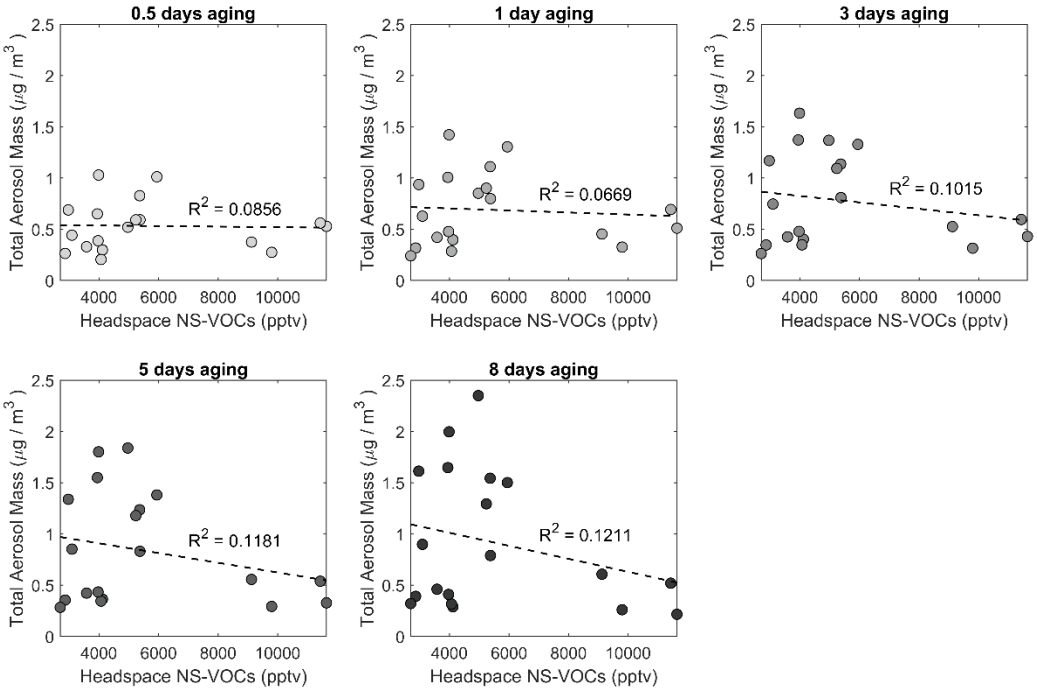

Figure 5.10 Correlation between non-sulfur VOC headspace (C5 and greater, siloxanes are omitted) concentrations and the SMA aerosol mass at each OH exposure.

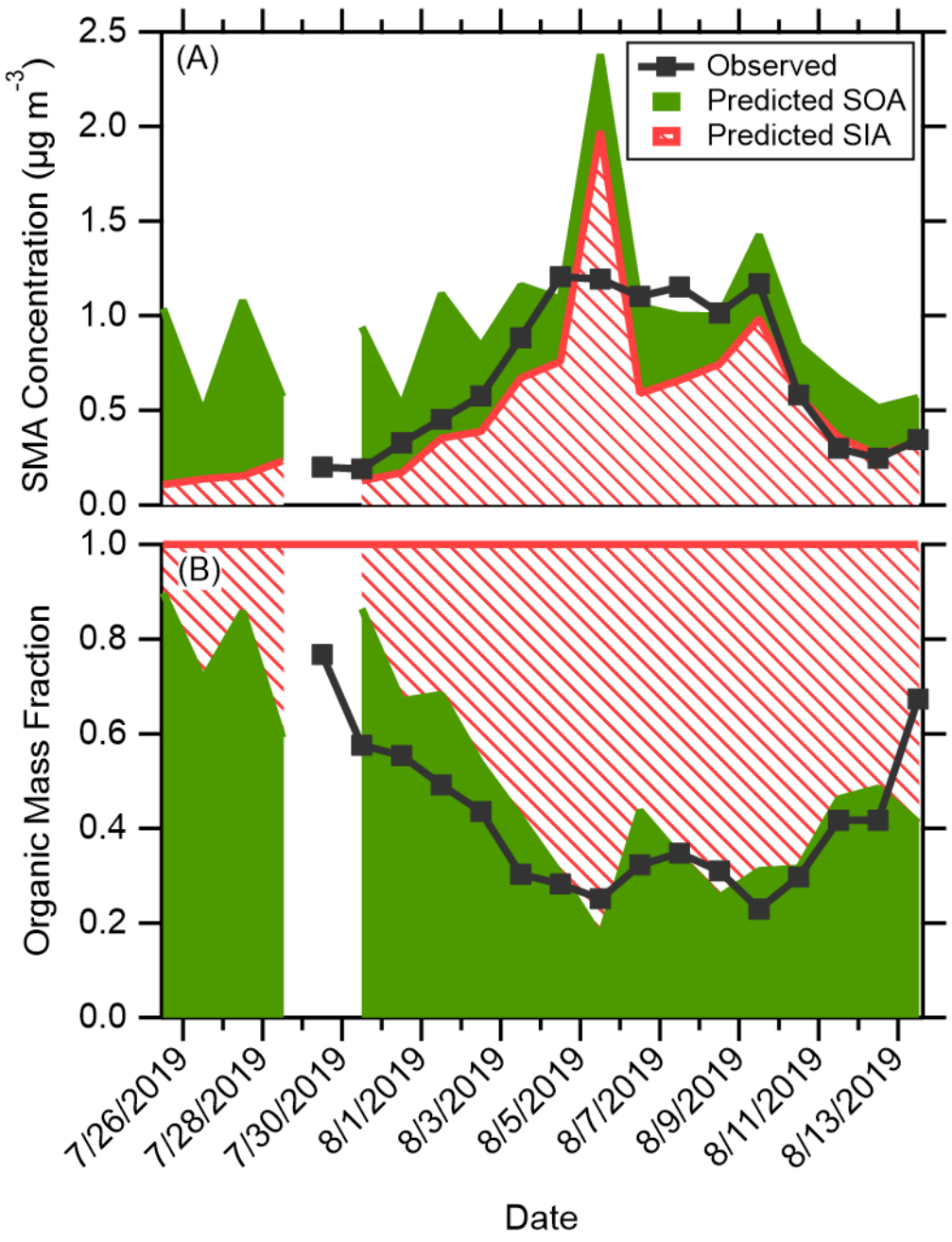

Figure 5.11 (A) Time-series of observed secondary marine aerosol (gray squares) averaged across photochemical ages compared with the sum of the predicted SOA (solid green) and SIA (hashed red) for the fixed-yield SMA model. (B) Time-series of observed organic mass fraction averaged across photochemical ages (gray squares) compared with the of the predicted OMF (solid green). Observations and results are shown as daily averages.

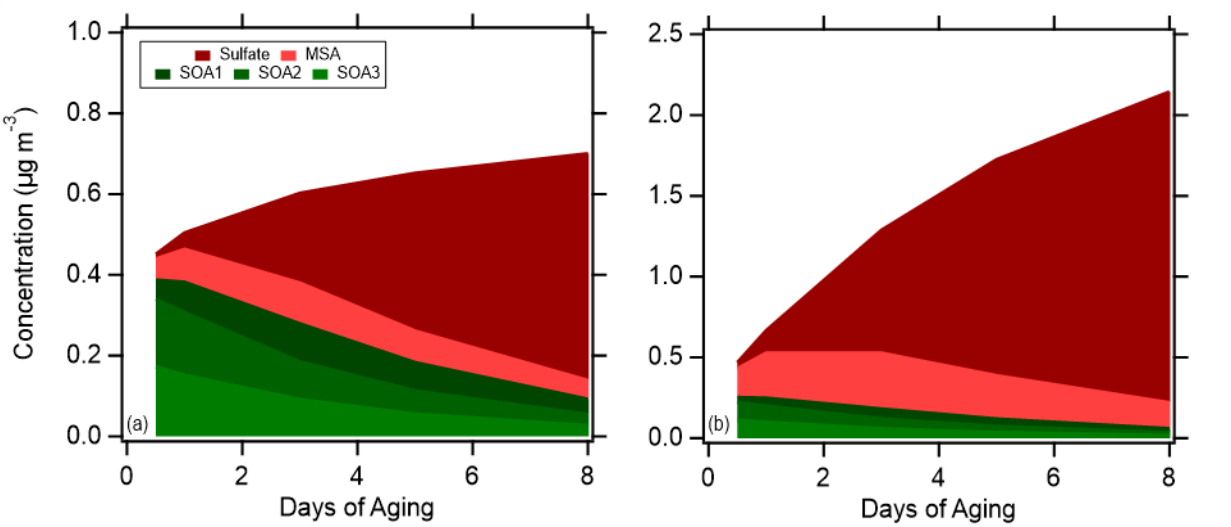

Figure 5.12 Calculated evolution of SMA composition with photochemical aging considering formation from organic species (green) and sulfur-containing species (red), for (a) Period 1 and (b) Period 3.

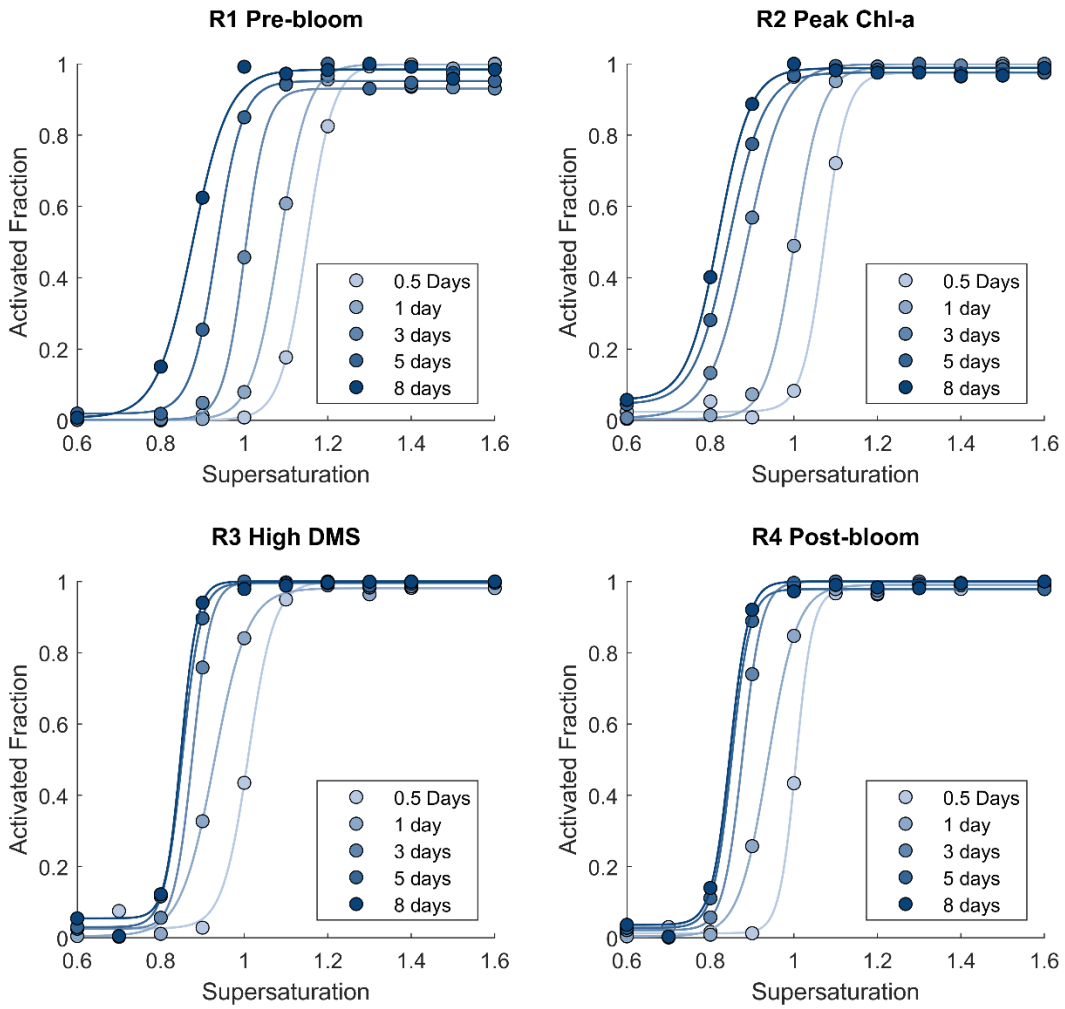

Figure 5.13 SR-CCN activation curves for SMA at each OFR condition (D_d = 30 nm) during the four bloom periods, illustrating typical CCN activation behavior. Each panel represents data from a single 4-hour OFR cycle.

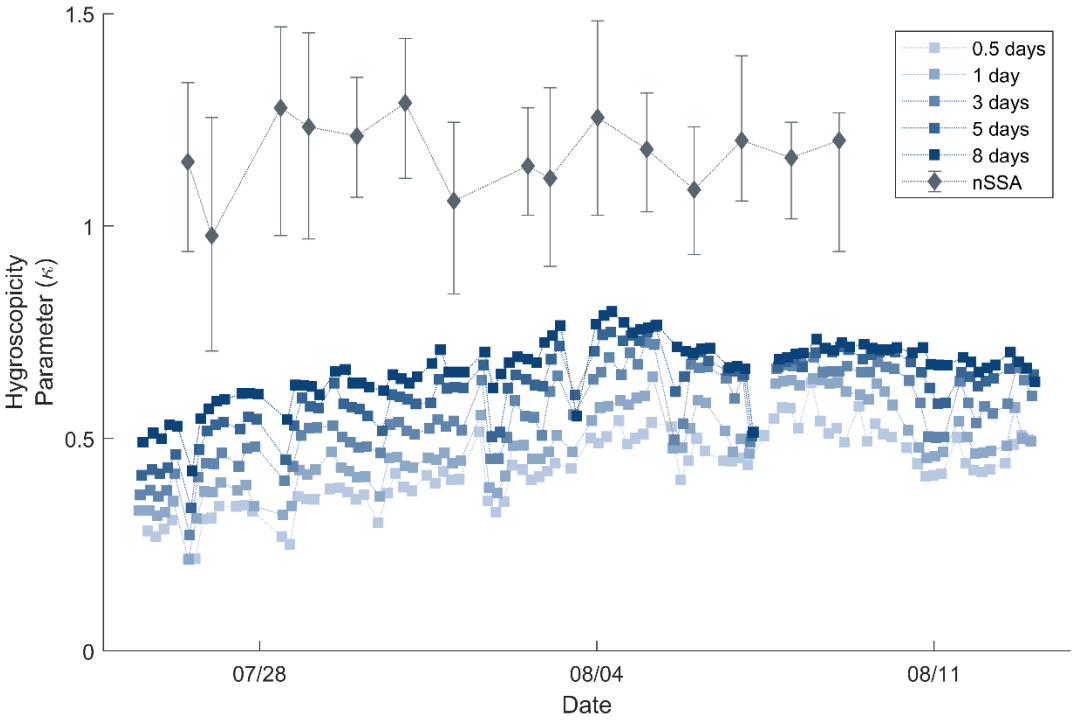

Figure 5.14 Time series showing the CCN activity of both nascent SSA and SMA at each OFR condition. The SSA data represents a daily average, whereas the SMA data points are calculated from individual sampling periods

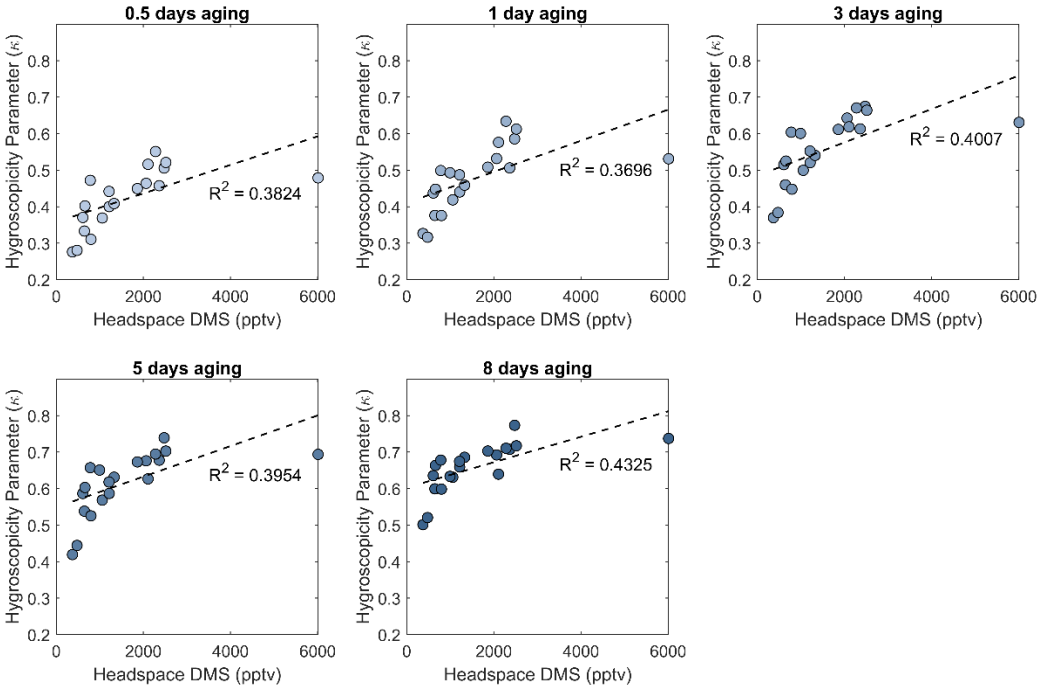

Figure 5.15 Hygroscopicity parameter versus headspace DMS concentrations at each oxidation level.

.

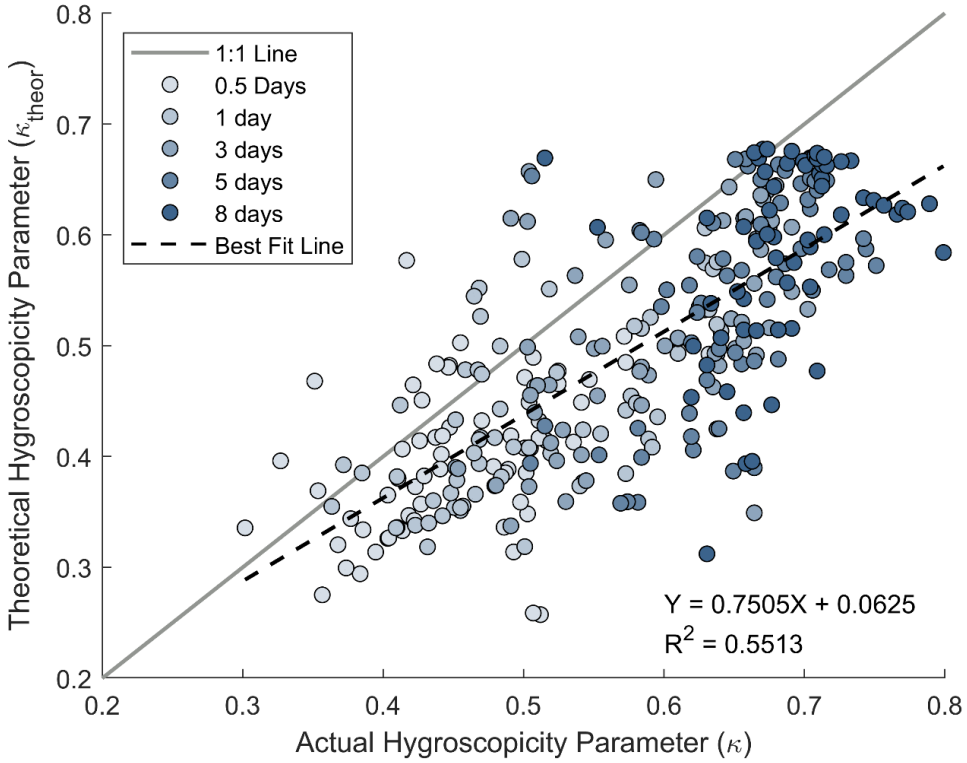

Figure 5.16 Correlation between the measured hygroscopicity parameter (κapp) and the theoretical values calculated from the HR-ToF-AMS using the simple mixing rule. The hygroscopicity of the organic fraction was assumed to be κorg = 0.2.

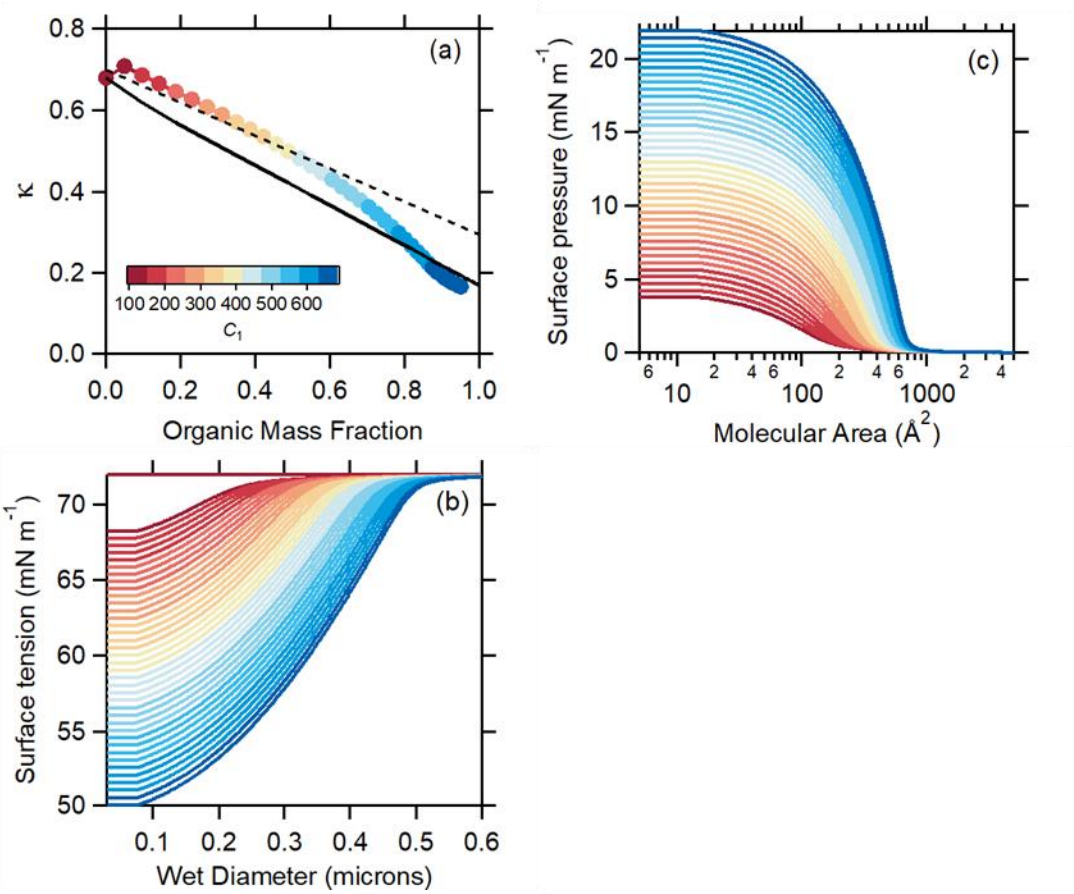

Figure 5.17 Results from the surface film model showing (a) the apparent κ versus the organic mass fraction, (b) the surface tension versus droplet wet diameter, and (c) the surface pressure versus molecular area. In (a), the colored points are the apparent κ values when the organic species can reduce the surface tension, the solid black line is the apparent κ assuming the organic to be fully soluble but not surface active, and the dashed line is a linear fit to the apparent k with surface tension reduction over the OMF range 0 to 0.6 (approximately equal to the range of the observations).

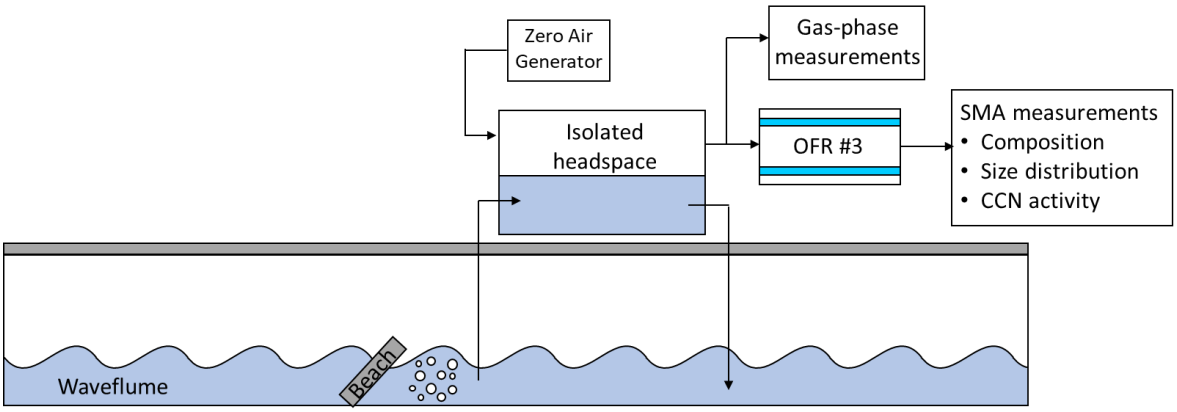

Figure 5.18 SeaSCAPE experimental setup, showing the wave channel, isolated headspace, OFR, and SMA and gas-phase measurements.

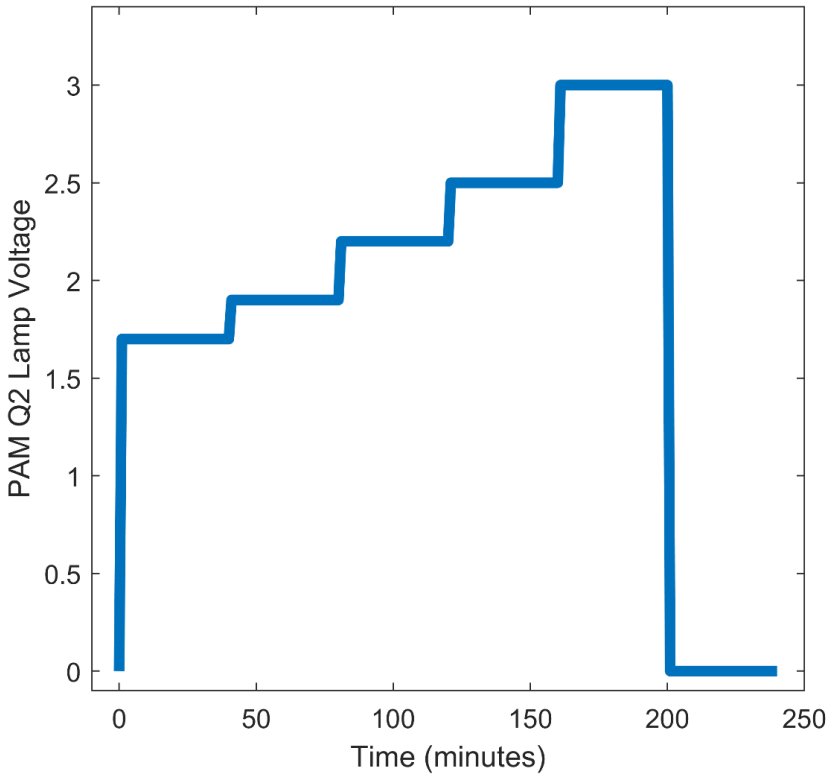

Figure 5.19 Example of the OFR cycle used during the bloom experiments, showing the different OH exposure steps used.

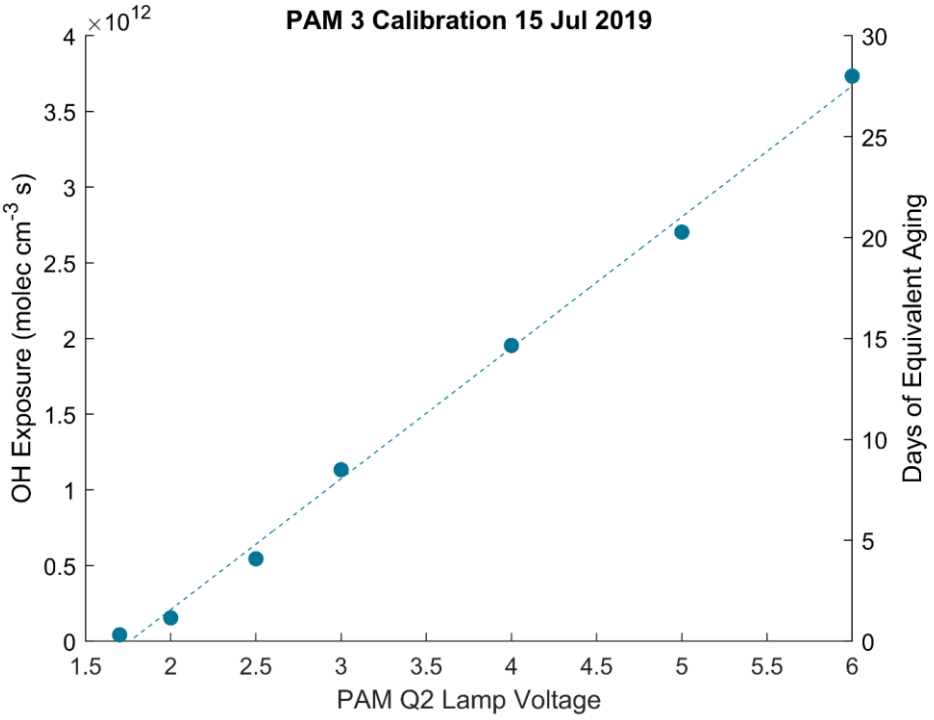

Figure 5.20 OFR calibration curve. Days of equivalent aging is calculated assuming a mean daily OH concentration of 1.5 x 10^6 molecules cm^{-3} (Seinfeld and Pandis, 2016).

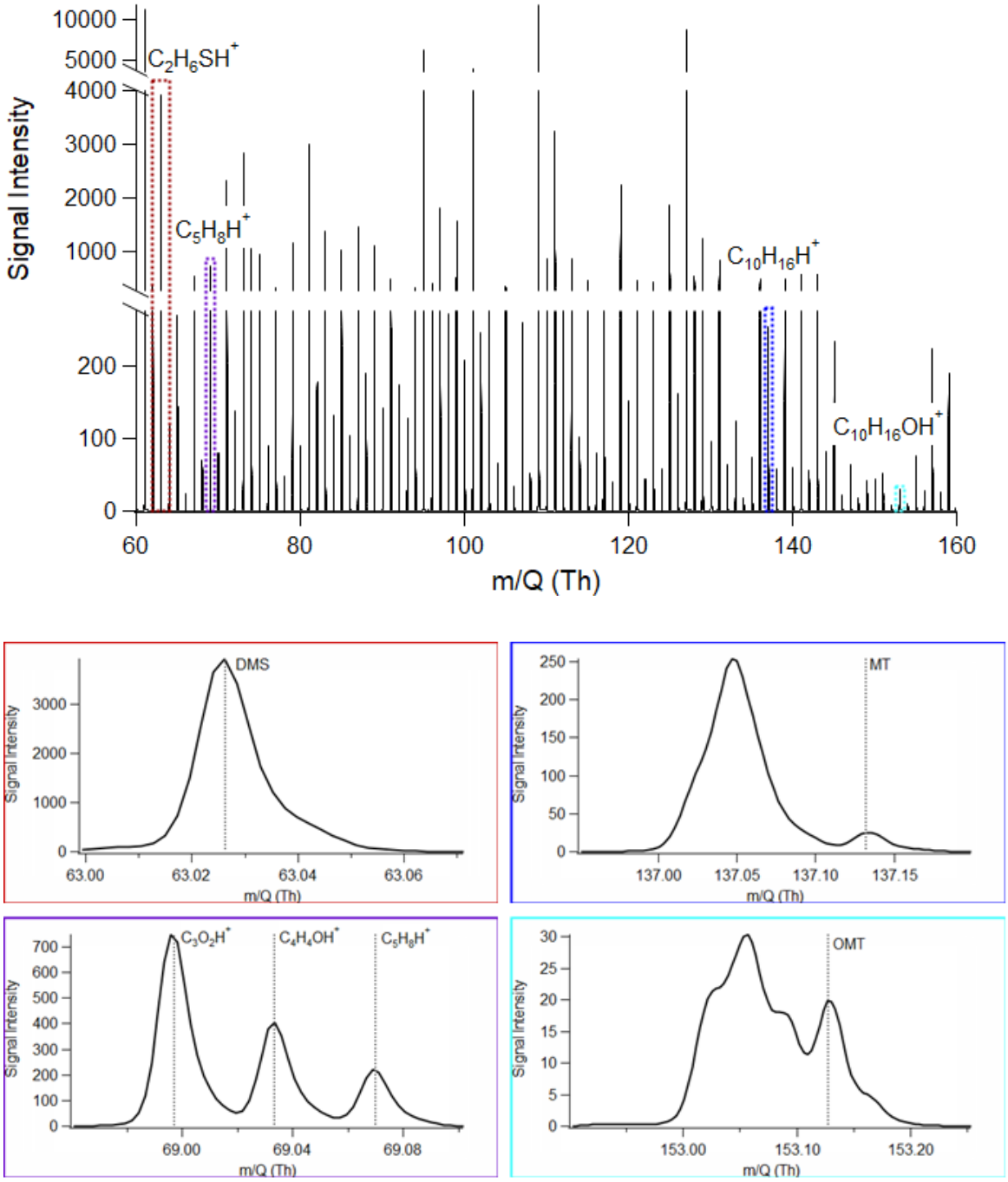

Figure 5.21 Sample mass spectrum from the PTR-MS corresponding to ISV measurement on August 8th. DMS, monoterpenes (MT), C5H8H+ ion, and oxygenated monoterpenes (OMT) are highlighted.

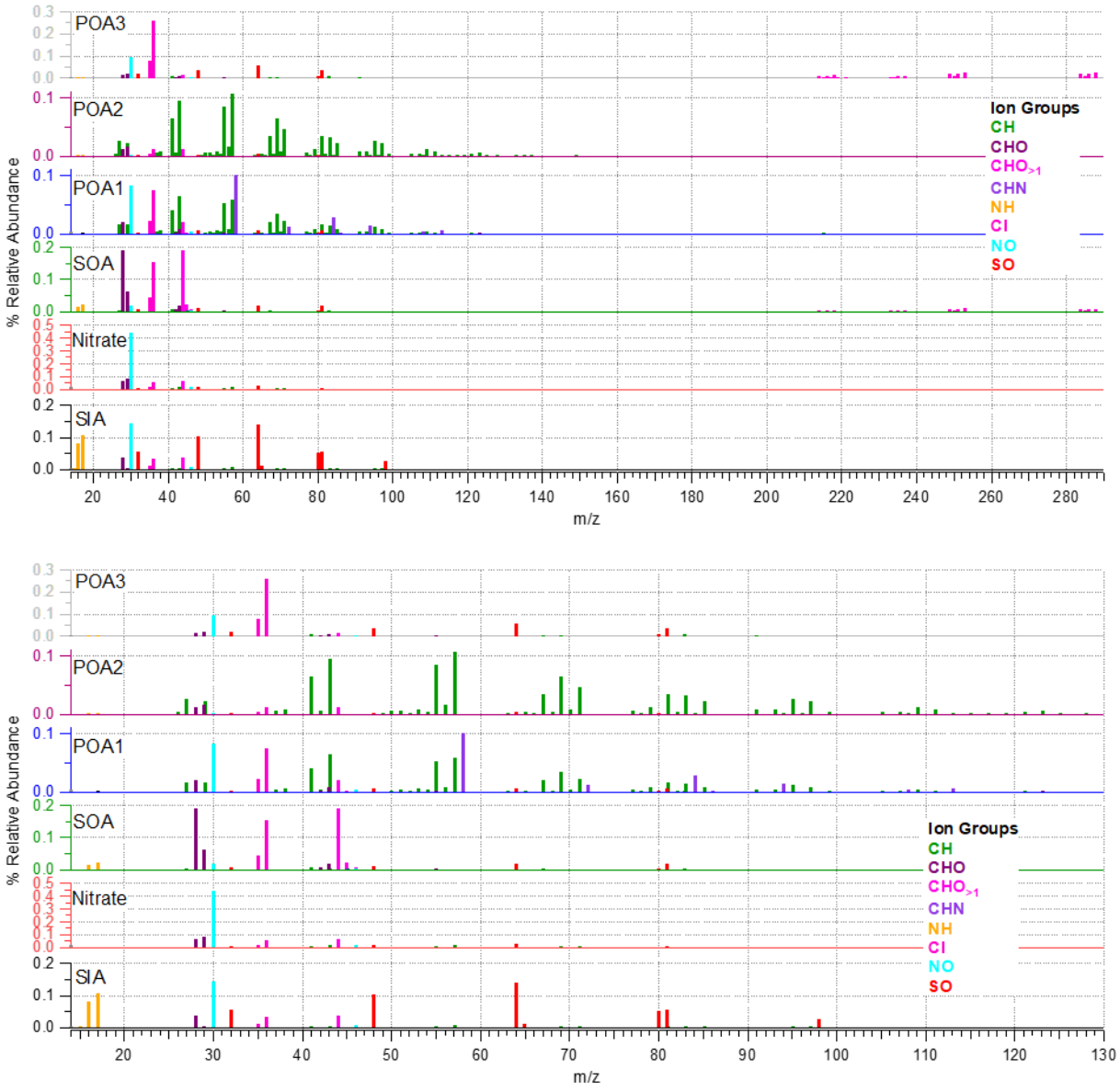

Figure 5.22 HR-ToF-AMS Mass Spectra of the Six Factors of the PMF Solution for Period 1 (top is the entire spectra and bottom is m/z <130).

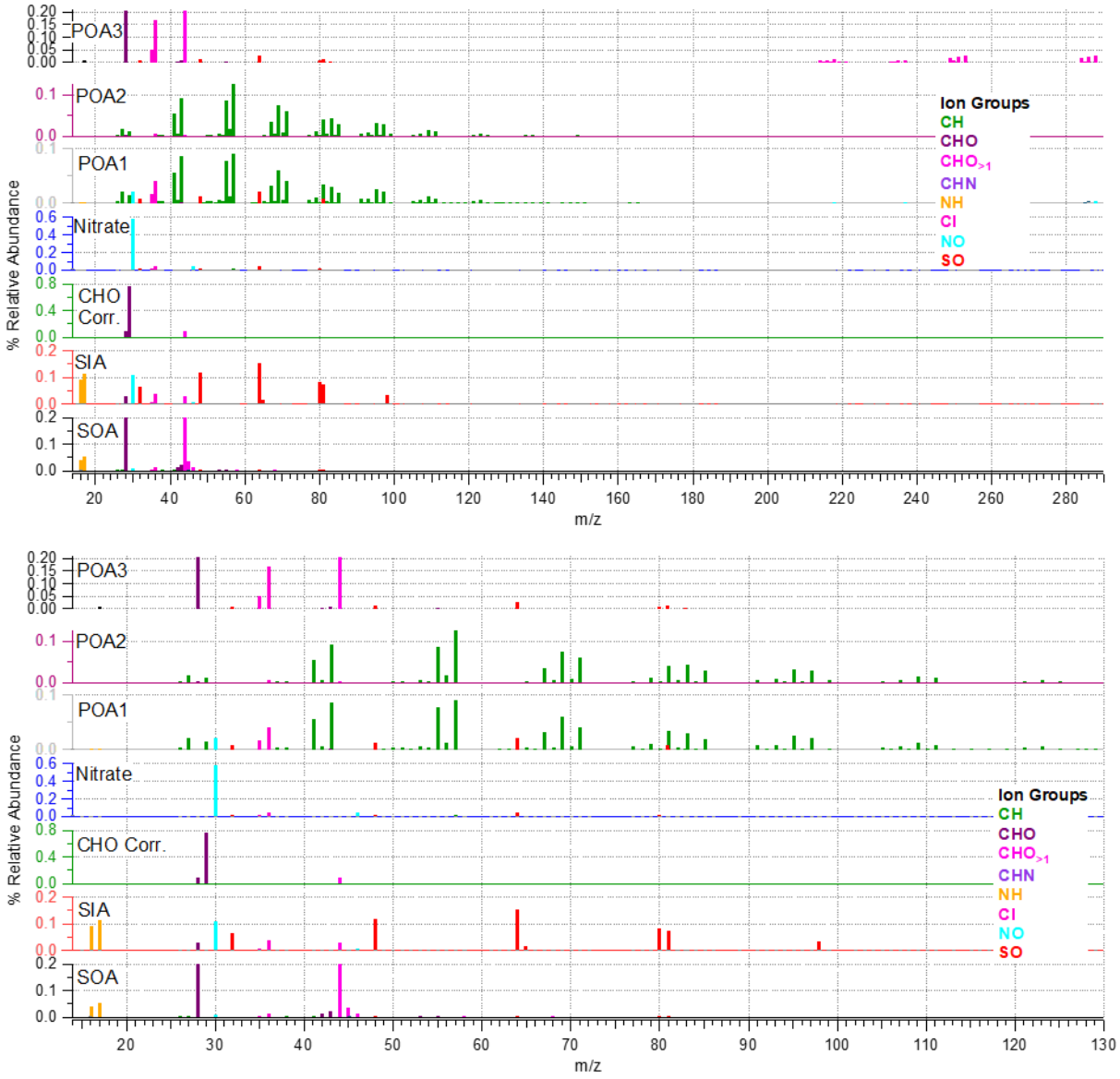

Figure 5.23 Mass Spectra of the Six Factors of the PMF Solution for Period 2 (top is the entire spectra and bottom m/z <130).

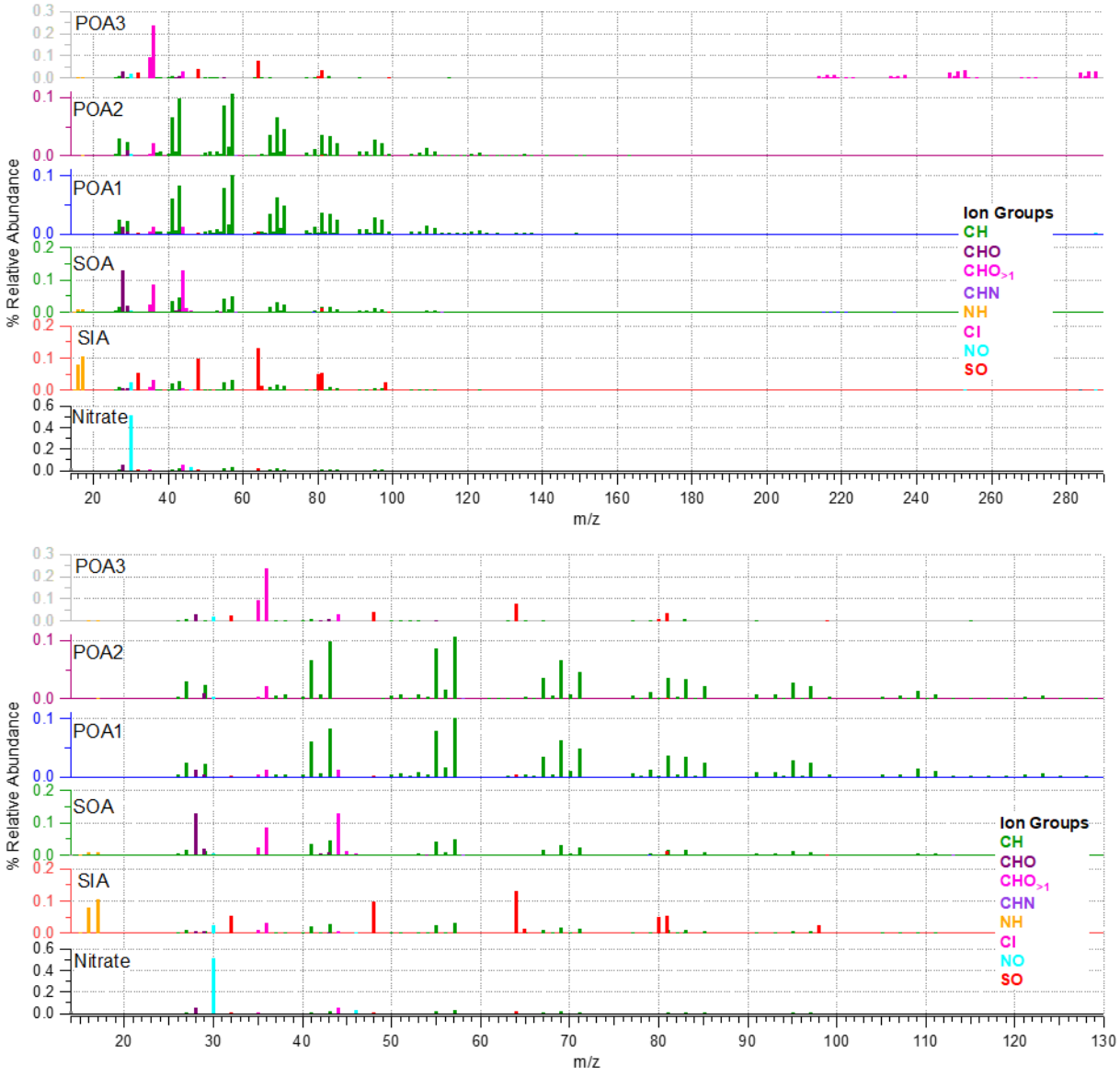

Figure 5.24 Mass Spectra of the Six Factors of the PMF Solution for Period 3 (top is the entire spectra and bottom m/z <130)

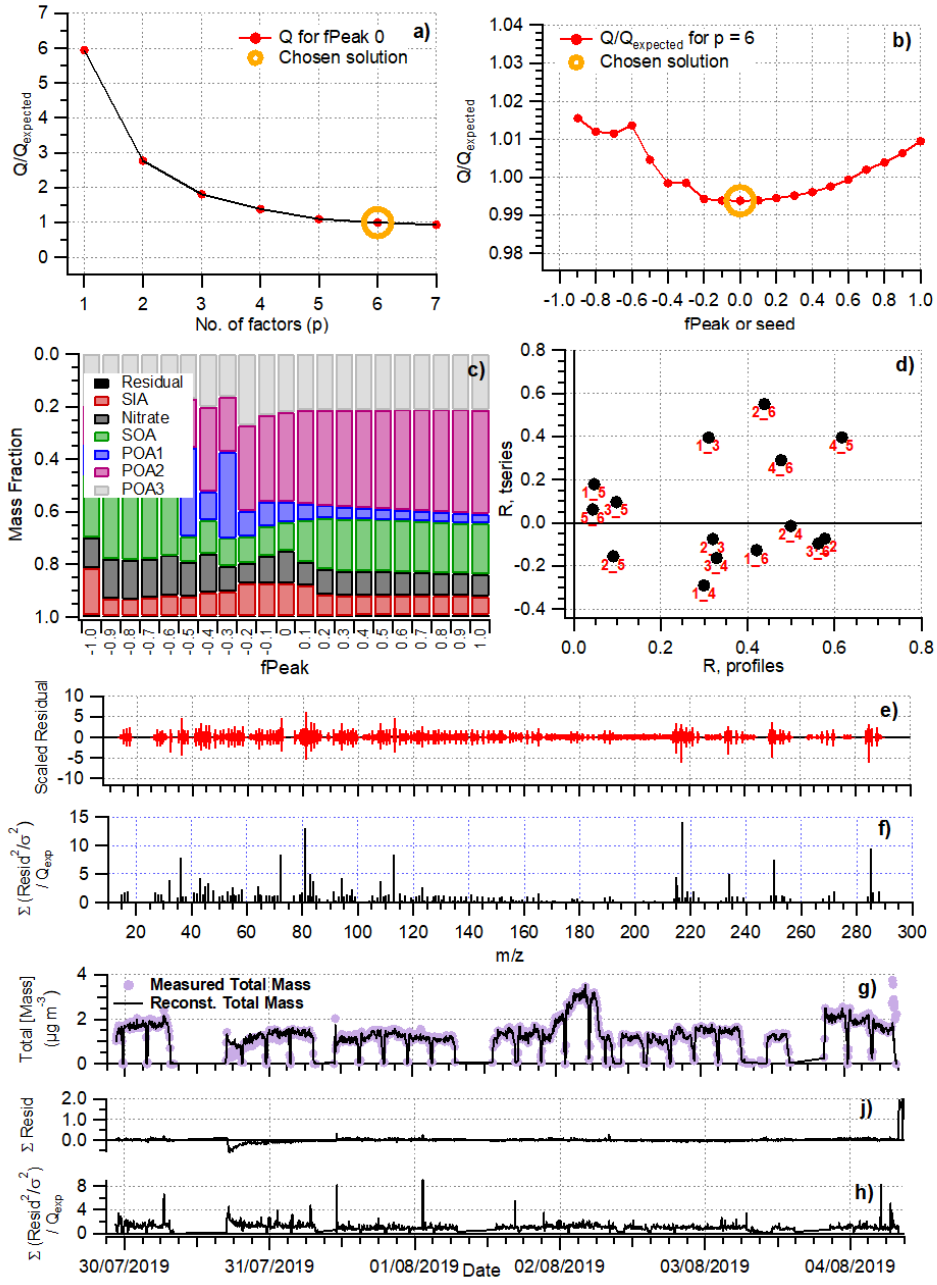

Figure 5.25 PMF Diagnostic Plots for Period 1. Panel (a) shows Q/Qexp of the solutions with a different number of factors tends to around 1, (b) presents Q/Qexp for the varying fPeak values showing the solution sets to be rotationally stable, (c) shows the relative changes of the mass fraction for the factors as the fPeak value was varied, (d) indicates the similarity of the time series and mass spectra of factors to each other with POA1 and POA2 being the most similar, (e-f) present the model-measured fit for each considered ion, and (g-i) present the model-measured fit for the total time series, all showing good agreement with the measurements.

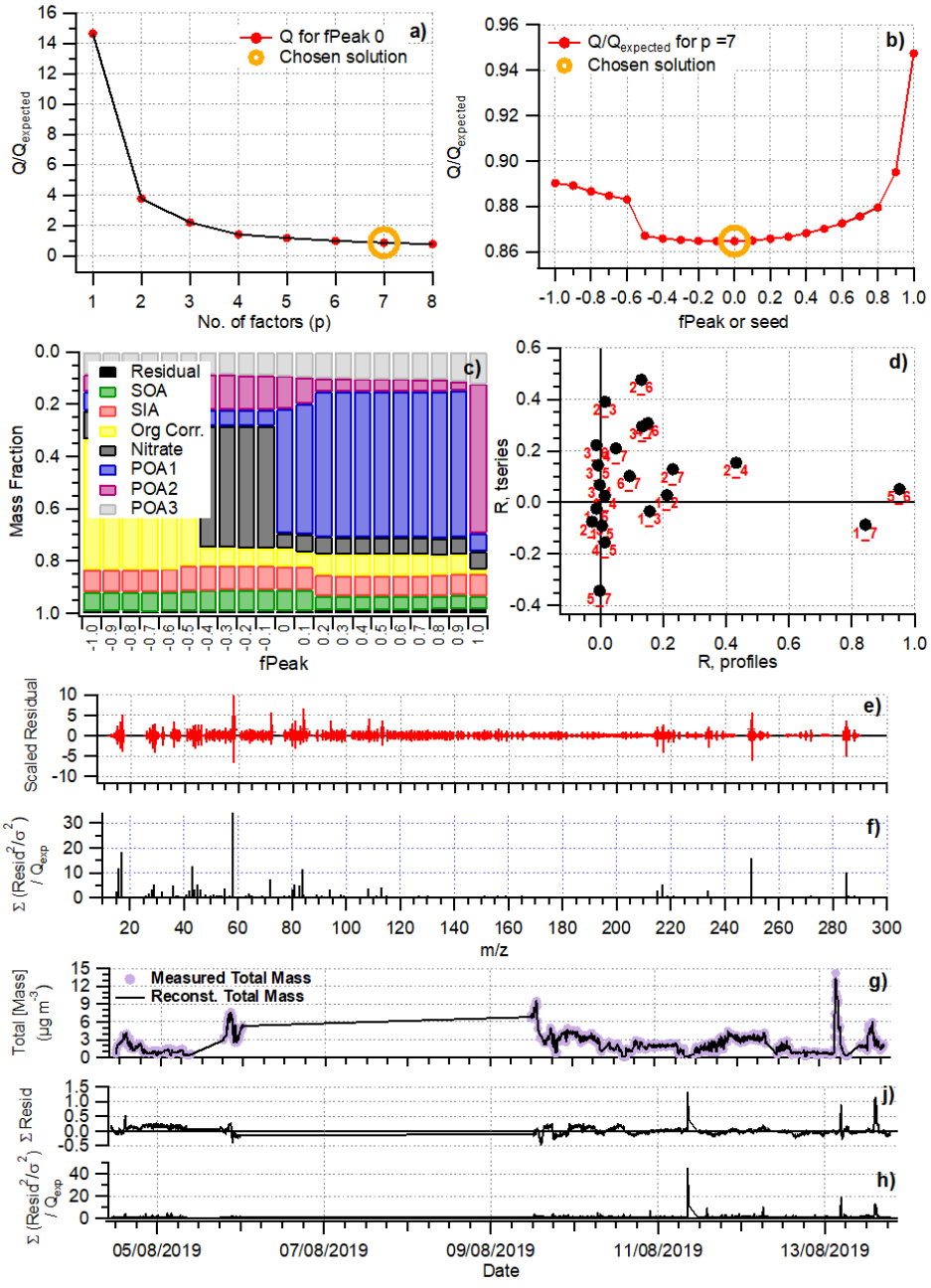

Figure 5.26 PMF Diagnostic Plots for Period 2. Panel (a) shows Q/Qexp of the solutions with a different number of factors tends to around 1, (b) presents Q/Qexp for the varying fPeak values showing the solution sets to be rotationally stable, (c) shows the relative changes of the mass fraction for the factors as the fPeak value was varied, (d) indicates the similarity of the time series and mass spectra of factors to each other with POA1 and POA2 being the most similar, (e-f) present the model-measured fit for each considered ion, and (g-i) present the model-measured fit for the total time series, all showing good agreement with the measurements.

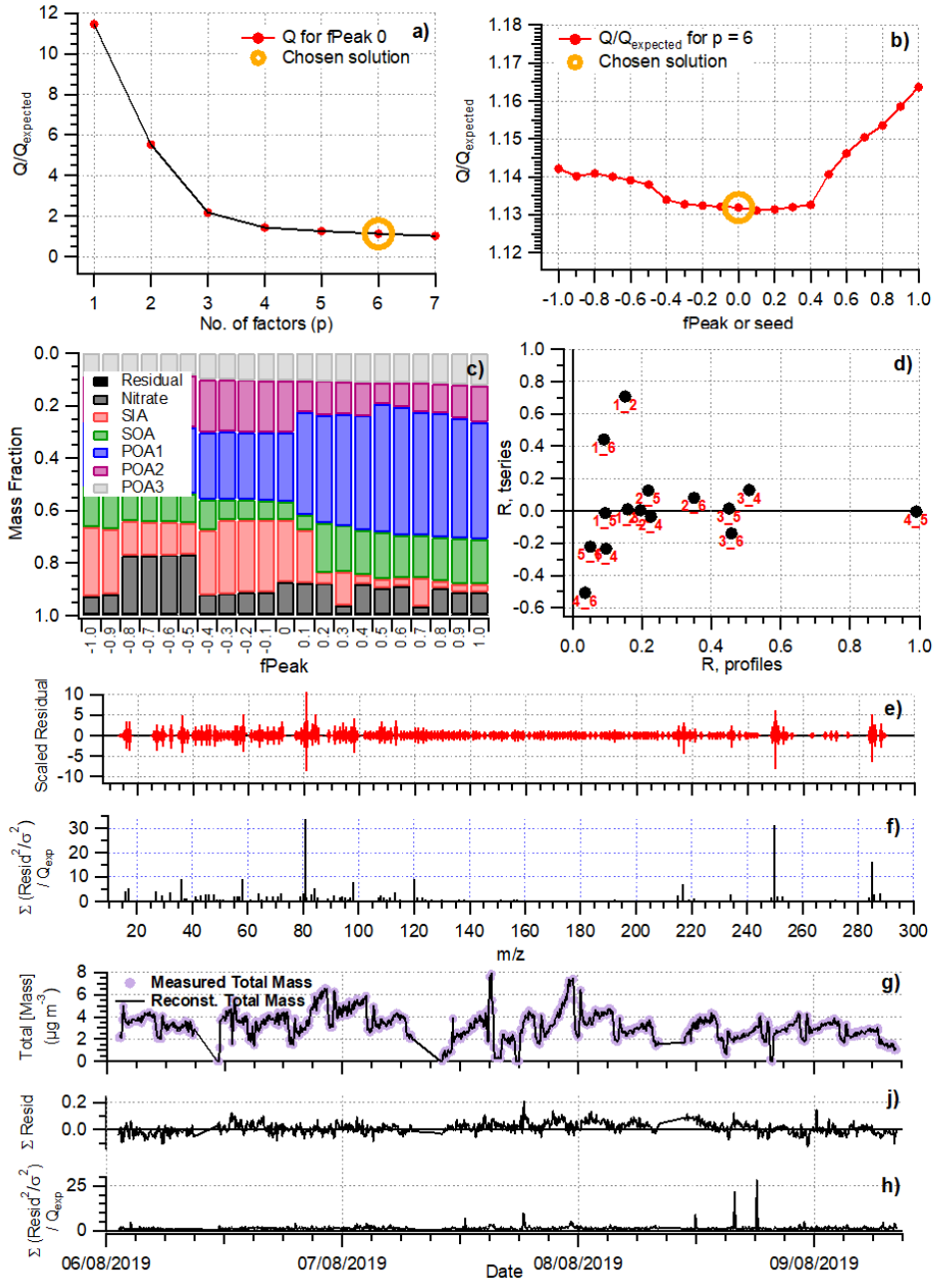

Figure 5.27 PMF Diagnostic Plots for Period 3. Panel (a) shows Q/Qexp of the solutions with a different number of factors tends to around 1, (b) presents Q/Qexp for the varying fPeak values showing the solution sets to be rotationally stable, (c) shows the relative changes of the mass fraction for the factors as the fPeak value was varied, (d) indicates the similarity of the time series and mass spectra of factors to each other with POA1 and POA2 being the most similar, (e-f) present the model-measured fit for each considered ion, and (g-i) present the model-measured fit for the total time series, all showing good agreement with the measurements.

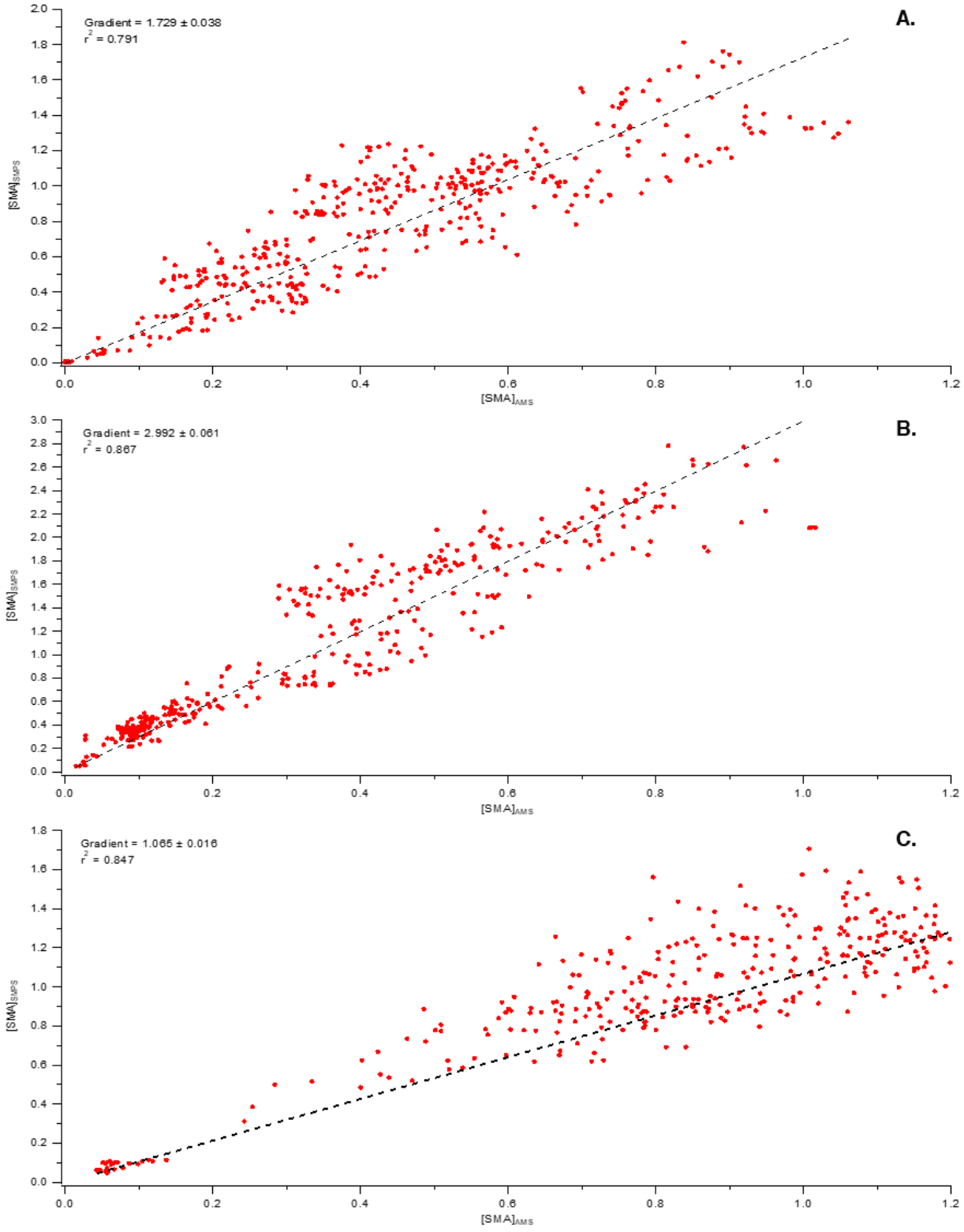

Figure 5.28 Scatter plot of [SMA]SMPS vs unverified [SMA]AMS for A) Period 1, B) Period 2, and C) Period 3.

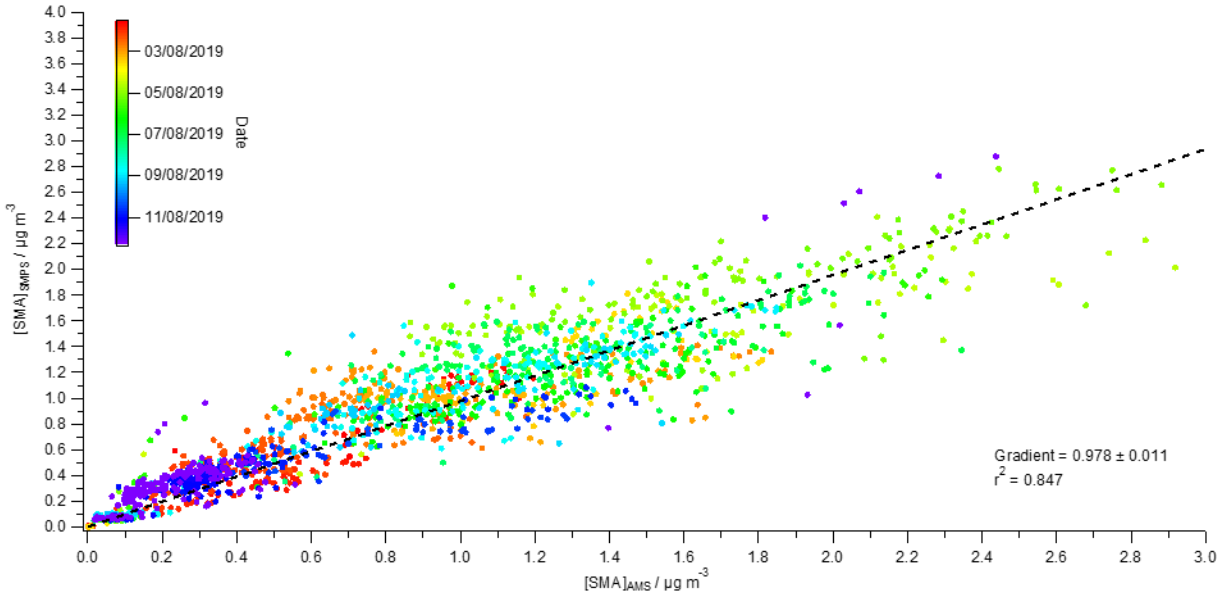

Figure 5.29 Scatter plot of [SMA]SMPS vs verified [SMA]AMS for all analysis periods

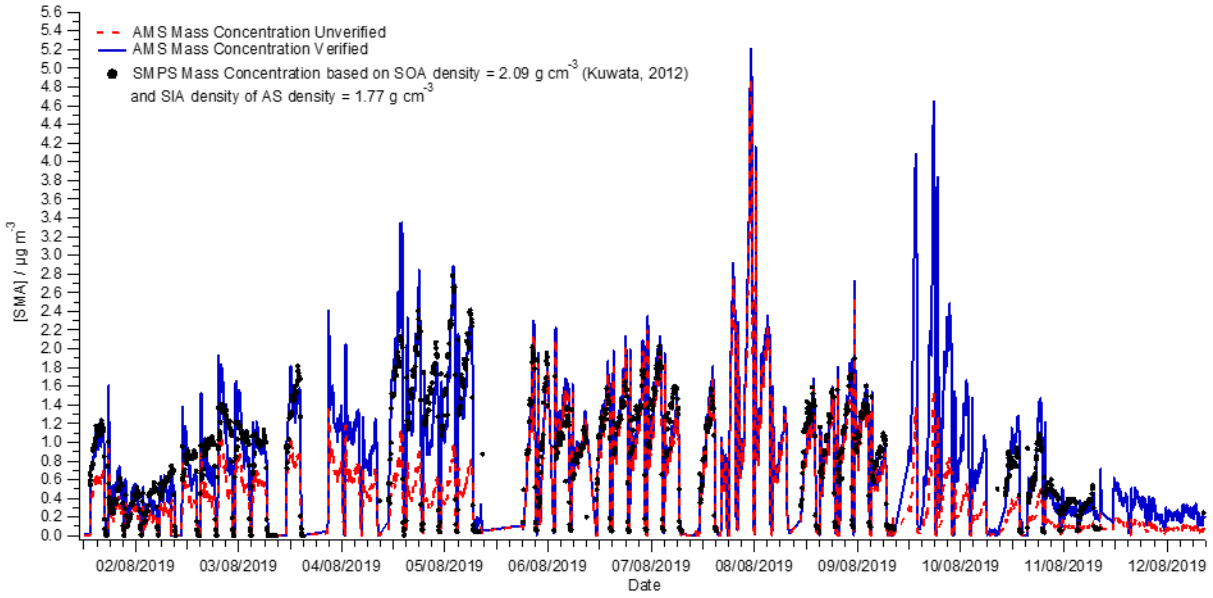

Figure 5.30 Comparison of time series for the mass concentration of unverified and verified SMA factor with SMPS

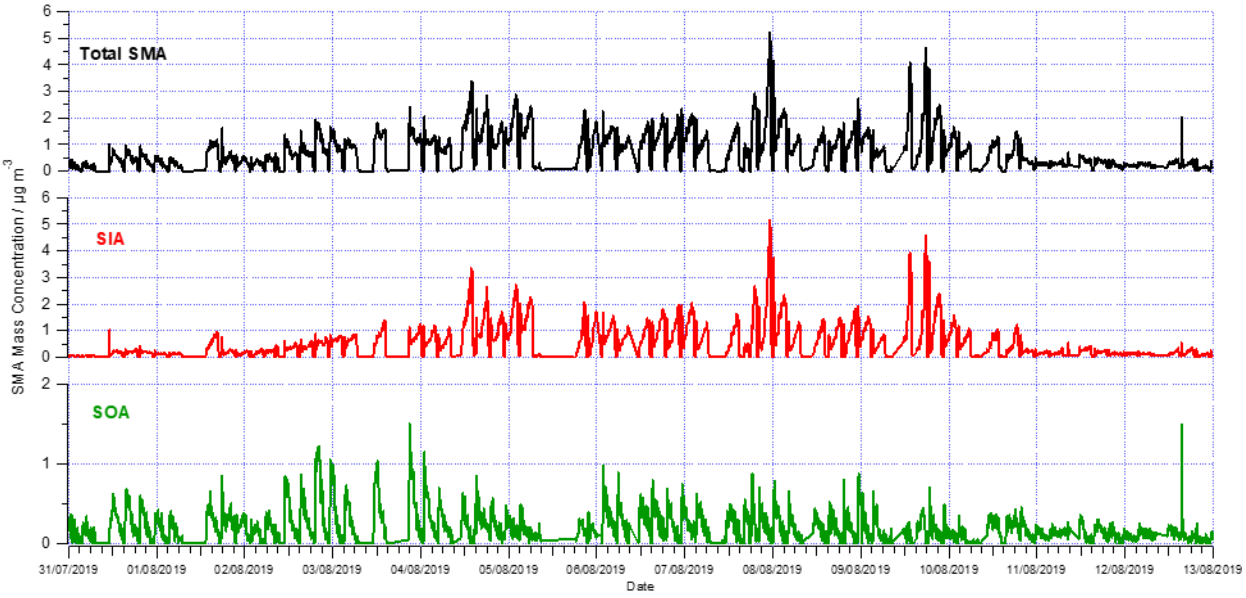

Figure 5.31 Verified Total SMA, SIA and SOA mass concentration time series

5.8.4 Supplementary Tables

Table 5.1 VOCs observed during SeaSCAPE with possible anthropogenic origins.

Compound Name	Structure	References
Styrene	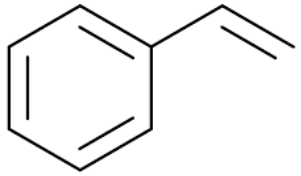	Plasticizer (Fuhrer et al., 2012)
Benzothiazole	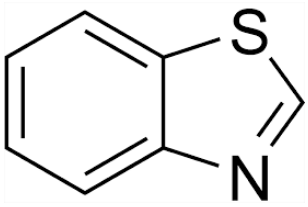	Runoff and wastewater, rubber derivatives (Liao et al., 2018; Reddy and Quinn, 1997)
o-Xylene	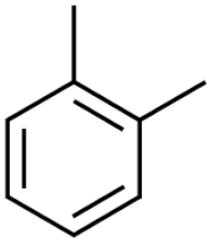	Fuel and chemical leaks, runoff (Duan et al., 2017)
Naphthalene	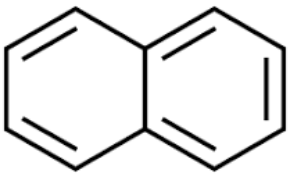	Oils, wastewater, fuels (Jing et al., 2014)
Benzophenone	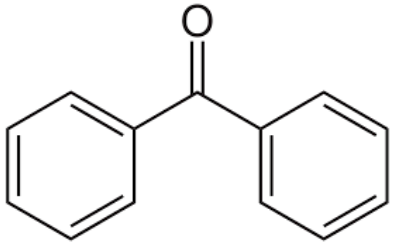	Personal care products, wastewater (Mao et al., 2019)

Table 5.2 Values of the mean, median, and standard deviation for the SMA hygroscopicity parameters (κ_{app}) measured for each OFR condition over the full bloom cycle.

OFR Condition	Mean	Median	Standard Deviation
0.5d	0.43	0.43	0.08
1d	0.48	0.47	0.10
3d	0.56	0.55	0.10
5d	0.62	0.63	0.09
8d	0.66	0.67	0.07

Table 5.3 Field observations of the hygroscopicity of secondary marine aerosols. Growth factors are converted to hygroscopicity parameters (κ) using the equation reported in Ref. 2.

Location	Hygroscopicity parameter	Diameter	Reference	Notes	Growth Factor
Western North Pacific	0.48 ± 0.06	50 nm	(Mochida et al., 2011)	Derived from growth factor (RH = 85%)	N/A
South China Sea	0.46 ± 0.17	Aitken mode	(Atwood et al., 2017)	Background marine type	N/A
Southern Ocean	0.47	42.2 nm	(Fossum et al., 2018)	Maritime polar (mP) type	N/A
Antarctic Coast	0.70	50 nm	(Asmi et al., 2010)	Calculated from growth factor (RH = 90%)	GF = 1.67
North Atlantic	0.68 ± 0.05	50 nm	(Maßling et al., 2003)	More hygroscopic type. Calculated from growth factor (RH = 90%)	GF = 1.66 +/- 0.03
Southern Atlantic (subtropical)	0.79 ± 0.09	50 nm	(Maßling et al., 2003)	More hygroscopic type. Calculated from growth factor (RH = 90%)	GF = 1.72 +/- 0.05
Indian Ocean	0.76 ± 0.06	50 nm	(Maßling et al., 2003)	More hygroscopic type. Calculated from growth factor (RH = 90%)	GF = 1.70 +/- 0.03
Southern Ocean	0.68	50 nm	(Berg et al., 1998)	Identified as nss-SO_4. Calculated from growth factor (RH = 90%)	GF = 1.66
North Pacific	0.61	50 nm	(Berg et al., 1998)	Identified as nss-SO_4. Calculated from growth factor (RH = 89%)	GF = 1.59

Table 5.4 Assumptions used in the theoretical hygroscopicity model.

Compound	Hygroscopicity parameter	Reference	Density
NH_4NO_3	0.67	(Petters and Kreidenweis, 2007)	1.72 g cm^{-3}
$(NH_4)_2SO_4$	0.61	(Petters and Kreidenweis, 2007)	1.77 g cm^{-3}
H_2SO_4	0.90	(Petters and Kreidenweis, 2007)	1.83 g cm^{-3}
OA	0.2	(Massoli et al., 2010)	2.09 g cm^{-3}

5.10 References

Allan, J. D., Delia, A. E., Coe, H., Bower, K. N., Alfarra, M. R., Jimenez, J. L., Middlebrook, A. M., Drewnick, F., Onasch, T. B., Canagaratna, M. R., Jayne, J. T. and Worsnop, D. R.: A generalised method for the extraction of chemically resolved mass spectra from Aerodyne aerosol mass spectrometer data, J. *Aerosol Sci.*, 35(7), 909–922, doi:10.1016/j.jaerosci.2004.02.007, 2004.

Anku, W. W., Mamo, M. A. and Govender, P. P.: Phenolic Compounds in Water: Sources, Reactivity, Toxicity and Treatment Methods, in Phenolic Compounds - Natural Sources, Importance and Applications., 2017.

Asmi, E., Frey, A., Virkkula, A., Ehn, M., Manninen, H. E., Timonen, H., Tolonen-Kivimaki, O., Aurela, M., Hillamo, R. and Kulmala, M.: Hygroscopicity and chemical composition of antarctic sub-micrometre aerosol particles and observations of new particle formation, *Atmos. Chem. Phys.*, 10(9), 4253–4271, doi:10.5194/acp-10-4253-2010, 2010.

Atwood, S. A., Reid, J. S., Kreidenweis, S. M., Blake, D. R., Jonsson, H. H., Lagrosas, N. D., Xian, P., Reid, E. A., Sessions, W. R. and Simpas, J. B.: Size-resolved aerosol and cloud condensation nuclei (CCN) properties in the remote marine South China Sea-Part 1: Observations and source classification, *Atmos. Chem. Phys.*, 17(2), 1105–1123, doi:10.5194/acp-17-1105-2017, 2017.

Ayers, G. P. and Gras, J. L.: Seasonal relationship between cloud condensation nuclei and aerosol methanesulphonate in marine air, *Nature*, 354, 56–58, doi:10.1038/353834a0, 1991.

Barger, W. R. and Means, J. C.: Clues to the structure of marine organic material from the study of physical properties of surface films, Mar. Estuar. Geochemistry, Lewis Publ. Chelsea Michigan. 1985. p 47-67, 6 fig, 6 tab, 25 ref., 1985.

Bates, T. S., Quinn, P. K., Coffman, D. J., Johnson, J. E., Upchurch, L., Saliba, G., Lewis, S., Graff, J., Russell, L. M. and Behrenfeld, M. J.: Variability in Marine Plankton Ecosystems Are Not Observed in Freshly Emitted Sea Spray Aerosol Over the North Atlantic Ocean, *Geophys. Res. Lett.*, 47(1), doi:10.1029/2019GL085938, 2020.

Berg, O. H., Swietlicki, E. and Krejci, R.: Hygroscopic growth of aerosol particles in the marine boundary layer over the Pacific and Southern Oceans during the First Aerosol Characterization Experiment (ACE 1), *J. Geophys. Res. Atmos.*, 103(D13), 16535–16545, doi:10.1029/97JD02851, 1998.

Le Bozec, L. and Moody, C. J.: Naturally occurring nitrogensulfur compounds. the benzothiazole alkaloids, *Aust. J. Chem.*, 62(7), 639–647, doi:10.1071/CH09126, 2009.

Burkholder, J. B., Sander, S. P., Abbatt, J., Barker, J. R., Cappa, C., Crounse, J. D., Dibble, T. S., Huie, R. E., Kolb, C. E., Kurylo, M. J., Orkin, V. L., Percival, C. J., Wilmouth, D. M. and Wine, P. H.: Chemical Kinetics and Photochemical Data for Use in Atmospheric Studies, Evaluation No. 19, Pasadena, CA. Available from: http://jpldataeval.jpl.nasa.gov/, 2019.

Canagaratna, M. R., Jayne, J. T., Jimenez, J. L., Allan, J. D., Alfarra, M. R., Zhang, Q., Onasch, T. B., Drewnick, F., Coe, H., Middlebrook, A., Delia, A., Williams, L. R., Trimborn, A. M., Northway, M. J., DeCarlo, P. F., Kolb, C. E., Davidovits, P. and Worsnop, D. R.: Chemical and microphysical characterization of ambient aerosols with the aerodyne aerosol mass spectrometer, *Mass Spectrom. Rev.*, 26(2), 185–222, doi:10.1002/mas.20115, 2007.

Carpenter, L. J., Archer, S. D. and Beale, R.: Ocean-atmosphere trace gas exchange, *Chem. Soc. Rev.*, 41(19), 6473–6506, doi:10.1039/c2cs35121h, 2012.

Charlson, R. J., Lovelock, J. E., Andreae, M. O. and Warren, S. G.: Oceanic phytoplankton, atmospheric sulphur, cloud albedo and climate, *Nature*, 326, 655–661, 1987.

Chen, W.-C. and Marcus, R. A.: On the theory of the reaction rate of vibrationally excited CO molecules with OH radicals, *J. Chem. Phys.*, 124(2), 024306, doi:10.1063/1.2148408, 2006.

Chen, Y., Xu, L., Humphry, T., Hettiyadura, A. P. S., Ovadnevaite, J., Huang, S., Poulain, L., Schroder, J. C., Campuzano-Jost, P., Jimenez, J. L., Herrmann, H., O'Dowd, C., Stone, E. A. and Ng, N. L.: Response of the Aerodyne Aerosol Mass Spectrometer to Inorganic Sulfates and Organosulfur Compounds: Applications in Field and Laboratory Measurements, *Environ. Sci. Technol.*, 53(9), 5176–5186, doi:10.1021/acs.est.9b00884, 2019.

Clarke, A. D., Davis, D., Kapustin, V. N., Eisele, F., Chen, G., Paluch, I., Lenschow, D., Bandy, A. R., Thornton, D., Moore, K., Mauldin, L., Tanner, D., Litchy, M., Carroll, M. A., Collins, J. and Albercook, G.: Particle Nucleation in the Tropical Boundary Layer and Its Coupling to Marine Sulfur Sources, *Science* (80-.)., 282(5386), 89–92, doi:10.1126/science.282.5386.89, 1998.

Collins, D. B., Bertram, T. H., Sultana, C. M., Lee, C., Axson, J. L. and Prather, K. A.: Phytoplankton blooms weakly influence the cloud forming ability of sea spray aerosol, *Geophys. Res. Lett.*, 9975–9983, doi:10.1002/2016GL069922, 2016.

Decarlo, P. F., Kimmel, J. R., Trimborn, A., Northway, M. J., Jayne, J. T., Aiken, A. C., Gonin, M., Fuhrer, K., Horvath, T., Docherty, K. S., Worsnop, D. R. and Jimenez, J. L.: Field-Deployable, High-Resolution, Time-of-Flight Aerosol Mass Spectrometer, *Anal. Chem.*, 78(24), 8281–8289, doi:8410.1029/2001JD001213.Analytical, 2006.

Duan, W., Meng, F., Wang, F. and Liu, Q.: Environmental behavior and eco-toxicity of xylene in aquatic environments: A review, Ecotoxicol. Environ. Saf., 145, 324–332, doi:10.1016/j.ecoenv.2017.07.050, 2017.

Ehn, M., Thornton, J. A., Kleist, E., Sipilä, M., Junninen, H., Pullinen, I., Springer, M., Rubach, F., Tillmann, R., Lee, B., Lopez-Hilfiker, F., Andres, S., Acir, I. H., Rissanen, M., Jokinen, T., Schobesberger, S., Kangasluoma, J., Kontkanen, J., Nieminen, T., Kurtén, T., Nielsen, L. B., Jørgensen, S., Kjaergaard, H. G., Canagaratna, M., Maso, M. D., Berndt, T., Petäjä, T., Wahner, A., Kerminen, V. M., Kulmala, M., Worsnop, D. R., Wildt, J. and Mentel, T.

F.: A large source of low-volatility secondary organic aerosol, *Nature*, 506(7489), 476–479, doi:10.1038/nature13032, 2014.

Facchini, M. C., Decesari, S., Rinaldi, M., Carbone, C., Finessi, E., Mircea, M., Fuzzi, S., Moretti, F., Tagliavini, E., Ceburnis, D. and O'Dowd, C. D.: Important Source of Marine Secondary Organic Aerosol from Biogenic Amines, *Environ. Sci. Technol.*, 42(24), 9116–9121, doi:10.1021/es8018385, 2008.

Fletcher, C. A., Johnson, G. R., Ristovski, Z. D. and Harvey, M.: Hygroscopic and volatile properties of marine aerosol observed at Cape Grim during the P2P campaign, *Environ. Chem.*, 4(3), 162–171, doi:10.1071/EN07011, 2007.

Forestieri, S. D., Staudt, S. M., Kuborn, T. M., Faber, K., Ruehl, C. R., Bertram, T. H. and Cappa, C. D.: Establishing the impact of model surfactants on cloud condensation nuclei activity of sea spray aerosol mimics, *Atmos. Chem. Phys.*, 18(15), 10985–11005, doi:10.5194/acp-18-10985-2018, 2018a.

Forestieri, S. D., Moore, K. A., Martinez Borrero, R., Wang, A., Stokes, M. D. and Cappa, C. D.: Temperature and Composition Dependence of Sea Spray Aerosol Production, *Geophys. Res. Lett.*, 45(14), 7218–7225, doi:10.1029/2018GL078193, 2018b.

Fossum, K. N., Ovadnevaite, J., Ceburnis, D., Dall'Osto, M., Marullo, S., Bellacicco, M., Simó, R., Liu, D., Flynn, M., Zuend, A. and O'Dowd, C.: Summertime Primary and Secondary Contributions to Southern Ocean Cloud Condensation Nuclei, *Sci. Rep.*, 8(1), 1–14, doi:10.1038/s41598-018-32047-4, 2018.

Fries, E., Gocht, T. and Klasmeier, J.: Occurrence and distribution of benzothiazole in the Schwarzbach watershed (Germany), J. Environ. Monit., 13(10), 2838–2843, doi:10.1039/C1EM10474H, 2011.

Fuhrer, M., Péron, O., Höfer, T., Morrissette, M. and Le Floch, S.: Offshore experiments on styrene spillage in marine waters for risk assessment, Mar. Pollut. Bull., 64(7), 1367–1374, doi:10.1016/J.MARPOLBUL.2012.04.022, 2012.

Gras, L. J. and Keywood, M.: Cloud condensation nuclei over the Southern Ocean: Wind dependence and seasonal cycles, *Atmos. Chem. Phys.*, 17(7), 4419–4432, doi:10.5194/acp-17-4419-2017, 2017.

Halsey, K. H., Giovannoni, S. J., Graus, M., Zhao, Y., Landry, Z., Thrash, J. C., Vergin, K. L. and de Gouw, J.: Biological cycling of volatile organic carbon by phytoplankton and bacterioplankton, *Limnol. Oceanogr.*, 62(6), 2650–2661, doi:10.1002/lno.10596, 2017.

Hatch, L. E., Jen, C. N., Kreisberg, N. M., Selimovic, V., Yokelson, R. J., Stamatis, C., York, R. A., Foster, D., Stephens, S. L., Goldstein, A. H. and Barsanti, K. C.: Highly Speciated Measurements of Terpenoids Emitted from Laboratory and Mixed-Conifer Forest Prescribed Fires, *Environ. Sci. Technol.*, 53(16), 9418–9428, doi:10.1021/acs.est.9b02612, 2019.

Hoffmann, E. H., Tilgner, A., Schrödner, R., Bräuer, P., Wolke, R. and Herrmann, H.: An advanced modeling study on the impacts and atmospheric implications of multiphase dimethyl sulfide chemistry, *Proc. Natl. Acad. Sci. U. S. A.*, 113(42), 11776–11781, doi:10.1073/pnas.1606320113, 2016.

Jenkin, M. E., Valorso, R., Aumont, B., Rickard, A. R. and Wallington, T. J.: Estimation of rate coefficients and branching ratios for gas-phase reactions of OH with aromatic organic compounds for use in automated mechanism construction, *Atmos. Chem. Phys.*, 18(13), 9329–9349, doi:10.5194/acp-18-9329-2018, 2018.

Jing, L., Chen, B., Zhang, B., Zheng, J. and Liu, B.: Naphthalene degradation in seawater by UV irradiation: The effects of fluence rate, salinity, temperature and initial concentration, Mar. Pollut. Bull., 81(1), 149–156, doi:10.1016/j.marpolbul.2014.02.003, 2014.

Kang, E., Root, M. J. and Brune, W. H.: Introducing the concept of Potential Aerosol Mass (PAM), *Atmos. Chem. Phys*., 7, 5727–5744, https://doi.org/10.5194/acp-7-5727-2007, 2007.

Kim, M. J., Zoerb, M. C., Campbell, N. R., Zimmermann, K. J., Blomquist, B. W., Huebert, B. J. and Bertram, T. H.: Revisiting benzene cluster cations for the chemical ionization of dimethyl sulfide and select volatile organic compounds, *Atmos. Meas. Tech.*, 9(4), 1473–1484, doi:10.5194/amt-9-1473-2016, 2016.

Kim, M. J., Novak, G. A., Zoerb, M. C., Yang, M., Blomquist, B. W., Huebert, B. J., Cappa, C. D. and Bertram, T. H.: Air-Sea exchange of biogenic volatile organic compounds and the impact on aerosol particle size distributions, *Geophys. Res. Lett.*, 44(8), 3887–3896, doi:10.1002/2017GL072975, 2017.

Korhonen, H., Carslaw, K. S., Spracklen, D. V., Mann, G. W. and Woodhouse, M. T.: Influence of oceanic dimethyl sulfide emissions on cloud condensation nuclei concentrations and seasonality over the remote Southern Hemisphere oceans: A global model study, *J. Geophys. Res. Atmos.*, 113(15), 1–16, doi:10.1029/2007JD009718, 2008.

Krechmer, J., Lopez-Hilfiker, F., Koss, A., Hutterli, M., Stoermer, C., Deming, B., Kimmel, J., Warneke, C., Holzinger, R., Jayne, J., Worsnop, D., Fuhrer, K., Gonin, M. and De Gouw, J.: Evaluation of a New Reagent-Ion Source and Focusing Ion-Molecule Reactor for Use in Proton-Transfer-Reaction Mass Spectrometry, *Anal. Chem.*, 90(20), 12011–12018, doi:10.1021/acs.analchem.8b02641, 2018.

Kuwata, M., R. Zorn, S. and T. Martin, S.: Using Elemental Ratios to Predict the Density of Organic Material Composed of Carbon, Hydrogen, and Oxygen, *Environ. Sci. Technol.*, 46(2), 787–794, doi:10.1021/es202525q, 2011.

Kwong, K. C., Chim, M. M., Hoffmann, E. H., Tilgner, A., Herrmann, H., Davies, J. F., Wilson, K. R. and Chan, M. N.: Chemical Transformation of Methanesulfonic Acid and Sodium Methanesulfonate through Heterogeneous OH Oxidation, *ACS Earth Sp. Chem.*, 2(9), 895–903, doi:10.1021/acsearthspacechem.8b00072, 2018.

Lambe, A. T., Onasch, T. B., Massoli, P., Croasdale, D. R., Wright, J. P., Ahern, A. T., Williams,

L. R., Worsnop, D. R., Brune, W. H. and Davidovits, P.: Laboratory studies of the chemical composition and cloud condensation nuclei (CCN) activity of secondary organic aerosol (SOA) and oxidized primary organic aerosol (OPOA), *Atmos. Chem. Phys.*, 11(17), 8913–8928, doi:10.5194/acp-11-8913-2011, 2011.

Lambe, A. T., Onasch, T. B., Croasdale, D. R., Wright, J. P., Martin, A. T., Franklin, J. P., Massoli, P., Kroll, J. H., Canagaratna, M. R., Brune, W. H., Worsnop, D. R. and Davidovits, P.: Transitions from functionalization to fragmentation reactions of laboratory Secondary Organic Aerosol (SOA) generated from the OH oxidation of alkane precursors, *Environ. Sci. Technol.*, doi:10.1021/es300274t, 2012.

Lambe, A. T., Chhabra, P. S., Onasch, T. B., Brune, W. H., Hunter, J. F., Kroll, J. H., Cummings, M. J., Brogan, J. F., Parmar, Y., Worsnop, D. R., Kolb, C. E. and Davidovits, P.: Effect of oxidant concentration, exposure time, and seed particles on secondary organic aerosol chemical composition and yield, *Atmos. Chem. Phys.*, 15(6), 3063–3075, doi:10.5194/acp-15-3063-2015, 2015.

Lana, A., Simó, R., Vallina, S. M. and Dachs, J.: Potential for a biogenic influence on cloud microphysics over the ocean: A correlation study with satellite-derived data, *Atmos. Chem. Phys.*, 12(17), 7977–7993, doi:10.5194/acp-12-7977-2012, 2012.

Liao, C., Kim, U. J. and Kannan, K.: A Review of Environmental Occurrence, Fate, Exposure, and Toxicity of Benzothiazoles, *Environ. Sci. Technol.*, 52(9), 5007–5026, doi:10.1021/acs.est.7b05493, 2018.

Mao, F., He, Y. and Gin, K. Y.-H.: Occurrence and fate of benzophenone-type UV filters in aquatic environments: a review, *Environ. Sci. Water Res. Technol.*, 5(2), 209–223, doi:10.1039/C8EW00539G, 2019.

Maßling, A., Wiedensohler, A., Busch, B., Neusüß, C., Quinn, P., Bates, T. and Covert, D.: Hygroscopic properties of different aerosol types over the Atlantic and Indian Oceans, *Atmos. Chem. Phys.*, 3(5), 1377–1397, doi:10.5194/acp-3-1377-2003, 2003.

Massoli, P., Lambe, A. T., Ahern, A. T., Williams, L. R., Ehn, M., Mikkilä, J., Canagaratna, M. R., Brune, W. H., Onasch, T. B., Jayne, J. T., Petäjä, T., Kulmala, M., Laaksonen, A., Kolb, C. E., Davidovits, P. and Worsnop, D. R.: Relationship between aerosol oxidation level and hygroscopic properties of laboratory generated secondary organic aerosol (SOA) particles, *Geophys. Res. Lett.*, 37(24), 1–5, doi:10.1029/2010GL045258, 2010.

Mayer, K. J., Wang, X., Santander, M. V, Mitts, B. A., Sauer, J. S., Sultana, C. M., Cappa, C. D. and Prather, K. A.: Secondary Marine Aerosol Plays a Dominant Role over Primary Sea Spray Aerosol in Cloud Formation, *ACS Cent. Sci.*, doi:10.1021/acscentsci.0c00793, 2020.

McCoy, D. T., Burrows, S. M., Wood, R., Grosvenor, D. P., Elliott, S. M., Ma, P.-L., Rasch, P. J. and Hartmann, D. L.: Natural aerosols explain seasonal and spatial patterns of Southern Ocean cloud albedo., *Sci. Adv.*, 1(6), e1500157, doi:10.1126/sciadv.1500157, 2015.

Meskhidze, N. and Nenes, A.: Phytoplankton and Cloudiness in the Southern Ocean, *Science* (80-

.)., 314(5804), 1419–1423, 2006.

Middlebrook, A. M., Bahreini, R., Jimenez, J. L. and Canagaratna, M. R.: Evaluation of composition-dependent collection efficiencies for the Aerodyne aerosol mass spectrometer using field data, *Aerosol Sci. Technol.*, 46(3), 258–271, doi:10.1080/02786826.2011.620041, 2012.

Mochida, M., Nishita-Hara, C., Furutani, H., Miyazaki, Y., Jung, J., Kawamura, K. and Uematsu, M.: Hygroscopicity and cloud condensation nucleus activity of marine aerosol particles over the western North Pacific, *J. Geophys. Res. Atmos.*, 116(6), 1–16, doi:10.1029/2010JD014759, 2011.

Modini, R. L., Johnson, G. R., He, C. and Ristovski, Z. D.: Observation of the suppression of water uptake by marine particles, *Atmos. Res.*, 98(2–4), 219–228, doi:10.1016/j.atmosres.2010.03.025, 2010.

Ovadnevaite, J., Zuend, A., Laaksonen, A., Sanchez, K. J., Roberts, G., Ceburnis, D., Decesari, S., Rinaldi, M., Hodas, N., Facchini, M. C., Seinfeld, J. H. and O' Dowd, C.: Surface tension prevails over solute effect in organic-influenced cloud droplet activation, *Nature*, 546(7660), 637–641, doi:10.1038/nature22806, 2017.

Paatero, P. and Tapper, U.: Positive matrix factorization: A non-negative factor model with optimal utilization of error estimates of data values, Environmetrics, 5(2), 111–126, doi:10.1002/env.3170050203, 1994.

Palmer, P. I. and Shaw, S. L.: Quantifying global marine isoprene fluxes using MODIS chlorophyll observations, *Geophys. Res. Lett.*, 32(9), 1–5, doi:10.1029/2005GL022592, 2005.

Peng, Z. and Jimenez, J. L.: KinSim: A Research-Grade, User-Friendly, Visual Kinetics Simulator for Chemical-Kinetics and Environmental-Chemistry Teaching, *J. Chem. Educ*., 96(4), 806–811, doi:10.1021/acs.jchemed.9b00033, 2019.

Petters, M. D. and Kreidenweis, S. M.: A single parameter representation of hygroscopic growth and cloud condensation nucleus activity, *Atmos. Chem. Phys.*, 7, 1961–1971, doi:10.5194/acp-7-1961-2007, 2007.

Prather, K. a, Bertram, T. H., Grassian, V. H., Deane, G. B., Stokes, M. D., Demott, P. J., Aluwihare, L. I., Palenik, B. P., Azam, F., Seinfeld, J. H., Moffet, R. C., Molina, M. J., Cappa, C. D., Geiger, F. M., Roberts, G. C., Russell, L. M., Ault, A. P., Baltrusaitis, J., Collins, D. B., Corrigan, C. E., Cuadra-Rodriguez, L. a, Ebben, C. J., Forestieri, S. D., Guasco, T. L., Hersey, S. P., Kim, M. J., Lambert, W. F., Modini, R. L., Mui, W., Pedler, B. E., Ruppel, M. J., Ryder, O. S., Schoepp, N. G., Sullivan, R. C. and Zhao, D.: Bringing the ocean into the laboratory to probe the chemical complexity of sea spray aerosol., *Proc. Natl. Acad. Sci. U. S. A.*, 110(19), 7550–5, doi:10.1073/pnas.1300262110, 2013.

Quinn, P. K., Coffman, D. J., Johnson, J. E., Upchurch, L. M. and Bates, T. S.: Small fraction of marine cloud condensation nuclei made up of sea spray aerosol, *Nat. Geosci.*, 10(9), 674–679, doi:10.1038/ngeo3003, 2017.

Reddy, C. M. and Quinn, J. G.: Environmental chemistry of benzothiazeles derived from rubber, *Environ. Sci. Technol.*, 31(10), 2847–2853, doi:10.1021/es970078o, 1997.

Ruehl, C. R., Davies, J. F. and Wilson, K. R.: An interfacial mechanism for cloud droplet formation on organic aerosols, *Science* (80-.)., 351(6280), 1447–1450, doi:10.1126/science.aad4889, 2016.

Saathoff, H., Naumann, K. H., Möhler, O., Jonsson, Å. M., Hallquist, M., Kiendler-Scharr, A., Mentel, T. F., Tillmann, R. and Schurath, U.: Temperature dependence of yields of secondary organic aerosols from the ozonolysis of α-pinene and limonene, *Atmos. Chem. Phys.*, 9(5), 1551–1577, doi:10.5194/acp-9-1551-2009, 2009.

Sanchez, K. J., Chen, C. L., Russell, L. M., Betha, R., Liu, J., Price, D. J., Massoli, P., Ziemba, L. D., Crosbie, E. C., Moore, R. H., Müller, M., Schiller, S. A., Wisthaler, A., Lee, A. K. Y., Quinn, P. K., Bates, T. S., Porter, J., Bell, T. G., Saltzman, E. S., Vaillancourt, R. D. and Behrenfeld, M. J.: Substantial Seasonal Contribution of Observed Biogenic Sulfate Particles to Cloud Condensation Nuclei, *Sci. Rep.*, 8(1), 1–14, doi:10.1038/s41598-018-21590-9, 2018.

Schneider, S. R., Collins, D. B., Lim, C. Y., Zhu, L. and Abbatt, J. P. D.: Formation of Secondary Organic Aerosol from the Heterogeneous Oxidation by Ozone of a Phytoplankton Culture, *ACS Earth Sp. Chem.*, 3(10), 2298–2306, doi:10.1021/acsearthspacechem.9b00201, 2019.

Seinfeld, J. H. and Pandis, S. N.: Atmospheric Chemistry and Physics: From Air Pollution to Climate Change, Third Ed., John Wiley & Sons, Inc., Hoboken, New Jersey., 2016.

Shaw, S. L., Gantt, B. and Meskhidze, N.: Production and Emissions of Marine Isoprene and Monoterpenes: A Review, edited by O. Stetzer, *Adv. Meteorol.*, 2010, 408696, doi:10.1155/2010/408696, 2010.

Trueblood, J. V., Wang, X., Or, V. W., Alves, M. R., Santander, M. V., Prather, K. A. and Grassian, V. H.: The Old and the New: Aging of Sea Spray Aerosol and Formation of Secondary Marine Aerosol through OH Oxidation Reactions, *ACS Earth Sp. Chem.*, 3(10), 2307–2314, doi:10.1021/acsearthspacechem.9b00087, 2019.

Ulbrich, I. M., Canagaratna, M. R., Zhang, Q., Worsnop, D. R. and Jimenez, J. L.: Interpretation of organic components from Positive Matrix Factorization of aerosol mass spectrometric data, *Atmos. Chem. Phys.*, 9(9), 2891–2918, doi:10.5194/acp-9-2891-2009, 2009.

Vaattovaara, P., Huttunen, P. E., Yoon, Y. J., Joutsensaari, J., Lehtinen, K. E. J., O'Dowd, C. D., and Laaksonen, A.: The composition of nucleation and Aitken modes particles during coastal nucleation events: evidence for marine secondary organic contribution, *Atmos. Chem. Phys.*, 6, 4601–4616, https://doi.org/10.5194/acp-6-4601-2006, 2006.

Veres, P. R., Andrew Neuman, J., Bertram, T. H., Assaf, E., Wolfe, G. M., Williamson, C. J., Weinzierl, B., Tilmes, S., Thompson, C. R., Thames, A. B., Schroder, J. C., Saiz-Lopez, A., Rollins, A. W., Roberts, J. M., Price, D., Peischl, J., Nault, B. A., Møller, K. H., Miller, D. O., Meinardi, S., Li, Q., Lamarque, J. F., Kupc, A., Kjaergaard, H. G., Kinnison, D.,

Jimenez, J. L., Jernigan, C. M., Hornbrook, R. S., Hills, A., Dollner, M., Day, D. A., Cuevas, C. A., Campuzano-Jost, P., Burkholder, J., Paul Bui, T., Brune, W. H., Brown, S. S., Brock, C. A., Bourgeois, I., Blake, D. R., Apel, E. C. and Ryerson, T. B.: Global airborne sampling reveals a previously unobserved dimethyl sulfide oxidation mechanism in the marine atmosphere, *Proc. Natl. Acad. Sci. U. S. A.*, 117(9), 4505–4510, doi:10.1073/pnas.1919344117, 2020.

Wang, X., Sultana, C. M., Trueblood, J., Hill, T. C. J., Malfatti, F., Lee, C., Laskina, O., Moore, K. A., Beall, C. M., McCluskey, C. S., Cornwell, G. C., Zhou, Y., Cox, J. L., Pendergraft, M. A., Santander, M. V., Bertram, T. H., Cappa, C. D., Azam, F., DeMott, P. J., Grassian, V. H. and Prather, K. A.: Microbial Control of Sea Spray Aerosol Composition: A Tale of Two Blooms, *ACS Cent. Sci*., 1(3), 124–131, doi:10.1021/acscentsci.5b00148, 2015.

Wohl, C., Brown, I., Kitidis, V., Jones, A. E., Sturges, W. T., Nightingale, P. D. and Yang, M.: Underway seawater and atmospheric measurements of volatile organic compounds in the Southern Ocean, Biogeosciences, 17(9), 2593–2619, doi:10.5194/bg-17-2593-2020, 2020.

Zhang, Q., Jimenez, J. L., Canagaratna, M. R., Ulbrich, I. M., Ng, N. L., Worsnop, D. R. and Sun, Y.: Understanding atmospheric organic aerosols via factor analysis of aerosol mass spectrometry: A review, Anal. Bio*Anal. Chem.*, 401(10), 3045–3067, doi:10.1007/s00216-011-5355-y, 2011.

Chapter 6 Conclusions and Future Work

6.1 Synopsis

This dissertation investigates the complex relationship between biological activity in seawater and the cloud-forming ability of both primary and secondary marine aerosols. Chapter 2 describes the use of laboratory ocean-atmosphere simulators for investigations of marine aerosol production and properties, and reviews the recent discoveries enabled by these systems. Chapter 3 directly compares the CCN activity and flux of SSA and SMA during a mesocosm bloom experiment. Chapter 4 gives a detailed overview of the Sea Spray Chemistry and Particle Evolution (SeaSCAPE) campaign, a large-scale wave channel experiment which sought to understand how atmospheric aging processes influence marine aerosols. Finally, Chapter 5 investigates the influence of photochemical aging timescales on the chemical composition and CCN activity of SMA generated during SeaSCAPE.

6.2 Conclusions

6.2.1 CAICE Studies: Insights from a Decade of Ocean–Atmosphere Experiments in the Laboratory

Laboratory ocean-atmosphere experiments have great utility for studying the complex relationships between marine biota, aerosol chemistry, and cloud formation. Chapter 2 describes the development of ocean-atmosphere simulators, as well as their important applications towards the study of marine aerosols and gases. In addition, this chapter presents new results regarding the CCN activity and flux of freshly emitted SSA, which show both properties are relatively insensitive to biological activity in seawater. This key discovery was enabled by ocean-atmosphere experiments in the laboratory and highlights their importance for understanding ocean-climate

interactions. Finally, an outlook on the future of ocean-atmosphere experiments is provided, with a key emphasis on the SOARS facility, which is currently under development.

6.2.2 Secondary Marine Aerosol Plays a Dominant Role over Primary Sea Spray Aerosol in Cloud Formation

Field observations showing a link between marine clouds and seawater chl-a concentrations have suggested a role for biogenic aerosols (McCoy et al., 2015); however, the exact mechanisms underlying this relationship have remained unclear. Chapter 3 of this dissertation presents results from a novel experimental approach, in which SSA and SMA were generated concurrently from a phytoplankton bloom grown in natural seawater. Notably, this experiment represents one of the first applications of OFRs for marine aerosol research and provides the foundation for the oxidation experiments described in Chapters 4 and 5. The results show SMA formation is much more sensitive to biological activity than SSA. In addition, the chemical composition and CCN activity of the OFR-generated SMA is consistent with field observations of marine aerosols (Asmi et al., 2010; Swietlicki et al., 2008). Overall, these findings suggest that the observed link between seawater chl-a concentrations and cloud droplet number concentrations is likely driven by SMA formation, rather than changes in the production and CCN activity of primary SSA.

6.2.3 The Sea Spray Chemistry and Particle Evolution Study (SeaSCAPE): Overview and Experimental Methods

Building upon previous wave channel experiments (Prather et al., 2013; Wang et al., 2015), the SeaSCAPE study sought to understand the complex interactions between marine biological activity and aerosols, with a specific emphasis on the role of VOC emissions, atmospheric aging processes, and secondary aerosol formation. Chapter 4 describes the methods and wave channel

characterization experiments necessary to facilitate the SeaSCAPE experiment, as well as a full inventory of seawater, gas-phase, and aerosol measurements conducted during the study. In addition, key results are presented which highlight the experimental capabilities of the campaign.

6.2.4 Atmospheric Aging Drives Variability in Secondary Marine Aerosol Composition and Cloud-Forming Ability

Chapter 6 reports on results from measurements taken during SeaSCAPE, which show a strong relationship between the degree of photochemical aging and cloud-forming abilities of SMA. Throughout the bloom experiment, increased oxidation levels led to a shift in chemical composition from organic-rich to sulfate-rich aerosol. This compositional change led to an increase in the CCN activity of SMA, as sulfate tends to be more hygroscopic than organic aerosol species. In addition, changes in the SMA properties were also linked to the biological activity in the seawater through the emission of different VOCs. The ratio between DMS and non-sulfur-VOCs was strongly controlled by the state of the phytoplankton bloom, which in turn influenced the properties of the SMA. This study demonstrates that chemical composition and CCN activity of SMA evolve temporally in the atmosphere, on timescales linked to both photochemical oxidation and biological dynamics.

6.3 Ongoing and Future Work

6.3.1 Model Studies of SMA Precursors

Oxidation flow reactors have been used extensively for studies of terrestrial and anthropogenic aerosols; however, their application to the marine atmosphere have been extremely limited. Chapter 3 of this dissertation represents one of the first experiments in which the PAM-OFR system was used for generating SMA during a phytoplankton bloom. While there is overlap

between terrestrial and marine VOCs (i.e. isoprene and monoterpenes), many of the compounds observed in the marine atmosphere are unique to that environment (i.e. DMS). Model studies of marine VOCs are necessary to understand how these compounds react in the OFR and to optimize experimental conditions for marine systems.

Prior studies have shown that the presence of inorganic seed particles increases SOA yield in OFRs (Lambe et al., 2015). Additionally, work done in environmental chambers suggests that DMS can increase the aerosol yield of isoprene SOA by creating acidic seed particles (Chen and Jang, 2012). Future studies are necessary to understand how the presence of DMS may affect the reactions and aerosols yields of non-sulfur-VOCs in the OFR. Additionally, it is known that the reaction of SOA products with H_2SO_4 can result in the formation of organosulfates (Darer et al., 2011; Hatch et al., 2011). As H_2SO_4 is a major product of DMS oxidation, it is possible that organosulfates may be a significant component of SMA; however, these compounds are difficult to measure using the aerosol mass spectrometer (AMS), which was described in Chapters 3, 4, and 5 of this thesis, due to fragmentation in the instrument (Chen et al., 2019). Future studies should focus on using alternative instrumentation with softer ionization methods in order to investigate the potential formation of organosulfates in SMA.

6.3.2 The Development of New Ocean-Atmosphere Interaction Facilities

A major disadvantage of the OFR system is that due to the fast reaction times, it strongly favors new particle formation over condensation and aerosol growth processes. While nucleation is observed in the marine atmosphere, these newly formed particles will grow over time to larger sizes through coagulation and condensation (Brock, 1972; Mulholland and Baum, 1980). Additionally, if there are particles already present in the atmosphere, secondary species may condense onto the particles, as opposed to forming new particles, transforming both their size

distribution and chemical composition (Sanchez et al., 2018). OFRs are not capable of accurately reproducing these processes. There have also been questions of the environmental relevance of OFR experiments, due to the high oxidant concentrations and UV light flux (Peng and Jimenez, 2020).

Environmental chambers (also called smog chambers) have traditionally been used for the study of secondary organic aerosol and are an important alternative to flow reactors. The typical design is a Teflon bag with a volume of up to 30 m^2, with the large size being necessary to increase the volume to surface area ratio within the chamber and minimize wall losses (Bruns et al., 2015). A major limitation of these chambers is that due to their size, they are not portable, which has limited their application in ocean-atmosphere studies thus far. However, with the development of the new Scripps Ocean Atmosphere Research Simulator (SOARS), these types of experiments will become feasible. The SOARS facility, which will be completed in Summer 2021, is a 36 m long wind-wave channel with a built-in environmental chamber. This will enable chamber studies of secondary marine aerosols during mesocosm bloom experiments under realistic conditions. While extensive work will be necessary to characterize both the wind-wave channel and the chamber, SOARS has the potential to answer many important questions about the reactions of particles and gases in the marine atmosphere, and their possible impact on clouds and climate.

6.3.3 Role of Anthropogenic Contaminants in SMA Formation

Chapter 5 of this dissertation describes results from the SeaSCAPE experiment, focusing specifically on the chemical properties of SMA. However, it is important to note that the seawater used to fill the wave channel was taken from the coast of San Diego, a major city with a metro population of 3.3 million people. Several of the gas-phase compounds which evolved from the seawater during SeaSCAPE have been identified as potentially being anthropogenic in origin,

including benzothiazole, styrene, xylene, and benzophenone (Table 5.1) (Duan et al., 2017; Fuhrer et al., 2012; Liao et al., 2018; Mao et al., 2019). There is a strong possibility that these contaminants may have been present in the seawater when it was collected from the ocean, as a result of pollution from runoff or wastewater effluence (Lopes and Dionne, 1998). However, marine phytoplankton and bacteria have been observed to produce a wide range of compounds, many of which overlap with anthropogenic contaminants, including chlorinated organics (Colomb et al., 2008). For example, benzothiazole is a well-known anthropogenic contaminant, originating from rubber (Reddy and Quinn, 1997); however, it also has natural sources in the marine environment (Le Bozec and Moody, 2009). Thus, it is difficult to confidently attribute some of these compounds to a purely anthropogenic origin without further studies to investigate their origins.

Future work should seek to differentiate between the anthropogenic and natural volatile compounds found in natural seawater. For example, stable carbon isotope ratios have been used in other studies to determine the source of atmospheric VOCs (Kawashima and Murakami, 2014). In addition, experiments which seek to examine marine aerosol formation and properties under pristine conditions may benefit from collecting seawater from further offshore, in order to minimize contributions from terrestrial runoff. Finally, the volatilization of anthropogenic pollutants from seawater has significant implications for air quality in coastal cities. Bubble-mediated transfer from breaking waves on the coast can enhance the sea-air transfer of VOCs, especially for gases with low solubilities in seawater (Bell et al., 2017). Further studies are necessary to determine how the transfer of pollutants from seawater to the air via breaking waves could affect air quality and human health.

6.4 Acknowledgements

Alexia N. Moore is acknowledged for assisting in the editing of this chapter.

6.5 References

Asmi, E., Frey, A., Virkkula, A., Ehn, M., Manninen, H. E., Timonen, H., Tolonen-Kiviḿaki, O., Aurela, M., Hillamo, R. and Kulmala, M.: Hygroscopicity and chemical composition of antarctic sub-micrometre aerosol particles and observations of new particle formation, *Atmos. Chem. Phys.*, 10(9), 4253–4271, doi:10.5194/acp-10-4253-2010, 2010.

Bell, T. G., Landwehr, S., Miller, S. D., De Bruyn, W. J., Callaghan, A. H., Scanlon, B., Ward, B., Yang, M. and Saltzman, E. S.: Estimation of bubble-mediated air-sea gas exchange from concurrent DMS and CO2 transfer velocities at intermediate-high wind speeds, *Atmos. Chem. Phys.*, 17(14), 9019–9033, doi:10.5194/acp-17-9019-2017, 2017.

Le Bozec, L. and Moody, C. J.: Naturally occurring nitrogensulfur compounds. the benzothiazole alkaloids, *Aust. J. Chem.*, 62(7), 639–647, doi:10.1071/CH09126, 2009.

Brock, J. R.: Condensational growth of atmospheric aerosols, *J. Colloid Interface Sci.*, 39(1), 32–36, doi:10.1016/0021-9797(72)90139-7, 1972.

Bruns, E. A., El Haddad, I., Keller, A., Klein, F., Kumar, N. K., Pieber, S. M., Corbin, J. C., Slowik, J. G., Brune, W. H., Baltensperger, U. and Prévôt, A. S. H.: Inter-comparison of laboratory smog chamber and flow reactor systems on organic aerosol yield and composition, *Atmos. Meas. Tech.*, 8(6), 2315–2332, doi:10.5194/amt-8-2315-2015, 2015.

Chen, T. and Jang, M.: Secondary organic aerosol formation from photooxidation of a mixture of dimethyl sulfide and isoprene, *Atmos. Environ.*, 46, 271–278, doi:10.1016/j.atmosenv.2011.09.082, 2012.

Chen, Y., Xu, L., Humphry, T., Hettiyadura, A. P. S., Ovadnevaite, J., Huang, S., Poulain, L., Schroder, J. C., Campuzano-Jost, P., Jimenez, J. L., Herrmann, H., O'Dowd, C., Stone, E. A. and Ng, N. L.: Response of the Aerodyne Aerosol Mass Spectrometer to Inorganic Sulfates and Organosulfur Compounds: Applications in Field and Laboratory Measurements, *Environ. Sci. Technol.*, 53(9), 5176–5186, doi:10.1021/acs.est.9b00884, 2019.

Colomb, A., Yassaa, N., Williams, J., Peeken, I. and Lochte, K.: Screening volatile organic compounds (VOCs) emissions from five marine phytoplankton species by head space gas chromatography/mass spectrometry (HS-GC/MS), *J. Environ. Monit.*, 10(3), 325–330, doi:10.1039/b715312k, 2008.

Darer, A. I., Cole-Filipiak, N. C., O'Connor, A. E. and Elrod, M. J.: Formation and stability of

atmospherically relevant isoprene-derived organosulfates and organonitrates, *Environ. Sci. Technol.*, 45(5), 1895–1902, doi:10.1021/es103797z, 2011.

Duan, W., Meng, F., Wang, F. and Liu, Q.: Environmental behavior and eco-toxicity of xylene in aquatic environments: A review, *Ecotoxicol. Environ. Saf.*, 145, 324–332, doi:10.1016/j.ecoenv.2017.07.050, 2017.

Fuhrer, M., Péron, O., Höfer, T., Morrissette, M. and Le Floch, S.: Offshore experiments on styrene spillage in marine waters for risk assessment, *Mar. Pollut. Bull.*, 64(7), 1367–1374, doi:10.1016/J.MARPOLBUL.2012.04.022, 2012.

Hatch, L. E., Creamean, J. M., Ault, A. P., Surratt, J. D., Chan, M. N., Seinfeld, J. H., Edgerton, E. S., Su, Y. and Prather, K. A.: Measurements of isoprene-derived organosulfates in ambient aerosols by aerosol time-of-flight mass spectrometry - Part 2: Temporal variability and formation mechanisms, *Environ. Sci. Technol.*, 45(20), 8648–8655, doi:10.1021/es2011836, 2011.

Kawashima, H. and Murakami, M.: Measurement of the stable carbon isotope ratio of atmospheric volatile organic compounds using chromatography, combustion, and isotope ratio mass spectrometry coupled with thermal desorption, *Atmos. Environ.*, 89, 140–147, doi:10.1016/j.atmosenv.2014.02.033, 2014.

Lambe, A. T., Chhabra, P. S., Onasch, T. B., Brune, W. H., Hunter, J. F., Kroll, J. H., Cummings, M. J., Brogan, J. F., Parmar, Y., Worsnop, D. R., Kolb, C. E. and Davidovits, P.: Effect of oxidant concentration, exposure time, and seed particles on secondary organic aerosol chemical composition and yield, *Atmos. Chem. Phys.*, 15(6), 3063–3075, doi:10.5194/acp-15-3063-2015, 2015.

Liao, C., Kim, U. J. and Kannan, K.: A Review of Environmental Occurrence, Fate, Exposure, and Toxicity of Benzothiazoles, *Environ. Sci. Technol.*, 52(9), 5007–5026, doi:10.1021/acs.est.7b05493, 2018.

Lopes, T. J. and Dionne, S. G.: A Review of Semivolatile and Volatile Organic Compounds in Highway Runoff and Urban Stormwater., 1998.

Mao, F., He, Y. and Gin, K. Y.-H.: Occurrence and fate of benzophenone-type UV filters in aquatic environments: a review, *Environ. Sci. Water Res. Technol.*, 5(2), 209–223, doi:10.1039/C8EW00539G, 2019.

McCoy, D. T., Burrows, S. M., Wood, R., Grosvenor, D. P., Elliott, S. M., Ma, P.-L., Rasch, P. J. and Hartmann, D. L.: Natural aerosols explain seasonal and spatial patterns of Southern Ocean cloud albedo., *Sci. Adv.*, 1(6), e1500157, doi:10.1126/sciadv.1500157, 2015.

Mulholland, G. W. and Baum, H. R.: Effect of initial size distribution on aerosol coagulation, *Phys. Rev. Lett.*, 45(9), 761–763, doi:10.1103/PhysRevLett.45.761, 1980.

Peng, Z. and Jimenez, J. L.: Radical chemistry in oxidation flow reactors for atmospheric chemistry research, *Chem. Soc. Rev.*, 49(9), 2570–2616, doi:10.1039/C9CS00766K, 2020.

Prather, K. A, Bertram, T. H., Grassian, V. H., Deane, G. B., Stokes, M. D., Demott, P. J., Aluwihare, L. I., Palenik, B. P., Azam, F., Seinfeld, J. H., Moffet, R. C., Molina, M. J., Cappa, C. D., Geiger, F. M., Roberts, G. C., Russell, L. M., Ault, A. P., Baltrusaitis, J., Collins, D. B., Corrigan, C. E., Cuadra-Rodriguez, L. a, Ebben, C. J., Forestieri, S. D., Guasco, T. L., Hersey, S. P., Kim, M. J., Lambert, W. F., Modini, R. L., Mui, W., Pedler, B. E., Ruppel, M. J., Ryder, O. S., Schoepp, N. G., Sullivan, R. C. and Zhao, D.: Bringing the ocean into the laboratory to probe the chemical complexity of sea spray aerosol., *Proc. Natl. Acad. Sci. U. S. A.*, 110(19), 7550–5, doi:10.1073/pnas.1300262110, 2013.

Reddy, C. M. and Quinn, J. G.: Environmental chemistry of benzothiazeles derived from rubber, *Environ. Sci. Technol.*, 31(10), 2847–2853, doi:10.1021/es970078o, 1997.

Sanchez, K. J., Chen, C. L., Russell, L. M., Betha, R., Liu, J., Price, D. J., Massoli, P., Ziemba, L. D., Crosbie, E. C., Moore, R. H., Müller, M., Schiller, S. A., Wisthaler, A., Lee, A. K. Y., Quinn, P. K., Bates, T. S., Porter, J., Bell, T. G., Saltzman, E. S., Vaillancourt, R. D. and Behrenfeld, M. J.: Substantial Seasonal Contribution of Observed Biogenic Sulfate Particles to Cloud Condensation Nuclei, *Sci. Rep.*, 8(1), 1–14, doi:10.1038/s41598-018-21590-9, 2018.

Swietlicki, E., Hansson, H. C., Hämeri, K., Svenningsson, B., Massling, A., Mcfiggans, G., Mcmurry, P. H., Petäjä, T., Tunved, P., Gysel, M., Topping, D., Weingartner, E., Baltensperger, U., Rissler, J., Wiedensohler, A. and Kulmala, M.: Hygroscopic properties of submicrometer atmospheric aerosol particles measured with H-TDMA instruments in various environments - A review, *Tellus, Ser. B Chem. Phys. Meteorol*., 60 B(3), 432–469, doi:10.1111/j.1600-0889.2008.00350.x, 2008.

Trueblood, J. V., Wang, X., Or, V. W., Alves, M. R., Santander, M. V., Prather, K. A. and Grassian, V. H.: The Old and the New: Aging of Sea Spray Aerosol and Formation of Secondary Marine Aerosol through OH Oxidation Reactions, *ACS Earth Sp. Chem.*, 3(10), 2307–2314, doi:10.1021/acsearthspacechem.9b00087, 2019.

Wang, X., Sultana, C. M., Trueblood, J., Hill, T. C. J., Malfatti, F., Lee, C., Laskina, O., Moore, K. A., Beall, C. M., McCluskey, C. S., Cornwell, G. C., Zhou, Y., Cox, J. L., Pendergraft, M. A., Santander, M. V., Bertram, T. H., Cappa, C. D., Azam, F., DeMott, P. J., Grassian, V. H. and Prather, K. A.: Microbial Control of Sea Spray Aerosol Composition: A Tale of Two Blooms, *ACS Cent. Sci*., 1(3), 124–131, doi:10.1021/acscentsci.5b00148, 2015.